Synthesis and Coordination Chemistry of Scorpionate Ligands and their Applications in ^{11}C–Positron Emission Tomography

Steven Kealey

Submitted in Partial Fulfilment of the Requirements
for the Degree of Doctor of Philosophy

Supervisor: Prof. N. J. Long

Department of Chemistry
Imperial College London

April 2008

STATEMENT OF COPYRIGHT

The copyright of this thesis rests with the author. No quotation from it should be published without the prior written consent of the author and information derived from it should be acknowledged appropriately.

DECLARATION

The work described in this thesis was carried out in the Department of Chemistry, Imperial College London, between October 2004 and December 2007. The entire body of work is my own unless otherwise stated to the contrary and has not been submitted previously for a degree at this or any other university.

ABSTRACT

This thesis is concerned with the synthesis and coordination chemistry of a range of poly(pyrazolyl)borate 'scorpionate' ligands and examines their suitability in facilitating rapid [^{11}C]carbonylation reactions to form radiotracers for application in positron emission tomography (PET).

The synthesis of a series of tris(pyrazolyl)borate (Tp) ligands and their corresponding copper(I) carbonyl complexes is described. The copper(I) carbonyls were formed by reaction of potassium Tp salts with copper chloride in the presence of carbon monoxide.

The second part of this thesis concerns the use of a copper(I)-Tp system for selectively solubilising ^{11}CO from nitrogen-rich gas streams for subsequent use in palladium-catalysed carbonylation reactions between amines and aryl-halides to form amides. These reactions were performed on a microfluidic device and in Schlenk apparatus using unlabelled carbon monoxide. These reactions were transferred to the radiochemical laboratory whereby efficient ^{11}CO trapping was observed prior to the formation of ^{11}C-radiolabelled amides.

The third part of this thesis explores the coordination chemistry of palladium(II) towards a novel hybrid ligand consisting of pyrazolyl and triphenylphosphine moieties. The potential hemilabile behaviour of this ligand and its derivatives towards palladium was investigated and the use of these complexes as catalysts for carbonylation reactions is described.

The final part of this thesis examines the coordination chemistry of poly(pyrazolyl)borates bearing additional coordinating groups appended to the 3- or 5-position of the pyrazolyl rings. Reactions of the 3-substituted derivatives were carried out with a range of metals and found to display varied coordination behaviour depending on the specific coordination requirements of the metal.

PUBLICATIONS

Publications resulting from this work are listed below and are reproduced in full in the appendix (Chapter 8).

Variable Coordination Behaviour of Pyrazole-Containing N,P and N,P(O) Ligands Towards Palladium(II),
Steven Kealey, Nicholas J. Long, Philip W. Miller, Andrew J. P. White, Peter B. Hitchcock, Antony D. Gee.
Dalton Transactions, 2007, 2823.

A Novel Tetrakis(pyrazolyl)borate Ligand Bearing Triphenylphosphine Oxide Substituents,
Steven Kealey, Nicholas J. Long, Andrew J. P. White and Antony D. Gee.
Dalton Transactions, 2007, 4763.

ScorpoPhos: A Novel Phosphine-Nitrogen Ligand Containing a Tris(pyrazolyl)borate Ligand Core,
Steven Kealey, Nicholas J. Long, Philip W. Miller, Andrew J. P. White and Antony D. Gee.
Dalton Transactions, 2008, 2677.

ABBREVIATIONS

Å	angstrom, 10^{-10} m
AD	Alzheimer's disease
ADME	absorption, distribution, metabolism and excretion
AIBN	azobis(isobutyronitrile)
Ani	anilinyl
Ar	aryl
Bp	bis(pyrazolyl)borate
Bp*	bis(3,5-dimethyl(pyrazolyl))borate
Bq	Becquerel (one disintegration per second)
^{t}Bu	tert-butyl, $C(CH_3)_3$
COD	1,5-cyclooctadiene
CORM	CO-releasing molecule
CT	computed tomography
DCEA	bis(2-cyanoethyl)amine
DCM	dichloromethane
DRIFT	diffuse reflectance infrared fourier transformation
DMA-DMA	dimethylacetamide dimethylacetal
DMF	dimethylformamide
DMF-DMA	dimethylformamide dimethylacetal
DMSO	dimethylsulphoxide
dppp	1,3-bis(diphenylphosphino)propane
EGDMA	ethylene glycol dimethacrylate
EI	electron ionization
EOB	end of bombardment
ESI	electrospray ionisation
Et	ethyl, CH_2CH_3
eV	electron volt
FAB	fast atom bombardment
FDG	fluoro-2-deoxy-D-glucose
GC	gas chromatography
HOMO	highest occupied molecular orbital
HPLC	high performance liquid chromatography

IR	infra red
^{i}Pr	iso-propyl, $CH(CH_3)_2$
l	litre
L	ligand
LUMO	lowest unoccupied molecular orbital
M	metal
Me	methyl, CH_3
MeCN	acetonitrile
MLCT	metal to ligand charge transfer
MO	molecular orbital
MRI	magnetic resonance imaging
m/z	mass to charge ratio
NMR	nuclear magnetic resonance
s	singlet
d	doublet
dd	double doublet
t	triplet
Hz	hertz
δ	chemical shift
ppm	parts per million
OAc	acetate, CH_3COO^-
PET	positron emission tomography
Ph	phenyl
Py	pyridyl
pz	pyrazolyl
TACN	1,4-diisopropyl-1,4,7-triazacyclononane
THF	tetrahydrofuran
Tim	tris(imidazole-2-ylidene)borate
TMPA	tris(2-pyridylmethyl)amine
Tp	tris(pyrazolyl)borate
Tp*	tris(3,5-dimethyl(pyrazolyl))borate
T_kp	tetrakis(pyrazolyl)borate
UV-vis	ultra violet-visible
υ	vibrational frequency, cm^{-1}

ACKNOWLEDGEMENTS

Probably the most challenging aspect of any thesis is to construct an acknowledgements section that is not overwhelmingly cringe-worthy when re-read in years to come. Having failed at this in less than two lines I shall carry on regardless.

Firstly, I would like to thank my supervisors Nick and Tony who have provided me with so much support throughout my project and for allowing me to work with a fantastic amount of freedom. Thanks to Nick and Phil for putting up with my constant knocking on their doors to provide the tiniest update on the progress of any given reaction. My thanks to Phil especially for so much help with syntheses and for those countless discussions which usually started with 'I think you should try making...'. Sometimes I did, and sometimes it worked, so for that, I am most grateful. Obviously I'd like to thank all the members of the Long group, past and present, whom I have been most fortunate to work with, and go to the Holland Club with, over the years.

I'm very grateful to GSK, EPSRC and the Department of Chemistry for providing funding for my project. Within the chemistry department I would like to thank Dick and especially Pete for going above-and-beyond their duties in helping me with all matters NMR. Thanks to Andrew White for X-ray analysis of my compounds, without which my thesis would be substantially barer. I am also grateful to John Barton and Stephen Boyer for mass spectrometry and elemental analysis.

Outside the department there are so many people who have made my last few years in London so enjoyable that I can't possibly name them all – In my head I am very grateful to you. More specifically, I would like to thank my housemates of years gone by, especially Mark, Dan and Dom for so many good laughs and probably an equal number of unaccountable headaches the next day. I would like to thank my family for being brilliant all of the time and for coming to visit me, taking me to concerts and buying me dinner. Finally, and this almost goes without saying, thank you Sophie for being so loving and supportive and managing to do so even when sharing the same living space as me. I feel extremely lucky.

TABLE OF CONTENTS

Declaration i

Abstract ii

Publications iii

Abbreviations iv

Acknowledgements vi

1. Introduction 1

1.1 Positron Emission Tomography 2

1.1.1 Positron Emitting Isotopes 4

1.1.2 Applications of PET 5

1.1.3 ^{11}C-Radiolabelling 9

1.2 Carbon Monoxide 10

1.2.1 [^{11}C]Carbon Monoxide as a Reagent 10

1.2.2 Palladium–Mediated [^{11}C]Carbonylations 11

1.2.3 Alternative [^{11}C]Carbonylation Methods 17

1.2.4 Coordination Chemistry of Carbon Monoxide 18

1.2.5 Metal Carbonyl Complexes in Nature 19

1.3 Copper(I) Carbonyl Complexes 25

1.3.1 Background 25

1.3.2 No Supporting Ligand 27

1.3.3 Bidentate Ligands 28

1.3.4 Tridentate Ligands 30

1.3.5 Flexible Tetradentate Ligands 31

1.3.6 Macrocyclic Tetradentate Ligands 34

1.3.7 Immobilized Copper(I) Complexes 35

1.3.8 Summary 37

1.4 Poly(pyrazolyl)borate Ligands 37

1.4.1 Background 37

1.4.2 Features 38

1.4.3 Naming of Scorpionates 39

1.4.4 Tris(pyrazolyl)borates 40

1.4.5 Tp-Supported Copper Carbonyls 41

1.4.6 Applications of Tp Ligands 43
1.5 Research Objectives 45
1.6 References 46

2. Synthesis and Copper Coordination Chemistry of Scorpionate Ligands 51
2.1 Synthesis of Known Scorpionates 53
2.1.1 Tris(pyrazolyl)borates 53
2.1.2 Bis(pyrazolyl)borates 55
2.2 Synthesis of Novel Tp Ligands 56
2.2.1 Background 56
2.2.2 Attempted Synthesis of Alkoxy-Substituted Tp 57
2.2.3 Synthesis of Methylthio-Substituted Tp 59
2.2.4 Summary 65
2.3 Synthesis of Copper Carbonyls 66
2.3.1 Synthesis of CuTpCO (**2.10**) 67
2.3.2 Synthesis of CuTp*CO (**2.11**) 68
2.3.3 Synthesis of Cu[$Tp^{Ph,SMe}$]CO (**2.12**) 69
2.3.4 Summary of Carbonyls 74
2.4 Rapid Carbonylation Reactions 75
2.4.1 Background 75
2.4.2 Rapid Carbonylation with Tp* 75
2.5 CO Displacement Reactions 77
2.5.1 Decarbonylation of CuTp*CO 78
2.5.2 Decarbonylation of Cu[$Tp^{Ph,SMe}$]CO 80
2.5.3 Summary 81
2.6 Future Work 81
2.6.1 Novel Electron-Rich Tps 81
2.6.2 Carbene Chemistry 83
2.6.3 UV-Triggered Decarbonylation 84
2.7 References 85

3. Palladium-Mediated Carbonylation Reactions 87
3.1 ^{11}CO Trapping Reactions 88
3.1.1 Background 88

3.1.2 Reaction Setup 90
3.1.3 Calculations 91
3.1.4 Results and Discussion 92
3.2 'Cold' Amide Syntheses 93
3.2.1 Background 93
3.2.2 Microfluidic Reactions 94
3.2.3 Schlenk Reactions 98
3.2.4 Carbonylation Summary 100
3.3 'Hot' Amide Syntheses 101
3.3.1 Reaction Setup 101
3.3.2 Results and Discussion 102
3.3.3 Summary 105
3.4 Future Work 107
3.4.1 [^{11}C]Carbonylations 107
3.5 References 108

4. Coordination Chemistry of Hemilabile Ligands 109
4.1 Introduction 110
4.1.1 Hemilability 110
4.1.2 Pyrazole-Donor Ligands 112
4.2 Novel Hybrid N,P Ligand 114
4.2.1 Proposed Ligand System 114
4.2.2 Proposed Synthetic Pathway 115
4.2.3 Synthesis of Enone (**4.1**) 115
4.2.4 Synthesis of Hpz^{phos} (**4.2**) 116
4.2.5 Synthesis of Hpz$^{phos(O)}$ (**4.3**) 117
4.2.6 Synthesis of Hpz$^{phos(S)}$ (**4.4**) 118
4.2.7 Summary 119
4.2.8 Coincidental Research 120
4.3 Palladium(II) Coordination Chemistry of Hpz^{phos} (**4.2**) 121
4.3.1 Synthesis of Mono-Chelate (**4.5**) 122
4.3.2 Synthesis of Bis-Chelate (**4.6**) 123
4.3.3 Synthesis of Perchlorate Bis-Chelate (**4.7**) 126
4.3.4 Summary 129

4.4 Palladium(II) Coordination Chemistry of $Hpz^{phos(O)}$ (**4.3**) 131
4.4.1 Attempted Synthesis of Mono-Chelate (**4.8**) 132
4.4.2 Synthesis of Bis-Adduct (**4.9**) 132
4.4.3 Synthesis of Perchlorate Bis-Chelate (**4.10**) 135
4.4.4 Synthesis of COD-Insertion Product (**4.11**) 136
4.4.5 Summary 140
4.5 Palladium(II) Coordination Chemistry of $Hpz^{phos(S)}$ (**4.4**) 141
4.5.1 Synthesis of Mono-Chelate (**4.12**) 142
4.5.2 Attempted Synthesis of Bis-Adduct (**4.13**) 143
4.5.3 Synthesis of Perchlorate Bis-Chelate (**4.14**) 143
4.5.4 Summary 144
4.6 Summary of Palladium Chemistry 145
4.7 Applications in Catalysis 146
4.7.1 Carbonylation Reactions 146
4.7.2 Heck Reaction 147
4.8 Future Work 148
4.8.1 Ligand Fine-Tuning 148
4.8.2 Supramolecular Chemistry 149
4.9 References 150

5. New Scorpionate Ligands Containing Appended Donor Groups 152
5.1 Introduction 153
5.1.1 Potentially Hemilabile Scorpionates 154
5.2 Nitrogen-Appended Scorpionates 155
5.2.1 Synthesis of $Cu_4[Tp^{py}]_4$ (**5.2**) 156
5.2.2 Synthesis of $Cu[Tp^{py}]CO$ (**5.3**) 159
5.2.3 Summary 162
5.3 Phosphine-Appended $T_k$ps 164
5.3.1 Background 164
5.3.2 Synthesis of $K[T_kp^{phos}]$ (**5.4**) 166
5.3.3 Synthesis of $Zn[T_kp^{phos}]OAc$ (**5.5**) 167
5.3.4 Summary 167
5.4 Phosphine Oxide-Appended $T_k$ps 169
5.4.1 Synthesis of $K[T_kp^{phos(O)}]$ (**5.6**) 169

5.4.2 Synthesis of Tl[$T_kp^{phos(O)}$] (**5.7**) 170
5.4.3 Synthesis of Cu[$T_kp^{phos(O)}$]CO (**5.8**) 173
5.4.4 Synthesis of [Eu($T_kp^{phos(O)}$)NO_3][NO_3] (**5.9**) 174
5.4.5 Summary 177
5.5 Phosphine Sulphide-Appended $T_k$ps 178
5.5.1 Synthesis of K[$T_kp^{phos(S)}$] (**5.10**) 178
5.5.2 Synthesis of Tl[$T_kp^{phos(S)}$] (**5.11**) 179
5.5.3 Summary 179
5.6 Phosphine-Appended Bulky Pyrazoles 180
5.6.1 Introduction 180
5.6.2 Synthesis of Enone (**5.12**) 181
5.6.3 Synthesis of $Hpz^{phos,Me}$ (**5.13**) 182
5.6.4 Synthesis of $Hpz^{phos(O),Me}$ (**5.14**) 183
5.6.5 Summary 183
5.7 Phosphine-Appended Tps 184
5.7.1 Synthesis of K[$Tp^{phos,Me}$] (**5.15**) 184
5.7.2 Synthesis of Tl[$Tp^{phos,Me}$] (**5.16**) 185
5.7.3 Synthesis of Cu[$Tp^{phos,Me}$] (**5.17**) 188
5.7.4 Synthesis of [Ru($Tp^{phos,Me}$)]Cl (**5.18**) 192
5.7.5 Synthesis of Zn[$Tp^{phos,Me}$]OAc (**5.19**) 194
5.7.6 Summary 195
5.8 Summary of Scorpionate Chemistry 197
5.9 Future Work 198
5.9.1 Donor Scorpionates in Catalysis 198
5.9.2 Coordination Chemistry of 'Crowned Scorpionates' 199
5.9.3 Supramolecular Chemistry of T_kp Ligands 202
5.9.4 Novel Nitrogen-Donor Scorpionates 203
5.10 References 203

6. Conclusion 206
6.1 References 210

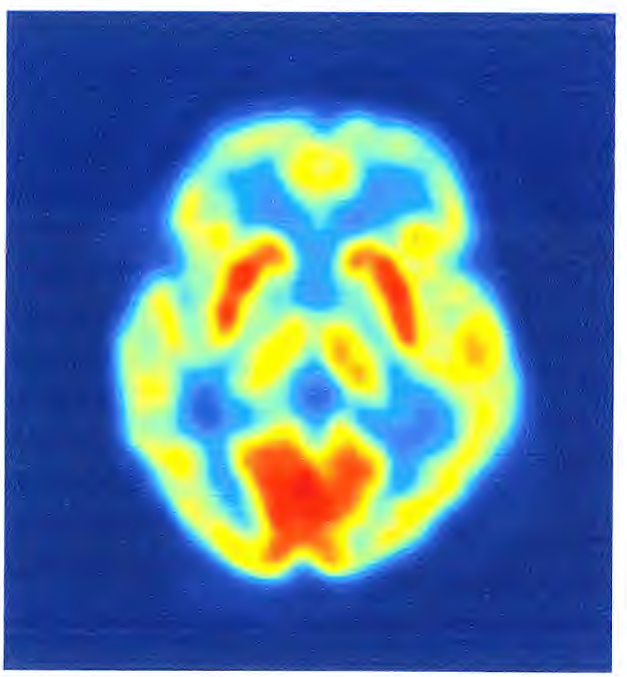
7. Experimental 211
7.1 Synthesis of Ligands and Complexes 212

7.1.1 Experimental Procedures for Chapter 2 212
7.1.2 Experimental Procedures for Chapter 3 219
7.1.3 Experimental Procedures for Chapter 4 220
7.1.4 Experimental Procedures for Chapter 5 228
7.2 References 238

8. Appendix 239
8.1 Crystal Structure Determinations 240
8.2 Crystal Data for Complex **5.16** 255
8.3 Publications 258

CHAPTER 1

INTRODUCTION



1. Introduction

1.1 Positron Emission Tomography

Positron Emission Tomography (PET) is a powerful technique in medical imaging, drug development and clinical research that is used to study biochemical and physiological processes in living organisms. PET experiments can provide information on the functioning of organs, tissues and enzymes/receptors as well as providing metabolic information. This is in contrast to other imaging techniques such as computed tomography (CT) and magnetic resonance imaging (MRI) which are generally used to provide detailed anatomical images.

PET works by detecting the emission of positrons from the body after a microgram quantity of a positron-emitting radiopharmaceutical (often called a tracer or a probe) has been administered to the subject, usually by injection. As the tracer molecule travels around the body, positrons will be emitted as the radioactive isotope decays (Figure 1.1).

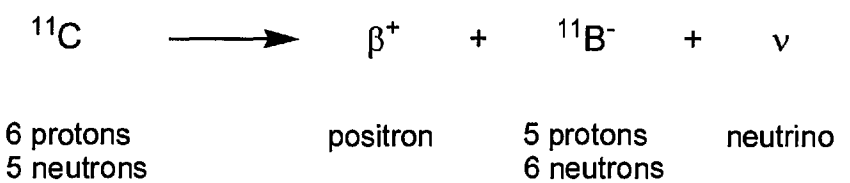


Figure 1.1. Decay of the ^{11}C isotope by positron emission.

The emitted positron itself is not detected as it quickly annihilates in collision with its anti-matter particle, the electron. This occurs in close proximity to the site of emission – typically 0.5 – 2.0 cm. This annihilation event produces a pair of gamma photons (γ) of a specific energy (511 keV) which travel away from the annihilation site in opposite directions (Figure 1.2).

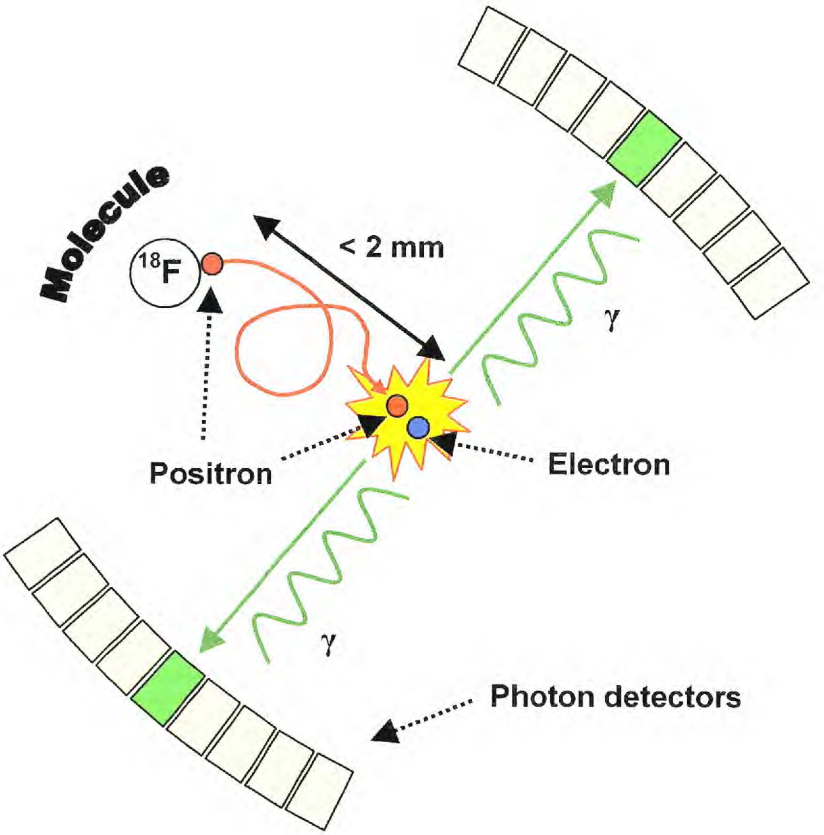


Figure 1.2. Annihilation event between a positron and an electron.

The PET technique depends on simultaneous detection of pairs of γ photons – those that do not coincide are not used for analysis. The PET scanner consists of a series of photon detectors around the body and uses the pair-detection events to map the location and density of the isotope in the body, in the form of sliced or 'tomographic' images (Figure 1.3). Many millions of individual annihilation events are required to provide enough data to provide such an image.

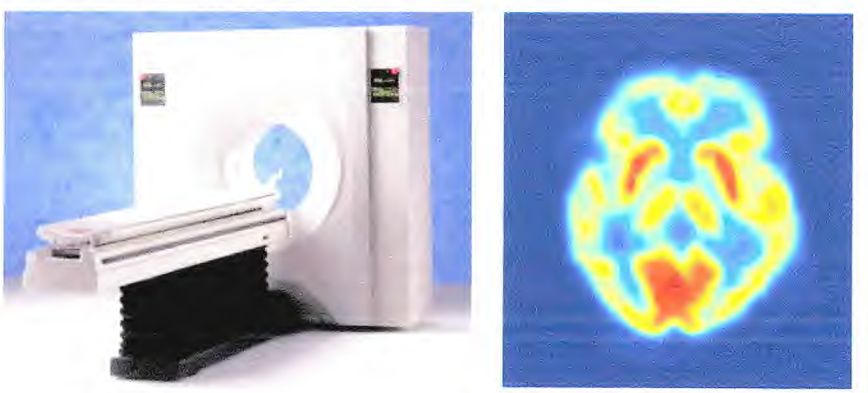


Figure 1.3. Left: A PET scanner (source: summitradiology.com); Right: ^{18}FDG PET scan of the human brain (source: en.wikipedia.org).

1.1.1 Positron Emitting Isotopes

Positron emitting isotopes are generally short-lived and those commonly used in PET are shown in Table 1.1 along with their corresponding half lives.

Table 1.1. PET radioisotopes and their corresponding half lives

Radioisotope	$t_{1/2}$ / min
^{18}F	110
^{11}C	20.4
^{13}N	10.0
^{15}O	2.0

One of the biggest challenges facing the PET chemist is the rapid incorporation of the radioisotope into the desired tracer molecule. The whole process of running a PET scan, from isotope production, synthesis of the radio-tracer, purification, quality control to administration into the patient, must be carried out within approximately three half-lives, in order for the radioactivity to be great enough. These constraints mean that PET facilities often have the cyclotron, radiochemical laboratories, quality control laboratory and PET scanner all under one roof so that the process, from start to finish, can be completed as rapidly as possible in order to maximise radiochemical yields.

When planning a radiolabelling experiment, the first decision that needs to be made is the choice of isotope to be used in the study. Too short a half-life and the majority of the radioactivity could be lost in the time it takes the radiotracer to reach its desired target. Conversely, one wants to avoid, where possible, the use a radioisotope with too long a half-life in order to minimise the potentially harmful effects of radiation on the body.

Once the isotope has been chosen, the PET chemist must then decide upon how to incorporate it into the desired tracer molecule through organic transformations. These are like any other chemical reactions but with two significant differences: (1) the quantity of the isotope produced (typically nanomoles) means that reactions are performed on a very small scale; (2) the radioactivity of these species means that the reactions must be performed in shielded fume hoods (hot-cells). The position of the

radiolabel within the tracer molecule is also significant. If the tracer molecule is metabolised in the body, metabolites will form and these may contain the positron-emitting isotope that is detected in the PET scan. Given that metabolites will have different properties to the parent molecule, it is possible for labelled metabolites to confuse the scan and increase the levels of noise.

In order to maximise the radioactivity of the radiotracer, it is common for the radioisotope to be incorporated during the last step of the synthesis. For example, it would be useless to incorporate ^{11}C into a molecule in the first step of a multi-step procedure as the short half-life would mean that most of the ^{11}C had decayed by the time the synthesis was complete. This constraint again adds to the challenge faced by the radiochemist in the successful synthesis of PET probes and as such some creative thinking is often required in order to circumvent these problems.

1.1.2 Applications of PET

The most commonly used PET tracer is the ^{18}F-labelled glucose derivative 2-[^{18}F]fluoro-2-deoxy-D-glucose, [^{18}F]FDG. The short but manageable half-life of ^{18}F (110 minutes) means that it has been possible to synthesise [^{18}F]FDG on a commercial level for distribution to PET centres on demand. This has fuelled the increase in use of PET throughout the world and is one of the reasons why PET is a rapidly growing field.

i. Oncology

PET is most commonly used for the detection of cancers and for early feedback into the effectiveness of cancer therapy. By far the most common radiotracer used for these studies is [^{18}F]FDG. Within the body, [^{18}F]FDG is transported in an analogous manner to glucose. It is carried around the bloodstream and taken up into tissues requiring high glucose usage. Inside the cell it is phosphorylated by the hexokinase enzyme to form [^{18}F]FDG-6-phosphate. Since a 2-oxy substituent (which has been replaced by ^{18}F) is required for glycolosis, further metabolism of [^{18}F]FDG-6-phosphate is inhibited. This causes [^{18}F]FDG-6-phosphate to accumulate in cells and

means that its distribution around the body, as detected by PET, reflects the glucose uptake and rate of phosphorylation by cells in the body.[1]

This process allows [^{18}F]FDG to highlight cancerous tissue whereby the high metabolic rate of cancer cells (as a result of elevated levels of hexokinase) mean that [^{18}F]FDG-6-phosphate rapidly accumulates due to the phosphorylation of [^{18}F]FDG. This build-up can be detected in the PET scan and therefore provides a means to differentiate between malignant and benign lesions. As such, a negative PET scan can avoid the need for surgical biopsy. Since a PET scan can be used for whole-body imaging, any non-local metastasis can be observed which can alter treatment plans in certain cases (for example from surgical intervention to a course of chemotherapy).

Through PET, it is also possible to determine therapeutic effectiveness. If a course of chemotherapy has been successful in killing the cancerous cells, they will no longer be visible on the PET scan. This technique can be advantageous over the anatomical images produced by MRI or CT which rely on observing tumour shrinkage which can occur slowly after the cancer cells have become inactive. The advent of new integrated PET/CT or PET/MRI scanners allows the overlap of functional images with detailed anatomical images to significantly aid disease treatment and detection.

ii. Neurology

The brain is highly dependent on glucose metabolism – about 95 % of ATP required for the brain to function properly is provided by glucose metabolism.[2] It is therefore possible to study the brain by monitoring the uptake and distribution of [^{18}F]FDG. This can be used to provide early diagnosis of Alzheimer's disease (AD), where brain functions in specific regions are decreased.[3, 4] These patterns can be spotted very early in the course of the disease, where other imaging techniques would show the brain to appear normal. Since medical treatments for AD are most effective when started early, a reliable early diagnosis can have significant ramifications for the patient. PET is also used for distinguishing AD from other types of dementia, such as Parkinson's disease and Huntington's disease or the benign effects of aging.[5, 6] [^{18}F]FDG can also be applied to the detection of brain tumours. It is possible to study specific

neuroreceptors by the use of specific radioligands. For example, [^{11}C]raclopride has been used to study the dopamine D2 receptors in the human brain.[7]

PET neuroimaging works on the assumption that areas of high radioactivity are associated with increased brain activity. By following the [^{18}F]FDG uptake in the brain one can visualise the specific regions of the brain that are being used to perform specific different tasks.[1, 8, 9] For example, Figure 1.4 shows the corresponding areas of increased brain activity from a study where subjects look at a visual scene (visual cortex), listen to a mystery story (left and right auditory cortices), count backwards from 100 by sevens (frontal cortex), recollect learned objects (hippocampus bilaterally) and touch thumb to fingers of right hand (left motor cortex and supplementary motor systems).[1]

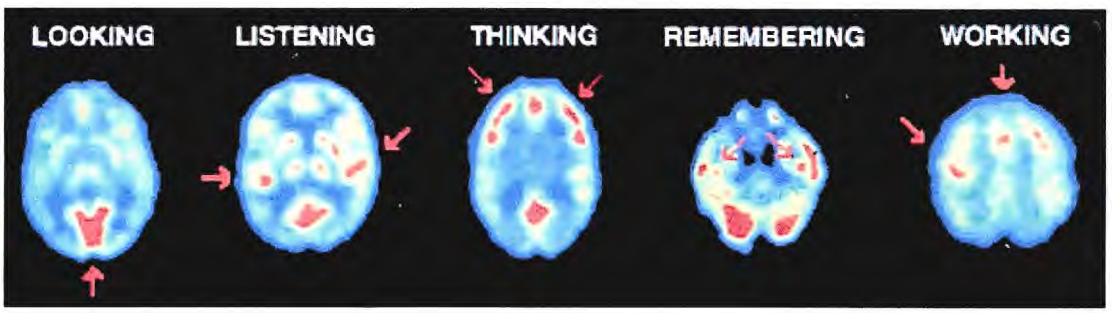


Figure 1.4. Areas of increased [^{18}F]FDG uptake corresponding to increased brain activity during specific tasks (source: reference [1]).

iii. Drug Discovery

PET has the potential to improve the lengthy and costly process of drug development. In 2003, the cost associated with the development of a new drug was estimated to be around US $800 million.[10] Much of this cost is associated with those drugs that do not make it onto the market – approximately three out of four new chemical entities under development as drug candidates fail in clinical trials. Of particular importance to the success of a drug is the way in which it is absorbed and metabolized by the human body. These 'pharmacokinetic' and 'pharmacodynamic' properties define the drug's absorption, distribution, metabolism and excretion (ADME) characteristics. It is estimated that around 40 % of all drug candidates that fail in the first stage of human

trials (Phase I) do so because of poor ADME properties.[11, 12] This huge cost and the increased demand to minimise preclinical animal experiments provide a strong incentive for improvements in the early screening process of new drugs in humans.

The incorporation of positron-emitting isotopes into drug molecules, has made it possible to study *in vivo* the biodistribution of drug molecules and the level of receptor occupancy.[13] This is particularly important as the drug's binding ability at the active site is a crucial factor that governs its efficacy. Moreover, to perform a PET scan, non-pharmacological doses (approximately 1 to 10 nanomoles) of the radiolabelled drug are administered to the patient. This is known as 'microdosing' and means that no physiological response to the drug will occur during these studies. With this technique, potential drug candidates can be studied *in vivo* much earlier in the clinical trials, thus facilitating smarter drug development through early identification of the molecule with the optimum metabolism characteristics.[10] Similarly, drugs that display low occupancy or poor pharmacokinetic properties can be identified early in the drug development process thus eliminating them from further costly clinical trials.

At present, the use of PET for drug discovery is not widespread, and restrictions to its extensive use are not only based on access to PET facilities, but also to the challenges faced by the radiochemist to successfully label the desired molecule. As more advances are made within this field, new synthetic procedures and chemical pathways should facilitate the synthesis of target molecules. If PET microdosing were to be successfully applied to drug development, the tremendous cost of this process could be greatly reduced, which in turn, could fund research into new drugs and treatments which otherwise might have never progressed.

iv. Cardiology

PET can be used to detect Coronary Artery Disease by measuring myocardial blood flow and perfusion. Typcially [^{13}N]ammonia is used for perfusion studies[14] while [^{18}F]FDG studies can be performed in conjunction for imaging of the metabolism.[15]

1.1.3 ^{11}C-Radiolabelling

The ubiquitous nature of carbon within drug molecules and natural products makes ^{11}C a particularly attractive isotope for PET. Upon substituting a stable carbon isotope for the positron-emitting ^{11}C there will be zero substance alteration, *i.e* the molecule will behave identically to its unlabelled parent molecule. These advantageous features have led to the development of a wide array of ^{11}C-labelled molecules which have been extensively studied by PET. However, the synthesis of these molecules is not trivial as it is not possible to simply pluck out the ^{12}C isotopes and replace them with ^{11}C! In reality, the synthesis of ^{11}C-labelled tracers relies on the use of a handful of ^{11}C-containing reagents. Furthermore, the short half-life of ^{11}C (20 mins) provides a time constraint which essentially factors out any lengthy multi-step syntheses.

^{11}C is produced in the cyclotron by proton bombardment of ^{14}N (^{14}N (p,α)^{11}C).[16] Once formed in the target, the ^{11}C is then immediately converted to $^{11}CO_2$ or $^{11}CH_4$ by reaction with oxygen or hydrogen, respectively. All the commonly used ^{11}C synthons are derived from these two parent molecules (Figure 1.5).

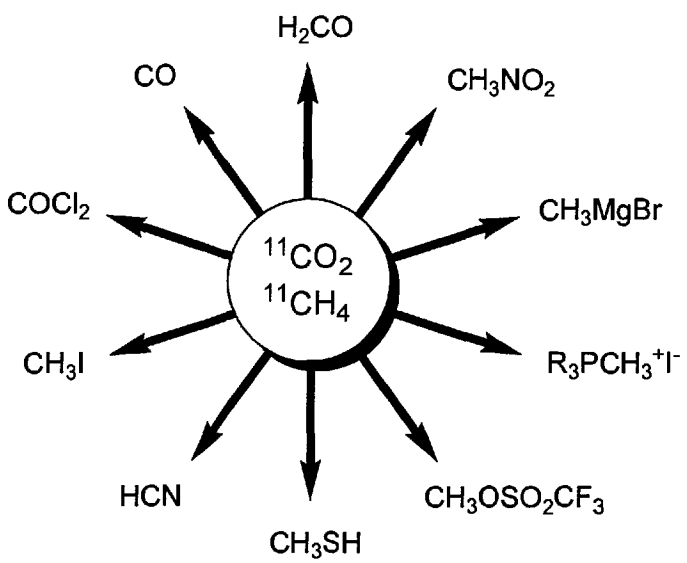


Figure 1.5. Common ^{11}C-containing synthons derived from $^{11}CO_2$ and $^{11}CH_4$.

[^{11}C]Methylation using [^{11}C]methyl iodide is the most frequently used reagent to incorporate ^{11}C into a radiotracer. Its widespread use is based on the relative simplicity and speed of its reactions as well as the commercial availability of the

apparatus needed to produce the [^{11}C]methyl iodide. Incorporation of the $^{11}CH_3$ group into the radiotracer is usually performed by N-, O- or S- methylation reactions. These feature nucleophilic substitution via attack of an amine (primary, secondary or tertiary), an alcohol or a thiol upon $^{11}CH_3I$ to produce a ^{11}C-labelled amine (secondary, tertiary or quaternary), ether or thioether, as shown in Figure 1.6.

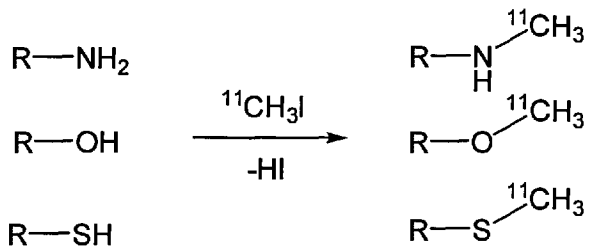


Figure 1.6. Methylation of common substrates with $^{11}CH_3I$.

1.2 Carbon Monoxide

1.2.1 [^{11}C]Carbon Monoxide as a Reagent

[^{11}C]Carbon monoxide is a particularly desirable and versatile labelling reagent due to the sheer number of biologically active functional groups that the CO unit is incorporated within. Furthermore, the ^{11}CO synthon can be produced in one step by the reduction of $^{11}CO_2$ at elevated temperatures using zinc or molybdenum. The widespread use of this reagent, however, has been hindered by two significant factors: (i) the poor solubility of CO in organic solvents at low pressure,[17] and (ii) high dilution of the ^{11}CO within the carrier gas stream which results in a very low partial pressure. The combination of these two factors lowers the reactivity of ^{11}CO to such an extent that it cannot be used under mild conditions that are generally suitable for [^{11}C]methylation reactions, for example.

Until recently, the use of ^{11}CO had been inhibited due to these problems of low solubility and high dilution. Over the last 10 years, however, there have been major advancements in the handling of this reagent, thus making it a viable synthon for PET labelling experiments. Carbonylation reactions are rapidly becoming a highly versatile ^{11}C-labelling strategy and have been used to produce a range of biologically active molecules including amides, ketones, imides, acrylamides, ureas and esters.

1.2.2 Palladium–Mediated [^{11}C]Carbonylations

To date, the most frequently encountered method of [^{11}C]carbonylation has been through palladium(0)-mediated reactions. This process was first reported by Heck in 1974,[18] to couple an amine nucleophile and an aryl-halide with carbon monoxide (Figure 1.7).

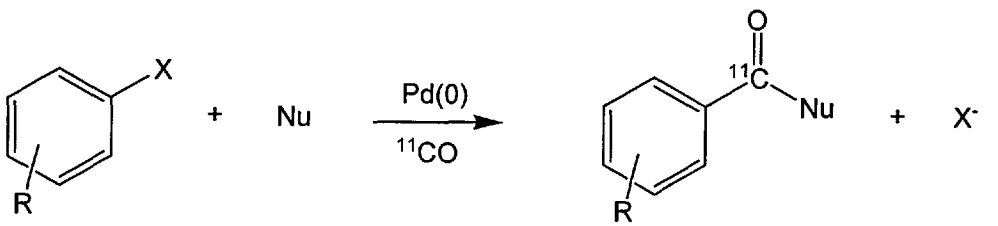


Figure 1.7. Carbonylative cross-coupling reaction between an aryl-halide and a nucleophile.

When these reactions are performed on the nanomolar scale necessary to produce radiotracers for PET, the palladium 'catalyst' is typically present in a vast excess when compared to the coupling reactants. As such, when describing this process within PET experiments, they are more accurately to referred to as palladium-'mediated' reactions.

Palladium-mediated carbonylations proceed via a four-step cycle as shown in Figure 1.8: (i) oxidative addition of the aryl halide to form the Pd–aryl complex; (ii) migratory insertion of the CO into the Pd–C bond to form the Pd–acyl species; (iii) nucleophilic attack at the palladium(II) centre, displacing the halide; (iv) reductive elimination to yield the carbonylated product and the regenerated palladium(0) species.

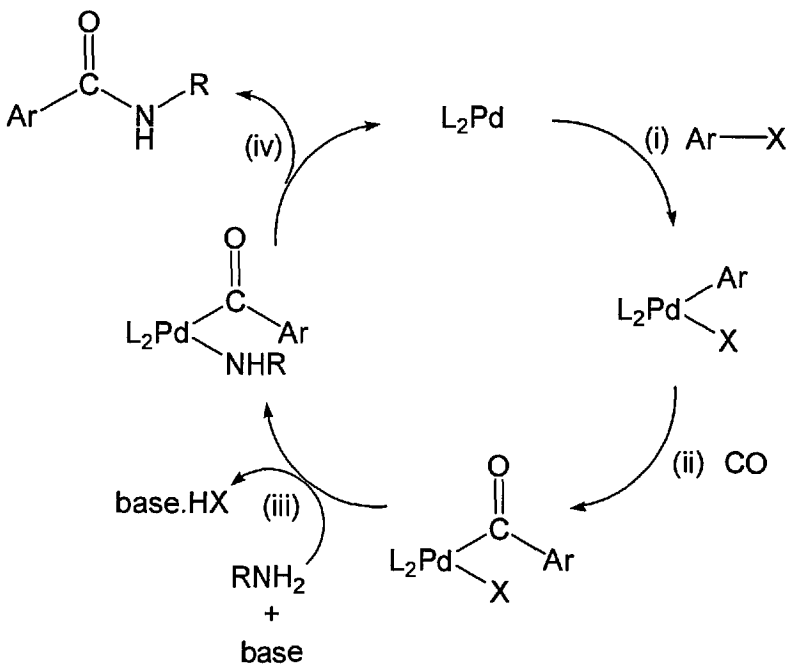


Figure 1.8. Catalytic cycle for Pd-catalysed carbonylative cross-coupling reaction.

The following section describes literature examples that have successfully overcome the problems associated with low CO reactivity for the synthesis of ^{11}C-labelled molecules via palladium-mediated [^{11}C]carbonylation reactions.

i. Recirculation

In 1997 Langstrom *et al.*[19] reported a new gas handling technique which enabled [^{11}C]carbonylation reactions to be performed successfully via a Stille coupling reaction. In this system, the radioactive carbon monoxide was allowed to recirculate through the reaction media thus overcoming the problems of poor solubility. These reactions produced [*carbonyl*-^{11}C]ketones by coupling arylhalides and an organotin nucleophile (Figure 1.11).

ii. Borane System

Audrain *et al.*[20] have performed [^{11}C]carbonylation reactions at low pressures using a BH_3.THF solution to sequester ^{11}CO in the form of BH_3.^{11}CO. This trapping reaction was performed at -78°C and once the borane-carbonyl complex had formed, the ^{11}CO could then be released from the complex by heating the reaction vessel at 70°C. The

released ^{11}CO was used for palladium-mediated cross-couplings between aryl-halides and an amine or alcohol nucleophile to form the coupled [*carbonyl*-^{11}C]-amides or esters, respectively (Figure 1.11). Using this technique, [*carbonyl*-^{11}C]*N*-benzylbenzamide could be synthesised in 47 % radiochemical yield by carbonylative cross-coupling of benzylamine and iodobenzene.

iii. Microfluidics and Microtube Reactors

The recent appearance of microfluidic systems for performing chemical and biochemical reactions on the microscale[21] has created much interest due to their many favourable properties over conventional techniques. Microfluidic reactions offer enticing advantages such as low sample and reagent consumption, acceleration of reactions through improved mass and heat transfer, faster analysis, high reproducibility and automation.[22] These features are well suited to the challenges associated with the synthesis of radiotracers for PET studies, where shorter reaction times are essential due to the short half-lifes of the isotopes involved. Furthermore, the scale of the microchip reactions is well suited to PET reactions, where microgram quantities of radiolabelled material are required. Microfluidic reactions have been used for the synthesis of [^{18}F]FDG,[23-25] and have the potential to be used for [^{11}C]carbonylation reactions with ^{11}CO.

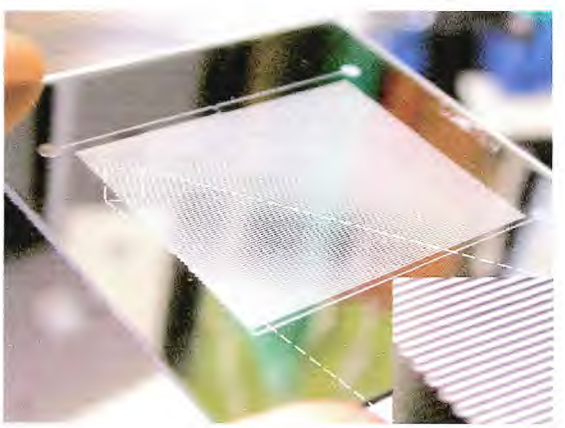


Figure 1.9. A microfluidic chip. (Inset: Close-up view of the microchannels).

In 2006, Miller *et al.*[26] successfully used a microreactor (Figure 1.9) for gas-liquid phase carbonylation reactions using non-^{11}C-labelled carbon monoxide. In this

system, the increased interfacial gas-liquid contact area and the increased pressure of carbon monoxide enhanced the reactivity. Reactions performed between arylhalide and benzylamine in the presence of *in situ*-generated palladium(0) produced amides in 46-58 % yield in just two minutes. Similar micro-reactions have also been reported using ionic liquids as solvents[27] and elevated pressures[28] to enhance yields.

Miller *et al.*[29] recently extended these carbonylations into the radiochemical laboratory but rather than performing the reactions in a microfluidic device, the reagents were instead passed through a 'micro-tube' reactor containing a silica-supported palladium catalyst (Figure 1.10). This reactor was used to synthesise [*carbonyl*-^{11}C]amides via the coupling of substituted aryl-halides and benzylamine with ^{11}CO (Figure 1.11). Radiochemical yields ranging from 33-79 % were obtained depending on the substitutent on the aryl ring. The microtube reactor was found to provide a cost-effective, reusable labelling route which, through the use of a solid-supported catalyst, provided an improvement to the purification process.



Figure 1.10. A microtube reactor.

iv. Iodonium Salts as Electrophiles

Al-Qahtani *et al.* have performed [^{11}C]carbonylative coupling of diaryliodonium salts with aryltributylstannanes to form aryl [^{11}C]ketones (Figure 1.11). These reactions were performed using a DME/water solvent system at room temperature and atmospheric pressure.[30, 31] The reaction between diphenyliodonium bromide and aryltributylstannanes produced [^{11}C]benzophenones in >98 % yield based on the amount of radioactivity initially trapped in the solvent. Unsymmetrical iodonium salts resulted in a mixture of labelled products. The main drawback to this approach was

the low trapping efficiency of the solvent (6 %) meaning that the majority of the ^{11}CO delivered to the system escaped unreacted.

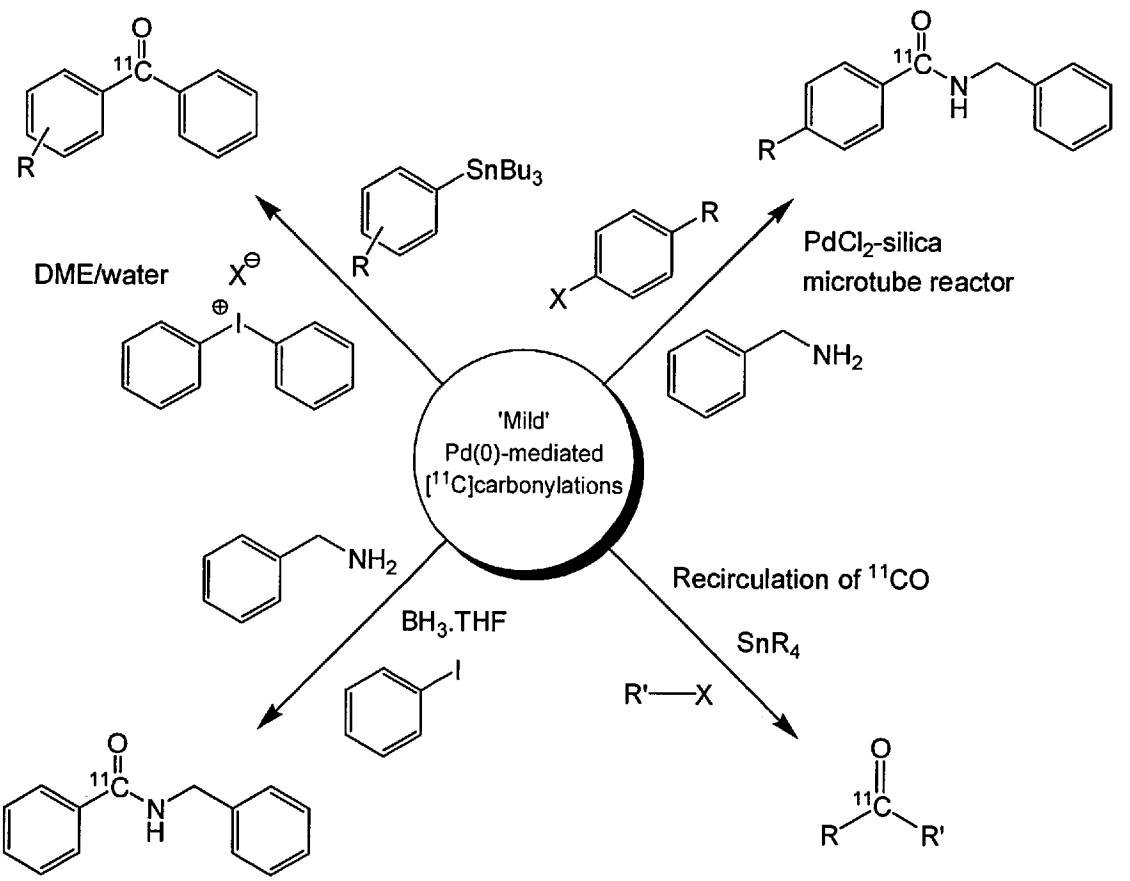


Figure 1.11. Palladium-mediated carbonylation reactions employing mild conditions.

iv. Micro-Autoclave

Langstrom *et al.* have performed a range of [^{11}C]carbonylation reactions using a stainless steel micro-autoclave reactor.[32] Inside the micro-autoclave, forcing reaction conditions (temperatures up to 150°C and pressures exceeding 35 MPa) can be employed to increase the reactivity of CO. This has led to the synthesis of [*carbonyl*-^{11}C]-amides,[33-36] hydrazides,[37] ketones[38-40] and acrylamides[41] (Figure 1.12).

This technique was first reported in 1999 for the synthesis of [*carbonyl*-^{11}C]amides through the carbonylative cross-coupling of aryl halides and primary or secondary amines in good to excellent radiochemical yields.[33] [*Carbonyl*-^{11}C]hydrazides were synthesised in the same manner when using hydrazine as the nucelophile.[37] This work

has since been extended to cover less basic amines such as aniline and indole derivatives, via *in situ* activation using lithium bis(trimethylsilyl)amide[34] and 1,2,2,6,6-pentamethylpiperidine.[35] This work was extended into the synthesis of acrylamides.[41] Two routes were chosen to synthesise *N*-benzyl[*carbonyl*-^{11}C]acrylamide. Firstly [1-^{11}C]acrylic acid was synthesised from ^{11}CO by palladium-mediated hydroxycarbonylation of acetylene. The labelled carboxylic acid was then converted into the acyl chloride and subsequently treated with amine to yield *N*-benzyl[*carbonyl*-^{11}C]acrylamide. The second method used ^{11}CO in a palladium-mediated carbonylative cross-coupling of the vinyl halide and amine. A higher radiochemical yield was achieved with the latter method (up to 81 %, decay corrected).

In 2004, the micro-autoclave was applied to the Suzuki coupling of aryl triflates, alkyl- or aryl-boronic acids, and ^{11}CO to form [*carbonyl*-^{11}C]ketones.[38, 39] Labelled products were obtained with radiochemical yields in the range of 10-70 % when LiBr was used as an additive with no extra base.[39] Improvements in the radiochemical yield were achieved by use of tetrabutylammonium fluoride in the synthesis of [*carbonyl*-^{11}C]ketones incorporating alkyl groups, while potassium *tert*-butoxide was the best base among those tested for improving the radiochemical yields in the syntheses of biaryl ketones.[38]

Stille coupling reactions were later performed between ^{11}CO, alkyl/aryl iodides and organostannanes, to produce [*carbonyl*-^{11}C]ketones.[40] These micro-autoclave reactions utilised the activated palladium(0) species Pd{P(*o*-Tol)$_3$}$_2$, generated in situ from $Pd_2(dba)_3$ and P(*o*-Tol)$_3$. Radiochemical yields of [*carbonyl*-^{11}C]-alkyl/aryl ketones were in the range of 37-98 % for these reactions.

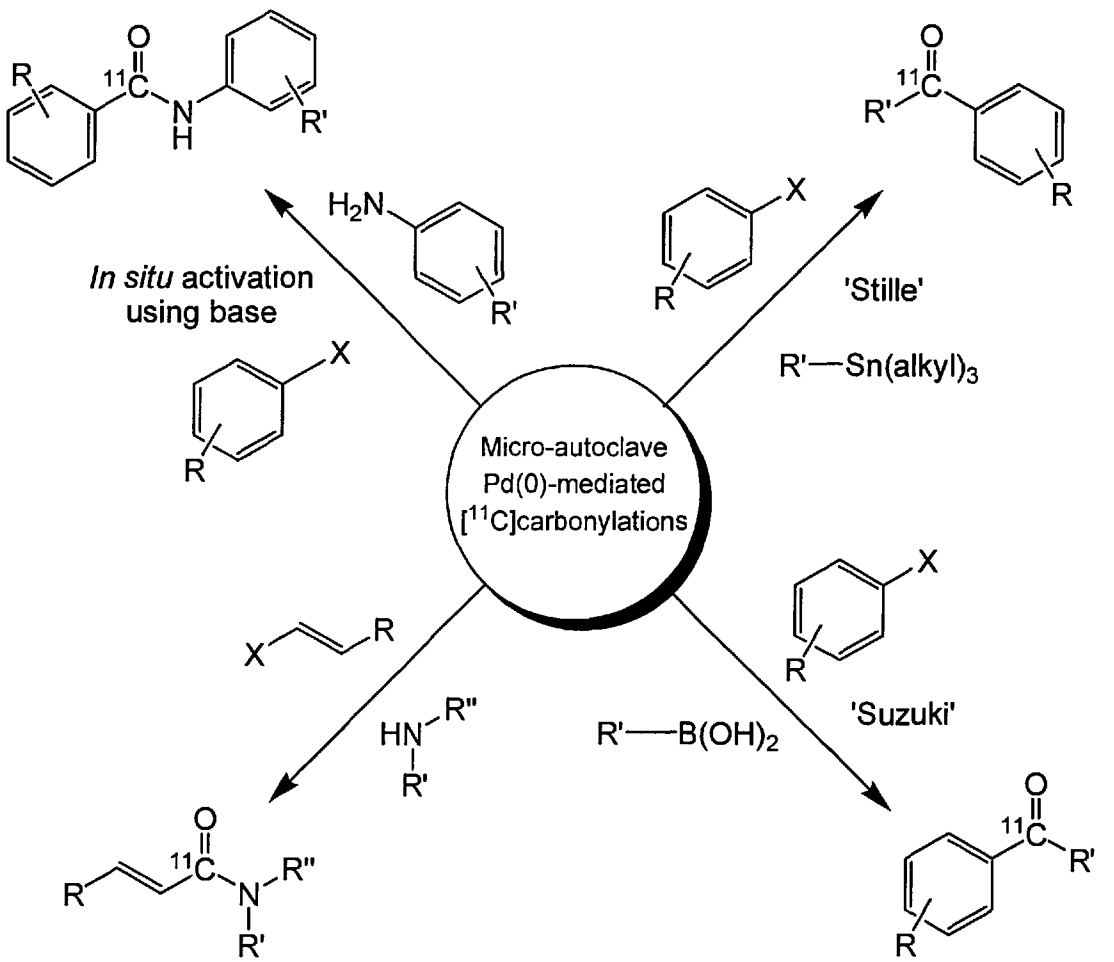


Figure 1.12. Palladium-mediated carbonylation reactions using micro-autoclave.

1.2.3 Alternative [^{11}C]Carbonylation Methods

Rhodium–mediated [^{11}C]carbonylations provide a viable route to a range of carbonyl-containing molecules that cannot be synthesised with palladium-mediated reactions. Molecules that have been synthesised in this way include ureas,[42, 43] carbamates,[43] and malonates.[44] Langstrom *et al.* have recently employed free radical photo-initiated [^{11}C]carbonylation reactions to synthesise labelled long and short chain aliphatic carboxylic acids,[45, 46] esters[46-48] and amides.[48, 49] These reactions were carried out in a modified micro-autoclave containing a sapphire window to allow irradiation with UV light. High pressure selenium-mediated [^{11}C]carbonylations have also been used by Langstom *et al.* for the synthesis of ureas, carbamates and carbonates.[50]

1.2.4 Coordination Chemistry of Carbon Monoxide

Given the greater electronegativity of oxygen compared to carbon, one might presume that the CO ligand would bind to a metal centre via the oxygen atom. In fact this coordination mode is very rarely observed and bonding usually occurs through the carbon atom. The experimental value of the electric dipole is small (0.1 D), with the negative end of the dipole residing on the *carbon* atom despite it being the less electronegative atom. This slightly odd situation can be explained when considering the molecular orbitals (Figure 1.13).

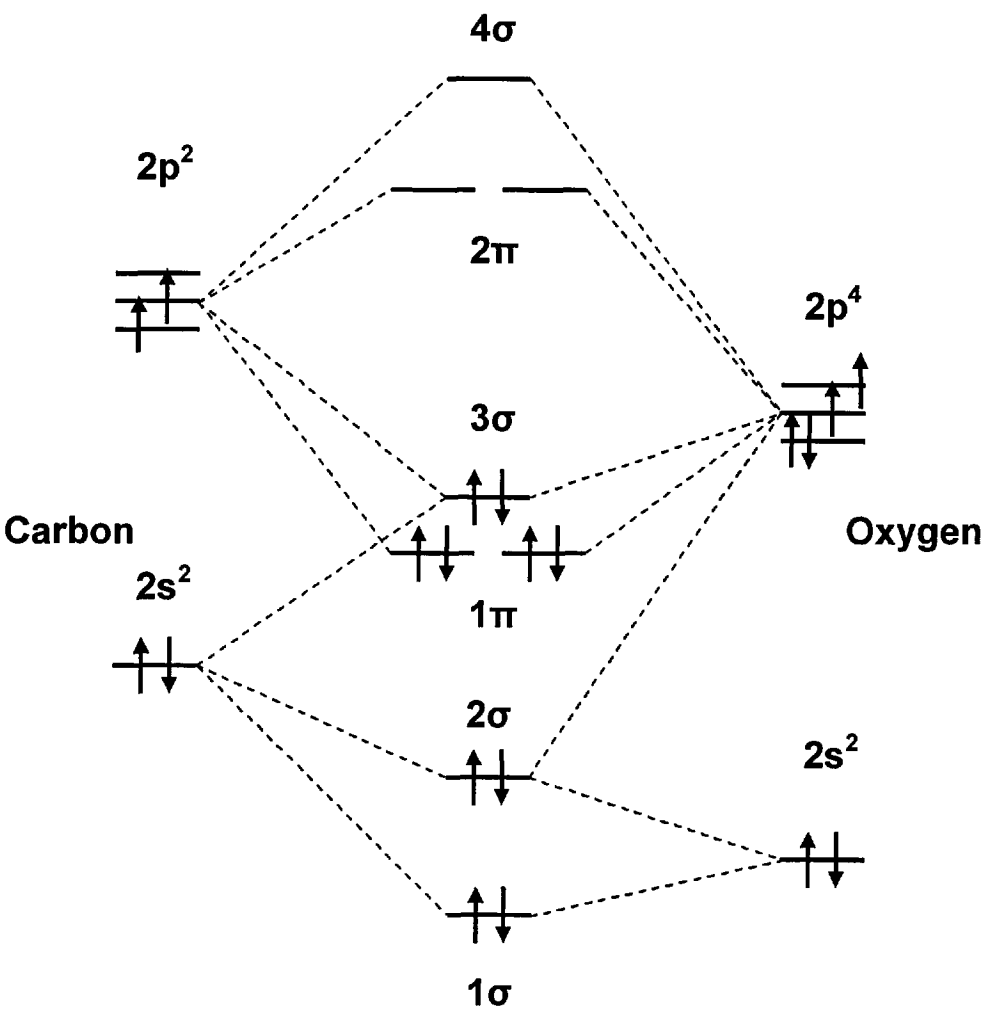


Figure 1.13. Molecular orbital diagram of carbon monoxide.

Examination of the molecular orbitals of CO finds that the HOMO is largely non-bonding and is essentially a lone pair that points away from the carbon atom. When CO coordinates, this σ-orbital acts as a weak donor thus forming a metal-carbon σ-

bond. The LUMO is a doubly degenerate pair of antibonding π-orbitals which allows for metal to ligand backbonding to occur, thus strengthening the metal-carbon bond (Figure 1.14). So even though the bonding electrons reside mainly on the oxygen atom, they are more than balanced by the non-bonding and anti-bonding electrons that reside towards carbon atom.

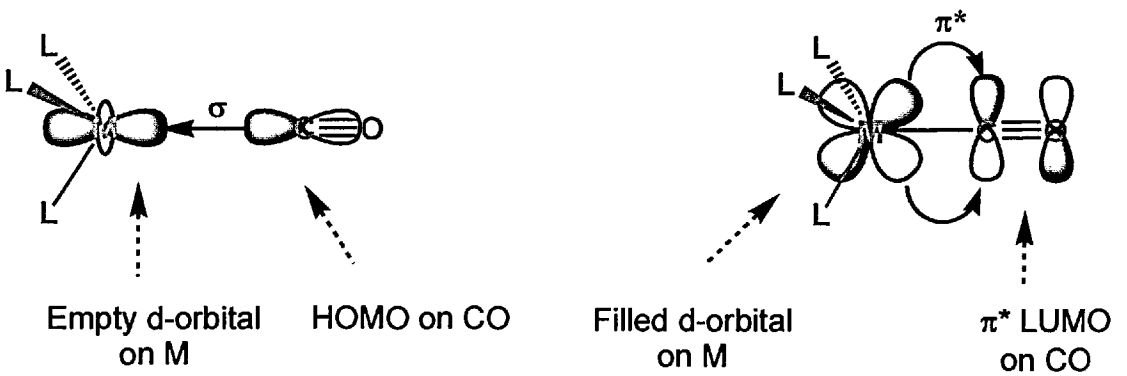


Figure 1.14. Bonding of the HOMO and LUMO of the carbonyl ligand within a M-CO complex.

1.2.5 Metal Carbonyl Complexes in Nature

The reversible binding of carbon monoxide at metal centres has the potential to lessen the problems of low ^{11}CO concentration and solubility which hinder its widespread use in PET. Before doing so it is useful to examine the chemistry of carbon monoxide within Nature.

i. Natural Oxygen Carriers: Hemoglobin and Myoglobin

It is well known that inhalation of carbon monoxide is toxic to mammals. This is a result of the interaction of carbon monoxide with the oxygen carrying metalloproteins found in red blood cells. In the oxygen-carrying hemoproteins (myoglobin and hemoglobin), the active site consists of an iron(II) protoporphyrin IX (heme) encapsulated in a water resistant pocket and bound through a single coordination bond between the imidazole group of the proximal histidine residue and the iron atom (Figure 1.15).[51]

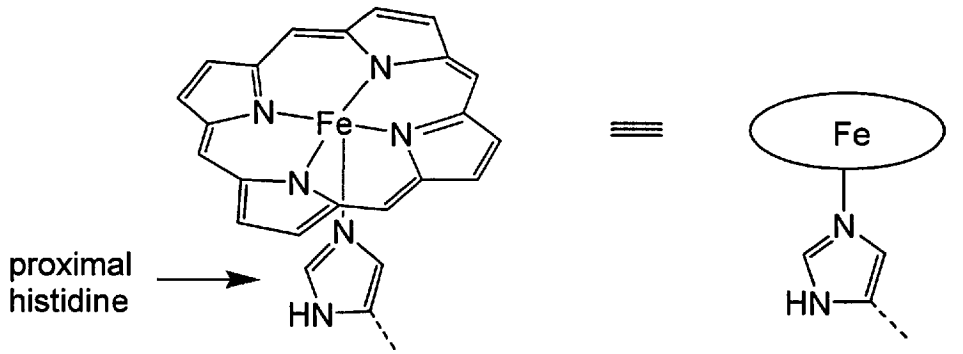


Figure 1.15. The heme unit in myoglobin/hemoglobin.

The protein environment surrounding the heme moiety plays a key role in dioxygen and carbon monoxide binding. Carbon monoxide has a significant affinity to the iron sites in unhindered iron-porphyrins. Hemoglobin, however, has a lower affinity for carbon monoxide relative to dioxygen when compared to simple iron-porphyrin systems. This is due to steric hindrance on the distal side of the heme, porphyrin skeletal deformations and polar factors associated with the distal pocket that destabilise the Fe-CO bond. Most significantly, a histidine residue (His E7)[52] located on the distal side blocks the otherwise unhindered access to the sixth 'free' coordination site at the iron centre (Figure 1.16 and Figure 1.17).[53] This can exploit the different coordination modes of oxygen and carbon monoxide to lower the affinity of the metal towards the latter: The carbonyl ligand, which prefers to bond linearly to the heme unit, is forced to bend as a result of steric hindrance from the distal histidine residue. Dioxygen, which bonds to the heme unit in a bent mode, is stabilised by favourable hydrogen bonding to the imidazolyl proton of same histidine residue.

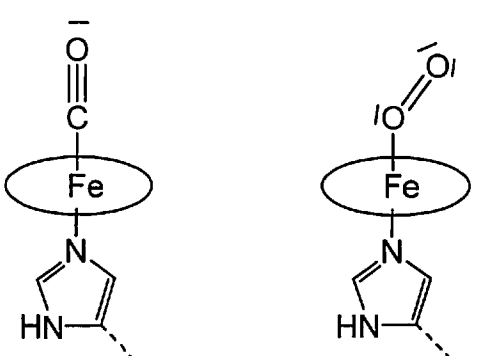


Figure 1.16. Free heme complexes bonded to CO (left) and O_2 (right).

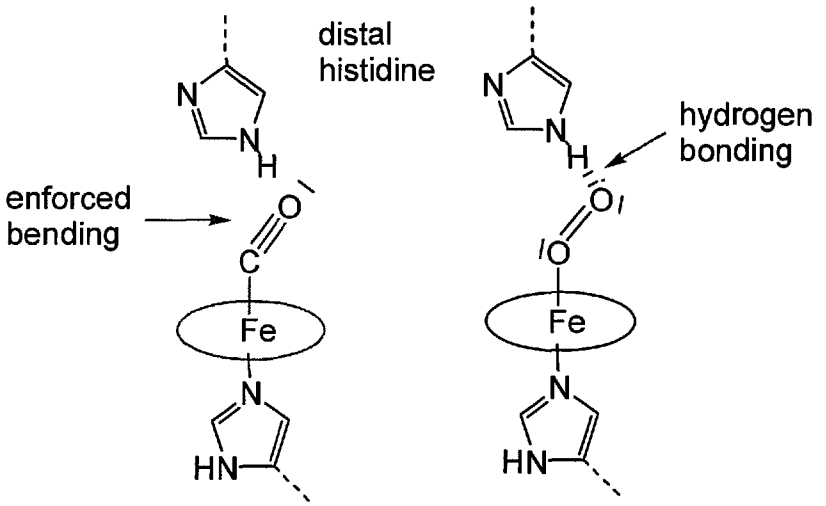


Figure 1.17. Hemoglobin bonded to CO (left) and O_2 (right).

Despite these obstacles to CO binding, its high reactivity is such that the affinity between carbon monoxide and hemoglobin is 240 times stronger than the affinity between hemoglobin and dioxygen. As a result, the gas is highly toxic upon prolonged exposure to low doses or short exposure to high doses. This is believed to be due to the formation of carboxyhemoglobin, which decreases the oxygen-carrying capacity of the blood.

ii. CO Binding to Synthetic Iron(II) Porphyrins

The formation of synthetic analogues of heme compounds is of interest as chemists endeavour to fully understand the nature of the heme binding site. This understanding should allow chemists to synthesise analogues that can reversibly bind to small molecules such as O_2 and CO.

In the laboratory, unhindered iron(II) hemes are oxidised rapidly and irreversibly in the presence of dioxygen, even in aprotic solvents. The mechanism of oxidation at low base concentration is summarised by the following equations (P = porphyrin, B = base):[51]

$$(B)PFe^{II} + O_2 \longrightarrow (B)PFe(O_2)$$

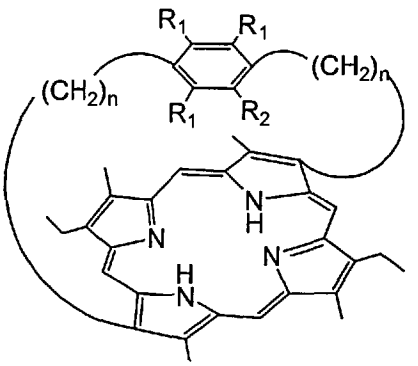
$$(B)PFe(O_2) + (B)PFe^{II} \longrightarrow PFe^{III}-O_2-Fe^{III}P + 2B$$

$$PFe^{III}-O_2-Fe^{III}P + 2B \longrightarrow 2\,(B)PFe^{IV}=O$$

$$2\,(B)PFe^{IV}=O + (B)PFe^{II} \longrightarrow PFe^{III}-O-Fe^{III}P + 2B$$

This irreversible oxidation upon exposure to dioxygen considerably limits the use of simple ferrous porphyrins, especially as models for the active site of hemoproteins. For the early models of the heme unit, ruthenium was often used rather than iron because the resultant complexes are more robust towards oxidation. Indeed, the first metalloporphyrin-carbonyl complex to be characterised by X-ray crystallography was the ruthenium-containing complex, Ru(TPP)$(CO)_2$ (TPP = tetraphenylporphyrin) by Cullen *et al.* in 1972.[54] Since this discovery, many iron(II) porphyrins have been synthesised which are stable to oxidation. This has been achieved by steric encumbrance of one or both porphyrin faces to inhibit the formation of the μ-peroxo dimer as well as creating a hydrophobic environment around the iron centre.

Among the many factors that affect dioxygen and carbon monoxide binding to synthetic heme models are the identity and oxidation state of the metal ion, distal steric hindrance, proximal ligand basicity, proximal base strain, ligand electronic effects and solvent polarity.[55] A series of porphyrins capped by benzene and amidobenzene rings was prepared by Dolphin *et al.*[52] In this report, the O_2 and CO binding to iron(II) porphyrin complexes were examined to see the effects of H-bonding on the stability of the dioxygen complexes relative to the carbon monoxide complexes. Figure 1.18 shows the amide-substituted benzene-capped porphyrin models (containing possible H-bonding sites) and the unsubstituted-benzene-capped porphyrin models (containing no possible H-bonding sites) that were synthesised.



1a: n = 4; $R_1 = R_2 = H$
1b: n = 5; $R_1 = R_2 = H$
1c: n = 4: $R_1 = H$, $R_2 = NHCOCH_3$
1d: n = 5: $R_1 = H$, $R_2 = NHCOCH$

Figure 1.18. Unsubstituted-benzene-capped porphyrin models (**1a-b**) and amide-substituted-benzene-capped porphyrin models (**1c-d**).

The sterically hindered base 1,5-dicyclohexylimidazole (DcIm) was chosen for the CO- and O_2-binding studies and K_b^{CO} values were obtained via addition of CO/N_2 mixtures to the 5-coordinate hemes, according to Figure 1.19. The results showed that there has been a remarkable reduction in CO affinities with these systems (**1a-d**) compared with the 'open' chelated hemes: Complex **1b** exhibited a 10^2-fold reduction in CO affinity and complex **1a** a 10^4-fold reduction compared to those of the 'open' chelated hemes. These complexes discriminated against CO binding so strongly that the 5-coordinate species can be readily regenerated by pumping. This is an important feature because normally, pumping CO complexes such as chelated protoheme would not remove the bound CO.[56] Using dioxygen as a ligand, the binding studies showed that the amide functionality present on hemes **1c** and **1d** increases their O_2 affinity due to the interaction between the polar amide function and the bound dioxygen. This supports the hypothesis that hydrogen bonding plays an important role in the differential binding of CO and O_2 by hemoglobin and myoglobin.

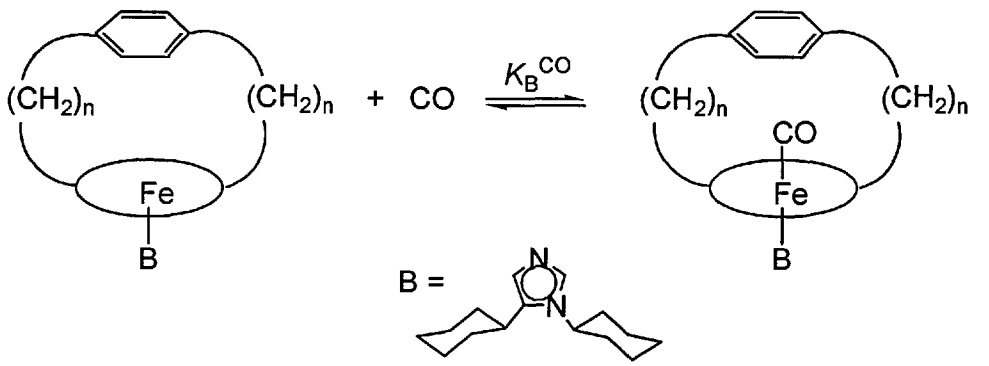


Figure 1.19. Reversible CO binding to capped iron porphyrins.

iii. CO Releasing Molecules (CORMs)

Although CO has traditionally been viewed as a toxic gas, over the last 10 years increasing evidence in the medical literature shows it to play a major role as a signalling molecule in mammals.[57] CO is generated in living organisms during the degradation of heme by the enzyme heme oxygenase. In humans, it is naturally produced at a rate of 3-6 cm^3 per day. This gas is particularly active within the cardiovascular system,[58] and is known to dilate blood vessels in a manner similar to nitric oxide. There are now a wide range of documented physiological effects of CO including reducing allergic inflammation, suppressing organ graft rejection and protecting tissues from ischemic injury (insufficient supply of blood to an organ) and apoptosis (programmed cell death).

Its therapeutic use, however, has been limited by the side-effects associated with CO inhalation. As such, alternative methods of artificially introducing small quantities of CO into the body are of interest. Recently, transition metal carbonyls have been researched as a safe and effective means of transporting and releasing CO *in vivo*. In one study,[58] $[Fe(CO)_5]$, $[Mn_2(CO)_{10}]$ and $[RuCl_2(CO)_3]_2$ were examined for their potential to act as CO Releasing Molecules (CORMs) *in vivo* for CO-based therapy of vascular- and immuno-related dysfunctions. With the iron and manganese carbonyl complexes, it was found that photolysis was necessary to release CO, hence these compounds were unsuitable for *in vivo* applications. The ruthenium species, $[RuCl_2(CO)_3]_2$, however, was soluble in DMSO, and was found to release CO without

stimulation. This compound was shown to cause sustained vasodilation in rat aortic rings and significantly reduced acute hypertension *in vivo*.

Further studies were carried out into water-soluble CORMs that could liberate CO under physiological conditions.[59, 60] In this work, the water-soluble ruthenium(II) complex, $[Ru(CO)_3Cl(glycinate)]$ (Figure 1.20), was found to be stable in water at acidic pH but in physiological buffers rapidly liberated CO. This was found to protect myocardial cells and tissue against ischemia injury and cardiac allograft rejection.

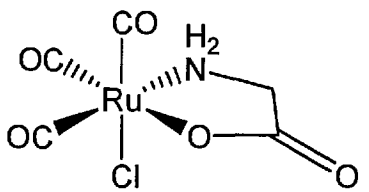


Figure 1.20. Water-soluble CO releasing molecule (CORM-3).

This field of research is still in its infancy and the current challenges for biochemists and bioinorganic chemists are to fully understand how CO can have such an important biological role. When this is further realised, CORMs may well find applications as pharmaceuticals for the treatment of cardiovascular-, neurodegenerative- or inflammatory-related diseases.

1.3 Copper(I) Carbonyl Complexes

1.3.1 Background

Controlled, reversible binding of carbon monoxide may be important in advancing the use of ^{11}CO in carbonylative cross-coupling reactions. Outside the field of PET, CO purification and separation techniques are of great significance given that CO is a key raw material in the synthetic routes for a variety of major chemical products including methanol, formaldehyde, acetic acid, isocyanates, aldehydes, formic acid, pesticides and herbicides. Rising energy and operating costs have underscored the need for energy efficient and selective separation processes for gaseous mixtures.

From searching the literature one finds that copper(I) solutions are widely regarded as the best means for reversibly absorbing CO under mild conditions. It has been found that copper(I) solutions usually absorb up to one molecule of CO per atom of copper.[61] The extent and reversibility of CO coordination in copper(I) complexes is dependent on three important features:

1. *Nature of the supporting ligands*: Many ligands stabilise the copper(I) oxidation state but only a few impart the appropriate properties for reaction with small molecules such as CO.[62] Copper(I) and CO are relatively poorly matched reaction partners and stabilisation of the Cu–CO bond depends heavily on π-backbonding from a filled copper d-orbital to the empty CO π* orbital (Figure 1.21).

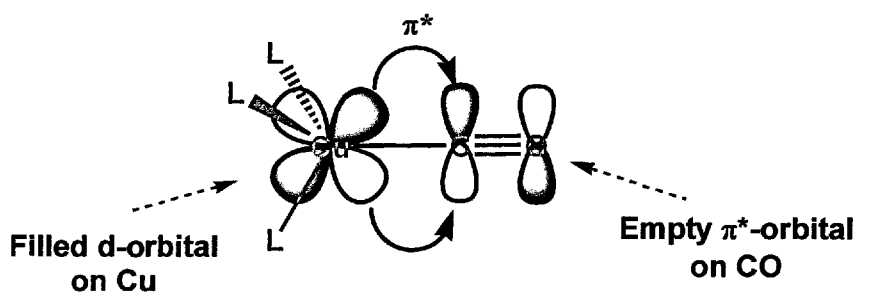


Figure 1.21. Backbonding from a filled d-orbital on copper to an empty π*-orbital on CO.

Molecules containing phosphorus and sulphur donor atoms are generally excellent ligands for copper(I), preventing the disproportionation reaction to copper(II) and copper metal. However, copper(I) complexes with P- and S-containing ligands do not react with CO.[63] Copper(I) carbonyl complexes are usually obtained in the presence of highly basic nitrogen donor atoms which are able to increase the metal electron density available for backbonding with CO. This results in a strengthened Cu–C bond and weakened C–O bond, as electron density has been donated into an antibonding orbital. The extent of π-backbonding is therefore conveniently quantified by observing νCO in the IR spectrum of the complex: Increased backbonding is observed by a reduction in the CO stretching frequency.

2. *The denticity of the supporting ligand*: This is related to the kinetic stability of the resulting carbonyl derivative. The most commonly observed copper(I) geometry is tetrahedral (four-coordinate), although linear (two-coordinate) and trigonal planar (three-coordinate) structures are known. Five-coordination is known for tetradentate macrocyclic ligands which can bind a fifth π-acceptor ligand. As such, tridentate ligands which allow binding of CO at the fourth coordination site of the copper centre are most frequently encountered.

3. *Nature of the solvent*: It has been presumed that the solvent is involved in coordination to many copper(I) species and the stability of the $Cu(CO)_x(solvent)_y$ species will be determined by the coordinating availability of the solvent. This stability refers not only to dissociation of the CO but also towards disproportionation to copper(II) and copper metal:[64]

$$2\ CuX \longrightarrow Cu^0 + CuX_2$$

Copper(I) may be stabilised against disproportionation under aprotic conditions.[65]

Some of the most significant $Cu(ligand)_nCO$ complexes that have been shown to exhibit reversible CO binding are discussed in the following sections. These examples have been grouped according to the defining characteristic of the supporting ligand (where present).

1.3.2 No Supporting Ligand

i. Industrial CO separation – The COSORB Process

The COSORB process[66] has been used for the separation and purification of CO from industrial gas streams and is based on the selective and reversible complexation of CO with an activating agent ($CuAlCl_4$) in an aromatic hydrocarbon solvent such as toluene. This mixture is known as the COSORB solution.[67]

Reaction between dissolved CO and COSORB solution may take place, with the CO displacing the toluene from the copper(I) complex. Heating of the CO-bound solution

causes the CO to be released from the complex. The high selectivity of this solvent for carbon monoxide at ambient temperature and the ease of decomplexation at higher temperatures are the basis for the simplicity of this process. Versteeg *et al.*[68] studied the kinetics of this reaction to gain an insight into the reaction mechanism. They concluded that when the toluene is used in excess (as observed for the experimentally used COSORB solutions), the $CuAlCl_4$ complex is bound to two toluene molecules. In their survey of the equilibrium experiments, a maximum of one mole of CO could be dissolved per mole of $CuAlCl_4$ complex. From this it could be deduced that the equilibrium reaction most likely to occur is as follows:

$$CO + CuAlCl_4.tol_2 \rightleftharpoons CuAlCl_4.tol.CO + tol$$

Gases such as H_2, CO_2, CH_4 and N_2 are chemically inert to this solvent, although H_2O, NH_3, H_2S, SO_2 and oxides of nitrogen are poisons to the complex. This process works well to produce high purity CO from a variety of gaseous mixtures, including N_2-rich gas streams.[67]

1.3.3 Bidentate Ligands

i. Early Research

Floriani *et al.* carried out a great deal of research into the reversible binding of CO to copper(I) complexes with amino ligands during the late 70s and 80s for their potential applications in CO activation.[69] It was found that a methanolic suspension of CuI in the presence of histamine (which is supposed to be the basic unit binding copper(I) in hemocyanins) absorbs CO reversibly at room temperature and atmospheric pressure and loses CO *in vacuo,* as depicted in Figure 1.22.[70] Here it is believed that the copper achieves tetracoordination in solution by coordination of a solvent molecule in addition to the CO and the bidentate histamine ligand.

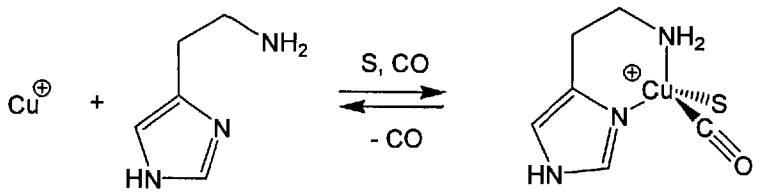


Figure 1.22. Reversible carbonylation of copper(I) histamine system.

In 1981, Kitagawa *et al.*[71] showed that binuclear copper(I) complexes of the formula $[CuX(bpy)]_2$ react with CO reversibly (X = Cl, Br, I). For example, $[CuCl(bpy)]_2$ could be carbonylated at low temperatures and CO release could be induced by purging the solution with N_2 or by raising the temperature (Figure 1.23). By analysing the absorption spectra upon variable CO partial pressures, it was found that the reaction stoichiometry was 1 CO / 2 Cu. Based on IR studies of the chloride species, it was hypothesised that the carbonyl adduct consists of a five-coordinate copper(I) species of the formula $[(bpy)CuCl_2Cu(bpy)(CO)]$. Some further five-coordinate copper(I) carbonyl species are discussed later on in this section.

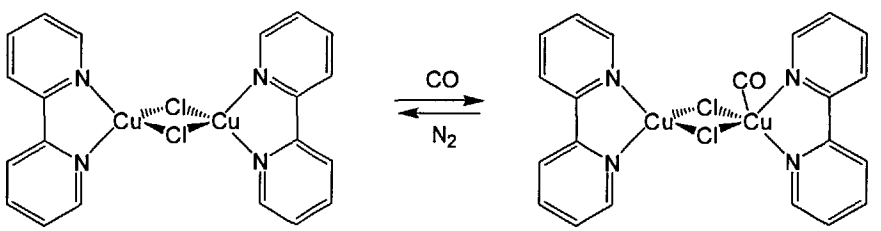


Figure 1.23. Reversible carbonylation of $[CuCl(bpy)]_2$.

ii. Bis(pyrazolyl)borates

Reversible CO/alkene coordination has also been explored at copper using bis(pyrazolyl)borate (Bp) ligands.[72] Bp ligands were chosen in preference to the tris(pyrazolyl)borates (Tp) analogues because the increased steric demand of Tp ligands has been found to prevent coordination of alkenes larger than ethylene.[73] Carbonylation reactions of copper-alkene complexes (alkene = cyclooctene, 4-vinylanisole, 4-chlorostyrene, triethylvinylsilane and fumaronitrile) were carried out in toluene solution according to the equation below.

$$[CuBp^{2(CF3)}(alkene)(solv)] + CO \overset{K}{\rightleftharpoons} [CuBp^{2(CF3)}(CO)(solv)] + alkene$$

Studies of the alkene/CO exchange were performed by gas volumetric analysis. For all of the alkenes except fumaronitrile, the carbonyl complex was thermodynamically favoured at one atmosphere of CO, with negative carbonylation enthalpies being observed in each case. The nitrile-containing alkene, fumaronitrile, was found to be unreactive towards CO due to coordination of the nitrile groups to the copper.

1.3.4 Tridentate Ligands

The formation of dinuclear copper(I) complexes has received interest in attempts to mimic the properties of the copper-containing dioxygen-carrying protein hemocyanin (Hc). Karlin *et al.* have investigated the reversible binding of O_2 and CO to copper(I) species containing dinucleating ligands.[74-76] One of the ligands used, N4PY2, is shown in Figure 1.24.[75]

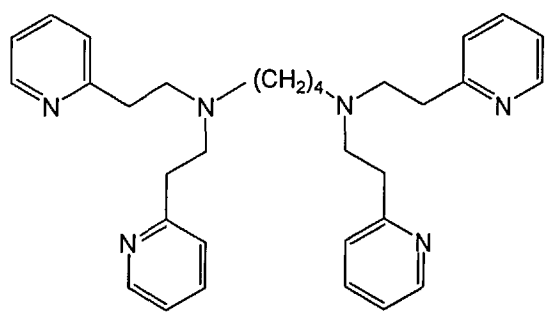


Figure 1.24. Dinucleating ligand N4PY2.

This molecule contains two tridentate PY2 units (PY2 = *bis*[2-(2-pyridyl)-ethyl]amine) connected by an alkyl chain consisting of four methylene units. Typically, dicopper(I) complexes were prepared by mixing $[Cu(MeCN)_4]Y$ ($Y = PF_6^-$ or ClO_4^-) with the N4PY2 ligand in polar organic solvents such as MeCN. Figure 1.25 shows the reactions of these dicationic dicopper complexes towards CO and O_2.

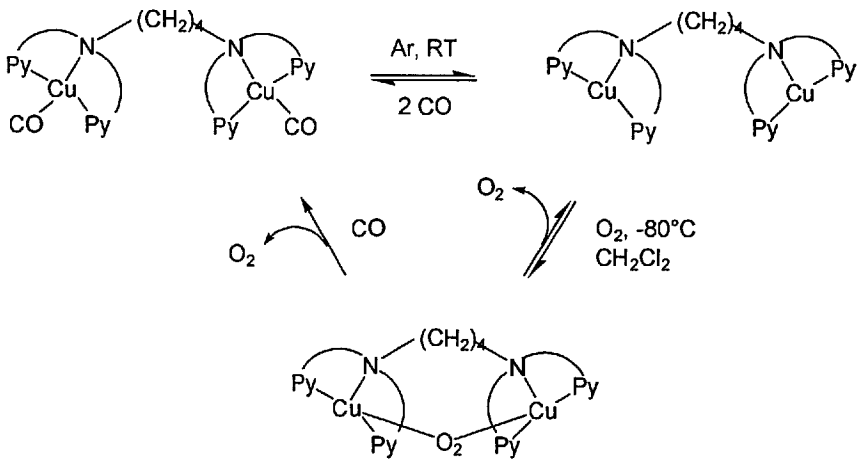


Figure 1.25. Reaction of dicationic copper complexes of the N4PY2 ligand.

Bubbling CO through solutions of $[Cu_2(N4PY2)]^{2+}$ readily gives the dicarbonyl complex $[Cu_2(N4PY2)(CO)_2]^{2+}$. This CO binding is reversible as decarbonylation can be achieved by vacuum/purge cycles. $[Cu_2(N4PY2)]^{2+}$ can also be reversibly oxygenated at -80°C in dichloromethane to give the dioxygen adduct, which is best described as a peroxo-dicopper(II) complex. The application of a vacuum to the dioxygen complex removes the bound O_2 and regenerates the dicopper(I) complex $[Cu_2(N4PY2)]^{2+}$. Saturating this dioxygen complex with CO causes displacement of the O_2 ligand and forms the dicopper(I) dicarbonyl complex $[Cu_2(N4PY2)(CO)_2]^{2+}$.

1.3.5 Flexible Tetradentate Ligands

i. TMPA

The tetradentate ligand tris(2-pyridylmethyl)-amine (TMPA) has been synthesised by Karlin *et al.*[77] and used to form Cu(I) complexes which can reversibly bind to carbon monoxide (Figure 1.26). It was observed that an acetonitrile solution of the TMPA ligand would react with $[Cu(MeCN)_4]^+Y$ ($Y = PF_6^-$ or ClO_4^-) in a 1:1 ratio to produce the copper(I) complex $[Cu(TMPA)(MeCN)]^+$ (1). The crystal structure of this species shows a pseudo-tetracoordinate structure around the copper centre, with strong bonding to all three pyridine nitrogen atoms and the MeCN donor as depicted in Figure 1.26. The lone pair on the central nitrogen atom is directed toward the copper ion thus giving the appearance of a trigonal bipyramidal Cu(I) complex.

The reversibility of this CO binding (Figure 1.26) was evidenced by UV/vis spectroscopy. The carbonylation of $[Cu(TMPA)(MeCN)]^+$ was performed by bubbling its RCN solution with CO, while decarbonylation was achieved by application of reduced pressure (at room temperature) to solutions of $[Cu(TMPA)CO]^+$. Replacement of the CO with PPh_3 gave a species which was studied by X-ray crystallography. This showed a four-coordinate tetradentate copper(I) complex in which one pyridyl 'arm' had been displaced from the coordination sphere of the copper and replaced by PPh_3. The triphenylphosphine adduct can also be formed directly from the acetonitrile adduct. These results suggest that the relative order of binding strength in solution is $PPh_3 > CO > RCN$.

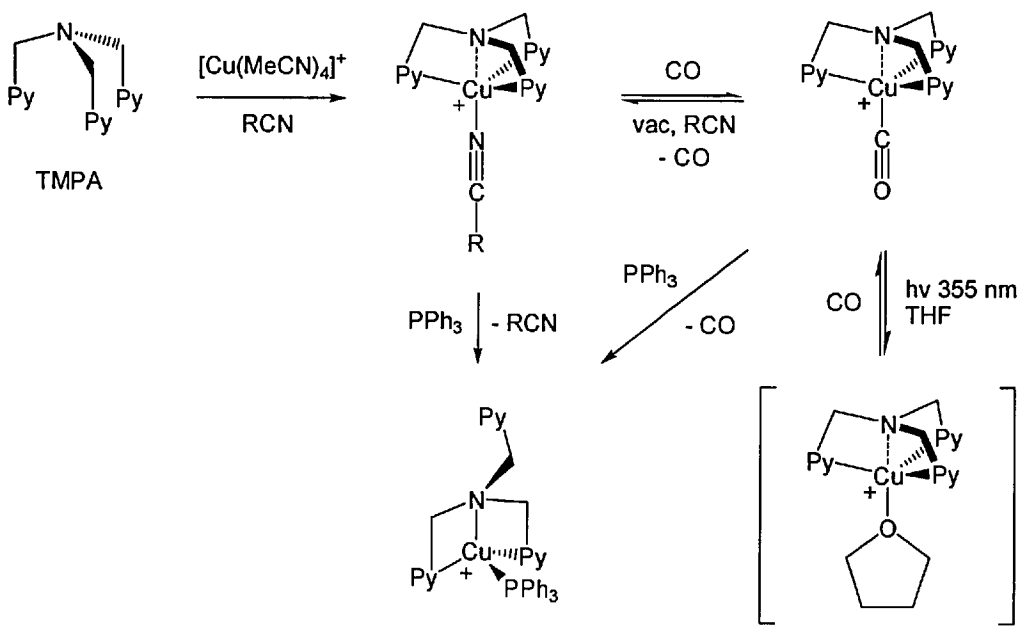


Figure 1.26. Reactivity of $Cu(TMPA)^+$ towards RCN, CO and PPh_3.

Further to these studies, Karlin *et al.*[78] observed that the acetonitrile adduct displays a UV absorption band at 350 nm that was assigned to a copper-to-pyridine MLCT transition, $(d\pi)^{10}(\pi^*)^0 \rightarrow (d\pi)^9(\pi^*)^1$. Absorbance measurements were then carried out in order to examine the effects of MLCT transitions on the coordination chemistry of the copper. Pulsed light excitations (355 nm) under one atmosphere of CO were found to induce reversible carbon monoxide dissociation to generate the transient intermediate $[Cu(TMPA)(THF)]^+$ (Figure 1.26). The CO loss was estimated to occur in less than 10 ns and CO rebinding was found to occur under first-order conditions. It

is believed that this CO dissociation occurs as a result of generation of the MLCT excited state, in which the copper is formally in a +2 oxidation state. CO loss is then triggered as a copper(II) species is not able to stabilise carbonyl adducts.

ii. TACN

Tolman *et al.*[79, 80] have studied copper(I) complexes supported by ligands comprising a single pyridyl donor appended to a 1,4-diisopropyl-1,4,7-triazacyclononane macrocycle. Reversible carbonylation was observed for the copper(I) complex $[(TACN\text{-}Py)Cu]^+$ (Figure 1.27).

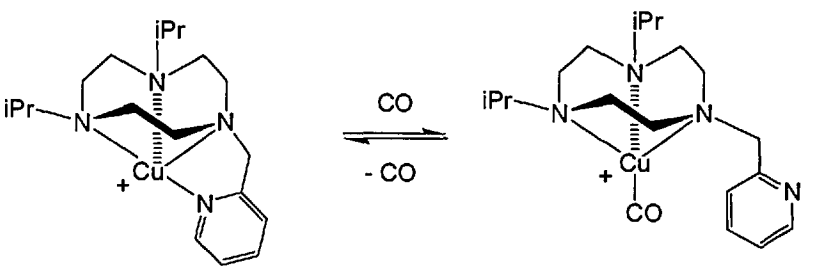


Figure 1.27. Reversible carbonylation of $[(TACN\text{-}Py)Cu]^+$.

UV-visible spectroscopy indicated the loss of the Cu-pyridyl MLCT upon binding of CO. This attests to displacement of the heterocyclic arm to yield a four coordinate adduct $[(\kappa^3\text{-}TACN\text{-}Py)Cu(CO)]^+$. Purging with nitrogen was found to cleanly reverse the process to regenerate the pyridyl-bound species. If the pyridyl side arm is not present, as in the 1,4,7-triazacyclononane (TACN) macrocyclic ligand, then irreversible CO binding with copper is observed.[81]

iii. Copper(I) Schiff-base complexes

Nelson *et al.*[82] reported the products of the reaction of Cu(I) with a series of acyclic Schiff-base ligands bearing appended alkenyl (L^1) (Figure 1.28) or alkyl groups (L^2). These ligands react with CuX salts (X = ClO_4^- or BPh_4^-) to give complexes with the empirical formula [CuL]X. NMR analysis showed that the alkyl complexes $[CuL^2]X$ are likely to form mononuclear three-coordinate structures in solution. $[CuL^1]X$ complexes contain additional olefinic groups and it is believed that in solution there is

an equilibrium between the three coordinate species and a four-coordinate species in which one double bond coordinates to the copper(I) centre (Figure 1.28). In MeCN solution these complexes bind CO reversibly at the fourth coordination site. Loss of CO is achieved by passing argon through the solutions, or degassing under vacuum.

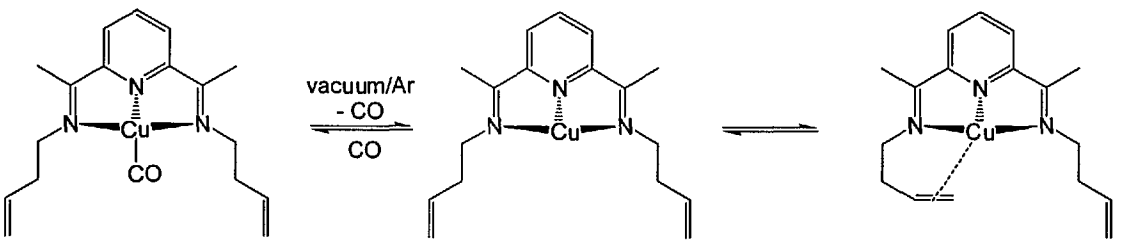


Figure 1.28. Competition between side arm-coordination and CO-coordination in complexes containing olefinic side groups.

The equilibrium constants for CO adduct formation were found to be dependent on the degree of competition between carbon monoxide binding and side-arm donor-group binding (where present) with the largest K_{eq} values being for the three-coordinate complexes having no side arm donor groups and the smallest being for complexes in which the pendant alkene groups provide strong competition to CO binding.

1.3.6 Macrocyclic Tetradentate Ligands

Copper(I) carbonyl complexes having rigid macrocylic ligands have been reported by Gagne *et al.*[83-86] In these species, the copper(I) centre is bound to four nitrogen atoms and therefore is formally an 18-electron system. Despite this stable electronic configuration, blue solutions of $[CuLBF_2]$ were found to react reversibly with CO to give light yellow solutions (Figure 1.29).[83] Decarbonylation could be induced by purging the solution with nitrogen. Structural characterisation of the carbonyl species showed a five-coordinate copper(I) centre which gives rise to a 20-electron count. The unusual coordination number and geometry of the copper(I) carbonyl complex may be explained by the rigid nature of the macrocyclic ligand as it cannot allow dissociation of a single nitrogen atom.

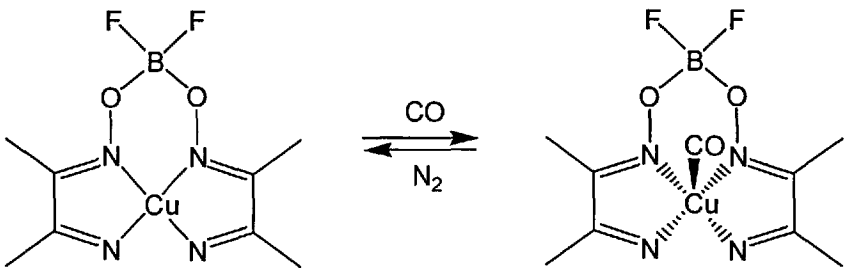


Figure 1.29. Reversible carbonylation of a tetradentate copper(I) complex, $Cu[LBF_2]$.

1.3.7 Immobilized Copper(I) Complexes

The previous examples demonstrate the reversible binding of Cu(I) solutions to carbon monoxide, but metal complexes that bind CO in solution often do not bind CO as a crystalline solid because of lattice constraints.[87] For this reason, relatively few studies have been carried out on solid-state absorbents. Two examples of polymer-supported Cu(I) complexes that reversibly bind carbon monoxide are discussed below.

It has been noted that solid copper(I) chloride binds CO only under extreme conditions, but when supported on active carbon, it is a reversible CO carrier that is stable to moisture.[88] From these observations, Drago *et al.*[87] reasoned that CO binding could occur in the solid state using copper(I) complexes covalently attached to polymer supports. In 1988 this group formed a cross-linked polystyrene derivative which would bind with Cu(I) in solution (Figure 1.30).

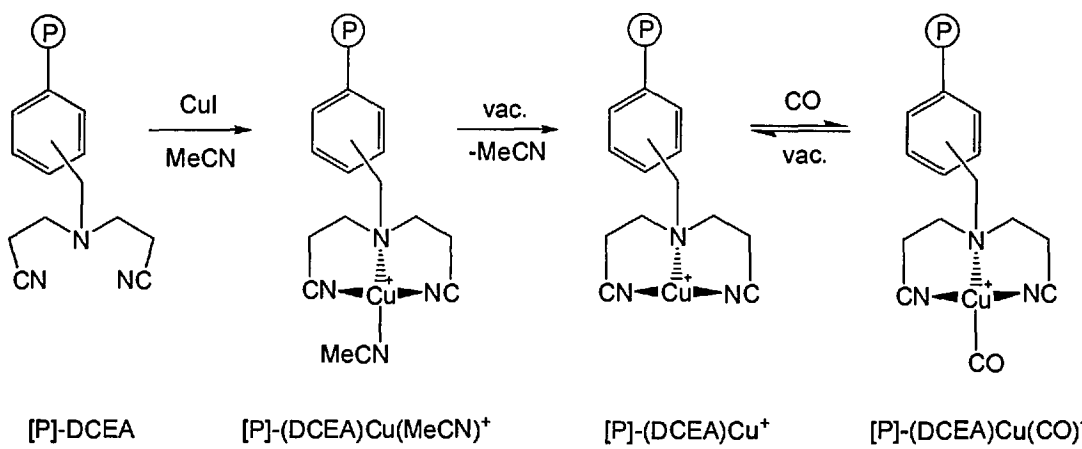


Figure 1.30. Formation of Cu(I)-containing cross-linked polymer and reversible reactions with CO.

The Cu(I)-containing resin formed by reaction of [P]-DCEA with CuI was unreactive toward carbon monoxide. However, if the polymer beads were placed under vacuum and then exposed to a CO atmosphere, binding of CO was observed. This led the authors to conclude that the Cu(I) complex is probably solvated prior to evacuation, rendering the Cu(I) coordinatively saturated and inert towards CO. The coordination of CO by exposure of [P]-(DCEA)Cu^{+} to carbon monoxide was observed by an increasingly strong absorption at 2091 cm^{-1} in the IR spectrum. The reversibility of this coordination was observed by placing the resin in a vacuum that caused the CO stretch to disappear from the IR spectrum.

Similarly, Borovik *et al.*[89] reasoned that CO coordination could occur within a network polymer if the CO-free form has a coordinatively unsaturated three-coordinate Cu(I) centre. Unlike the previous method, the copper(I) ions were incorporated into the monomer prior to polymerisation. The reaction scheme for polymer formation and the subsequent reactions with CO are shown in Figure 1.31.

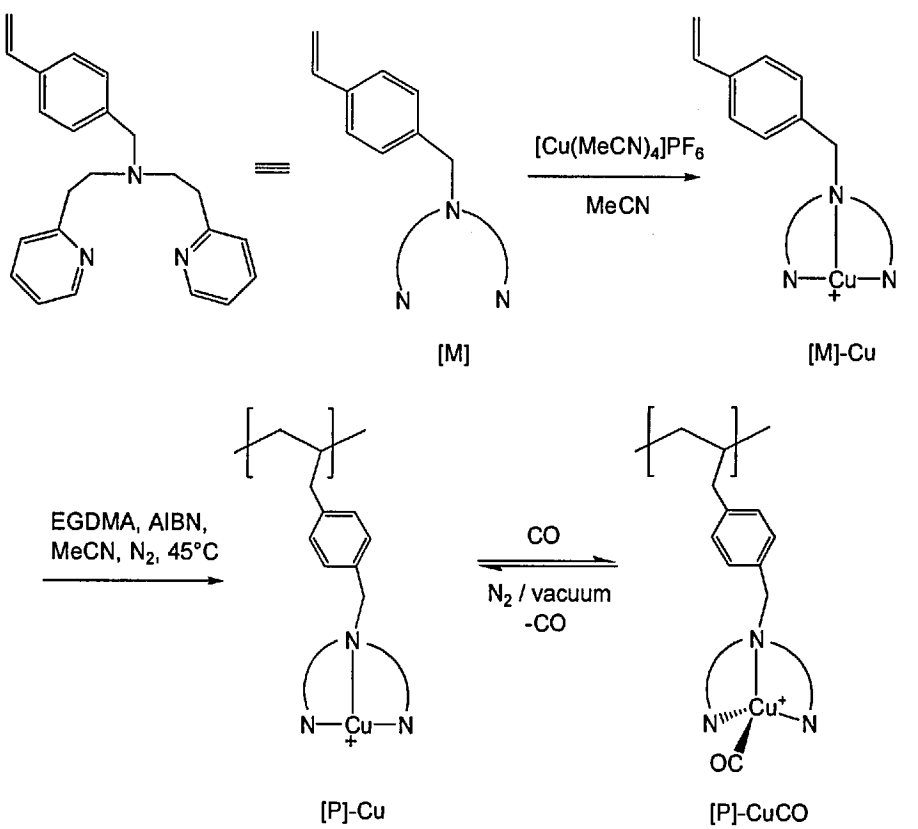


Figure 1.31. Formation of immobilized copper(I) complex and reversible binding to CO.

The solid state binding of CO to the polymer, [P]-Cu, was monitored using Diffuse Reflectance Infrared Fourier Transformation (DRIFT) spectroscopy. Upon exposure to CO, a new band at 2085 cm^{-1} appeared in the spectrum within five minutes, indicating coordination of the copper(I) centres to carbon monoxide to form [P]-Cu(CO). Decarbonylation was achieved by flushing the polymer with a stream of N_2 for 15 minutes resulting in loss of this absorption from the DRIFT spectrum.

1.3.8 Summary

Overall, the reversible coordination of CO with copper(I) complex appears to rely on the transient nature of the carbonyl ligand. As such, CO binding is often reversed by lowering the pressure or by purging the carbonyl solution with nitrogen. The reversibility of this process is generally facilitated by either a particularly weak Cu-CO bond or when a stronger Cu–CO bond is accompanied by a competing donor group. In the latter case, the competing donor group may be a strongly coordinating solvent molecule or an appendage to the ligand backbone which contains a potentially-containing donor group.

1.4 Poly(pyrazolyl)borate Ligands

1.4.1 Background

Just over 40 years ago, a landmark series of papers from Swiatoslaw Trofimenko was published in the Journal of the American Chemical Society that described the synthesis of a new ligand type, the poly(pyazolyl)borates.[90-93] In the years since, over 1500 publications have appeared describing the synthesis and application of these ligands in various areas of chemistry, from catalysis and material science through analytical chemistry to modelling the active site of metallo-enymes and organic chemistry. Their complexes have been described for all the elements in groups 1 to 13 (excluding francium and radium), for phosphorus, for all the lanthanides (except for promethium) and for some of the actinides (uranium, thorium, neptunium and plutonium). Their popularity is such that some of these ligands and their metal complexes are now commercially available (Aldrich, Acros, Strem) allowing the chemist instant access to their wide and varied chemistry.

1.4.2 Features

Poly(pyrazolyl)borate ligands contain two significant features: (i) a tetrasubstituted boron anion at the ligand core, and (ii) two or more pyrazolyl substituents attached to the central boron atom (Figure 1.32). This results in a negatively charged species in which the charge is delocalised throughout the aromatic pyrazolyl rings.

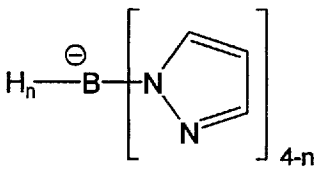


Figure 1.32. General formula of poly(pyrazolyl)borate ligands.

The name 'scorpionate' to describe these species was coined by Trofimenko as their coordination behaviour closely resembles the hunting habits of a scorpion: the animal grabs its prey with two claws (coordination of M through the two pyrazolyl N-donors) and then may, or may not, proceed to sting it with its tail (coordination of the third donor group 'L') (Figure 1.33). The defining feature of the resultant complexes is a six-membered $B(\mu\text{-}pz)_2M$ ring formed by the two pyrazolyl rings bridging between the boron atom and the metal atom (shown in blue in Figure 1.33).

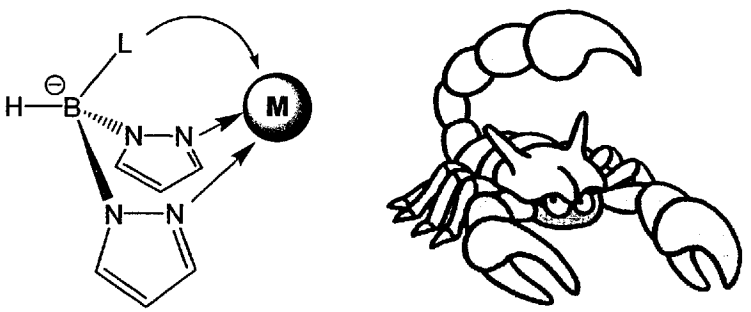


Figure 1.33. Scorpionate ligand (left) and Scorpion (right). Not to scale.

The most common types of scorpionate ligand are the bis(pyrazolyl)borates (L = H in Figure 1.33) and the tris(pyrazolyl)borates (L = pyrazole in Figure 1.33). In the case of the tris(pyrazolyl)borate (Tp) ligands, the L group is another pyrazolyl ring identical to the two others (thus the 'sting' is actually a third 'claw'), resulting in a

tridentate ligand of C_{3v} symmetry. In 1986, a 'second generation' of scorpionates were introduced,[94, 95] containing bulky substituents in the 3-position of the pyrazolyl rings. Nowadays, scorpionate ligands can contain R_1, R_2 and R_3 substituents in the 3-, 4-, and 5-positions of each pyrazolyl ring, and these substituents may themselves contain additional donor sites (this is further discussed in Chapter 5). This gives rise to a huge number of possible structural variations and allows their design with specific steric and electronic features thereby providing the chemist with greater control over their coordination chemistry (see review articles [96, 97]).

1.4.3 Naming of Scorpionates

The most frequently encountered scorpionates have been categorised according to the number of pyrazolyl units attached to the central boron (2, 3 or 4). These are known as bis(pyrazolyl)borates, tris(pyrazolyl)borates and tetrakis(pyrazolyl)borates and are usually denoted as Bp, Tp and pz^oTp, respectively. Throughout this thesis, however, the term T_kp has been adopted as the abbreviation for tetrakis(pyrazolyl)borates, rather than pz^oTp. Writing the systematic names for substituted scorpionates is time consuming and does not instantly allow one to visualise the ligand. As such, a system of abbreviation has been adopted to describe the substitution pattern (for corresponding examples see Figure 1.34):

1) Any non-hydrogen substituent in the 3-position is denoted by a superscript. For example, $[HB(3\text{-phenylpyrazole})_3]^-$ is written as Tp^{Ph}. This position is given priority because in the ligand forming reaction between a metal borohydride and a 3(5)-monosubstituted pyrazole, the substituent ends up in the 3-position of the ligand due to steric effects.

2) The 5-substituent follows the 3-substituent as a superscript, separated by a comma. For example $[HB(3\text{-}tert\text{-butyl-5-methylpyrazole})_3]^-$ is denoted as $Tp^{tBu,Me}$.

3) Where both the 3- and 5-substituents are identical, the superscript R is followed by a 2. Thus $[HB(3,5\text{-dibromopyrazole})_3]^-$ is denoted as Tp^{Br2}. For historical reasons, the frequently encountered Tp^{Me2} is referred to as Tp*.

4) A substituent in the 4-position is denoted as a 4R superscript. For example, [HB(3-isopropyl-4-chloropyrazole)$_3$]$^-$ is denoted as $Tp^{iPr,4Cl}$.

5) Boron substituents are written preceding the Tp. For example ferrocenylhydrotris(pyrazolyl)borate is abbreviated to FcTp.

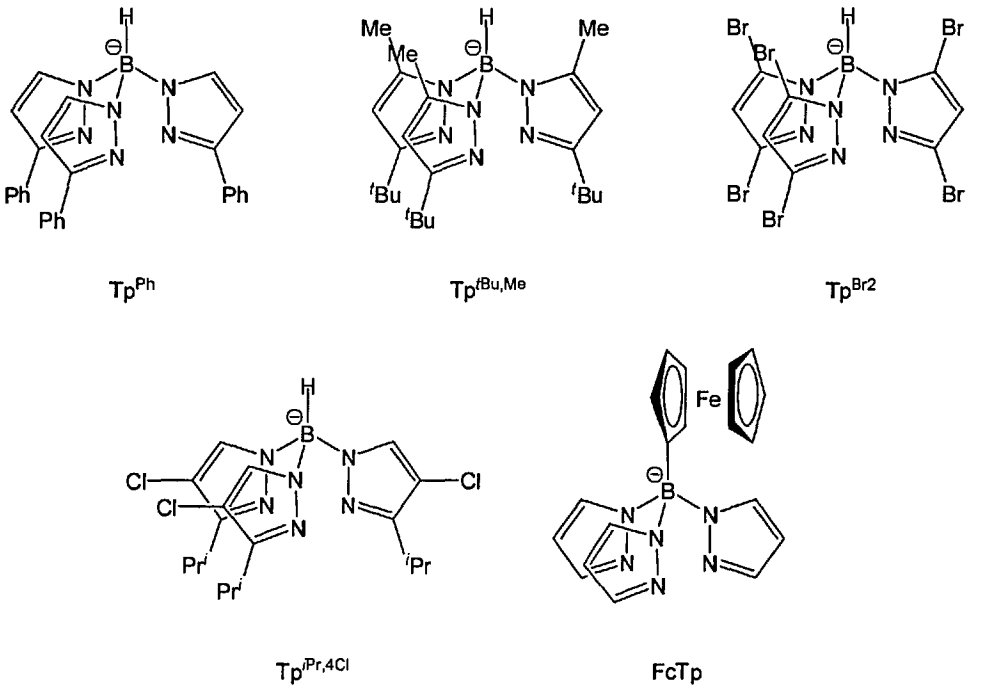


Figure 1.34. Examples of abbreviated naming of scorpionate ligands.

1.4.4 Tris(pyrazolyl)borates

The Tp ligand has frequently been compared with the cyclopentadienyl ions, Cp and Cp* because they have formed many similar metal complexes such as L_2M, and $[LM(CO)_3]^-$. Furthermore, both ligands carry a -1 charge, are capable of donating six electrons and they both occupy three coordination sites around a metal. There are, however, a number of differences including: (1) Symmetry – C_{3v} for TpM, C_{5v} for CpM; (2) Substitution – There are 10 substitutable positions on the Tp ring (1 on boron, and three on each of the 3-, 4- and 5-positions of the pyrazole rings; (3) Monomeric species – A wide range of Tp^RMX species can be formed (X = halide), while the only example with Cp is found with beryllium. This is because sterically hindered Tp ligands can be formed by placing large substituents in the 3-position of

the pyrazole rings; (4) The alkali metal salts of Tp ligands are air stable solids while Cp salts are air sensitive. These differences highlight the versatility of the Tp ligand which enables the chemist to fine-tune the ligand to suit their electronic and steric requirements.

The unsubstituted Tp ligand (right, Figure 1.35) was first synthesised in 1967 by Trofimenko.[91] In this case the 'tail' or third donor group of the scorpionate is a third pyrazolyl ring, thus the ligand is tridentate with local C_{3v} symmetry. This is a strongly electron donating ligand as a result of the negative charge.

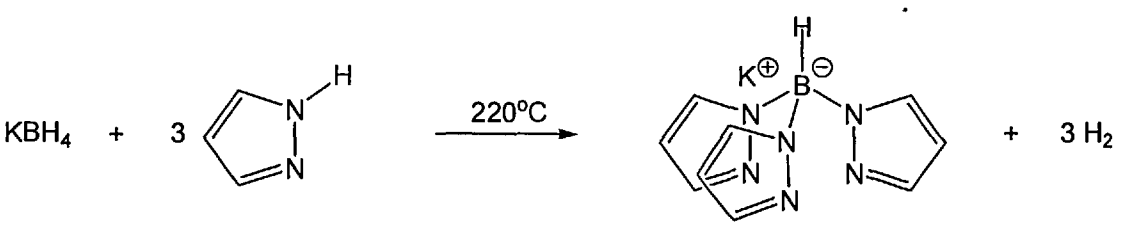


Figure 1.35. Formation of the tris(pyrazolyl)borate ligand (Tp).

This ligand is formed by a neat reaction *i.e.* heating a mixture of a metal borohydride (commonly KBH_4) with an excess of pyrazole (Figure 1.35). The extent of the reaction can be followed by hydrogen evolution. When the theoretical amount of hydrogen (three molar equivalents relative to the borohydride) has been evolved, the heating is stopped and the excess pyrazole is removed by sublimation. The Tp ligand coordinates with a range of metals, usually in a tridentate fashion to form octahedral sandwich complexes $[Tp]_2M$. The tetrahedral complexes [Tp]MX are more labile and can self-convert to the $[Tp]_2M$ species.

1.4.5 Tp-Supported Copper Carbonyls

One relatively stable [Tp]MX complex is the copper(I) carbonyl adduct, CuTpCO. In this case, the electron-donating properties of the Tp ligand are well suited to forming copper(I) carbonyl complexes, where an electron-rich, low valent metal centre is required to stabilise the Cu–CO bond via π-backbonding from a filled copper d-orbital to the empty CO π* orbital (Figure 1.21).

In 1973 Bruce *et al.* used the Tp ligand to form the first stable copper(I) carbonyl complex, CuTpCO (Figure 1.36, left).[98] Churchill *et al.* were later able to grow crystals of this complex to provide the first example of a copper carbonyl species structurally characterised by X-ray crystallography (Figure 1.36, right).[99]

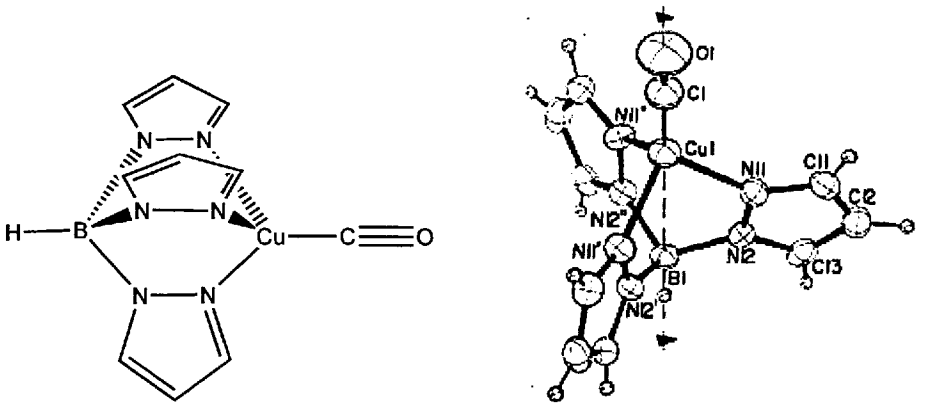


Figure 1.36. CuTpCO line drawing (left) and crystal structure (right).

Since this discovery many more tris(pyrazolyl)borate ligands have been synthesised, employing a range of substitution patterns and electron-withdrawing or electron-donating groups. The electronic properties of many of these ligands have been studied by IR spectroscopy by examining the stretching frequency for νCO in the Cu[Tp^{x}]CO complexes. A summary of these complexes and their corresponding CO stretching frequencies is shown below (Table 1.2). Here, the trend between ligand substitution and νCO is immediately apparent – the highest CO stretches are observed for Tp ligands bearing powerfully electron-withdrawing substituents and the lowest CO stretches are observed with Tp ligands containing electron-releasing substituents.

Table 1.2. Carbonyl stretching frequencies of known copper(I) scorpionate carbonyl complexes

Cu[Tp^x]CO complex			ν(CO) / cm^{-1}	Reference
3-pz:	*4-pz:*	*5-pz:*		
t-Bu	H	i-Pr	2054	100, 101
i-Pr	H	i-Pr	2056	102, 103
t-Bu	H	Me	2061	100, 101
Me	H	Me	2066	98
t-Bu	H	H	2069	104
Ph	H	i-Pr	2075	101
Ph(2-POPh$_2$)	H	H	2075 [a]	this report
p-(t-Bu)-Ph	H	Me	2078	105
Mes [b]	H	H	2079	106
2-pyridyl	H	H	2081	this report
H	H	H	2083	98, 107
H	H	H	2083 [a]	108
Ph	H	Ph	2086	102, 103
Ph	H	SMe	2087	this report
CF_3	H	H	2100	109
$CF_2CF_2CF_3$	H	H	2102	110
CF_3	H	Ph	2103	111
CF_3	H	Me	2109	106
Br	Br	Br	2100	112
CF_2CF_3	H	H	2110	110
camph [c]		H	2110 [a]	113
CF_3	H	CF_3	2137	114
free CO			2143	

(a) Tkp ligand; (b) Mes = 2,4,6-trimethylphenyl; (c) camph = camphorpyrazole.

1.4.6 Applications of Tp Ligands

The stabilising effect that the tridentate Tp ligand exerts upon a metal centre means that it does not normally interfere during reactions which might occur at any remaining coordination sites of the metal. This property of being a good 'spectator ligand' has allowed Tp ligands to be used in coordination with a range of metals for a host of applications.

i. Catalysis

Tp^x complexes have been found to catalyse a variety of chemical reactions. For example, transition metal-supported Tp complexes have been utilised for processes such as acyclic diene metathesis,[115] ethylene polymerisation,[116] ring opening metathesis polymerisations[117] and dimerisation of terminal alkynes.[118] Scorpionate

complexes, particularly of rhodium(I) and iridium(I), have been studied for their use in C–H bond activation.[119, 120]

ii. Enzyme Modelling

Scorpionate ligands have been used extensively for modelling the active site of enzymes in bio-inorganic systems, particularly those in which the metal is coordinated to three imidazolyl nitrogen atoms from three histidine residues. Frequently encountered metals are copper,[121] iron[122] and zinc,[123] with the last receiving considerable attention in attempts to mimic the active site of carbonic anhydrase,[124] the enzyme which catalyses the reversible hydration of carbon dioxide.

iii. Miscellaneous Studies

Recent advances in the chemistry of silver(I) carbonyl complexes highlights the versatility of the Tp ligand. Tp ligands containing electron-withdrawing substituents have previously been employed for the isolation and structural characterisation of silver(I) carbonyl complexes. For instance, the highly-fluorinated ligands $Tp^{(CF_3)2}$ and $MeTp^{(C_2F_5)2}$ have allowed the isolation and structural characterisation of silver(I) carbonyl complexes of the formula $[Tp^x]AgCO$.[125, 126] In contrast to the copper(I) species described in the previous section, these silver(I) carbonyls are unstable and exhibit stretching frequencies for νCO greater than that of free CO (2143 cm^{-1}). This suggests a lack of π-backbonding from the metal to the carbonyl, with the CO coordinating weakly via σ-donation from the HOMO. These are classified as non-classical metal carbonyl complexes.[127]

Recently, however, a Tp ligand was used to stabilise the first *classical* silver(I) carbonyl complex.[128] In this case, the non-fluorinated, electron-rich ligand $MeTp^{Mes}$ (Mes = 2,4,6-trimethylphenyl) was used to isolate the corresponding silver(I) carbonyl complex, $[MeTp^{Mes}]AgCO$, which exhibited a νCO of 2125 cm^{-1}. The lowering of the CO stretch relative to that of free CO is indicative of increased π-backbonding, much like the copper(I) complexes. It is notable that by tuning the steric and electronic properties of the Tp ligands through modification of the substituent groups it has been possible to stabilise both classical and non-classical silver carbonyl complexes.

1.5 Research Objectives

The growing use of PET for disease detection, disease treatment and drug discovery brings with it the need to produce a wider range of radiolabelled tracer molecules. At present the synthesis of new radiotracers for PET is hindered by the relatively few labelling reagents that are available to the radiochemist as well as the problems associated with the handling of these species. The incentive to incorporate ^{11}C, specifically, into tracer molecules is great since carbon is present in almost all biologically active compounds, hence no substance alteration would occur upon 'tagging' of a molecule with ^{11}C. Within this field, ^{11}CO has the potential to be one of the most versatile labelling reagents, yet its use has been restricted by its low solubility and low concentrations.

With these incentives, the aim of this project is to investigate new ways to utilise [^{11}C]carbon monoxide as a reagent for the development of PET tracers. Other groups have found success using harsh reaction conditions to boost reactivity and one of the objectives in this project is to develop milder alternatives which could allow [^{11}C]carbonylation reactions to be performed at lower temperatures and pressures. In order to do this the ^{11}CO must be selectively solubilised from within the dilute gas stream. In this project, the use of Tp ligands to stabilise carbon monoxide in the form of copper(I) complexes is to be explored.

Controllable release of the bound CO is also required, so that the gas can be used for carbonylation reactions. A specific trigger is needed to do this, such as a change in pH, increase in temperature, application of UV light or by displacement using a competing ligand. The tuneable electronics and sterics of the Tp ligand (by modification of the substituent groups) may play an important role in this process. Investigations into the synthesis of new Tp ligands will be explored for this purpose. As well as their applications in PET, any new Tp ligands are of interest because of their wide and varied coordination chemistry and their potential application in catalysis. For these reasons, the chemistry of any new Tp ligands will be duly explored.

1.6 References

1. M. E. Phelps, *Proc. Natl. Acad. Sci. U. S. A.*, 2000, **97**, 9226.
2. L. Sokoloff, in *Basic Neurology*, eds. G. Siegel, B. Agranoff, R. W. Albers and P. Molinoff, Raven, New York, 1989, p. 565.
3. R. Duara, C. Grady, J. Haxby, M. Sundaram, N. R. Cutler, L. Heston, A. Moore, N. Schlageter, S. Larson and S. I. Rapoport, *Neurology*, 1986, **36**, 879.
4. J. C. Mazziotta, R. S. J. Frackowiak and M. E. Phelps, *Semin. Nucl. Med.*, 1992, **22**, 233.
5. K. Herholz, *Alzheimer Dis. Assoc. Disord.*, 1995, **9**, 6.
6. D. H. S. Silverman, G. W. Small and M. E. Phelps, *Clin. Positron Imaging*, 1999, **2**, 119.
7. J. C. Baron, D. Comar, L. Farde, M. B. Martinot and B. Mazoyer, *Brain Dopaminergic Systems: Imaging with Positron Emission Tomography*, Kluwer, Dordrecht/Boston/London, 1991.
8. M. E. Phelps, D. E. Kuhl and J. C. Mazziotta, *Science*, 1981, **211**, 1445.
9. J. H. Greenberg, M. Reivich, A. Alavi, P. Hand, A. Rosenquist, W. Rintelmann, A. Stein, R. Tusa, R. Dann, D. Christman, J. Fowler, B. MacGregor and A. Wolf, *Science*, 1981, **212**, 678.
10. G. Lappin and R. C. Garner, *Nat. Rev. Drug Discovery*, 2003, **2**, 233.
11. J. A. Dimasi, *Clin. Pharmacol. Ther.*, 2001, **69**, 297.
12. R. A. Prentis, Y. Lis and S. R. Walker, *Br. J. Clin. Pharmacol.*, 1988, **25**, 387.
13. M. Bergstrom, A. Grahnen and B. Langstrom, *Eur. J. Clin. Pharmacol.*, 2003, **59**, 357.
14. T. Schepis, O. Gaemperli, V. Treyer, I. Valenta, C. Burger, P. Koepfli, M. Namdar, I. Adachi, H. Alkadhi and P. A. Kaufmann, *J. Nucl. Med.*, 2007, **48**, 1783.
15. C. K. Hoh, *Nucl. Med. Biol.*, 2007, **34**, 737.
16. D. J. Schlyer, *Annal. Acad. Med.*, 2004, **33**, 146.
17. H. M. Colquhoun, D. J. Thompson and M. V. Twigg, *Carbonylation*, Plenum Press, New York, 1991.
18. A. Schoenberg and R. F. Heck, *J. Org. Chem.*, 1974, **39**, 3327.
19. P. Lidstrom, T. Kihlberg and B. Langstrom, *J. Chem. Soc., Perkin Trans. 1*, 1997, 2701.
20. H. Audrain, L. Martarello, A. Gee and D. Bender, *Chem. Commun.*, 2004, 558.
21. R. F. Ismagilov, *Angew. Chem., Int. Ed.*, 2003, **42**, 4130.
22. H. Audrain, *Angew. Chem., Int. Ed.*, 2007, **46**, 1772.
23. J. M. Gillies, C. Prenant, G. N. Chimon, G. J. Smethurst, B. Dekker and J. Zweit, *Appl. Radiat. Isot.*, 2006, **64**, 333.
24. J. M. Gillies, C. Prenant, G. N. Chimon, G. J. Smethurst, W. Perrie, I. Hamblett, B. Dekker and J. Zweit, *Appl. Radiat. Isot.*, 2006, **64**, 325.
25. C. C. Lee, G. Sui, A. Elizarov, C. J. Shu, Y. S. Shin, A. N. Dooley, J. Huang, A. Daridon, P. Wyatt, D. Stout, H. C. Kolb, O. N. Witte, N. Satyamurthy, J. R. Heath, M. E. Phelps, S. R. Quake and H. R. Tseng, *Science*, 2005, **310**, 1793.
26. P. W. Miller, N. J. Long, A. J. De Mello, R. Vilar, J. Passchier and A. Gee, *Chem. Commun.*, 2006, 546.
27. M. T. Rahman, T. Fukuyama, N. Kamata, M. Sato and I. Ryu, *Chem. Commun.*, 2006, 2236.

28. E. R. Murphy, J. R. Martinelli, N. Zaborenko, S. L. Buchwald and K. F. Jensen, *Angew. Chem., Int. Ed.*, 2007, **46**, 1734.
29. P. W. Miller, N. J. Long, A. J. De Mello, R. Vilar, H. Audrain, C. Bender, J. Passchier and A. Gee, *Angew. Chem., Int. Ed.*, 2007, **46**, 2875.
30. M. H. Al-Qahtani and V. W. Pike, *J. Chem. Soc., Perkin Trans. 1*, 2000, 1033.
31. M. H. Al-Qahtani and V. W. Pike, *J. Label. Compd. Radiopharm.*, 2000, **43**, 825.
32. T. Kihlberg, B. Langstrom and F. T. J. Eriksson, *Method and apparatus for production and cse of [^{11}C]carbon monoxide in labelling synthesis, Patent Application, PCT/SE02/01222.*
33. T. Kihlberg and B. Langstrom, *J. Org. Chem.*, 1999, **64**, 9201.
34. F. Karimi and B. Langstrom, *Org. Biomolec. Chem.*, 2003, **1**, 541.
35. F. Karimi and B. Langstrom, *Eur. J. Org. Chem.*, 2003, 2132.
36. O. Rahman, T. Kihlberg and B. Langstrom, *J. Org. Chem.*, 2003, **68**, 3558.
37. F. Karimi and B. Langstrom, *J. Chem. Soc., Perkin Trans. 1*, 2002, 2111.
38. O. Rahman, J. Llop and B. Langstrom, *Eur. J. Org. Chem.*, 2004, 2674.
39. O. Rahman, T. Kihlberg and B. Langstrom, *Eur. J. Org. Chem.*, 2004, 474.
40. F. Karimi, J. Barletta and B. Langstrom, *Eur. J. Org. Chem.*, 2005, 2374.
41. J. Eriksson, O. Aberg and B. Langstrom, *Eur. J. Org. Chem.*, 2007, 455.
42. J. Barletta, F. Karimi and B. Langstrom, *J. Label. Compd. Radiopharm.*, 2006, **49**, 429.
43. H. Doi, J. Barletta, M. Suzuki, R. Noyori, Y. Watanabe and B. Langstrom, *Org. Biomolec. Chem.*, 2004, **2**, 3063.
44. J. Barletta, F. Karimi, H. Doi and B. Langstrom, *J. Label. Compd. Radiopharm.*, 2006, **49**, 801.
45. O. Itsenko and B. Langstrom, *J. Org. Chem.*, 2005, **70**, 2244.
46. O. Itsenko and B. Langstrom, *Org. Lett.*, 2005, **7**, 4661.
47. O. Itsenko, T. Kihlberg and B. Langstrom, *Eur. J. Org. Chem.*, 2005, 3830.
48. O. Itsenko, D. Norberg, T. Rasmussen, B. Langstrom and C. Chatgilialoglu, *J. Am. Chem. Soc.*, 2007, **129**, 9020.
49. O. Itsenko, T. Kihlberg and B. Langstrom, *J. Org. Chem.*, 2004, **69**, 4356.
50. T. Kihlberg, F. Karimi and B. Langstrom, *J. Org. Chem.*, 2002, **67**, 3687.
51. M. Momenteau and C. A. Reed, *Chem. Rev.*, 1994, **94**, 659.
52. H. Tang and D. H. Dolphin, *Inorg. Chem.*, 1996, **35**, 6539.
53. W. Kaim and B. Schwederski, *Bioinorganic Chemistry: Inorganic Elements in the Chemistry of Life*, Wiley, Chichester, 1994.
54. D. Cullen, M. Tsutsui, Srivasta.Ts and E. Meyer, *J. Chem. Soc., Chem. Commun.*, 1972, 584.
55. M. Buchalova, P. R. Warburton, R. vanEldik and D. H. Busch, *J. Am. Chem. Soc.*, 1997, **119**, 5867.
56. T. G. Traylor, M. J. Mitchell, S. Tsuchiya, D. H. Campbell, D. V. Stynes and N. J. Koga, *J. Am. Chem. Soc.*, 1981, **103**, 5234.
57. L. E. Otterbein, *Antioxid. Redox Signalling*, 2002, **4**, 309.
58. R. Motterlini, J. E. Clarke, R. Foresti, P. Sarathchandra, B. E. Mann and C. J. Green, *Circ. Res.*, 2002, **90**, e17.
59. J. E. Clarke, P. Naughton, S. Shurey, C. J. Green, T. R. Johnson, B. E. Mann, R. Foresti and R. Motterlini, *Circ. Res.*, 2003, **93**, e2.
60. R. Foresti, J. Hammad, J. E. Clarke, T. R. Johnson, B. E. Mann, A. Friebe, C. J. Green and R. Motterlini, *Br. J. Pharmacol.*, 2004, **142**, 453.
61. M. I. Bruce, *J. Organomet. Chem.*, 1972, **44**, 209.

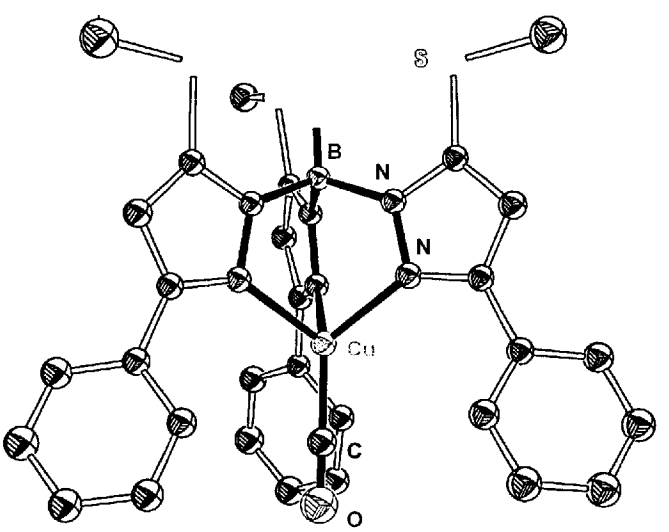
62. A. Toth, C. Floriani, M. Pasquali, A. Chiesivilla, A. Gaetani-Manfredotti and C. Guastini, *Inorg. Chem.*, 1985, **24**, 648.
63. F. A. Cotton and G. Wilkinson, *Advanced Inorganic Chemistry, 4th ed.*, Wiley, New York, 1980.
64. G. Wilkinson, *Comprehensive Coordination Chemistry: The Synthesis, Reactions, Properties and Applications of Coordination Compounds*, Pergamon Press, Oxford, 1987.
65. K. G. Caulton, G. Davies and E. M. Holt, *Polyhedron*, 1990, **9**, 2319.
66. D. J. Haase and D. G. Walker, *Chemical Engineering Progress*, 1974, **70**, 74.
67. N. N. Dutta and G. S. Patil, *Gas Separation & Purification*, 1995, **9**, 277.
68. J. A. Hogendoorn, W. P. M. Vanswaaij and G. F. Versteeg, *Chem. Eng. J., Biochem. Eng. J.*, 1995, **59**, 243.
69. C. Floriani, *Copper Coordination Chemistry: Chemical and Inorganic Perspectives*, Adenine Press, New York, 1982.
70. M. Pasquali, G. Marini, C. Floriani, A. Gaetanimanfredotti and C. Guastini, *Inorg. Chem.*, 1980, **19**, 2525.
71. S. Kitagawa and M. Munakata, *Inorg. Chem.*, 1981, **20**, 2261.
72. G. Pampaloni, R. Peloso, C. Graiff and A. Tiripicchio, *Dalton Trans.*, 2006, 3576.
73. D. J. Thompson, R. L. Harlow and J. F. Whitney, *J. Am. Chem. Soc.*, 1983, **105**, 3522.
74. K. D. Karlin, M. S. Haka, R. W. Cruse and Y. Gultneh, *J. Am. Chem. Soc.*, 1985, **107**, 5828.
75. K. D. Karlin, M. S. Haka, R. W. Cruse, G. J. Meyer, A. Farooq, Y. Gultneh, J. C. Hayes and J. Zubieta, *J. Am. Chem. Soc.*, 1988, **110**, 1196.
76. K. D. Karlin, Z. Tyeklar, A. Farooq, M. S. Haka, P. Ghosh, R. W. Cruse, Y. Gultneh, J. C. Hayes, P. J. Toscano and J. Zubieta, *Inorg. Chem.*, 1992, **31**, 1436.
77. Z. Tyeklar, R. R. Jacobson, N. Wei, N. N. Murthy, J. Zubieta and K. D. Karlin, *J. Am. Chem. Soc.*, 1993, **115**, 2677.
78. D. V. Scaltrito, H. C. Fry, B. M. Showalter, D. W. Thompson, H. C. Liang, C. X. Zhang, R. M. Kretzer, E. Kim, J. P. Toscano, K. D. Karlin and G. J. Meyer, *Inorg. Chem.*, 2001, **40**, 4514.
79. J. A. Halfen, V. G. Young and W. B. Tolman, *J. Am. Chem. Soc.*, 1996, **118**, 10920.
80. L. M. Berreau, J. A. Halfen, V. G. Young and W. B. Tolman, *Inorg. Chim. Acta*, 2000, **297**, 115.
81. P. Chaudhuri and K. Oder, *J. Organomet. Chem.*, 1989, **367**, 249.
82. S. M. Nelson, A. Lavery and M. G. B. Drew, *J. Chem. Soc., Dalton Trans.*, 1986, 911.
83. R. R. Gagne, J. L. Allison, R. S. Gall and C. A. Koval, *J. Am. Chem. Soc.*, 1977, **99**, 7170.
84. R. R. Gagne, J. L. Allison and G. C. Lisensky, *Inorg. Chem.*, 1978, **17**, 3563.
85. R. R. Gagne, C. A. Koval, T. J. Smith and M. C. Cimolino, *J. Am. Chem. Soc.*, 1979, **101**, 4571.
86. R. R. Gagne, J. L. Allison and D. M. Ingle, *Inorg. Chem.*, 1979, **18**, 2767.
87. K. J. Balkus, A. Kortz and R. S. Drago, *Inorg. Chem.*, 1988, **27**, 2955.
88. H. Hirai, K. Wada and M. Komiyama, *Chem. Lett.*, 1983, 361.
89. J. F. Krebs and A. S. Borovik, *J. Am. Chem. Soc.*, 1995, **117**, 10593.
90. S. Trofimenko, *J. Am. Chem. Soc.*, 1967, **89**, 3165.

91. S. Trofimenko, *J. Am. Chem. Soc.*, 1967, **89**, 3170.
92. S. Trofimenko, *J. Am. Chem. Soc.*, 1967, **89**, 4948.
93. S. Trofimenko, *J. Am. Chem. Soc.*, 1967, **89**, 6288.
94. J. C. Calabrese, S. Trofimenko and J. S. Thompson, *J. Chem. Soc., Chem. Commun.*, 1986, 1122.
95. S. Trofimenko, J. C. Calabrese and J. S. Thompson, *Inorg. Chem.*, 1987, **26**, 1507.
96. S. Trofimenko, *Scorpionates: The Coordination Chemistry of Polypyrazolylborate Ligands*, Imperial College Press, London, 1999.
97. J. A. McCleverty and T. J. Meyer, *Comprehensive Coordination Chemistry II - From Biotechnology to Nanotechnology*, Elsevier, 2003.
98. M. I. Bruce and A. P. P. Ostazewski, *J. Chem. Soc., Dalton Trans.*, 1973, 2433.
99. M. R. Churchill, B. G. DeBoer, F. J. Rotella, O. M. Abu Salah and M. I. Bruce, *Inorg. Chem.*, 1975, **14**, 2051.
100. S. Kiani, J. R. Long and P. Stavropoulos, *Inorg. Chim. Acta*, 1997, **263**, 357.
101. S. Imai, K. Fujisawa, T. Kobayashi, N. Shirasawa, H. Fujii, T. Yoshimura, N. Kitajima and Y. Moro-oka, *Inorg. Chem.*, 1998, **37**, 3066.
102. N. Kitajima, K. Fujisawa, C. Fujimoto and Y. Moro-oka, *Chem. Lett.*, 1989, 421.
103. N. Kitajima, K. Fujisawa, C. Fujimoto, Y. Moro-oka, S. Hashimoto, T. Kitagawa, K. Toriumi, K. Tatsumi and A. Nakamura, *J. Am. Chem. Soc.*, 1992, **114**, 1277.
104. C. E. Ruggiero, C. J. Carrano, W. E. Antholine, J. W. Whittaker, C. J. Cramer and W. B. Tolman, *J. Am. Chem. Soc.*, 1993, **115**, 11285.
105. R. R. Conry, G. Ji and A. A. Tipton, *Inorg. Chem.*, 1999, **38**, 906.
106. J. L. Schneider, S. M. Carrier, C. E. Ruggiero, V. G. Young and W. B. Tolman, *J. Am. Chem. Soc.*, 1998, **120**, 11408.
107. M. I. Bruce and A. P. P. Ostazewski, *J. Chem. Soc., Chem. Commun.*, 1972, 1124.
108. O. M. Abu Salah and M. I. Bruce, *J. Organomet. Chem.*, 1975, **87**, C15.
109. H. V. R. Dias, H. J. Kim, H. L. Lu, K. Rajeshwar, N. R. deTacconi, A. Derecskei-Kovacs and D. S. Marynick, *Organometallics*, 1996, **15**, 2994.
110. H. V. R. Dias and H. J. Kim, *Organometallics*, 1996, **15**, 5374.
111. H. V. R. Dias and T. K. H. H. Goh, *Polyhedron*, 2004, **23**, 273.
112. A. Caballero, M. M. Diaz-Requejo, T. R. Belderrain, M. C. Nicasio, S. Trofimenko and P. J. Perez, *J. Am. Chem. Soc.*, 2003, **125**, 1446.
113. H. Brunner, U. P. Singh, T. Boeck, S. Altmann, T. Scheck and B. Wrackmeyer, *J. Organomet. Chem.*, 1993, **443**, C16.
114. H. V. R. Dias and H. L. Lu, *Inorg. Chem.*, 1995, **34**, 5380.
115. L. L. Blosch, A. S. Gamble and J. M. Boncella, *J. Mol. Catal.*, 1992, **76**, 229.
116. A. Karam, E. Casas, E. Catari, S. Pekerar, A. Albornoz and B. Mendez, *J. Mol. Catal. A: Chem.*, 2005, **238**, 233.
117. H. Katayama, T. Yoshida and F. Ozawa, *J. Organomet. Chem.*, 1998, **562**, 203.
118. M. A. J. Tenorio, M. J. Tenorio, M. C. Puerta and P. Valerga, *Organometallics*, 2000, **19**, 1333.
119. C. Barrientos, C. K. Ghosh, W. A. G. Graham and M. J. Thomas, *J. Organomet. Chem.*, 1990, **394**, C31.

120. M. Paneque, M. L. Poveda, V. Salazar, S. Taboada and E. Carmona, *Organometallics*, 1999, **18**, 139.
121. N. Kitajima, *Adv. Inorg. Chem.*, 1992, **39**, 1.
122. R. S. Czernuszewicz, J. E. Sheats and T. G. Spiro, *Inorg. Chem.*, 1987, **26**, 2063.
123. C. Bergquist and G. Parkin, *Inorg. Chem.*, 1999, **38**, 422.
124. A. Looney, R. Han, K. McNeill and G. Parkin, *J. Am. Chem. Soc.*, 1993, **115**, 4690.
125. H. V. R. Dias and X. Wang, *Dalton Trans.*, 2005, 2985.
126. H. V. R. Dias and H. Jin, *J. Am. Chem. Soc.*, 1995, **117**, 11381.
127. A. J. Lupinetti, G. Frenking and S. H. Strauss, *Angew. Chem., Int. Ed.*, 1998, **37**, 2113.
128. H. V. R. Dias and M. Fianchini, *Angew. Chem., Int. Ed.*, 2007, **46**, 2188.

CHAPTER 2

SYNTHESIS AND COPPER COORDINATION CHEMISTRY OF SCORPIONATE LIGANDS



2. Synthesis and Copper Coordination Chemistry of Scorpionate Ligands

For over 100 years copper(I) solutions have been used for the reversible binding of carbon monoxide. The carbonyl complexes of copper(I) were investigated in some detail in the late 1970s and 1980s by various groups (see reviews [1, 2]), although this field of chemistry is by no means fully understood, as noted by Caulton *et al.*[2] who state; "the progress in copper(I) carbonyl chemistry has been severely inhibited by excessive focus on data which can be reliably gathered: solid state structures determined by X-ray diffraction. While such work is both objective and definitive, it provides no reliable guide to solution behaviour...We make a plea for more systematic characterisation of solution behaviour of newly isolated compounds". Clearly there is a demand for advances in this field of chemistry: generally, to provide a better understanding of the solution behaviour of copper(I) carbonyl species, and because of their potential applications in CO separation. In this case CO binding and release is sought in order to overcome some of the problems associated with the use of ^{11}CO in PET.

Within the field of copper-CO chemistry there is a wide array of ligands and solvents available for use depending on the particular system and its application. In the reversible carbonylation schemes described in Chapter 1, the Cu-CO bond is usually quite weak thus allowing the carbonyl ligand to drift on and off the copper centre. Due to their electron-releasing properties, tris(pyrazolyl)borate ligands were employed in the first stable copper(I) carbonyl adducts in an irreversible process. Tp ligands are regularly used as molecular vices to keep a metal ion in a firm tridentate 'grip' thus allowing other ligands to interact with the remaining coordination site(s). In coordination to copper(I) this creates a free coordination site for CO binding which can be strengthened by backbonding. With these favourable properties tris(pyrazolyl)borates were deemed an excellent ligand system to explore for their potential applications in CO trapping for PET.

2.1 Synthesis of Known Scorpionates

Research has been focussed on ligands that could combine with copper to give a strong Cu-CO bond. From the table of the known Tp ligands and their corresponding carbonyl stretching frequencies (Chapter 1), it is not surprising to find that the more electron-rich the Tp ligand, the stronger the Cu-CO bond (as observed by the lowering of νCO). As such, the initial research was conducted on the established scorpionates, hydrotris(pyrazolyl)borate (Tp) and hydrotris(3,5-dimethyl-pyrazolyl)borate (Tp*) due to their relative ease of synthesis and their electron-donating properties.

The most convenient route to scorpionate ligands is via reaction of the borohydride ion $[BH_4]^-$ and the desired pyrazole. By controlling the reaction conditions, this method can be used to form bis-, tris-, and in the case of 5-unsubstituted pyrazoles, tetrakis-(pyrazolyl)borates.[3] During these reactions (Figure 2.1), the amount of hydrogen gas produced depends of whether bis-, tris- or tetrakis-substitution has taken place. As such, the progress of the reaction can be followed by measuring the volume of hydrogen gas produced during the reaction. In the syntheses of the poly(pyrazolyl)borates described below, the volume of gas was measured by the displacement of water from a container.

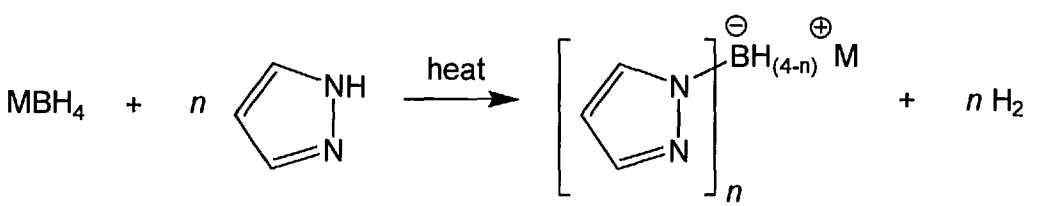


Figure 2.1. Synthesis of poly(pyrazolyl)borates.

2.1.1 Tris(pyrazolyl)borates

i. Synthesis of KTp (2.1)

The Tp ligand **2.1** was synthesised as the potassium salt by heating a 1:4 mixture of KBH_4 and pyrazole in the absence of solvent (Figure 2.2). In addition to the recrystallisation suggested in the literature,[4] increased purity of the final product was

achieved by initial removal of the excess pyrazole from the crude product by vacuum sublimation.

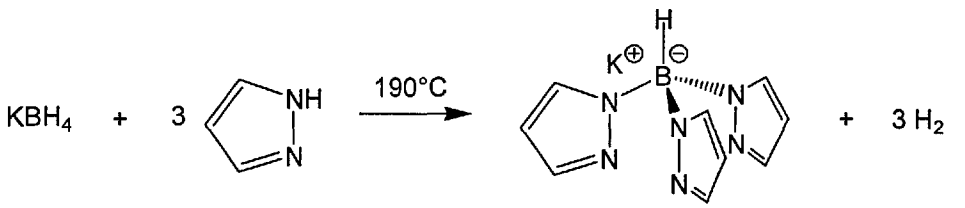


Figure 2.2. Synthesis of KTp (**2.1**).

ii. Synthesis of KTp (2.2)*

The 3,5-dimethyl substituted ligand, KTp* (**2.2**) was synthesised according to the procedure described by Young *et al.*[5] In this reaction tetrasubstitution to form the T_kp^* ligand cannot take place due to the extra steric bulk imposed by the methyl unit in the 5-position of the pyrazole ring (Figure 2.3). Due to the added steric hindrance of the methyl groups, higher temperatures are required to place the three pyrazolyl arms around the central boron. Since tetrasubstitution is hindered, careful control over the temperature is not necessary.

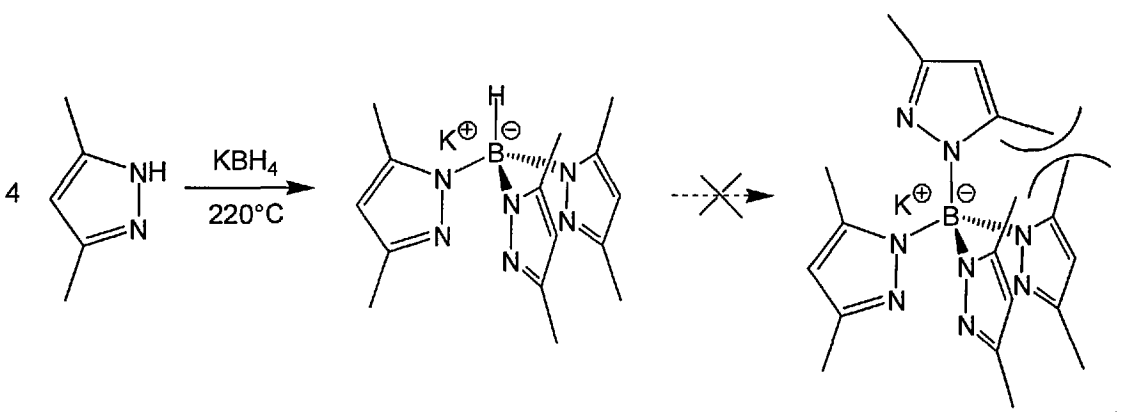


Figure 2.3. Formation of KTp*. Formation of T_kp^* is hindered by steric interactions between 5-methyl substituents.

These reactions proceeded in good yield to obtain the ligand salts as white powders which were pure as judged by ^1H and ^{11}B NMR spectroscopy and elemental analysis. A summary of their NMR and IR spectroscopic data is found in Table 2.3.

2.1.2 Bis(pyrazolyl)borates

The corresponding bis(pyrazolyl)borates were also isolated to aid the characterisation of the Tp analogues and for their potential to be used as precursors in the synthesis of asymmetric scorpionates. These reactions were performed at lower temperatures to minimise unwanted formation of the tri-substituted species.

i. Synthesis of KBp (2.3)

Potassium dihydrobis(pyrazolyl)borate (**2.3**) was prepared using the melt method as described by Trofimenko (Figure 2.4).[4]

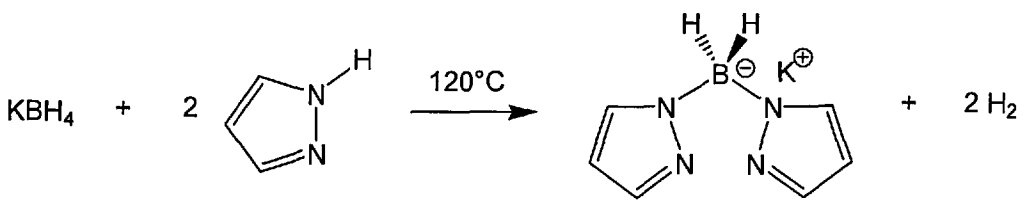


Figure 2.4. Synthesis of KBp (**2.3**).

ii Synthesis of KBp (2.4)*

The 3,5-dimethyl substituted analogue, **2.4** was synthesised using the melt method rather than using refluxing dimethylacetamide as suggested in the literature.[6] In this case, the melt was heated gently to 160°C and the reaction was worked up when two equivalents of H_2 had been evolved. The crude product showed traces of the tris(pyrazolyl) species **2.2** indicating that some over-reaction had occurred. By exploiting the slightly greater ether solubility possessed by KBp* over KTp* it was possible to isolate the desired species by Soxhlet extraction in ether followed by recrystallisation from hot anisole. This yielded a pure sample as judged by ^{1}H and ^{11}B NMR spectroscopy (Table 2.3) and elemental analysis.

2.2 Synthesis of Novel Tp Ligands

2.2.1 Background

From the table summarising all the known Cu[Tp^x]CO complexes (see Chapter 1), the varying pyrazole ring substituents can be split into three categories – electron releasing (alkyl), electron neutral (aryl) and electron withdrawing (bromo or fluorinated alkyl). It is surprising to find that amongst the electron-rich species, only alkyl substituents have been reported and there are no examples of heteroatom-substituted Tp ligands (with the exception of the electron-poor perbromo derivative Tp^{Br3} reported with copper).[7] This survey was subsequently extended to cover all the Tp and T$_k$p ligands produced to date and revealed, somewhat surprisingly, that no scorpionate ligands containing direct substitution of S, O, P or N onto all the pyrazolyl rings have been reported.

Adam *et al.*[8] have reported one example of a mono-hydroxylated Tp system in which a 4-hydroxy substituent has been introduced onto one pyrazolyl ring of the Tp* ligand. In this report, Tp*-stabilised allyl- and vinyl-tungsten oxides were treated with oxidising agents to examine the epoxidation products. In one case it was found that the more reactive oxidant, methyl(trifluoromethyl)dioxirane, would avoid epoxidation of the shielded vinylic double bond in favour of hydroxylation of one pyrazolyl rings (Figure 2.5).

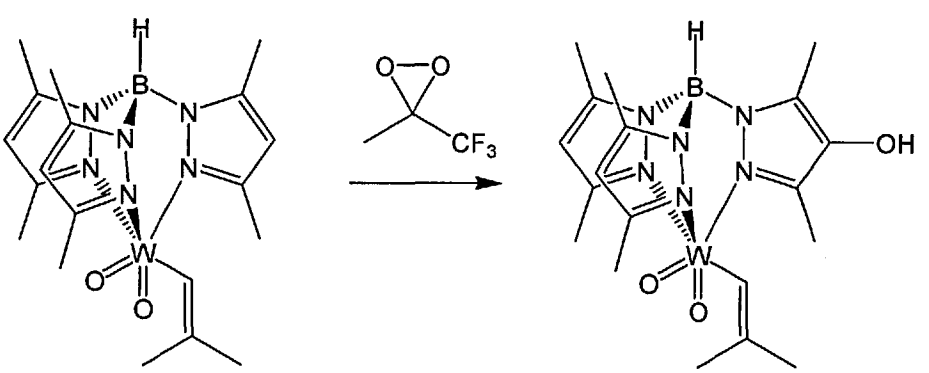


Figure 2.5. Formation of mono-hydroxylated Tp* ligand.

This absence of any symmetrical, heteroatom-substituted poly(pyrazolyl)borates was attributed to the relatively few examples of heteroatom-substituted pyrazoles in the

literature, and the obscure journals in which they often appear. It was also not known whether these functionalised pyrazoles are stable at the high temperatures involved during ligand synthesis, or if unwanted side reactions with the borohydride anion would occur. These heteroatom-substituted Tps could have novel electronic and coordinating properties. They may be more electron-rich than their alkyl-substituted counterparts due to the resonance effect in which the lone pairs are donated into the aromatic π-system (Figure 2.6). As such, the synthesis of alkoxy- and alkylthio-substituted pyrazoles was investigated.

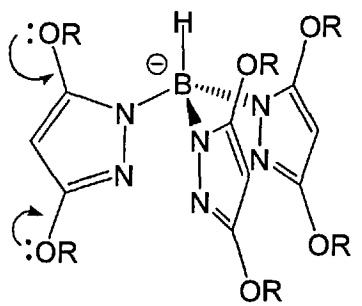


Figure 2.6. Resonance effects in 3,5-alkoxy-substituted Tp ligands.

2.2.2 Attempted Synthesis of Alkoxy-Substituted Tp

The 3,5-di-alkoxy-substituted pyrazoles (Figure 2.7; R = OMe, OEt) were chosen as potential precursors to novel electron-rich scorpionates. It has been reported by Kollipara *et al.*[9] that 3,5-dimethoxy- and 3,5-diethoxy-pyrazoles could be prepared via the condensation reaction between the corresponding diketone and hydrazine hydrate (Figure 2.7). This is a well-known reaction for the synthesis of alkyl-substituted pyrazoles (R = alkyl).

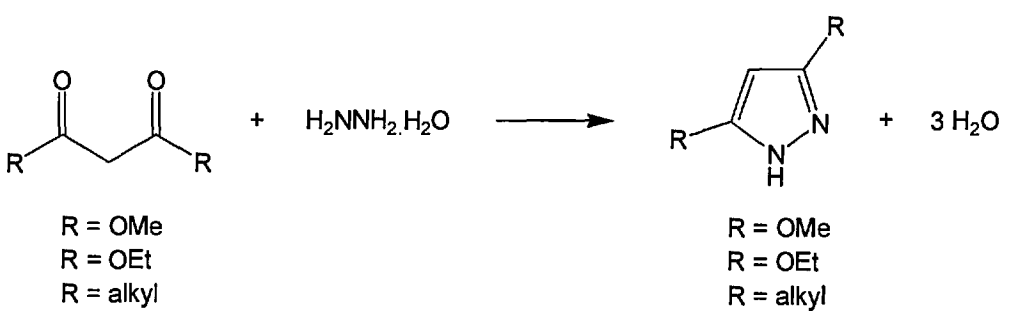


Figure 2.7. Proposed synthesis of 3,5-disubstituted pyrazoles.

The above reaction (R = OEt) was performed accordingly to produce a white solid precipitate that was expected to be the desired pyrazole. Examination of the solubility of this compound (**2.5**) revealed that it was completely insoluble in organic solvents but soluble in water. This was an unexpected observation given that alkyl-substituted pyrazoles are highly soluble in a range of polar organic solvents (e.g. acetone, ether, CH_2Cl_2, MeOH etc.). Elemental analysis of **2.5** (Table 2.1) suggested that the hydrazide shown in Figure 2.8 had formed preferentially. This was further supported by mass spectrometry, in which the molecular ion of the hydrazide was observed at 132 m/z.

Table 2.1. Elemental analysis of compound **2.5** versus predicted values of the pyrazole and hydrazide

		% C	% H	% N
Calc. for $C_7H_{12}N_2O_2$	(pyrazole)	53.8	7.74	17.9
Calc. for $C_3H_8N_4O_2.H_2O$	(hydrazide)	24.0	6.71	37.3
Found for compound **2.5**		25.2	6.84	38.3

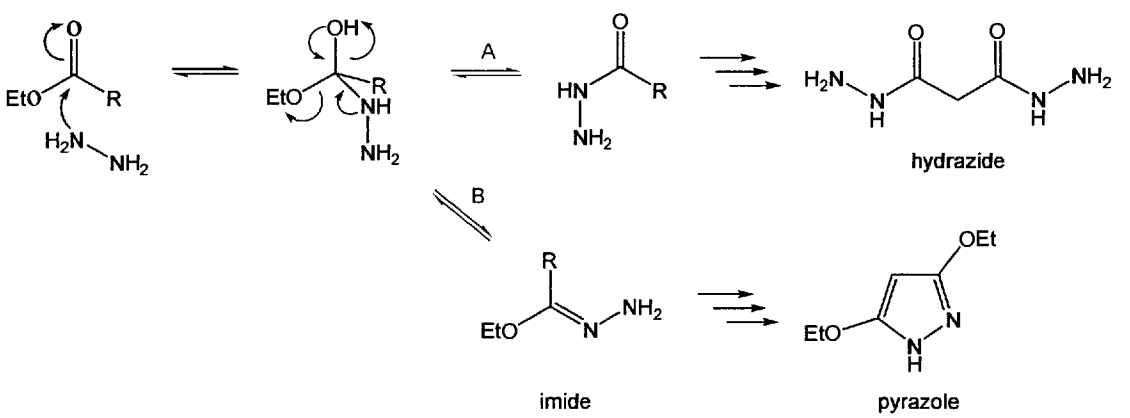


Figure 2.8. Suggested mechanism of amide/pyrazole formation.

By looking at the mechanistic pathways possible (Figure 2.8), it soon became clear that the reaction could not give the desired product. Attack of the hydrazine on the carbonyl group first forms a tetrahedral intermediate. This can then react via two separate pathways: when there is no competing leaving group, pathway B would occur in which collapse of the nitrogen lone pair and loss of H_2O forms the intermediate imide. This can then ring-close, by the intramolecular reaction of the

remaining -NH_2 group with the other carbonyl group, to form the pyrazole. In this case though, the presence of the ethoxy leaving group means that pathway A is followed. In this route, the ethoxy group leaves preferentially to the hydroxyl group thus forming the unwanted hydrazide derivative, **2.5**. This proposed product formation is supported by a paper published in *Acta Poloniae Pharmaceutica*,[10] in which this same hydrazide was synthesised under similar conditions.

2.2.3 Synthesis of Methylthio-Substituted Tp

i. Synthesis of 5(3)-methylthio-pyrazole (2.7)

Junjappa *et al.* reported in 1975 that 5(3)-methylthio- and alkoxy-pyrazoles could be synthesised in one step from α-ketoketene-*S,S*-diacetals.[11] These α-ketoketene-*S,S*-diacetals are themselves made in one step from commercially available starting materials, namely an acetyl-arene, carbon disulphide and methyl iodide.[12, 13] This pyrazole was proposed to be incorporated into a new methylthio-substituted Tp ligand according to the scheme shown in Figure 2.9.

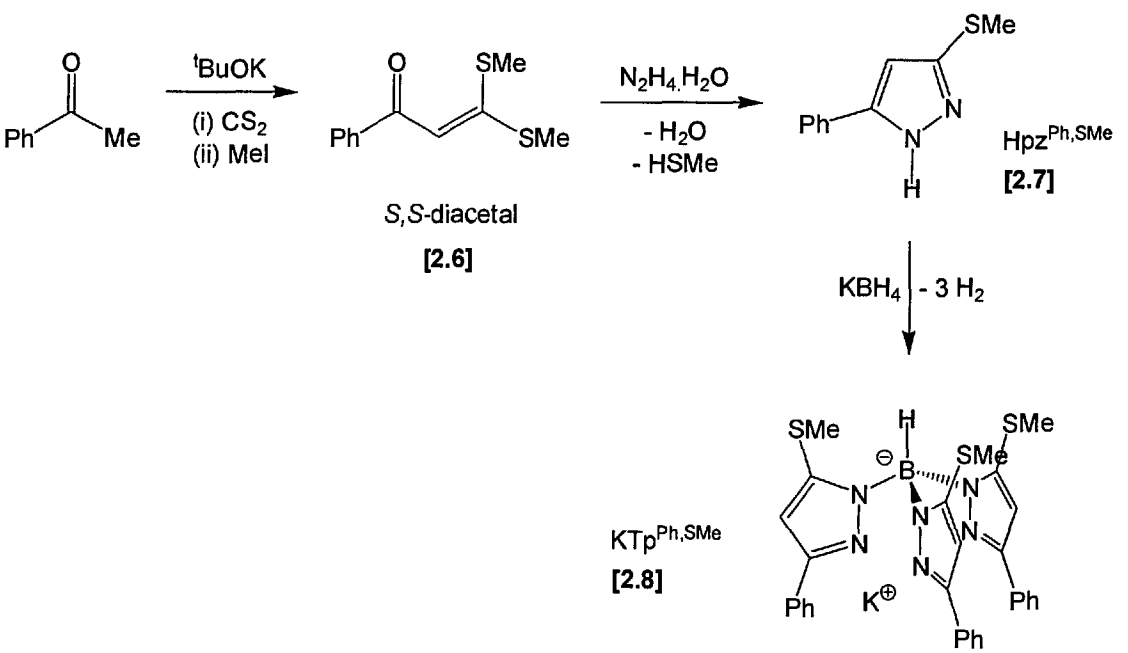


Figure 2.9. Synthetic pathway to new Tp species, K[$Tp^{Ph,SMe}$] (**2.8**).

The *S,S*-diacetal (**2.6**) was synthesised accordingly in 51 % yield and characterised by ^{1}H NMR spectroscopy. Subsequent reaction with hydrazine hydrate yielded the 3(5)-

phenyl-5(3)-methylthiopyrazole (**2.7**) in 80 % yield (lit.[11] 88 %) as confirmed by mass spectrometry ($[M]^+$ = 190 m/z) and ^{1}H NMR spectroscopy (Figure 2.10).

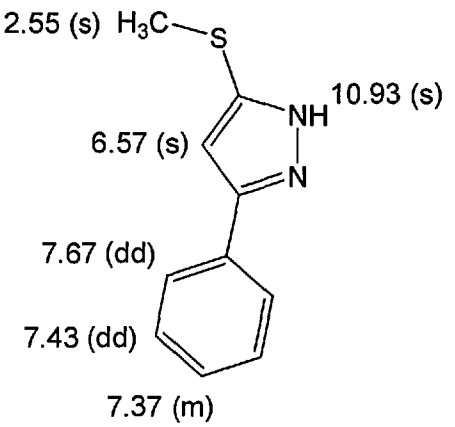


Figure 2.10. ^{1}H NMR environments in 3(5)-phenyl-5(3)-methylthiopyrazole (**2.7**).

ii. Synthesis and characterisation of K[Tp^{Ph,SMe}] (2.8)

The next step was the unreported conversion of this pyrazole to the corresponding tris(pyrazolyl)borate via the reaction with KBH_4. Given the unknown stability of **2.7** towards the borohydride anion and high reaction temperatures, it was decided to carry out this reaction under a nitrogen atmosphere to avoid oxidation/decomposition of the product. The 3,5-disubstitution pattern of **2.7** meant that over-reaction to form the tetrakis(pyrazolyl)borate was not possible. As such, a finely ground mixture of **2.7** and KBH_4 in a 5:1 molar ratio were heated gradually to 220°C followed by stirring for two hours at this temperature (Figure 2.11).

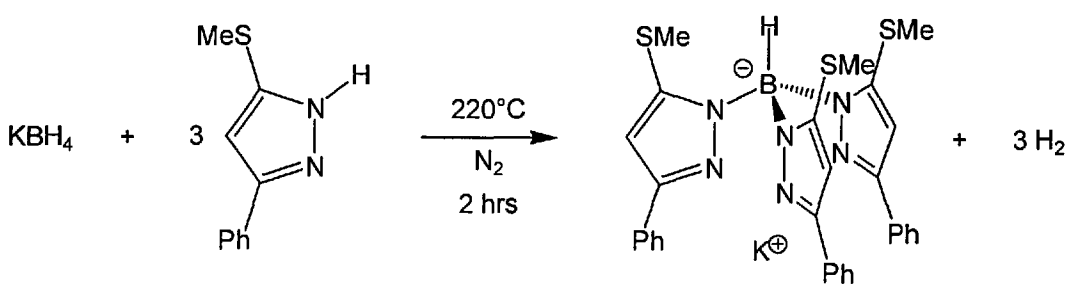


Figure 2.11. Synthesis of K[Tp^{Ph,SMe}] (**2.8**).

The white product precipitated during this reaction was found to be insoluble in ethanol (unlike the pyrazole starting material) indicating that the reaction had proceeded. Recrystallisation from THF/hexane gave **2.8** as a white powder in 66 % yield. Mass spectrometry (ESI –ve) confirmed the presence of the desired Tp anion ($[M]^-$ = 579 m/z). ^{1}H NMR spectroscopy (Figure 2.12) further confirmed the formation of the desired species.

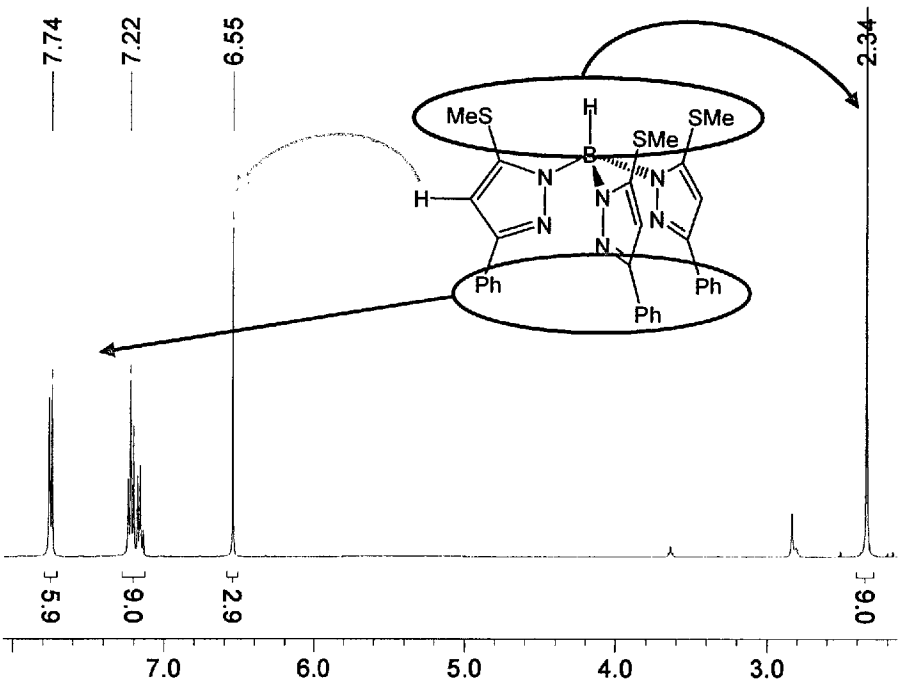


Figure 2.12. ^{1}H NMR spectrum of K[Tp^{Ph,SMe}] (**2.8**).

Upon formation of the tris(pyrazolyl)borate species the NH peak of the starting material (**2.7**) is no longer observed. A broad multiplet spread over the baseline is instead found at 5.43 ppm, corresponding to the new BH proton. Upon formation of the Tp ligand the 4-pyrazolyl proton is virtually unmoved, while the S-methyl protons shift upfield from 2.55 to 2.34 ppm.

The ^{11}B NMR spectrum produced a slightly broadened singlet at -5.6 ppm. In this case, a doublet was expected due to coupling to the adjacent proton. This broadening was attributed to possible weak H-bonding to the nearby sulphur atoms.

iii. Predicted regiochemistry

It is generally accepted that during poly(pyrazolyl)borate synthesis, steric factors control the regiochemistry of the resultant ligand. This is a consequence of the relative energies of the five-centre transition state that occurs during the formation of the pyrazole-boron bond. Since bulky pyrazolyl substituents in the proximity of the forming bond are energetically disfavoured, 3-substituted pyrazoles give rise to ligands in which the boron is bonded to the least sterically hindered nitrogen of the pyrazolyl ring (Figure 2.13). This results in a scorpionate in which the substituent ends up in the 3-position.

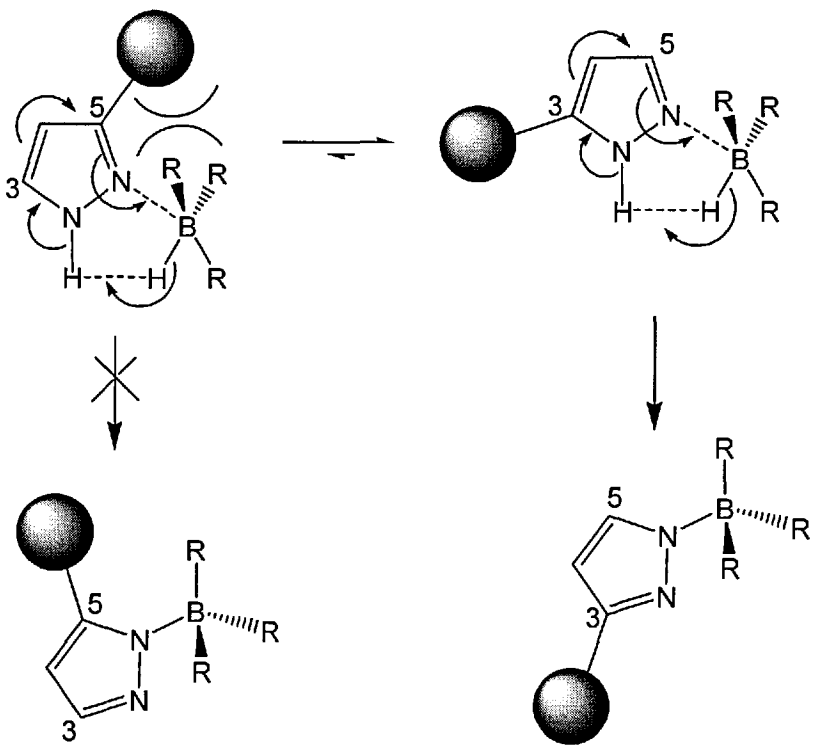


Figure 2.13. Steric clash (top left) between substituted pyrazole and boron moieties during scorpionate formation, resulting in 3-substituted species (bottom right).

The same effect occurs in 3,5-disubstituted pyrazoles whereby the boron will bind to the nitrogen atom adjacent to the smaller substituent, causing the bulkier group to end up in the 3-position. As such, it was estimated that in the case of **2.7**, the phenyl group would occupy the 3-position in the resultant Tp ligand (**2.8**) as it is larger than the S–Me group.

iv. Synthesis of Tl[Tp^{Ph,SMe}] (2.9)

To confirm the regiochemistry of this ligand, structural characterisation by X-ray crystallography was sought. Tp ligands are conventionally converted to their thallium salts for structural characterisation as a result of their crystallinity and organic solubility. As such, the corresponding thallium complex was obtained by 1:1 reaction of **2.8** and thallium nitrate (Figure 2.14).

$$K[Tp^{Ph,SMe}] + TlNO_3 \longrightarrow Tl[Tp^{Ph,SMe}] + KNO_3$$

Figure 2.14. Synthesis of Tl[Tp^{Ph,SMe}] (**2.9**).

This reaction proceeded cleanly and in high yield (84 %) and the product, **2.9**, was found to be pure by ^{1}H and ^{11}B NMR spectroscopy. The ^{11}B NMR revealed a broad singlet, now slightly shifted to -6.9 ppm. The ^{1}H NMR spectrum showed this BH proton as a characteristically broad multiplet spread over the baseline centred at 5.41 ppm. To confirm the coupling to boron, the $^{1}H\{^{11}B\}$ NMR spectrum was recorded, causing this peak to become significantly sharper (Figure 2.15).

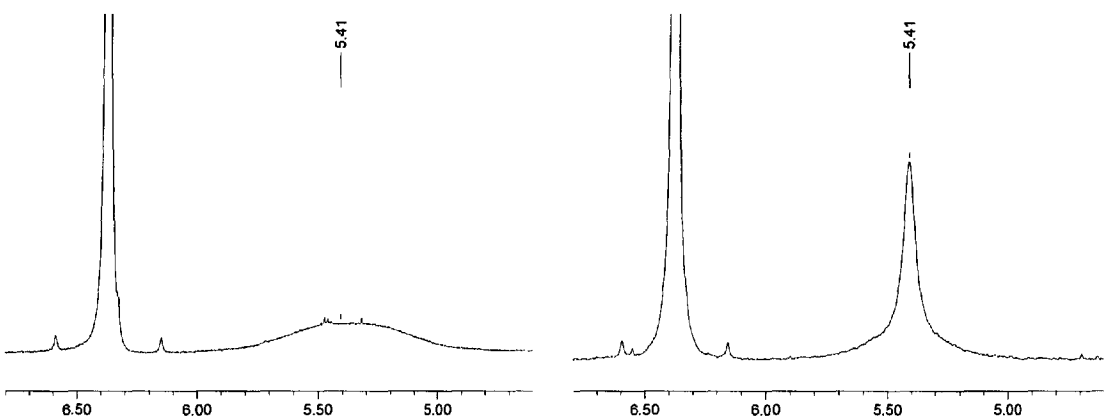


Figure 2.15. Close-up ^{1}H (left) and $^{1}H\{^{11}B\}$ (right) NMR spectra of **2.9**.

v. X-ray analysis

Single crystals of **2.9** were obtained by diffusion of pentane vapour into a chloroform solution and the solid-state structure was determined by X-ray crystallography.

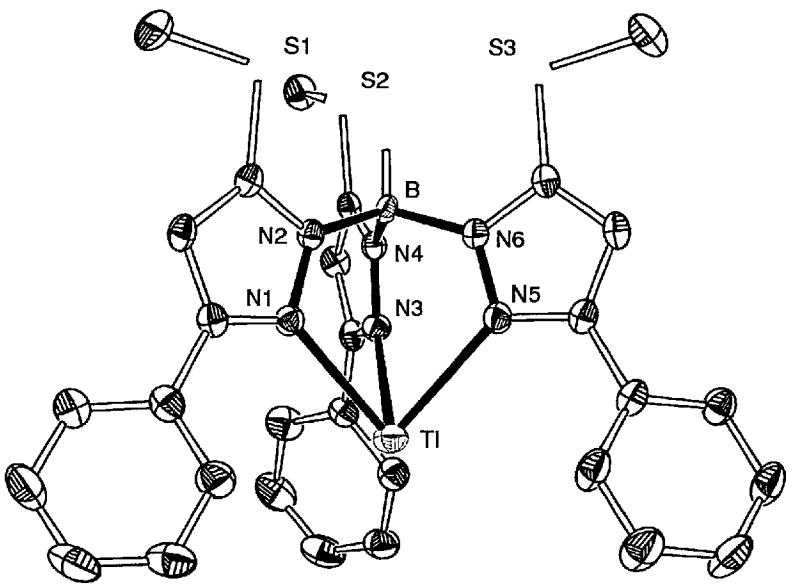


Figure 2.16. Molecular structure of Tl[$Tp^{Ph,SMe}$] (**2.9**) (50 % probability ellipsoids).

The solid state structure of **2.9** (Figure 2.16) shows the tridentate ligand adopting a near C_3 symmetric arrangement about the B···Tl axis. The B···Tl separation is 3.612(2) Å (the metal lying *ca.* 1.83 Å out of the {N(1),N(3),N(5)} plane). Similarly, in a close literature analogue, Tl[Tp^{Ph}],[14] the B···Tl separation is *ca.* 3.61 Å. A list of selected bond lengths and angles for **2.9** is given in Table 2.2.

Table 2.2. Selected bond lengths (Å) and angles (°) for Tl[$Tp^{Ph,SMe}$] (**2.9**)

Tl–N(1)	2.6100(19)	Tl–N(3)	2.5594(16)
Tl–N(5)	2.5910(16)	N(3)–N(4)	1.370(2)
N(1)–N(2)	1.375(2)	B–N(2)	1.555(3)
N(5)–N(6)	1.372(2)	B–N(6)	1.547(3)
B–N(4)	1.521(3)	Tl···B	3.612(2)
N(1)–Tl–N(3)	74.78(5)	N(1)–Tl–N(5)	76.01(5)
N(2)–B–N(4)	111.26(16)	N(3)–Tl–N(5)	75.66(5)
N(4)–B–N(6)	111.75(18)	N(2)–B–N(6)	111.48(15)

The structure shows that the phenyl groups are found in the 3-position of the pyrazolyl rings, and the methylthio groups are in the 5-position. This is in agreement with the predictions made upon steric grounds. This particular regiochemistry might be further encouraged by electronic effects in which the electron-releasing S–Me group increases the nucleophilicity of its vicinal nitrogen atom, thus making it more reactive towards boron.

Recently Trofimenko *et al.*[15] reported the first exception to the steric rule, whereby an atypical Tp ligand (Figure 2.17, right) was formed in which the bulkier group is found in the 5-position of the pyrazolyl ring.

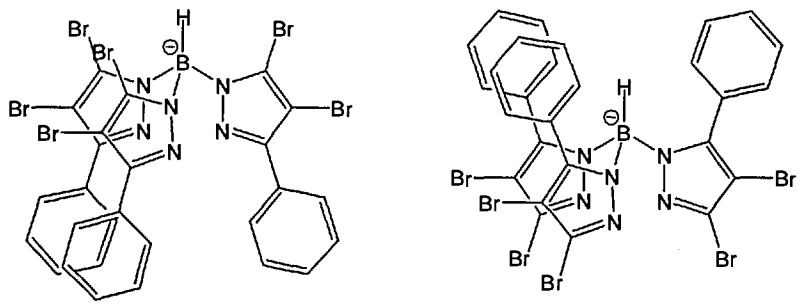


Figure 2.17. Normal (left) and atypical (right) geometries for the [$Tp^{Br,Ph,Br}$] ligand.

The formation of this atypical structure is proposed to result from electronic factors which surpass the unfavourable steric repulsions. The electronic effect occurs during the formation of the N-B bond, whereby the most electron rich nitrogen of pyrazole is preferred to bond to the boron atom. Since the phenyl group imparts greater electron density on its vicinal nitrogen atom than the outer bromine, the N-B bond forms from the nitrogen atom nearest the phenyl ring despite it being the most sterically demanding substituent.

2.2.4 Summary

Table 2.3 contains a summary of the ^{1}H, ^{11}B and IR spectroscopic data of the three Tp and two Bp ligands synthesised.

Table 2.3. Summary of NMR and IR spectroscopic data for K[Scorpionate] species **2.1-2.4** and **2.8**

Ligand	Pz-substituent		δ ^{1}H / ppm			δ ^{11}B/ ppm	νBH/ cm^{-1}
	3-	*5-*	*3-*	*4-*	*5-*		
2.1[a] KTp	*H*	*H*	7.40	6.33	7.66	-2.4 (d)	2437[c]
2.2[b] KTp*	*Me*	*Me*	2.01 (Me)	5.53	2.17 (Me)	-7.9 (d)	2438[c]
2.8[b] K[Tp^{Ph,SMe}]	*Ph*	*S-Me*	7.8-7.1 (Ph)	6.55	2.34 (SMe)	-5.6 (s-br)	2448[c]
2.3[a] KBp	*H*	*H*	7.54	6.25	7.67	-5.3 (t)	2433[c] 2402
2.4[b] KBp*	*Me*	*Me*	2.02 (Me)	5.49	2.22 (Me)	-12.2 (t)	2592

(a) D_2O solution; (b) d_6-acetone solution; (c) KBr disc.

The ^{1}H chemical shift of the 4-pyrazolyl protons appears to reflect the 'electron-richness' of the scorpionate ligands. Going from Bp to Bp* and Tp to Tp*, the chemical shift of these protons move 0.76 and 0.80 ppm upfield, respectively. This is attributed to the addition of electron-releasing methyl substituents which result in more shielded pyrazolyl protons. The 4-pyrazolyl proton of Tp^{Ph,SMe} (**2.8**), is found furthest downfield of all the Tp ligands (6.55 ppm). This suggests that the ligand may not be as electron-rich as anticipated. In order to gain further information on ligand electronics and their potential to be applied to CO trapping, their respective copper(I) carbonyls were synthesised.

2.3 Synthesis of Copper Carbonyls

The Cu[Tp^{x}]CO species were formed by bubbling CO through a solution of the K[Tp^{x}] salt and CuCl in THF solution (Figure 2.18). These reactions must be performed under anaerobic conditions as oxidation of Cu[Tp^{x}]CO solution occurs quickly in air. Despite this, the solids, when isolated, are fairly air stable.

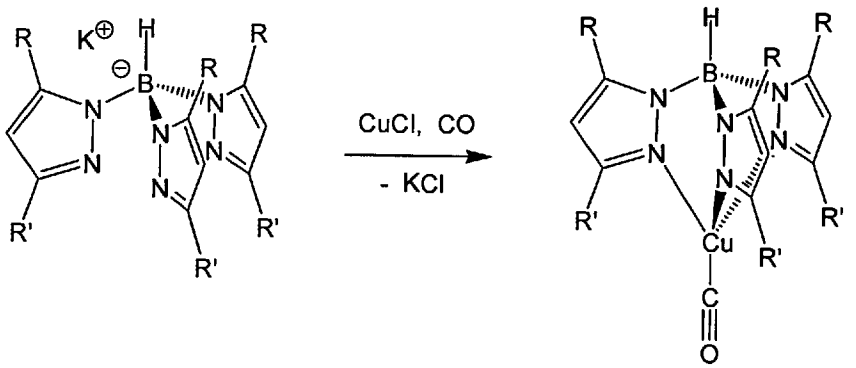


Figure 2.18. Carbonylation of Tp^x ligands with Cu(I).

2.3.1 Synthesis of CuTpCO (2.10)

CuTpCO (**2.10**) (R = R' = H in Figure 2.18) was formed from KTp (**2.1**) and isolated in 94 % yield. The ^1H and ^{11}B NMR and IR spectroscopic data for this complex are summarised in Figure 2.19.

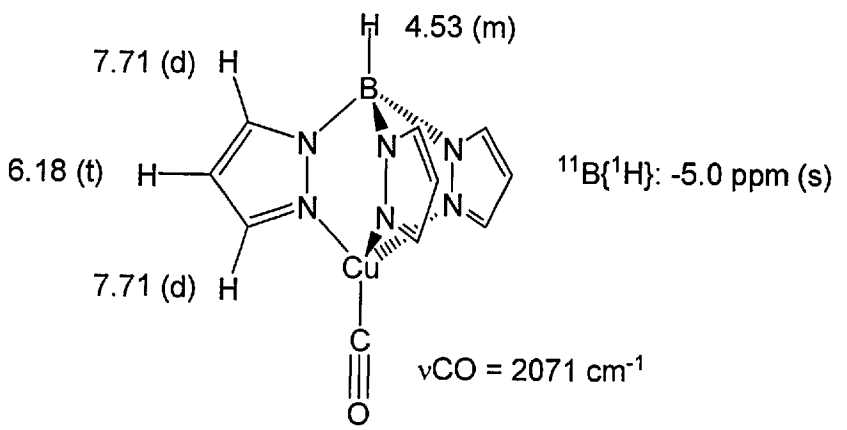


Figure 2.19. Summary of ^1H, ^{11}B and IR spectroscopic data of CuTpCO (**2.10**).

Upon formation of the copper carbonyl complex, the 3- and 5-pyrazolyl protons coincide on the ^1H NMR to give overlapping doublets at 7.71 ppm. The 4-pyrazolyl proton is observed as a pseudo-triplet at 6.18 ppm as a result of ^3J coupling to the 3- and 5- pyrazolyl protons. In forming the carbonyl, the CO stretch is lowered in frequency from that of free CO (2143 cm^{-1}) to 2077 cm^{-1} due to backbonding from the copper d-orbital to the CO π^* orbital.

2.3.2 Synthesis of CuTp*CO (2.11)

CuTp*CO (**2.11**) (R = R' = Me in Figure 2.18) was formed from KTp* (**2.2**). The ^{1}H and ^{11}B NMR and IR spectroscopic data for this complex are summarised in Figure 2.20.

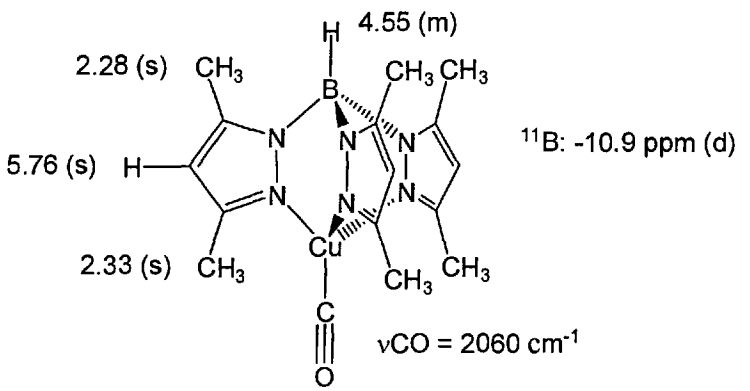


Figure 2.20. Summary of ^{1}H, ^{11}B and IR spectroscopic data of CuTp*CO (**2.11**).

2.11 was isolated as a white solid which is more air-stable that the unsubstituted species, CuTpCO (**2.10**) due to the increased steric bulk of the methyl groups that protect the copper centre. Electronic effects also strengthen the Cu-CO bond as judged by IR spectroscopy and NMR spectroscopy (Figure 2.20). νCO of this complex (2060 cm^{-1}) is 11 cm^{-1} lower than that of **2.10**. This reduction in νCO reflects an increase in donation of electron density from filled copper d-orbitals into CO π*-orbitals. This is caused by the inductive effect of the methyl groups in the 3- and 5-positions, which impart greater electron density into the system.

Under normal conditions, it is not possible to observe the carbonyl ligand in the ^{13}C NMR spectrum due to the low natural abundance of ^{13}CO and the broadening of the signal. In order to observe the carbonyl ligand, a sample of **2.11** was prepared using ^{13}C-enriched CO. The resultant spectrum (Figure 2.21) shows an interesting splitting pattern centred at 177.3 ppm resulting from coupling of ^{13}C to the two spin active isotopes of copper.

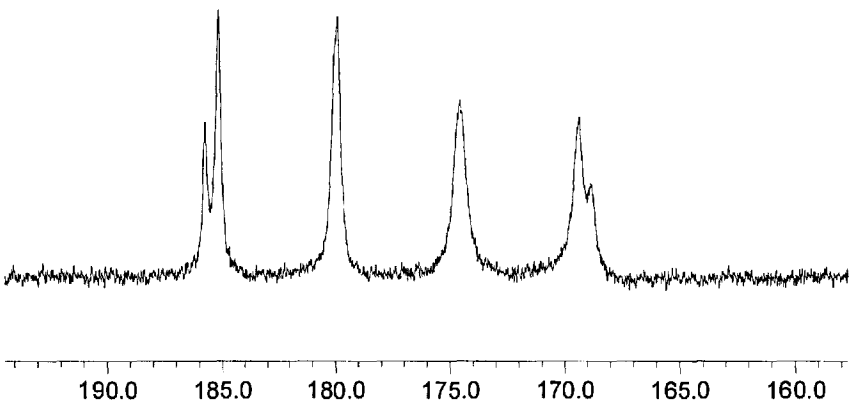


Figure 2.21. Upfield region of $^{13}C\{H\}$ NMR spectrum of CuTp*^{13}CO (**2.12–^{13}C**).

These isotopes, ^{63}Cu (I = 3/2, abundance = 69 %, γ = 7.11) and ^{65}Cu (I = 3/2, abundance = 31 %, γ = 7.60) result in two overlapping 1:1:1:1 quartets. Coupling to ^{63}Cu (^1J = 660 Hz) produces the more intense quartet due to its higher natural abundance. Coupling to ^{65}Cu causes larger splitting (^1J = 709 Hz) due to its greater gyromagnetic ratio and this is observed by the shoulder peaks at each extreme (the inner most ones overlap with the ^{63}Cu signals).

The only other literature example studying similar Cu[Tp^x]CO complexes is reported by Fujisawa *et al.*[16] They observed a similar splitting pattern for the complexes Cu[Tp^{2iPr}]CO and Cu[Tp^{tBu,iPr}]CO but interestingly reported that the complex Cu[Tp^{2Ph}]CO only produces one broad ^{13}C-signal at 173.8 ppm.

The ^{13}C NMR signal of ^{13}CO gas (in CH_2Cl_2) is observed at 184 ppm, hence an upfield shift of 7 ppm occurs upon binding to the copper(I) ion.[17] This is in contrast to the ^{13}C NMR signals of ^{13}CO bound to iron-heme units which are detected downfield of free ^{13}CO at approximately 200 ppm.[18, 19]

2.3.3 Synthesis of Cu[Tp^{Ph,SMe}]CO (2.12)

This new copper carbonyl species, Cu[Tp^{Ph,SMe}]CO (**2.12**) (R = SMe, R' = Ph in Figure 2.18) , was obtained as a white, reasonably air-stable solid in moderate yield (60 %). ESI +ve mass spectrometry showed $[M\text{-}CO]^+$ at 581 m/z and its purity was

confirmed by ^{1}H NMR, ^{11}B NMR and IR spectroscopy (Figure 2.22) as well as elemental analysis.

i. *IR spectroscopy*

The carbonyl stretch (νCO) of **2.12** was observed at 2087 cm^{-1}. This fairly high value may be caused by poor orbital overlap between the sulphur lone pair (third row element) and the conjugated π-system of the pyrazolyl ring (second row elements). As such the inductive electron withdrawing effect of the fairly electronegative sulphur atom is thought to outweigh the weak electron-releasing resonance effect. The presence of the weakly electron-withdrawing phenyl group in the 3-position may also contribute to this effect.

ii. NMR spectroscopy

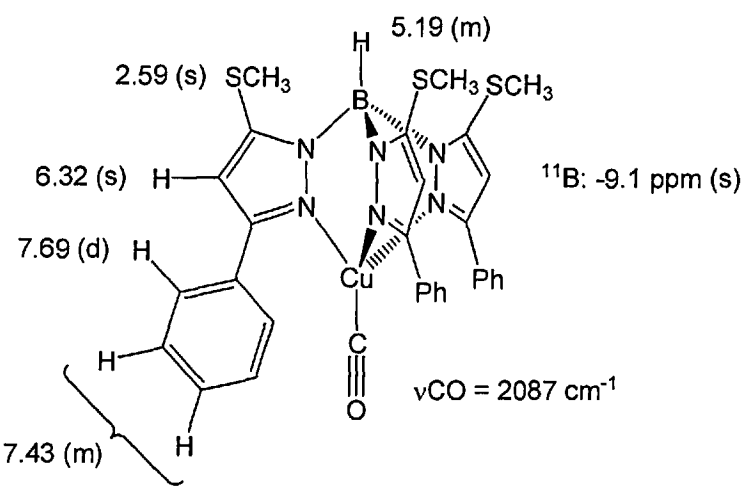


Figure 2.22. Summary of ^{1}H, ^{11}B and IR spectroscopic data of Cu[$Tp^{Ph,SMe}$]CO (**2.12**).

The $^{13}C\{^{1}H\}$ NMR spectrum of **2.12** was recorded using a sample prepared from ^{13}C-enriched CO (Figure 2.23). In contrast to the Tp* species, the ^{13}CO resonance is observed as a broad singlet at 174.8 ppm. This might be caused by fast quadrupole relaxation processes of the adjacent copper(I) nucleus.

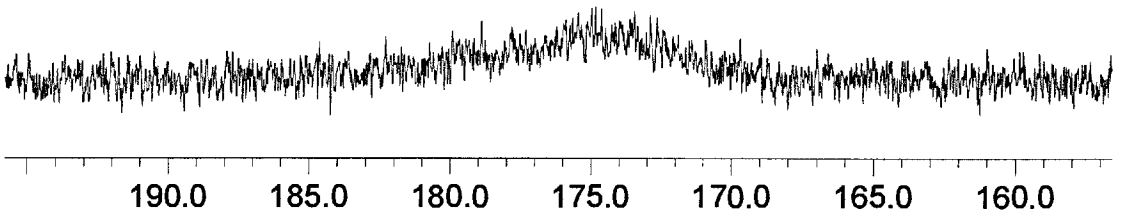


Figure 2.23. Carbonyl region of the $^{13}C\{^{1}H\}$ NMR spectrum of $Cu[Tp^{Ph,SMe}]^{13}CO$ (**2.12**–^{13}**C**).

iii. X-ray analysis

The solid-state structure of **2.12** (Figure 2.24) was obtained from crystals grown by slow evaporation of a DCM solution.

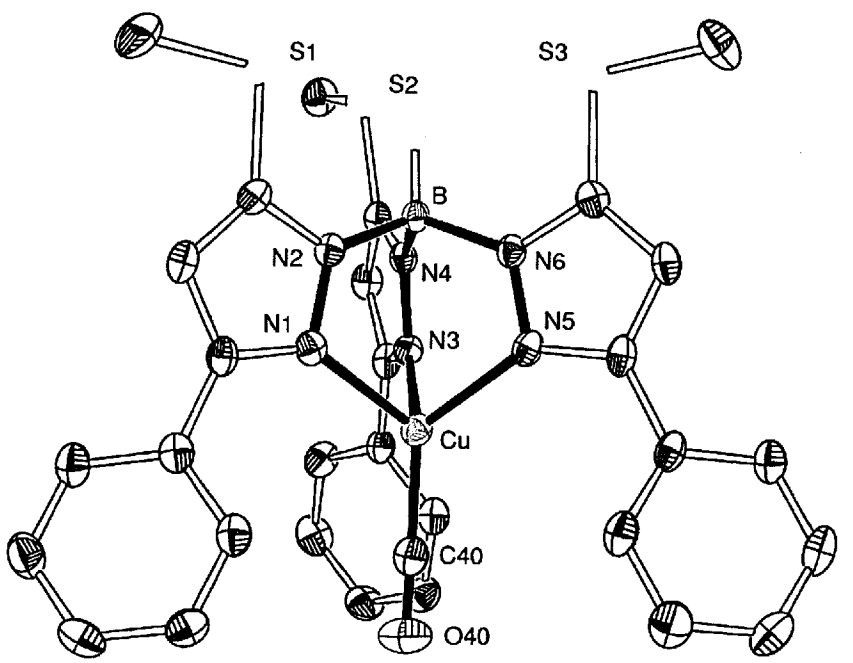


Figure 2.24. Molecular structure of $Cu[Tp^{Ph,SMe}]CO$ (**2.12**) (50 % probability ellipsoids).

In **2.12** the ligand binds in a tridentate fashion to the copper in a near C_3 symmetric arrangement about the B···Cu axis. The carbonyl ligand binds at the fourth coordination site to form a tetrahedron about this metal. This 'head on' coordination is slightly distorted, the angle between C(40), Cu and the {N(1),N(3),N(5)} centroid being *ca.* 175.6°. The carbonyl unit itself is also slightly bent, with a Cu–C(40)–O(40) angle of 178.5(3). A list of selected bond lengths and angles is given in Table 2.4.

Table 2.4. Selected bond lengths (Å) and angles (°) for Cu[$Tp^{Ph,SMe}$]CO (**2.12**)

Cu–N(1)	2.074(2)	Cu–N(3)	2.072(2)
Cu–N(5)	2.051(2)	Cu–C(40)	1.794(3)
N(1)–N(2)	1.377(3)	N(3)–N(4)	1.371(3)
N(5)–N(6)	1.377(3)	B–N(2)	1.539(3)
B–N(4)	1.549(3)	B–N(6)	1.537(3)
C(40)–O(40)	1.128(3)	Cu···B	3.014(3)
N(1)–Cu–N(3)	91.39(8)	N(1)–Cu–N(5)	93.24(8)
N(1)–Cu–C(40)	122.41(10)	N(3)–Cu–N(5)	91.64(8)
N(3)–Cu–C(40)	121.58(10)	N(5)–Cu–C(40)	127.15(10)
N(2)–B–N(4)	108.2(2)	N(2)–B–N(6)	110.3(2)
N(4)–B–N(6)	109.38(19)	Cu–C(40)–O(40)	178.5(3)

iv. Comparison of solid-state structures

In both complexes, all three of the BN_4M six-membered chelate rings have boat conformations with the N_4 atoms near coplanar and the boron and the metal centres out of plane. For each arm of the Tp ligand the S–Me unit is near coplanar with its associated pyrazolyl ring, the S(1)–C, S(2)–C and S(3)–C torsion angles being *ca.* 2, 6 and 4° respectively in **2.9**, and *ca.* 1, 6 and 1° respectively in **2.12**. This suggests significant overlap of a sulphur lone pair with the π-system of its adjacent pyrazolyl ring. The phenyl rings by contrast are noticeably twisted with respect to their parent pyrazolyl rings, the C–Ph torsion angles for the N(1), N(3) and N(5) arms being *ca.* 33, 35 and 36° respectively in **2.9**, and *ca.* 36, 31 and 34° respectively in **2.12**.

The B···Cu separation in the copper species (**2.12**) is 3.014(3) Å (the metal lying *ca.* 1.15 Å out of the {N(1),N(3),N(5)} plane). This is situated *ca.* 0.6 Å closer to the metal than the corresponding thallium species (**2.9**) in which the B···Tl separation is 3.612(2) Å (the metal lying *ca.* 1.83 Å out of the {N(1),N(3),N(5)} plane). In a close literature analogue to **2.12**, Cu[Tp^{2Ph}]CO,[20] the B···Cu separation is *ca.* 3.08. The M–N bond lengths in **2.12** are *ca.* 0.5 Å shorter than the corresponding thallium complex **2.9**.

The differences in metal position between **2.9** and **2.12** are associated with a pseudo "grabbing" distortion of the tridentate ligand (Figure 2.25). In the copper complex each of the three arms of the ligand are tilted towards the copper centre *cf.* the thallium centre in **2.9**, resulting in the pendant phenyl rings being pulled "inwards"

and the S–Me units being pushed "outwards"; the average separation between the phenyl ring centroids is *ca.* 8.02 Å in **2.9** *cf.* 7.58 Å in **2.12**, whilst the average separation between the sulphur atoms is *ca.* 4.28 Å in **2.9** *cf.* 4.51 Å in **2.12**.

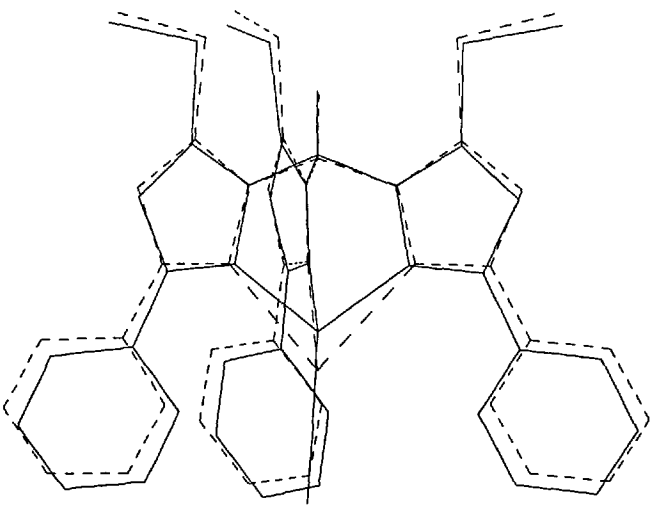


Figure 2.25. Overlay of the structures of **2.9** (dashed bonds) and **2.12** (solid line bonds) showing the similarities, and differences, in the ligand conformations.

It is interesting to note that the unit cells of the two complexes are somewhat similar; they are both monoclinic with space group $P2_1/c$, and for **2.9** a = 12.8755(2), b = 14.4834(2), c = 17.3040(3) Å, β = 109.588(2)°, V = 3040.12(8) Å^3, whilst for **2.12** a = 12.8579(3), b = 14.7465(3), c = 17.5158(4) Å, β = 111.388(3)°, V = 3092.43(12) Å^3. It is therefore not surprising that the two structures show the same packing pattern. In each case adjacent molecules are held together by a series of C–H···π interactions involving the pendant phenyl rings.

2.3.4 Summary of Carbonyls

Selected spectroscopic data for the three carbonyl complexes, **2.10** – **2.12**, are shown in Table 2.5.

Table 2.5. Summary of spectroscopic data for Cu[Tp^x]CO species, **2.10-2.12**

Complex	Pz-substituent		^{1}H NMR δ/ppm			δ ^{11}B/ ppm	δ ^{13}CO/ ppm	νCO/ cm^{-1}
	3-	*5-*	*3-*	*4-*	*5-*			
2.10[a] CuTpCO	H	H	7.71	6.18	7.71	-5.0	-	2071[c]
2.11[b] CuTp*CO	Me	Me	2.33 (Me)	5.76	2.28 (Me)	-10.9[a]	177.3 (m)	2060[c]
2.12[b] Cu[Tp^{Ph,SMe}]CO	*Ph*	*SMe*	2.59 (SMe)	6.32	7.7-7.4 (Ph)	-9.1	174.8 (s)	2087[c]

(a) d_6-acetone solution; (b) CD_2Cl_2 solution; (c) KBr disc.

The ^{1}H chemical shift of the 4-pyrazolyl proton is found furthest upfield for Tp* (5.76 ppm), followed by Tp (6.18 ppm), while the corresponding proton in Tp^{Ph,SMe} is found furthest downfield (6.32 ppm). This matches the trend in νCO (Figure 2.26) in which the lowest stretch is observed with Tp* (green - 2060 cm^{-1}), followed by Tp (orange - 2071 cm^{-1}), then Tp^{Ph,SMe} (red - 2087 cm^{-1}).

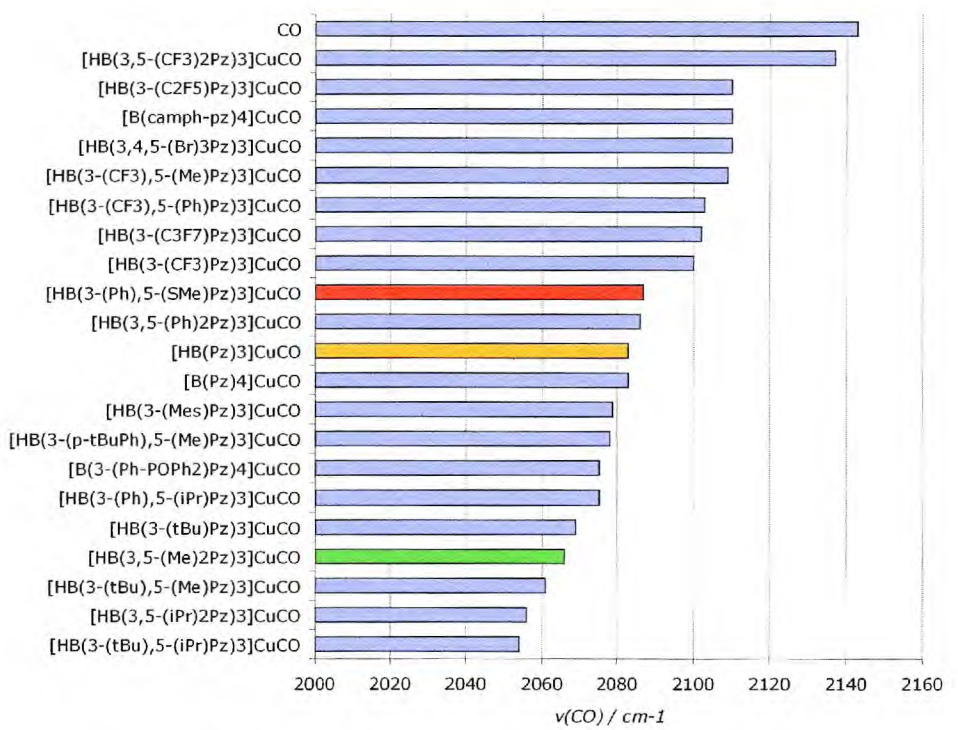


Figure 2.26. Graph of νCO of known copper(I) scorpionate carbonyls.

These trends give an insight into the relative 'electron-richness' of the ligands tested and their relative position amongst the other known scorpionate ligands. Out of the three tested, Tp*, was chosen for subsequent carbonylation studies due to its favourable donor properties.

2.4 Rapid Carbonylation Reactions

2.4.1 Background

Having selected a system for CO trapping, its suitability to the conditions of the radiolaboratory was explored using unlabelled CO. One of the most important objectives in radiosyntheses is the attainment of high radiochemical yields. To do so, one must have high chemical yields combined with short reaction times. When using ^{11}CO, it is delivered into the reaction medium in an inert gas stream that lasts for approximately two minutes. Since there is a finite amount of ^{11}CO produced, it is important to minimise the amount of this gas that goes to waste.

2.4.2 Rapid Carbonylation with Tp*

In order to assess how well the copper(I)-Tp* solution can trap CO in short periods of time, NMR-scale experiments were performed on a solution of CuCl and KTp* (**2.2**) in d_6-acetone. In these experiments, unlabelled CO was slowly bubbled through the solution for one minute and the ^1H NMR spectrum recorded. The resultant ^1H NMR spectrum is shown in Figure 2.27.

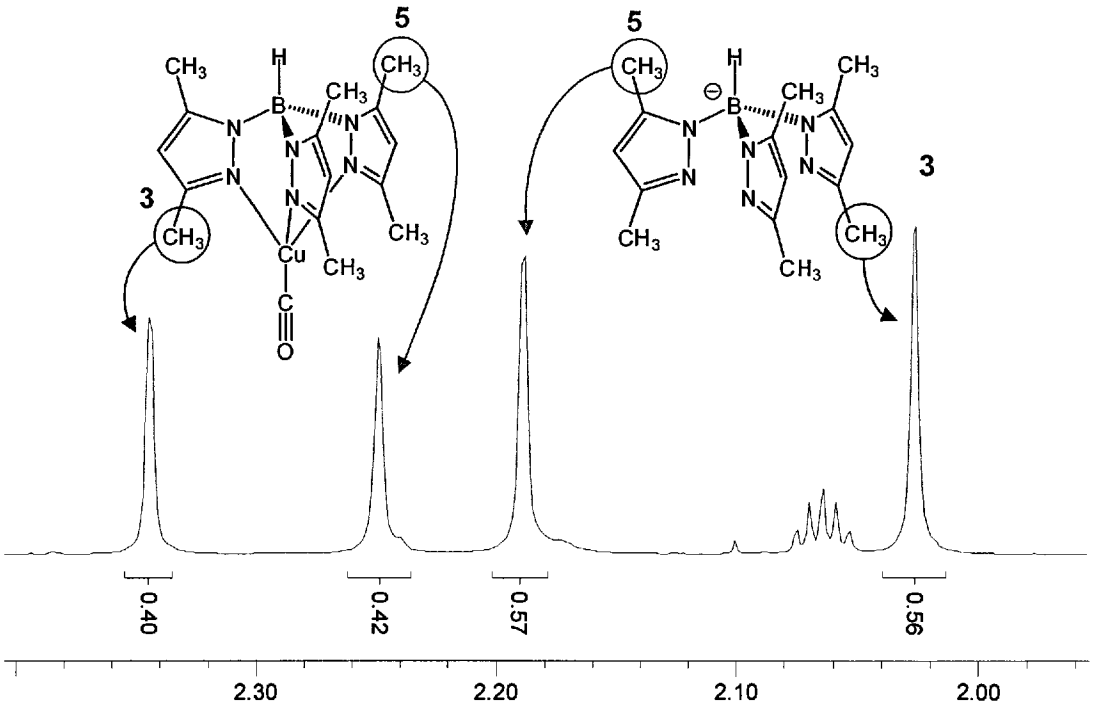


Figure 2.27. ^{1}H NMR spectrum recorded after rapid CO trapping reaction with CuCl/KTp* in d_6-acetone.

Since the carbonyl complex (CuTp*CO) and the uncoordinated ligand (Tp*) have been previously characterised by NMR, it is easy to identify these distinct species on the NMR spectrum obtained from this reaction. As such, the integrals of the 3- and 5-methyl groups of each species were measured to estimate the ratio of the carbonyl complex to the unreacted ligand. As seen in Figure 2.27, a *ca.* 4:6 carbonyl-to-ligand ratio was observed, corresponding to a 42 % trapping efficiency of the gas.

This trapping efficiency would be dependent on the flow rate of the gas (which was not measured). However, it was deemed a positive result since the gas stream consisted of undiluted CO. It was therefore hoped that when this system was applied to the hot cell, trapping efficiency would be increased due to the vast excess of trapping solution over ^{11}CO.

2.5 CO Displacement Reactions

Having successfully formed the carbonyl (thus solubilising the CO) via the reaction of CO with CuCl and KTp*, the next stage was to investigate the release of CO via a controlled trigger mechanism (Figure 2.28). In this case a fast concerted release of CO is required, such that the gas can be immediately used for carbonylation reactions.

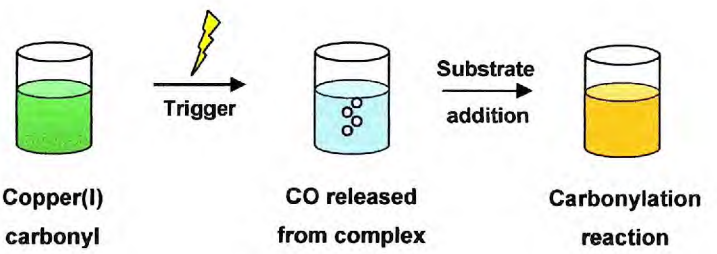


Figure 2.28. Schematic of CO release.

As discussed in Chapter 1, decarbonylation of copper(I) carbonyls can occur in a number of ways. In most reversible carbonylation systems, repeated vacuum/nitrogen cycles are used to displace the labile carbonyl ligand. This is not applicable in this instance as the CO gas must remain in the vessel for subsequent reaction. Furthermore, the high stability of the CuTp*CO solution renders it inert to decarbonylation under vacuum. UV-triggered release of CO is appealing, as it has been shown to occur rapidly with $[Cu(TMPA)CO]^+$.[21] The effect of UV on copper(I) scorpionate carbonyls is unknown, however, so it was decided not to explore this potential route.

Ligand displacement reactions are well established at the copper(I) centres. As a result of ligand binding studies of copper(I) species it has been shown that a phosphine ligand is able to displace a carbonyl ligand which in turn can displace a nitrile ligand from the coordination sphere of the copper:

$$\underset{\text{Lowest affinity}}{R\text{-}C{\equiv}N} < \underset{}{CO} < \underset{\text{Greatest affinity}}{PR_3}$$

The displacement of the carbonyl ligand in CuTp*CO upon addition of triphenylphosphine is reported to occur rapidly and at room temperature.[22] [23] With

this literature precedent, it was decided that CO displacement via PPh_3 would be used in this system. These experiments have been repeated, as described below, in the hope that this decarbonylation step can be combined with carbonylative cross-coupling reactions.

2.5.1 Decarbonylation of CuTp*CO

The displacement reaction was performed by addition of an excess of solid PPh_3 to a stirred solution of CuTp*CO (**2.11**) at room temperature (Figure 2.29). This caused immediate effervescence of the solution, indicating release of CO.

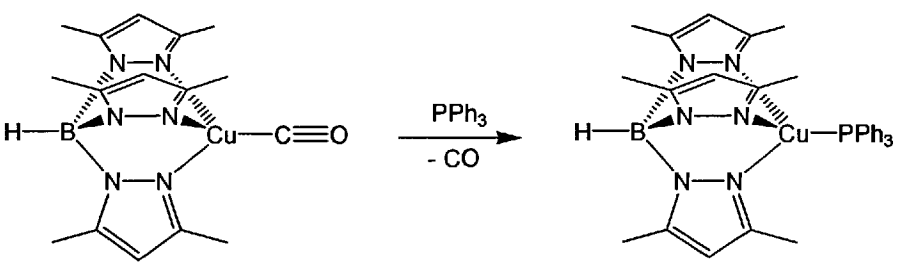


Figure 2.29. Displacement of CO from CuTp*CO (**2.11**) by PPh_3 to form CuTp*PPh_3 (**2.13**).

i. IR studies

IR spectra were recorded immediately prior to the addition of PPh_3 and two minutes after addition of PPh_3 to gauge the rate of the decarbonylation process (Figure 2.30).

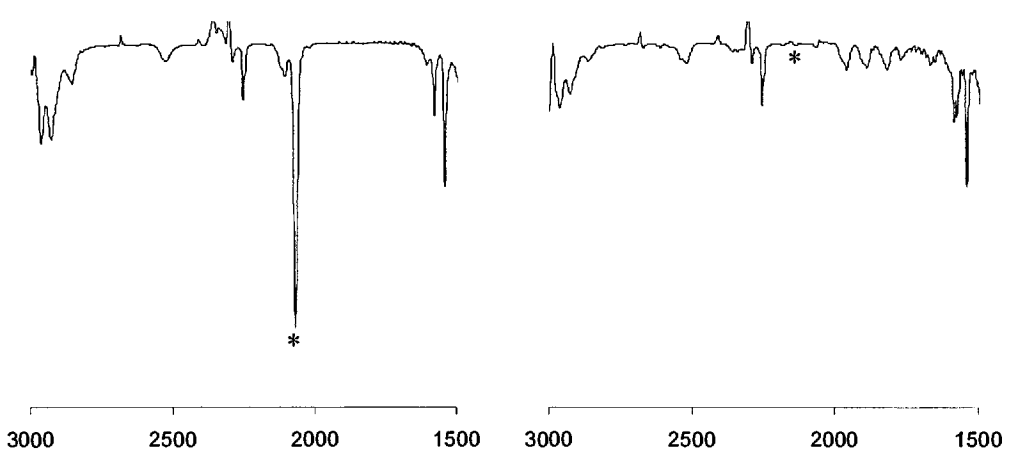


Figure 2.30. IR spectrum before (left) and two minutes after (right) addition of PPh_3 to CuTp*CO.

As can be seen from Figure 2.30, the carbonyl stretch (marked with a *) on the IR spectrum of the copper complex prior to addition of triphenylphosphine appears as a strong band at approximately 2060 cm^{-1}. Following the addition of the competing ligand, the carbonyl stretch completely disappeared, indicating that full decarbonylation has been effected in under two minutes. It is interesting to note the presence of some new peaks in the IR spectrum of the phosphine adduct – a series of weak absorptions between 1600 and 2000 cm^{-1}, corresponding to vibrations in the benzene rings of triphenylphosphine.

ii. NMR studies

The product, $CuTp^*PPh_3$ (**2.13**) has been isolated as an air stable white solid and characterised by ^1H and $^{31}P\{^1H\}$ NMR spectroscopy and IR spectroscopy (Figure 2.31).

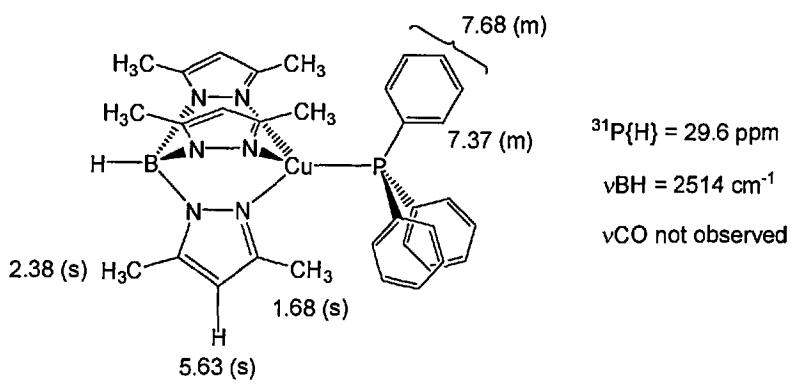


Figure 2.31. Summary of ^1H, $^{31}\{^1H\}$ and IR spectroscopic data of $CuTp^*PPh_3$ (**2.13**).

Replacement of the carbonyl ligand with triphenylphosphine causes the chemical shifts of the two non-equivalent methyl groups to become more separated in the ^1H NMR spectrum. The peak that is found furthest upfield (1.68 ppm) is assumed to be that of the methyl group in the 3-position (*c.f.* 2.33 ppm in $CuTp^*CO$) as it is closest to the copper centre and therefore most likely to be influenced by the coordination of PPh_3. The methyl group in the 5-position is further removed from the copper centre and its chemical shift would not be expected to change dramatically. Indeed, a small downfield shift (2.28 to 2.38 ppm) is observed upon ligand exchange. The proton in

the 4-position of the pyrazolyl ring is found slightly further upfield at 5.63 ppm relative to the parent carbonyl (5.76 ppm).

2.5.2 Decarbonylation of Cu[Tp^{Ph,SMe}]CO

The decarbonylation of Cu[Tp^{Ph,SMe}]CO (**2.12**) using triphenylphosphine was similarly investigated. IR spectra of a solution of Cu[Tp^{Ph,SMe}]CO in DCM were recorded prior to, and at intervals after, the addition of PPh_3 (Figure 2.32).

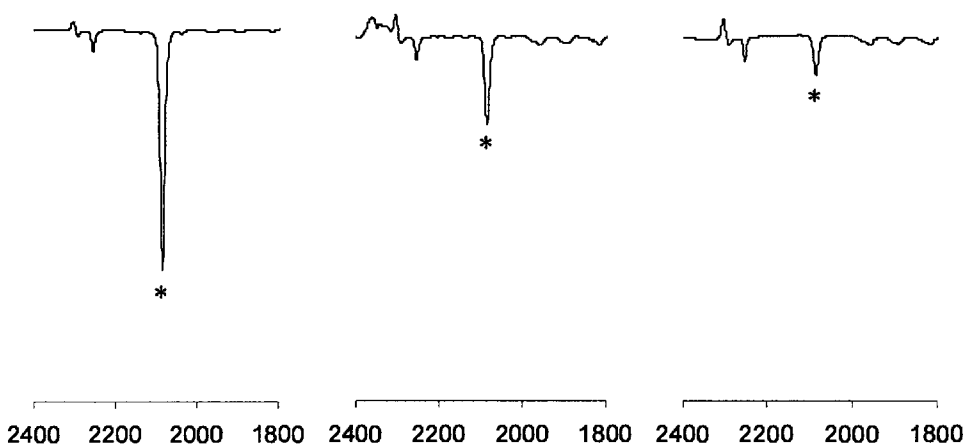


Figure 2.32. IR spectrum before (left), two minutes after (centre) and 10 minutes after (right) addition of PPh_3 to Cu[Tp^{Ph,SMe}]CO (**2.12**).

As can be seen in Figure 2.32, the carbonyl stretch (marked with a *) on the IR spectrum prior to addition of triphenylphosphine appears as a strong band at approximately 2080 cm^{-1}. This carbonyl stretch is weakened but *not* removed after two minutes stirring with excess PPh_3. After 10 minutes, this stretch is still visible. This incomplete decarbonylation can be contrasted with CuTp*CO which was shown to undergo complete decarbonylation in under two minutes. The difference in decarbonylation rate is attributed to the presence of bulky phenyl groups attached to the 3-position of the pyrazolyl rings in Cu[Tp^{Ph,SMe}]CO which provides a steric hindrance to approach of the bulky PPh_3 unit at the nearby copper centre.

2.5.3 Summary

The decarbonylation of CuTp*CO is observed by immediate effervescence and IR spectroscopy was used to gauge the rate of CO loss. This method of decarbonylation is irreversible as the triphenylphosphine adduct is stable due to its good π-acceptor and σ-donor properties. Despite this, the low cost of the reagents and the simplicity of the process make it ideal for application with ^{11}CO. The next challenge is to use the released CO for carbonylative cross-coupling reactions. This work is discussed in Chapter 3.

2.6 Future Work

2.6.1 Novel Electron-Rich Tps

The successful synthesis of the scorpionate $Tp^{Ph,SMe}$ provides the first example of a new class of heteroatom-substituted scorpionate ligands. There are many more variations to pursue in this field, including changing the heteroatom (e.g. alkoxy or amino substitution), varying the position of the substituent, and di-, or even tri-heteroatom substitution patterns. These species might be expected to possess interesting electronic properties and could find use in a range of applications. Some synthetic pathways to new Tp ligands are proposed below based on literature preparations of heteroatom-substituted pyrazoles.

i. Alkoxy and Amino–Substituted Tps

Junjappa *et al.* reported that as well as forming methylthio-pyrazoles, alkoxy and amino-pyrazoles can be synthesised directly from ketoketene-*S,S*-diacetals.[11] This is reported to occur by addition of one equivalent of the respective alkoxide or amine prior to the addition of hydrazine (Figure 2.33).

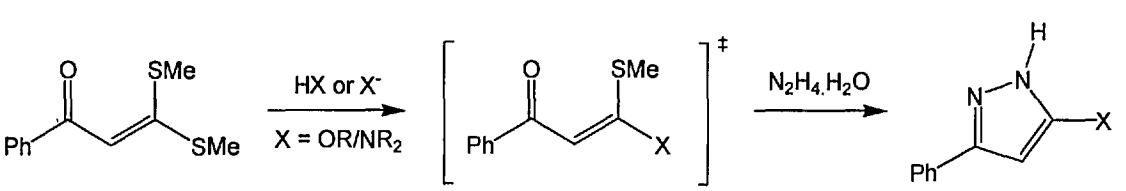


Figure 2.33. Synthesis of alkoxy/amino-substituted pyrazoles.

The resultant 5(3)-alkoxy/amino-pyrazoles could then be reacted with potassium borohydride to form Tp ligands bearing alkoxy or amino substituents.

ii. 3,5-Diethoxy-Substituted Tps

As discussed previously, the attempted synthesis of 3,5-diethoxypyrazole following the literature procedure described by Kollipara *et al.*[9] was unsuccessful. However, an alternative synthesis of 3,5-diethoxypyrazole is described in the journal *Archiv der Pharmazie*.[24] In this procedure, a dithiomalonester is reacted with hydrazine to give 3,5-diethoxypyrazole. The dithiomalonester can be synthesised in two steps[24, 25] from malonitrile as shown in Figure 2.34, below.

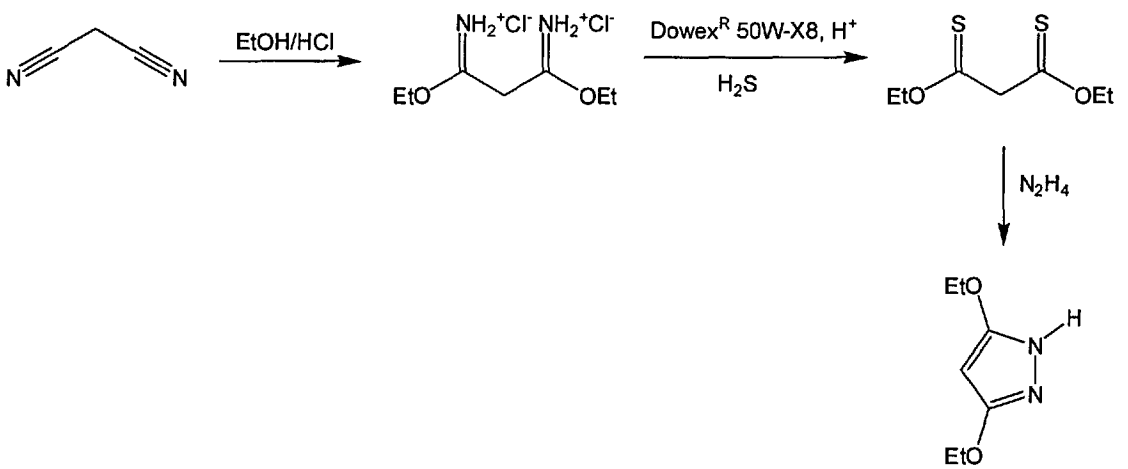


Figure 2.34. Proposed Synthesis of 3,5-diethoxypyrazole.

This pyrazole could then react with KBH_4 to produce the ligand, $K[Tp^{(OEt)2}]$ (Figure 2.35).

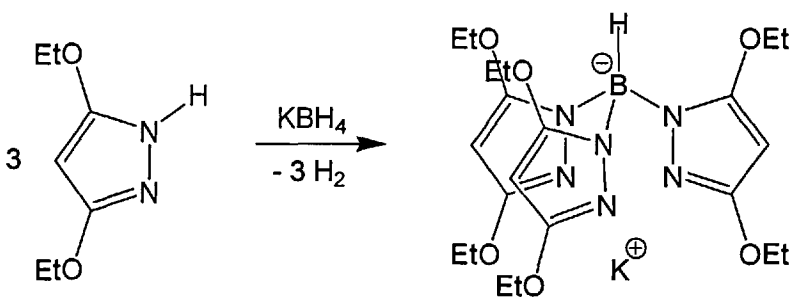


Figure 2.35. Proposed synthesis of electron rich ligand $K[Tp^{(OEt)2}]$.

2.6.2 Carbene Chemistry

A relatively unexplored class of tripodal ligands are the tris(imidazolylidene)borates (Figure 2.36).[26, 27] These N-heterocyclic ligands are topologically similar to the tris(pyrazolyl)borates but have N-substituted imidazole rings instead of the pyrazolyl units. Like the Tp ligands, they are negatively charged and provide a rigid tridentate bonding mode.

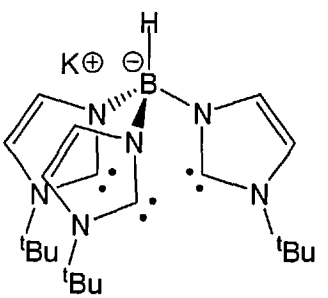


Figure 2.36. Tris(imidazole-2-ylidene)borate ligand, K[Tim^{tBu}].

Copper(I) complexes derived from these ligands have not been reported in the literature and would be expected to have different electronic properties to the Cu[Tp^{x}]CO species due to the strong σ-donating capabilities of the carbene ligand. These electron donating properties are hoped to promote the formation of copper carbonyls – stabilised via copper-d to CO-π* backbonding.

i. Synthesis of Cu[Tim^{tBu}]CO

The precursor to the [Tim] ligand is the stable dibromide salt shown in Figure 2.37. Deprotonation of the three imidazole units using strong base can be carried out *in situ* to yield the carbene. This species could then be reacted with copper(I) chloride under an atmosphere of CO in the hope that the carbonyl complex, Cu[Tim^{tBu}]CO, shown in Figure 2.37, would form.

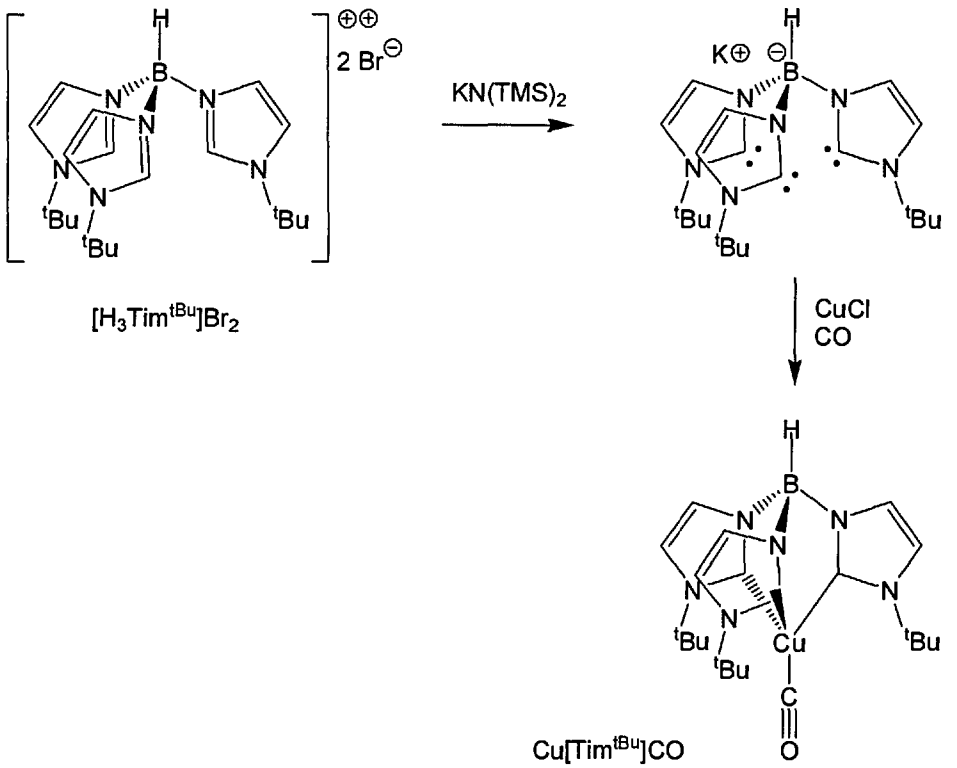


Figure 2.37. Proposed synthesis of copper(I)tris(imidazolylidene)borate carbonyl, Cu[Tim^{tBu}]CO.

Preliminary solution studies on this species[28] indicate a CO stretch at 2004 cm^{-1}, an unprecedented low value for a copper(I) carbonyl species. These reactions are worthy of further investigations. Displacement of the carbonyl ligand upon addition of phosphine ligands could also be investigated.

2.6.3 UV-Triggered Decarbonylation

The ability of [Cu(TMPA)CO]$^+$ to undergo reversible photo-induced decarbonylation could be similarly explored with Tp ligands. This process (Figure 2.38) may be dependent on the nature of the R groups attached to the ligand core as this will affect the electronic properties of the ligand.

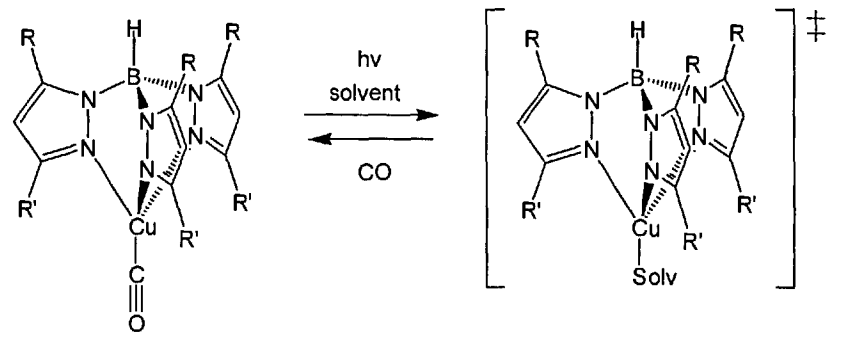


Figure 2.38. Proposed photodissociation from copper(I) scorpionate carbonyls.

Furthermore, photo-initiated carbonylation reactions have been described by Langstrom *et al.* for the synthesis of amides, esters and carboxylic acids under irradiation with UV light.[29-33] It might therefore be possible to design a system combining photo-induced ^{11}CO release with photo-initiated [^{11}C]carbonylation to form ^{11}C-labelled molecules for PET studies (Figure 2.39).

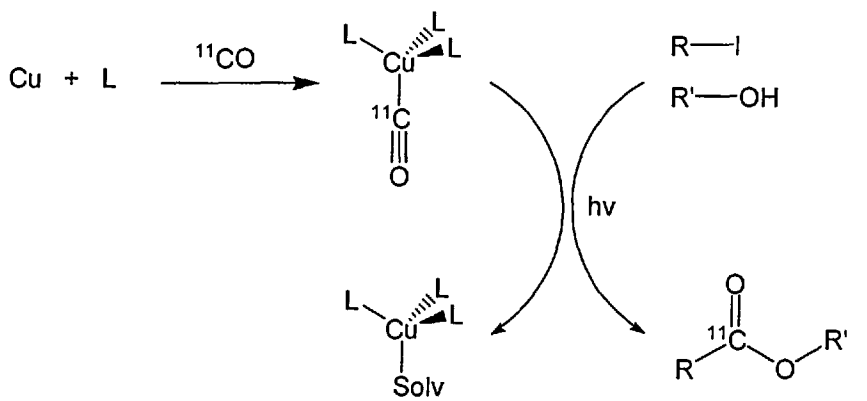


Figure 2.39. Proposed tandem photodissociation/photo-initiation reactions for ^{11}C-labelling.

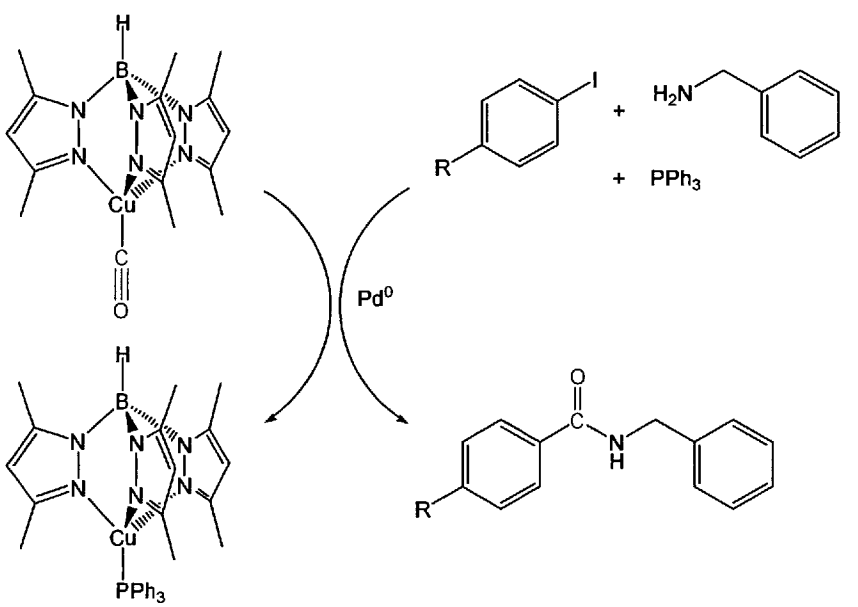
2.7 References

1. C. Floriani, *Copper Coordination Chemistry: Chemical and Inorganic Perspectives*, Adenine Press, New York, 1982.
2. K. G. Caulton, G. Davies and E. M. Holt, *Polyhedron*, 1990, **9**, 2319.
3. S. Trofimenko, *Scorpionates: The Coordination Chemistry of Polypyrazolylborate Ligands*, Imperial College Press, London, 1999.
4. S. Trofimenko, *Inorg. Synth.*, 1970, **12**, 99.
5. S. Thomas and C. G. Young, *Inorg. Synth.*, 2002, **33**, 218.
6. S. Trofimenko, *Inorg. Chem.*, 1970, **9**, 2493.
7. A. L. Rheingold, L. M. Liable-Sands, C. L. Incarvito and S. Trofimenko, *J. Chem. Soc., Dalton Trans.*, 2002, 2297.

8. W. Adam, J. Putterlik, R. M. Schuhmann and J. Sundermeyer, *Organometallics*, 1996, **15**, 4586.
9. N. R. Kollipara, P. Govindaswamy and Y. A. Mozharivskyj, *J. Organomet. Chem.*, 2004, **689**, 3265.
10. R. Balicki and P. Namirski-Nantka, *Acta Polon. Pharm.*, 1988, **45**, 1.
11. S. M. S. Chauhan and H. Junjappa, *Synthesis*, 1975, 798.
12. K. T. Potts, M. J. Cipullo, P. Ralli and G. Theodoridis, *J. Org. Chem.*, 1982, **47**, 3027.
13. K. T. Potts, P. Ralli, G. Theodoridis and P. Winslow, *Inorg. Synth.*, 1986, **64**, 189.
14. Z. Ciunik, T. Ruman, M. Lukasiewicz and S. Wolowiec, *J. Mol. Struct.*, 2004, **690**, 175.
15. G. P. A. Yap, F. Jove, J. Urbano, E. Alvarez, S. Trofimenko, M. M. Diaz-Requejo and P. J. Perez, *Inorg. Chem.*, 2007, **46**, 780.
16. K. Fujisawa, T. Ono, Y. Ishikawa, N. Amir, Y. Miyashita, K. Okamoto and N. Lehnert, *Inorg. Chem.*, 2006, **45**, 1698.
17. M. Kujime, T. Kurahashi, M. Tomura and H. Fujii, *Inorg. Chem.*, 2007, **46**, 541.
18. R. B. Moon and J. H. Richards, *Biochemistry*, 1974, **13**, 3437.
19. R. B. Moon, K. Dill and J. H. Richards, *Biochemistry*, 1977, **16**, 221.
20. S. Imai, K. Fujisawa, T. Kobayashi, N. Shirasawa, H. Fujii, T. Yoshimura, N. Kitajima and Y. Moro-oka, *Inorg. Chem.*, 1998, **37**, 3066.
21. D. V. Scaltrito, H. C. Fry, B. M. Showalter, D. W. Thompson, H. C. Liang, C. X. Zhang, R. M. Kretzer, E. Kim, J. P. Toscano, K. D. Karlin and G. J. Meyer, *Inorg. Chem.*, 2001, **40**, 4514.
22. M. I. Bruce and A. P. P. Ostazewski, *J. Chem. Soc., Dalton Trans.*, 1973, 2433.
23. N. Kitajima, T. Koda, S. Hashimoto, T. Kitagawa and Y. Moro-oka, *J. Am. Chem. Soc.*, 1991, **113**, 5664.
24. K. Hartke and H. G. Muller, *Archiv der Pharmazie*, 1988, **321**, 863.
25. A. Couture, P. Grandclaudon and E. Huguerre, *Synthesis*, 1989, **6**, 456.
26. I. Nieto, F. Cervantes-Lee and J. M. Smith, *Chem. Commun.*, 2005, 3811.
27. W. A. Herrmann, *Angew. Chem., Int. Ed.*, 2002, **41**, 1290.
28. S. Kealey and N. J. Long, *Preliminary studies, Imperial College, London.*
29. O. Itsenko and B. Langstrom, *J. Org. Chem.*, 2005, **70**, 2244.
30. O. Itsenko and B. Langstrom, *Org. Lett.*, 2005, **7**, 4661.
31. O. Itsenko, T. Kihlberg and B. Langstrom, *Eur. J. Org. Chem.*, 2005, 3830.
32. O. Itsenko, D. Norberg, T. Rasmussen, B. Langstrom and C. Chatgilialoglu, *J. Am. Chem. Soc.*, 2007, **129**, 9020.
33. O. Itsenko, T. Kihlberg and B. Langstrom, *J. Org. Chem.*, 2004, **69**, 4356.

CHAPTER 3

PALLADIUM-MEDIATED CARBONYLATION REACTIONS



3. Palladium-Mediated Carbonylation Reactions

In Chapter 2 the trapping and release of CO through the use of a copper(I)-scorpionate complex was shown to be viable for application with ^{11}CO in the radiochemical laboratory. To be useful, the trapping/release system must be compatible with some means of incorporating the CO into the desired target molecule. The various types of [^{11}C]carbonylation reactions were discussed in Chapter 1, and it was found that palladium-mediated cross-coupling reactions are most frequently employed. These reactions provide access to a range of common CO-containing functional groups, namely amides, esters and ketones. Due to this literature precedence, palladium-catalysed carbonylation reactions were chosen to be performed in conjunction with the copper(I)-scorpionate system.

The ^{11}CO trapping and [^{11}C]carbonylation reactions were performed with the help of Idriss Bennacef, Christophe Plisson and Philip Miller at the GSK laboratories at Mount Vernon Hospital, Middlesex and with Hélène Audrain at the PET Centre, Aarhus University Hospital, Denmark.

3.1 ^{11}CO Trapping Reactions

3.1.1 Background

Before attempting any palladium-catalysed carbonylation reactions it was decided to investigate the suitability of the CuCl/KTp* CO-trapping system towards the conditions of the radiolaboratory, specifically the low concentrations and short delivery times of the [^{11}C]carbon monoxide. The proposed scheme of ^{11}CO trapping is shown in Figure 3.1. These reactions were performed in sealed sample vials containing a rubber septum to allow infusion of the $^{11}CO/N_2$ gaseous mixture and the waste gases to escape.

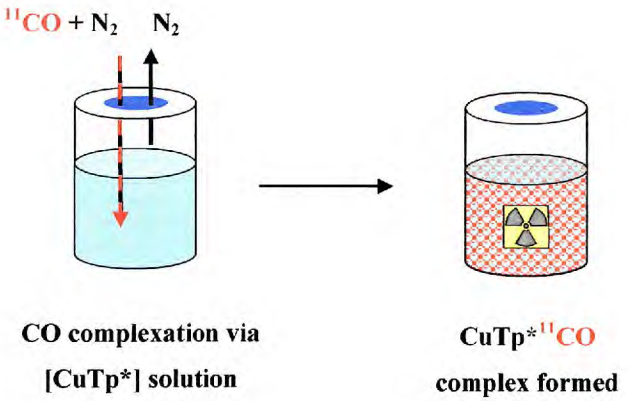


Figure 3.1. Schematic showing proposed trapping mechanism of ^{11}CO.

Working with radioactivity brings about restrictions in the handling of these species compared to working in an ordinary laboratory. It is essential to perform reactions in shielded 'hot-cells' (Figure 3.2) and as a consequence, processes that would normally be performed by hand such as addition of reagents and the switching of gas flows are often automated in such a way that they can be controlled externally. In the experiments described in this section, valve towers situated inside the hot-cell have been used to control gas flows and the raising and lowering of reaction vials for heating/cooling. It is also possible to perform these actions sequentially, leading to an automated system for radiolabelling experiments.



Figure 3.2. A hot-cell in the radiochemical laboratory.

3.1.2 Reaction Setup

The 'CO complexation' stage, shown in Figure 3.1 has been performed in a sample vial containing a saturated solution of CuCl and KTp* in THF. This process consists of two stages, ^{11}CO preconcentration and ^{11}CO trapping, as discussed below.

Step 1: Production and preconcentration of ^{11}CO (Figure 3.3)

Having formed $^{11}CO_2$ in the cyclotron, it is pushed through the system via a flow of nitrogen gas. The $^{11}CO_2$ is then reduced to ^{11}CO by passing the gas over a molybdenum reductant at 800°C and any remaining $^{11}CO_2$ is removed from the gas stream by passing the gases through an Ascarite CO_2 trap. At this stage, the ^{11}CO is preconcentrated by passing the gas stream through a loop containing molecular sieves, suspended in liquid nitrogen. Any gases not trapped on the Ascarite or sieves are collected in bag 1.

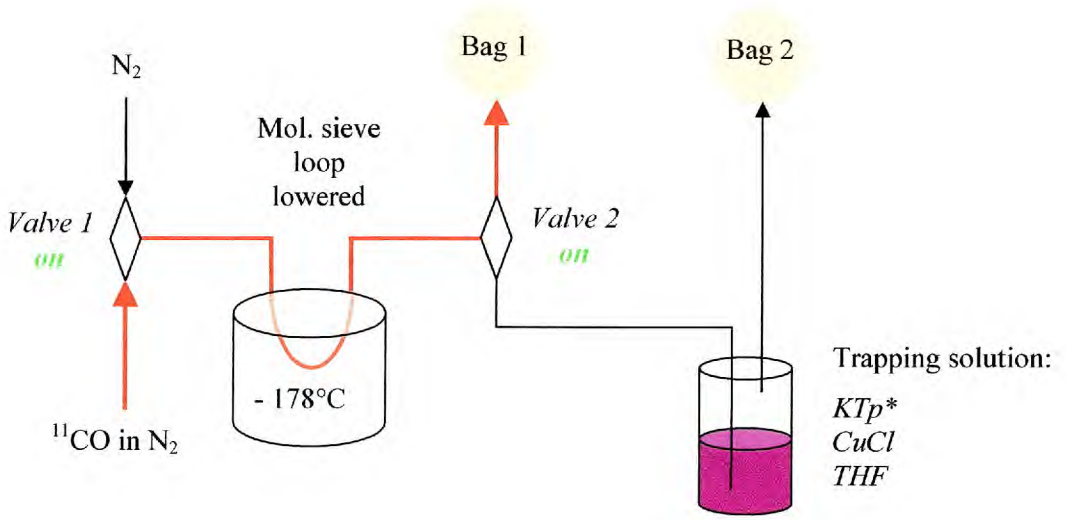


Figure 3.3. Preconcentration of ^{11}CO on molecular sieves.

Step 2: Trapping of ^{11}CO via formation of Cu(Tp)^{11}CO (Figure 3.4)*

When the activity of this loop reaches its maximum (*i.e.* the maximum amount of ^{11}CO has been trapped) it is removed from the liquid nitrogen by raising a piston. Valve 1 is switched thus providing a nitrogen flow to push the ^{11}CO off the loop as it

warms up to room temperature. Simultaneously, Valve 2 is switched allowing the $^{11}CO/N_2$ to be bubbled through the vial containing KTp* and CuCl in THF (the trapping reagents). The remaining, uncoordinated gases are then collected in bag 2. Collecting the waste gases enables the total amount of radioactivity to be measured and compared to the activity present in the sample vial. By doing this it is possible to calculate the trapping efficiency of the complex solution.

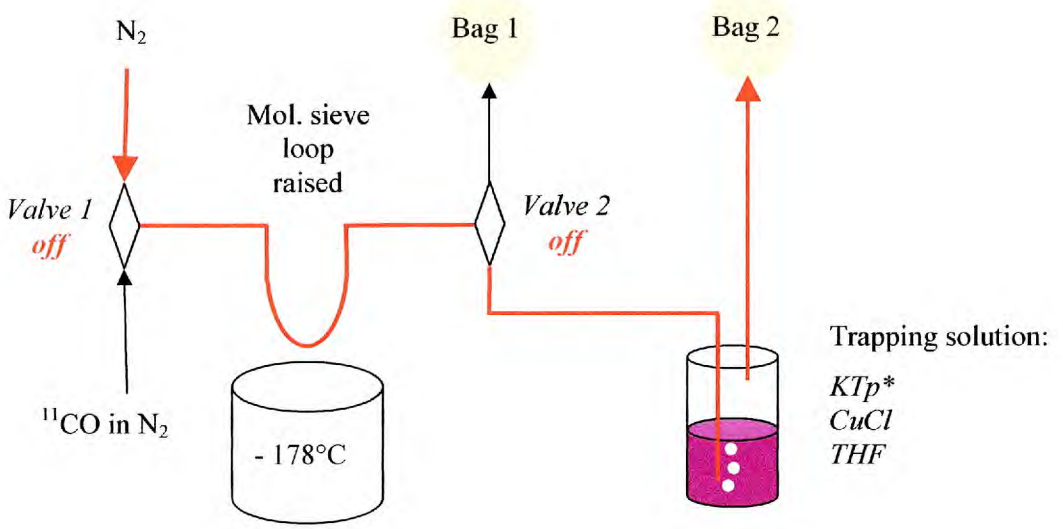


Figure 3.4. Release of ^{11}CO from sieves and subsequent complexation.

3.1.3 Calculations

The trapping reactions were performed four times and in each case the progress of the reaction was followed by measuring the radioactivity of the waste gases until a constant maximum reading was observed or by measuring the radioactivity of the molecular sieve loop until the activity had reached a minimum. This corresponds to having flushed all the hot reagents through the system. In each case, the trapping efficiency has been measured by the following equation:

$$\text{Trapping efficiency} = \frac{\text{Total radioactivity in vial}}{\text{Total radioactivity passed through vial}}$$

The total radioactivity resulting from ^{11}CO is made up of the waste gases collected in bag 2 and the trapped radioactivity in the sample vial. When performing calculations with these data, it is necessary to correct the radioactivities at time, *t*, to their theoretical values at time, $t = 0$. These are known as decay corrected radioactivities and enable comparisons to be made between the radioactivities of the waste gases and the sample vial as they are often recorded at different times and hence different stages in the decay process. In these calculations, $t = 0$ is defined as the moment when bombardment of the target in the cyclotron ceases. This is known as the 'end of bombardment' (EOB) and corresponds to the point at which the maximum amount of ^{11}C is present.

3.1.4 Results and Discussion

As shown in Table 3.1, the CuCl/KTp* trapping solution was able to trap an average of 96 % of the ^{11}CO based on the assumption that the ^{11}CO was the only radioactive gas passing through the system. This is a promising result and provides the basis for further reactions to incorporate ^{11}CO into organic molecules. The large excess of trapping reagents (micromoles) compared to the amounts of ^{11}CO being produced (picomoles) is thought to favour the trapping process.

Table 3.1. Radioactivity log during ^{11}CO trapping reactions

Run[a]	Max. bag radioactivity / MBq		Max. sample radioactivity / MBq		Total radioactivity (corrected) / MBq	Trapping efficiency
	A_t (min:sec)	A_0 (corrected)	A_t (min:sec)	A_0 (corrected)		
1[b]	370 (9:30)	511	4000 (15:00)	6662	7173	93 %
2	16.7 (7:00)	21	349 (6:20)	433	454	95 %
3	0.3 (12:20)	0.5	8.1 (13:30)	12.8	13	97 %
4	0.5 (13:30)	0.8	32.0 (16:20)	55.8	57	99 %
					Average	96 %

(a) Performed at GSK laboratories, Mount Vernon Hospital, Middlesex unless indicated otherwise; (b) performed at the PET centre, Aarhus University Hospital, Denmark.

On average the preconcentration step lasted approximately five minutes, with the gas sweep to flush the activity through the vial lasting a further five minutes. With such a high trapping efficiency, future reactions will be performed without the pre-concentration stage as it increases the reaction time, possibly unnecessarily.

3.2 'Cold' Amide Syntheses

3.2.1 Background

Having designed a system for CO trapping and displaying its suitability to the radiolaboratory, it was decided to investigate the subsequent carbonylation reactions utilising the trapped CO. Palladium-mediated [^{11}C]carbonylation reactions were chosen as they provide access to a range of CO-containing functionalities. Initial research within this field was focussed on the carbonylative cross-coupling reactions between an aryl-halide and benzylamine to form the amide, *N*-benzylbenzamide (Figure 3.5).

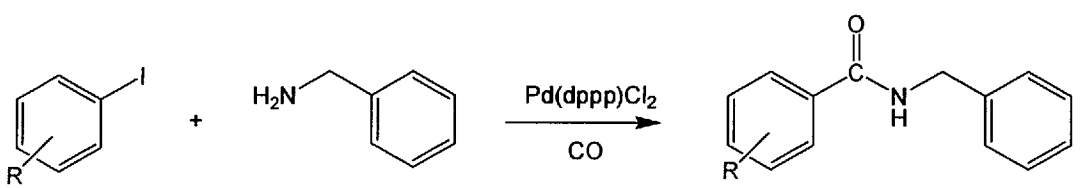


Figure 3.5. Carbonylation reaction between an aryl-halide and an amine in the presence of CO.

In this case the CO is sourced from the CuTp*CO species, which is decarbonylated by addition of triphenylphosphine. By performing this step in tandem with the addition of cross-coupling reagents (aryl-halide, palladium catalyst and benzylamine) it is hoped to allow the CO to be incorporated into amide functionalities as shown in Figure 3.6.

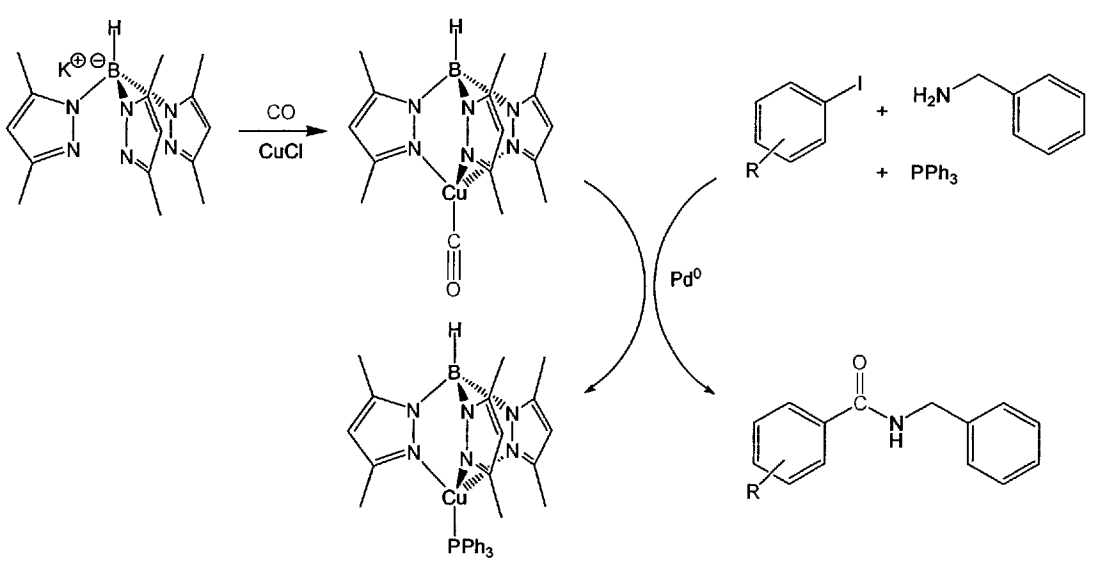


Figure 3.6. CO trapping followed by tandem CO release/carbonylation reaction.

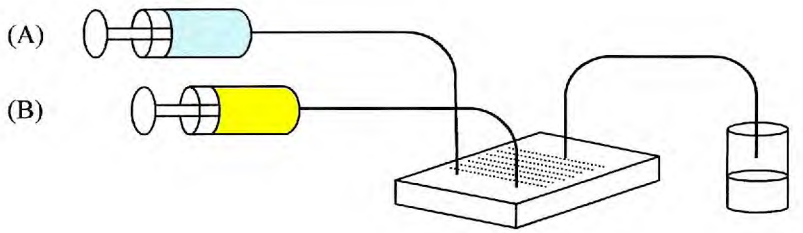
These reactions will allow the examination of any effect that the presence of the copper complexes have on the catalytic activity of the palladium. To ascertain the performance of these reactions and their suitability to the hot-cell, these reactions have been performed using unlabelled 'cold' CO. These reactions have been performed on a microfluidic device and in Schlenk apparatus.

3.2.2 Microfluidic Reactions

As outlined in Chapter 1, microfluidic reactors are well suited to the synthesis of radiolabelled molecules as they can reduce reaction times through improved mass and heat transfer. Rapid reactions are important in the synthesis of ^{11}C-labelled molecules due to the short half-life of the isotope. The scale of microchip reactions is well suited with the desire to produce microgram quantities of radiolabelled molecules for *in vivo* studies. Microchip reactions are expected to be useful for these tandem carbonylations as any CO released inside the chip cannot directly escape to the atmosphere until the reagents have passed along the channels. It is hoped that this will facilitate the CO insertion step in the catalytic cycle, thus improving reaction rates.

i. Reaction Setup

These reactions were performed on a micromolar scale by infusing the cross-coupling reagents (benzylamine, aryl-halide, palladium catalyst, triphenylphosphine) with a solution of CuTp*CO in a microfluidic reactor which was heated to 85°C for the course of the reaction (Figure 3.7). The flow rate of each syringe was 6 µl/minute to give a combined flow rate of 12 µl/minute through the microchannels.



Syringe (A): CuTp*CO (0.50 mmol)
in THF (7.5 ml)

Syringe (B): PPh_3 (0.50 mmol)
$Pd(dppp)Cl_2$ (0.01 mmol)
Aryl-halide (0.50 mmol)
Benzylamine (7.5 ml, excess)

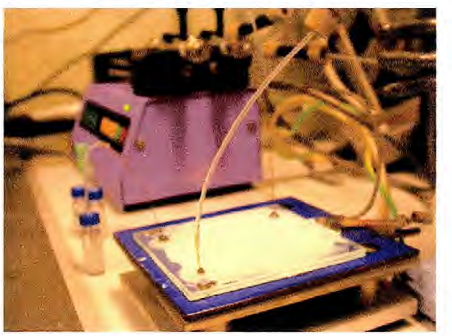
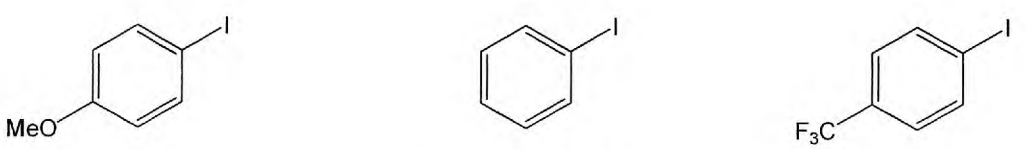


Figure 3.7. Reaction set-up for carbonylative cross-couplings on a microchip. (Inset: photograph of microchip and syringe pump in use).

The aryl-halide substrates that were examined in these chip carbonylation reactions are shown in Figure 3.8. These three substrates were chosen as they vary from electron-rich to electron-poor. It is expected that the electron-rich substrate will give the lowest yields as it slowly undergoes oxidative addition to palladium. Conversely the electron-withdrawing *para*-trifluoromethyl group facilitates oxidative addition of the C–I bond thus enhancing yields.



Electron-rich substrate

Electronically 'neutral' substrate

Electron-poor substrate

Figure 3.8. Aryl-halide substrates used in carbonylation reactions.

ii. Results and Discussion

In every experiment, upon fusing of the reagents in the microfluidic chip, bubbles of gas could be seen to appear and flow along the micro-channels. This was attributed to CO being released inside the chip upon the reaction between PPh_3 and CuTp*CO. Figure 3.9 shows the chip during a carbonylation reaction. Here, the CO gas can be observed as the darker sections flowing along the channels, with the liquid reagents flowing in front of and behind these sections. This flow regime is known as 'slug flow' whereby the liquid phase flows along the microchannel in short sections separated by bubbles of gas. As the reagents passed through the channels the amount of gas visibly reduced, indicating that the CO was reacting.



Figure 3.9. Microfluidic chip in use during tandem CO release/carbonylation reactions.

Confirmation that these bubbles were not merely caused by vaporised solvent was provided from a run performed at 50°C (bpt. of THF = 66°C), during which time gas production in the microchannels was still observed.

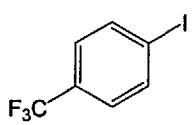
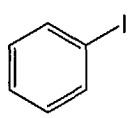
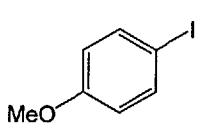
The time it takes for the reagents to pass through the length of the microchannel (*i.e.* the residence time) was calculated by the following equation:

$$\begin{aligned} \text{Residence time} &= \text{chip volume / total flow rate} \\ &= 75\ \mu l / 12\ \mu l/\text{minute} \\ &= 6.25\ \text{minutes} \end{aligned}$$

The actual residence time was estimated to be slightly shorter than this as the production of CO gas within the channels forced the reagents through the chip at an increased rate.

The results of the microfluidic reactions are summarised in Table 3.2. As expected, the electron-poor substrate gave the highest yields. In this case an average yield of 73 % was observed, with a residence time of six minutes. This is an encouraging result as it shows that amides can be synthesised rapidly and in good yields for potential application with ^{11}CO. However, a large decrease in reactivity was observed when the 'neutral' substrate, iodobenzene, was reacted, with an average yield of 13 %. This pattern extends to the electron-rich substrate, 4-iodoanisole, in which a negligible yield (4 %) was observed. Bearing in mind that the reactions performed were palladium-*catalysed* involving a two mole% loading of palladium catalyst and equimolar quantities of the carbonyl source and the cross-coupling reagents, it is quite possible that this process could be favoured under the conditions of the hot-cell where there is a large excess of palladium and cross-coupling reagents relative to the amount of ^{11}CO.

Table 3.2. Yield of amides from cross-coupling reactions performed on a microfluidic device

Substrate	Total flow rate	Residence time	Run duration	Amide yield[a]
	12 µL/min	6 mins	80 mins	73 %
	12 µL/min	6 mins	80 mins	13 %
	12 µL/min	6 mins	80 mins	4 %

(a) Average over three runs.

These results can be compared to the results obtained by Miller *et al.*[1] in which a microfluidic device was used to perform similar carbonylation reactions. Here the carbonyl source was CO gas which passed along the microchannels in an annular flow regime (a thin film of liquid reagents being forced onto the walls of the microchannel while the gas flows through the centre). This creates a high gas/liquid interfacial surface area and likely contributes towards enhanced yields. In these experiments carbon monoxide pressures of three to four atmospheres were produced which

facilitates the CO insertion step in the catalytic cycle. With a mean residence time of less than two minutes, amide yields of *ca.* 38 % were obtained with iodobenzene as a substrate. It is interesting to note that in these reactions, α-ketoamide formation was observed as a result of double carbonylation during the catalytic cycle. This is attributed to the high CO pressure in the system. It is thought that no α-ketoamide formation was observed with the CuTp*CO system as the pressures are likely to be much lower.

The yields observed with the CuTp*CO system are approximately one third of those obtained in the comparable system used by Miller *et al.*[1] This is likely to be a result of the high gas pressures involved in the latter system which results in the favourable annular flow regime. It cannot be ruled out that the presence of copper species, CuTp*CO and CuTp*PPh_3, contribute towards the poisoning of the palladium catalyst thus reducing its activity.

3.2.3 Schlenk Reactions

Following on from the microfluidic reactions, carbonylations using CuTp*CO as the CO source were performed on a larger scale inside sealed Schlenk flasks. It was hoped that if these reactions could be performed successfully then similar reactions could be applied to the hot-cell – by injection of the cross-coupling reagents into a sample vial containing freshly-trapped ^{11}CO.

i. Reaction Setup

For each reaction, a solution containing the cross-coupling reagents (aryl-halide, Pd(dppp)Cl_2 and triphenylphosphine dissolved in benzylamine) was added by syringe to a solution of CuTp*CO in THF in a Schlenk flask under an atmosphere of nitrogen (Figure 3.10). The flask was immediately sealed at the side arm and at the rotaflow adaptor to prevent any released CO escaping into the atmosphere. The flask was then immersed in an oil bath which had been preheated to 85°C. This was followed by vigorous stirring at this temperature for either 90 minutes or 20 minutes. After a standard acidic work-up, yields were monitored by GC using a phenyl ether standard.

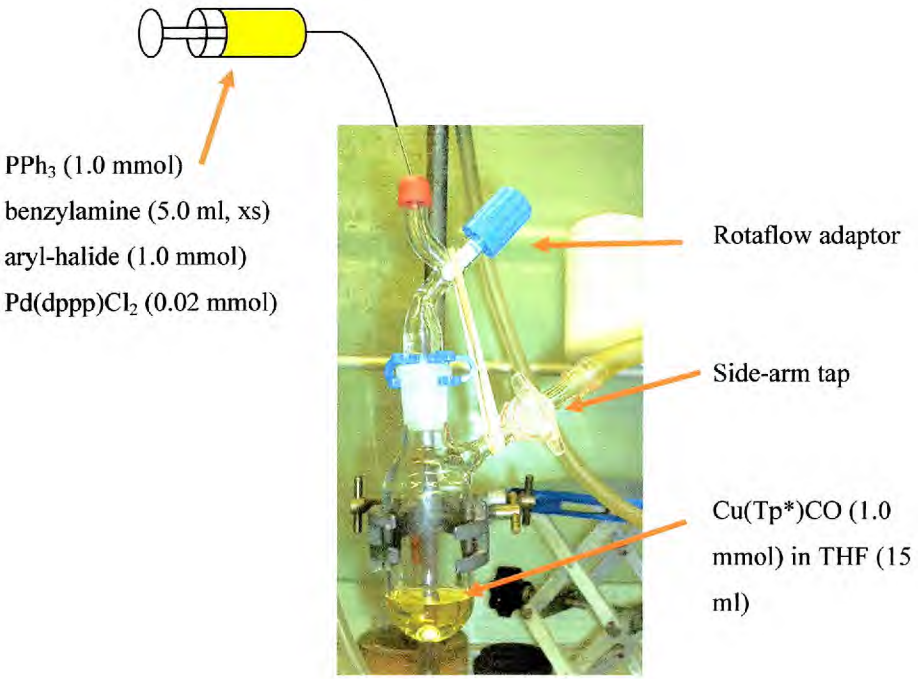
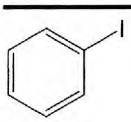


Figure 3.10. Reaction setup for bulk-scale tandem CO release/carbonylation reactions.

ii. Results and Discussion

Table 3.3 shows the results of the 90 minute cross-coupling reactions. These reactions proceeded in good yield (75 %), with significant improvements in yield over the corresponding control reactions. The control reactions were performed in order to monitor the extent of amide formation as a result of CO that was dissolved solely in the THF solvent. As expected, due to the low solubility of CO in this solvent, the control yields were very low.

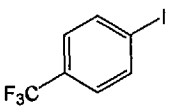
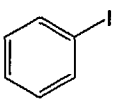
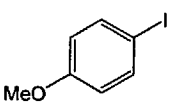
Table 3.3. Yields of *N*-benzylbenzamide from 90 minute Schlenk carbonylation reactions

Substrate	Reaction time	Amide yield[a]	Amide yield (control)[a,b]
	90 min	75 %	7 %

(a) Average of three runs; (b) 3 hr reaction.

Following these successful reactions, it was decided to perform further carbonylation reactions on a time-scale more comparable to the half life of ^{11}C. As such, 20 minute reactions were performed using a range of substrates, from electron-poor to electron-rich.

Table 3.4. Yields of amides from 20 minute Schlenk carbonylation reactions

Substrate	Reaction time	Yield of Amide (CuTp*CO)[a]	Yield of Amide (control)[a]
	20 min	18 %	2 %
	20 min	11 %	3 %
	20 min	5 %	1 %

(a) Average of two runs.

As shown in Table 3.4, these reactions followed the trend in reactivity observed with the microfluidic reactions. Here the yields are generally low, with the highest yields being observed for the electron-poor substrate (18 %). However, in each case the yields are significantly higher than their corresponding control reactions in which the carbonyl source is CO-saturated THF. This confirms the role of the CuCl/KTp* trapping solution in solubilising CO and its compatibility with palladium(0) carbonylation reactions. These yields are hoped to be improved when reactions are performed in the hot-cell as the palladium will be in excess over the ^{11}CO.

3.2.4 Carbonylation Summary

The microfluidic reactions were rapid and achieved high yields for the favourable electron-poor substrate. Significantly lower yields, however, were observed with the neutral and electron-rich substrates. Despite their mixed success these reactions were not chosen to be performed with ^{11}CO in the hot-cell. This is based on mechanistic difficulties in adapting this system to the hot-cell, such as complications in transferring the CuTp*^{11}CO solution, once formed, into the microfluidic device.

The Schlenk reactions were also performed with mixed success. While the 90 minute reactions gave very good yields with the 'neutral' iodobenzene substrate, shortening the reaction time to 20 minutes proved detrimental to yields. However, an improvement in yields was observed with respect to the CO-saturated-solvent runs.

3.3 'Hot' Amide Syntheses

3.3.1 Reaction Setup

The Schlenk carbonylation system was adapted for use with ^{11}CO in the hot-cell. These reactions were performed in a sealed sample vial, the first stage being the ^{11}CO trapping process described previously. However, given the high trapping efficiency of the CuCl/KTp* system, it was decided to attempt these experiments *without* the usual ^{11}CO preconcentration step using molecular sieves. This was hoped to maintain a high trapping efficiency of ^{11}CO whilst speeding-up and simplifying the process. As such the $^{11}CO/N_2$ gas stream was bubbled directly through the trapping solution (a saturated solution of CuCl and KTp* in 1 ml THF) at a controlled flow rate of 40 ml min^{-1} (Figure 3.11).

Once the trapping process was complete (*i.e.* the radioactivity of the sample vial had reached a maximum value), the gas flow was stopped and the cross-coupling reagents (aryl-halide, benzylamine, palladium catalyst and triphenylphosphine) were injected into the sample vial. The vial was then immediately lowered into a heating block at 130°C and heated for 10 minutes (Figure 3.11). In each instance, product formation was monitored by analytical HPLC using UV and radio detectors.

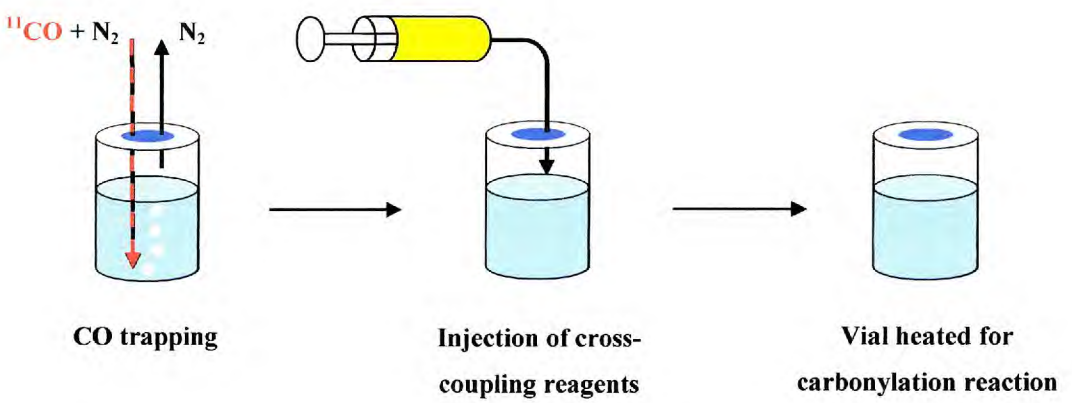


Figure 3.11. Schematic of ^{11}CO trapping followed by [^{11}C]carbonylation reaction.

3.3.2 Results and Discussion

Four carbonylation reactions were performed; in each case the reagents and conditions were slightly modified in attempts to optimise the carbonylation process. A summary of the key stages in these reactions is summarised in Table 3.5. The data analysis is split into two sections; calculations of trapping efficiency and product distribution based on HPLC data.

Table 3.5. Key steps in [^{11}C]carbonylation reactions

Time /min:sec	Comment
0:00	**end of bombardment**
0:00-3:00	**^{11}CO synthesis and $^{11}CO_2$ trapping**
3:00-9:00	**^{11}CO flow through vial**
3:00	bubbling observed in vial
4.00	radioactivity of vial rapidly increasing
	radioactivity of bag slowly increasing
8:30	maximum radioactivity in sample vial
9:00-19:00	**carbonylation reaction**
9:00	cross-coupling reagents added
	vial lowered into heating block
10:00	refluxing THF observed in vial
12:00	septum bulging indicating pressurised contents
19:00	sample vial raised and allowed to cool
21:00	radioactivity of bag measured
21:30	radioactivity of sample vial measured
21:30 +	**HPLC analysis**

i. *^{11}CO Trapping*

As before, the trapping efficiencies were calculated as a fraction of the radioactivity of the sample vial compared to the total radioactivity delivered to the system. In these reactions, the radioactivity of the waste gases and the sample vial were measured after the cross-coupling carbonylation reaction.

Table 3.6. Radioactivity log during ^{11}CO trapping reactions

Run[a]	Max. bag radioactivity		Max. vial radioactivity		Total radioactivity (corrected) / MBq	Trapping efficiency
	Time / min:sec	A_0 (corrected) / MBq	Time / min:sec	A_0 (corrected) / MBq		
1	21:00	79.9	21:30	4990.3	5070.2	98 %
2	21:00	47.8	26:00	3874.0	4110.6	99 %
3	21:00	60.2	22:30	4008.5	4068.7	99 %
4	20:00	28.9	22:00	1830.4	1859.3	98 %
					Average	99 %

(a) Reactions performed at the PET centre, Aarhus University Hospital, Denmark.

As shown in Table 3.6, the CuCl/KTp* solution was able to trap the ^{11}CO almost quantitatively (99 % average) with very little deviation over the four runs. This consistently high trapping efficiency, obtained without the use of the molecular sieve loop, is very encouraging as it should lead to increased radiochemical yields as a consequence of shorter reaction times.

ii. [^{11}C]Carbonylation Reactions To Form Amides

In each carbonylation reaction, the sample vial was heated at 130°C for 10 minutes. In every case, a build up of pressure inside the sample vial was evidenced by the bulging of the septum soon after heating had begun. This was accompanied by THF visibly refluxing inside the sample vial. Each run varied in the palladium species employed and the amount of benzylamine and triphenylphosphine used. The conditions employed in each carbonylation reaction are summarised in Table 3.7.

Table 3.7. Conditions employed in [^{11}C]carbonylation reactions

Run	Substrate (amount)	Benzylamine	PPh_3	Catalyst (loading)	Temperature	Reaction time
1	Iodobenzene (11 µmol)	0.1 ml (large excess)	20 µmol in THF (0.1 ml)	$Pd(OAc)_2$ (20 mol %)	130°C	10 min
2		3 mg (equivalent)	20 µmol in THF (0.3 ml)			
3		0.3 ml (large excess)	33 µmol (no THF)	$Pd(dppp)Cl_2$ (20 mol %)		
4		13 mg (slight excess)	33 µmol in THF (0.4 ml)			

Analytical HPLC was used to identify the product distribution using radio and UV detectors. By coinjecting the product mixture with a sample of unlabelled reference amide it was possible to identify the amide on the UV trace. This could then be superimposed onto the radio HPLC trace to identify the corresponding peak on the radio trace. In each case, the radiochemical purity of a species was calculated by integration of the peaks on the radio HPLC trace (Table 3.8).

At the end of each carbonylation reaction, air was purged through the sample vial in order to displace any unreacted ^{11}CO gas. The radioactivity of the liquid in the sample vial was then measured and this value was assumed to correspond to the total radioactivity of the ^{11}C-labelled products. From this, the amount of radioactivity used for product formation could be calculated as a fraction of the total radioactivity delivered to the system. Multiplication of this fraction by the radiochemical purity of the amide gave the corresponding radiochemical yield (Table 3.8).

Table 3.8. Product distribution in [^{11}C]carbonylation reactions

Run	Radiochemical purity[a] (acid) /%	Radiochemical purity[a] (amide) /%	Liquid radioactivity (corrected) /MBq	Total radioactivity (corrected) /MBq	Liquid radioactivity / total radioacitivity	Radiochemical yield[b] (amide) /%
1	16	64	2015	5070	0.40	26
2	55	14	3874	4111	0.94	13
3	1	82	2096	4069	0.52	43
4	<1	66	262	1859	0.14	9

(a) Radiochemical purity determined by analytical radio HPLC; (b) Decay corrected radiochemical yields are based on the measured radioactivity trapped in the liquid phase at the end of synthesis compared to the total radioactivity delivered to the system and are corrected by their radiochemical purities.

Runs 1 and 2, performed using $Pd(OAc)_2$ + PPh_3 as the catalytic species, were found to produce significant amounts of [*carbonyl*-^{11}C]benzoic acid. Run 2, which used a stoichiometric amount of benzylamine rather than a large excess, produced 55 % of this species based on integration of the radio trace. This species is believed to form as a consequence of the low concentration of benzylamine in the reaction solution, which is particularly significant in Run 2. In this instance, the reductive elimination step in the catalytic cycle becomes rate-limiting and results in build-up of the Pd-CO-aryl species by the end of the reaction. This species is then quenched by water during HPLC analysis resulting in the formation of [*carbonyl*-^{11}C]benzoic acid (Figure 3.12).

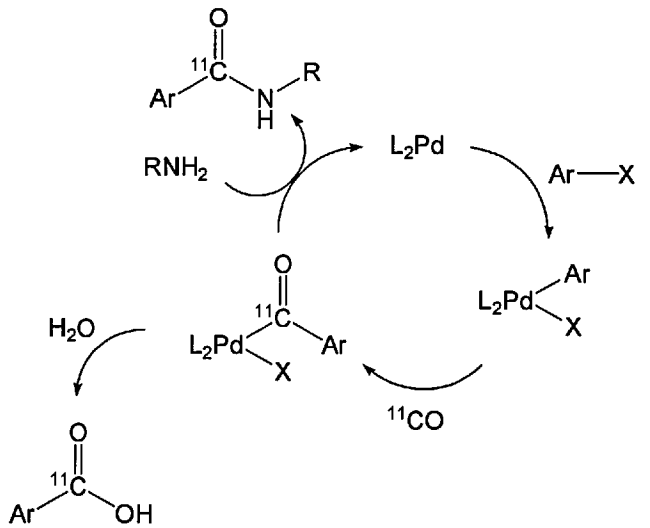


Figure 3.12. Catalytic cycle of [^{11}C]carbonylation reaction.

Runs 3 and 4, performed using Pd(dppp)Cl_2 as catalyst, resulted in negligible quantities of [*carbonyl*-^{11}C]benzoic acid being produced. The best results were obtained for Run 3, using a large excess of benzylamine, with [*carbonyl*-^{11}C]*N*-benzylbenzamide being obtained with a radiochemical purity of 82 %. This corresponds to a radiochemical yield of 43 % based on the total amount of ^{11}CO delivered to the system.

In each case, the amide peak on the radio HPLC was found to display a shoulder peak, indicating an unknown radiochemical impurity believed to result from impurities in the iodobenzene starting material.

3.3.3 Summary

The carbonylation reactions performed to date provide some very encouraging results, particularly as the CuCl/KTp* system has been shown to be capable of trapping ^{11}CO almost quantitatively in one sweep of the dilute gas stream. This shows that the gas can be efficiently and selectively solubilised using small quantities of trapping solution (1 ml).

The trapping efficiency compares very favourably to the results obtained by Al-Qahtani *et al.*[2, 3] in which Stille-type [^{11}C]carbonylation reactions were performed in a

DME/water solution. Here, radiochemical yields of [*carbonyl*-^{11}C]benzophenones greater than 98 % were reported based on the amount of radioactivity initially trapped by the solvent. However, only 6 % of the radioactivity was trapped by a single pass of the $^{11}CO/N_2$ gas stream through the DME/water solution.[3] Similarly, Langstrom *et al.*[4] have reported a ^{11}CO trapping efficiency of ~10 % when using DMSO, DMF and THF solutions for the synthesis of ^{11}C-labelled ketones. In 2004 Audrain *et al.*[5] reported trapping efficiencies of > 90 % using a BH_3.THF solution. This process involved use of the molecular sieve ^{11}CO-preconcentration step followed by passing the $^{11}CO/N_2$ gas stream through a solution of BH_3.THF at -78°C. The resultant BH_3CO complex was then passed through an empty vial at -60°C to condense the THF and finally through a reaction vial containing the cross-coupling reagents in solution at -78°C.

The CuCl/KTp* trapping system may prove advantageous over the above methods as it is an easily-assembled, one-pot procedure which requires inexpensive reagents and provides highly reproducible results. Furthermore, it allows the trapping process to be performed rapidly at room temperature without the need for any ^{11}CO preconcentration or harsh reaction conditions.

The previous difficulties in solubilising ^{11}CO have led to alternative handling techniques including gas recirculation[6] and high pressure microautoclave devices.[7, 8] The relative simplicity of the CuCl/KTp* system in that there is no need for complicated apparatus or harsh reaction conditions is hoped to allow its application in the synthesis of a range of ^{11}C-labelled molecules. The results obtained so far indicate that a [*carbonyl*-^{11}C]-labelled amide, *N*-benzylbenzamide, can be produced using this system, and in moderate radiochemical yield. Clearly further studies are necessary to optimise the conditions of this reaction and to prove its reproducibility. These have not been possible to date due to restricted access to the radiochemical laboratory.

3.4 Future Work

3.4.1 [^{11}C]Carbonylations

The preliminary results for the carbonylation reactions performed with the trapped ^{11}CO provide scope for a wide range of follow-up experiments. When performing future reactions it would be advisable to use freshly distilled reagents to minimise the formation of unwanted side-products. Repeat experiments would then be performed in order to gain an insight into the consistency and reproducibility of the results.

Following this, a range of different aryl-halide substrates could be investigated to see the effect that substituent groups have on the radiochemical yields and purity. For example, substituted aryl-halides, such as those containing *para*-trifluoromethyl and -methoxy groups could be used to study the effects of substrate electronics on product formation (Figure 3.13). It is estimated that these reactions will follow the trends observed for the 'cold' carbonylation reactions, in which the greatest yields were obtained with the electron-poor substrates, due to their increased rate of oxidative addition to palladium.

As well as the synthesis of ^{11}C-labelled amides, it would be worthwhile to extend these investigations into the Stille- and Suzuki-type coupling reactions used to produce ^{11}C-labelled ketones from organotin reagents and alkyl/aryl-boronic acids, respectively (Figure 3.13).

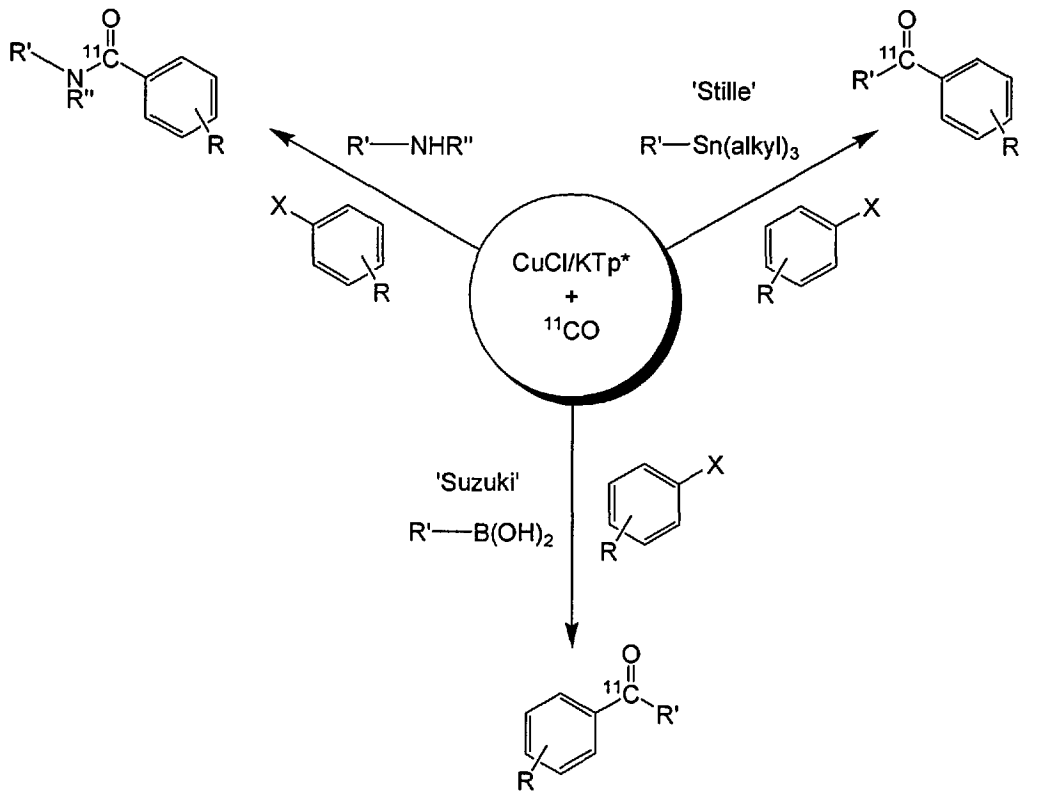


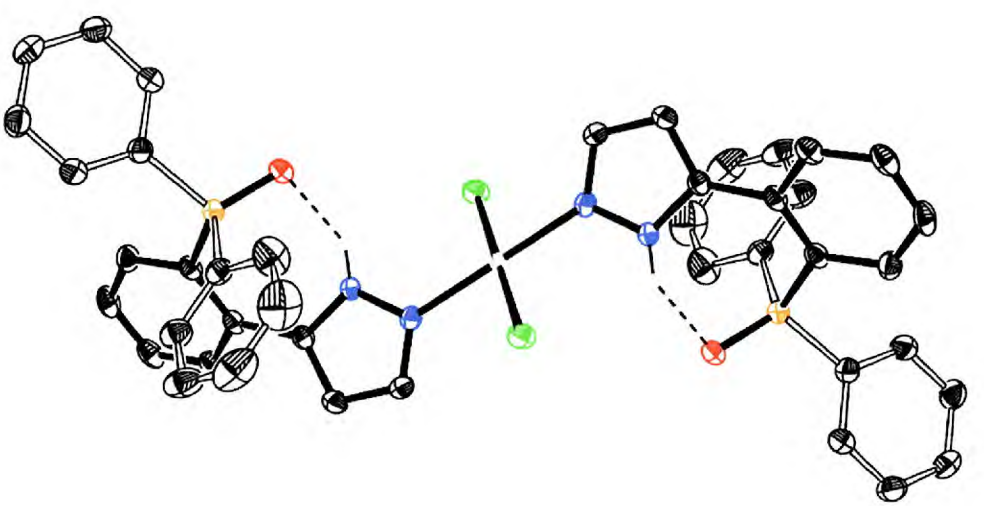
Figure 3.13. Alternative functional groups to be synthesised using tandem ^{11}CO trapping/carbonylation reactions

3.5 References

1. P. W. Miller, N. J. Long, A. J. De Mello, R. Vilar, J. Passchier and A. Gee, *Chem. Commun.*, 2006, 546.
2. M. H. Al-Qahtani and V. W. Pike, *J. Label. Compd. Radiopharm.*, 2000, **43**, 825.
3. M. H. Al-Qahtani and V. W. Pike, *J. Chem. Soc., Perkin Trans. 1*, 2000, 1033.
4. Y. Andersson and B. Langstrom, *J. Chem. Soc., Perkin Trans. 1*, 1995, 287.
5. H. Audrain, L. Martarello, A. Gee and D. Bender, *Chem. Commun.*, 2004, 558-559.
6. P. Lidstrom, T. Kihlberg and B. Langstrom, *J. Chem. Soc., Perkin Trans. 1*, 1997, 2701.
7. T. Kihlberg, B. Langstrom and F. T. J. Eriksson, *Method and apparatus for production and cse of [^{11}C]carbon monoxide in labelling synthesis, Patent Application, PCT/SE02/01222.*
8. E. D. Hostetler and H. D. Burns, *Nucl. Med. Biol.*, 2002, **29**, 845.

CHAPTER 4

COORDINATION CHEMISTRY OF HEMILABILE LIGANDS



4. Coordination Chemistry of Hemilabile Ligands

4.1 Introduction

4.1.1 Hemilability

Over recent years, considerable attention has been drawn towards the coordination chemistry of hybrid ligands, *i.e.* those molecules containing significantly different donor groups. Of particular interest are the metal complexes of hybrid 'hemilabile' ligands,[1, 2] containing at least one substitutionally inert donor group and one or more substitutionally labile donor groups. These ligands can allow the donor group with the lowest affinity towards the metal to dissociate to create a vacant coordination site which is then available to accommodate a new substrate. The 'anchor' effect of the stronger, permanently-bound donor group means that after the substrate has left the coordination sphere of the metal, chelation can again occur to stabilise the metal (Figure 4.1).

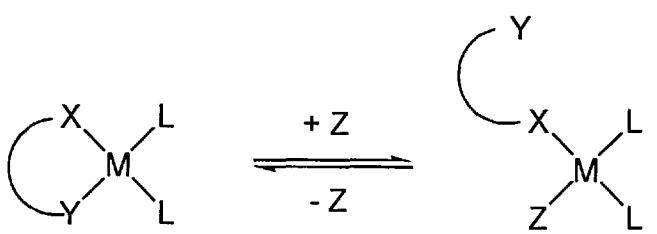


Figure 4.1. Hemilabile ligand behaviour: Stabilisation of a metal in the absence of a small molecule substrate (left) and partial dissociation to allow substrate binding (right).

These enticing properties of hemilabile ligands have led them to receive much interest in the field of catalysis (see for example reviews [1, 3] and references therein), as well as in functional materials,[3-5] and molecular activation.[6-12] Due to their ability to reversibly bind to analytes, hemilabile coordination complexes have recently been explored for application as small-molecule chemosensors (see review [13] and references therein). It is interesting to note that hemilabile ligands have been applied in the sensing of CO.[14, 15] For this application, a hemilabile rhodium(I) phosphine-ether complex was found to exhibit a change in absorbance spectrum in the presence and absence of CO.

The most studied class of hemilabile ligands are bifunctional molecules containing a phosphorus donor moiety as the substitutionally inert anchor group. This is owed largely to the widespread use of transition metal phosphine complexes in homogeneous catalysis. The most common ligand types within this field are P,O, P,N and P,S[16] ligands. The P,N ligands have found application in a range of catalytic processes including cross-coupling reactions, carbonylation reactions, ring-opening and ring-closing metathesis polymerisation.

An example of the ability of hemilabile ligands to facilitate catalytic processes is described with reference to the palladium-catalysed carbonylations, discussed previously in Chapter 3. In this modified catalytic cycle (Figure 4.2) the hemilabile ligand is able to stabilise the Pd–Ar species by coordination of the phosphine anchor group, P, and the substitutionally labile donor, D. In the presence of carbon monoxide this donor group may dissociate to allow coordination of the carbonyl. The migratory insertion step to form the Pd–Acyl species creates a vacant site which can be stabilised once more by chelation of the P,D ligand. Once this is complete, reductive elimination yields the carbonylated product and the regenerated palladium(0) species. In this example, the potential beneficial effect of the hemilabile ligand is two-fold: (i) to prevent decomposition of the palladium complex in the absence of substrate and (ii) to stabilise the migratory insertion product by occupation of the vacant site.

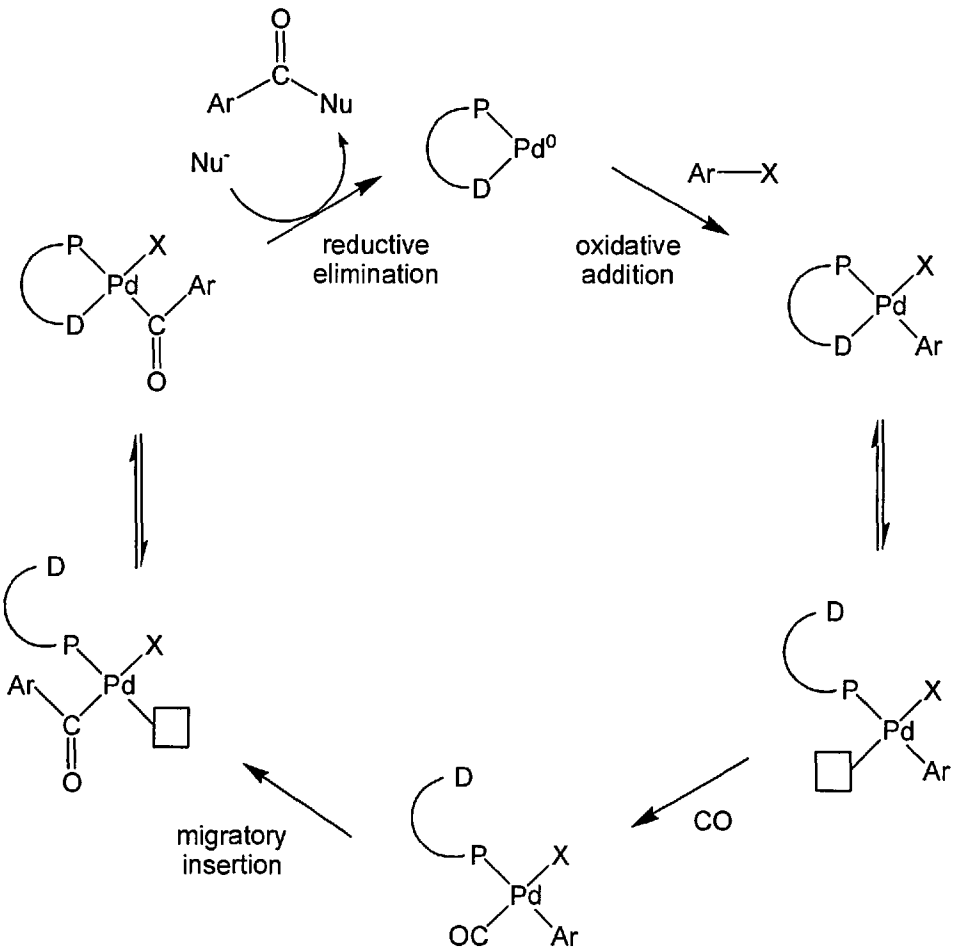


Figure 4.2. Proposed application of hemilabile ligands to palladium-catalysed carbonylation reactions.

4.1.2 Pyrazole-Donor Ligands

The chemistry of pyrazole and its derivatives has been established for over 100 years.[17] This heterocyclic species can act as a ligand via coordination of the lone pair of the unprotonated nitrogen atom. The two most common synthetic routes to pyrazoles (Figure 4.3) are through a 1,3-dipolar cycloaddition between a diazomethane derivative and an acetylene (route **A**) or by ring closure of a β-diketone (or derivative thereof) with hydrazine (route **B**).

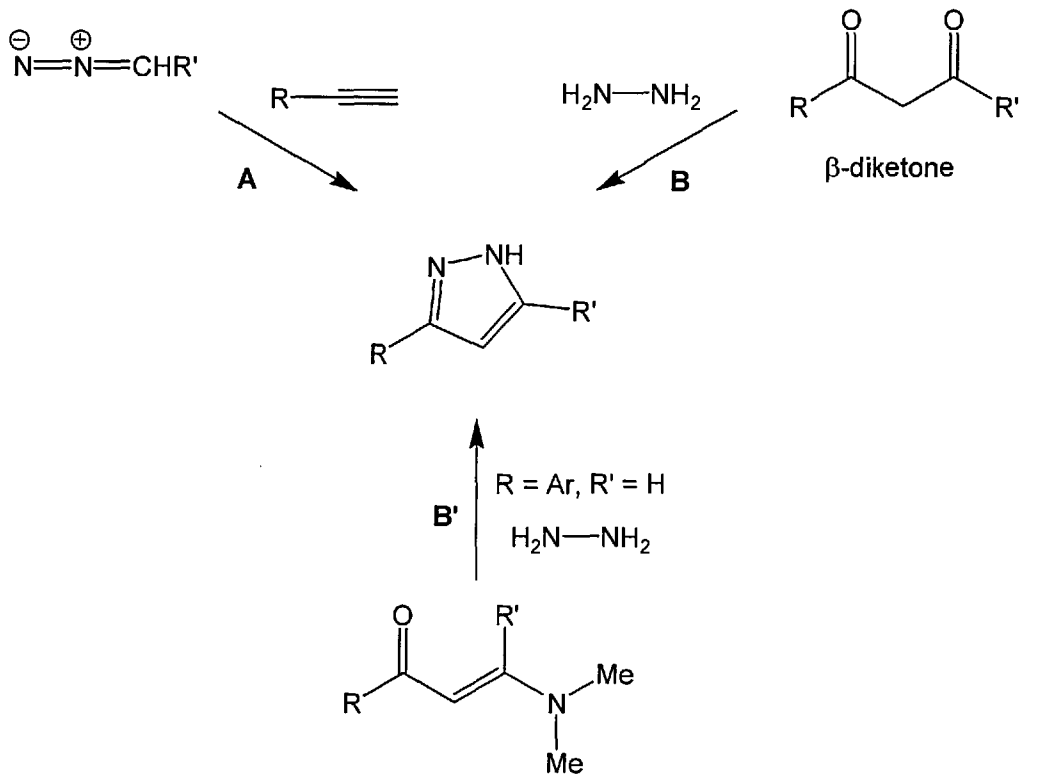


Figure 4.3. Synthetic pathways to form pyrazoles.

The latter strategy is favourable as the substitution pattern of the resultant pyrazole is determined by the substitution pattern of the β-diketone starting material. Analogous compounds which possess similar reactivity to β-diketones can also be applied to the synthesis of pyrazoles. One such example is 1-aryl-3-dimethylaminoprop-2-enones which can be thought of as 'masked' aromatic β-diketo aldehydes as they undergo analogous condensation reactions with hydrazine to form 3(5)-aryl pyrazoles (route **B'** in Figure 4.3).[18] In 2001 Thiel *et al.* reported a simple and rapid synthesis of 1-aryl-3-dimethylaminoprop-2-enones using microwave irradiation of an aromatic acetyl compound and *N,N*-dimethylformamide dimethylacetal (Figure 4.4).[18]

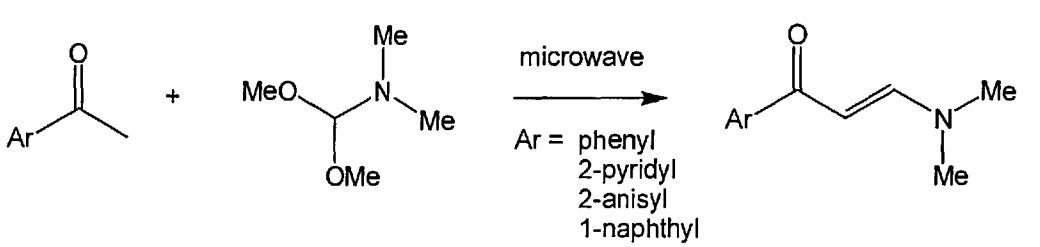


Figure 4.4. Synthesis of 1-aryl-3-dimethylaminoprop-2-enones.

With this reactivity in mind, it was decided to investigate the use of phosphino-substituted aromatic acetyls for the synthesis of new phosphino-substituted pyrazoles.

4.2 Novel Hybrid N,P Ligand

4.2.1 Proposed Ligand System

The proposed ligand, Hpz^{phos}, (Figure 4.5) is an N,P donor consisting of a triphenylphosphine unit (soft donor) bearing a pyrazole group (hard donor) in the *ortho*-position of one phenyl ring.

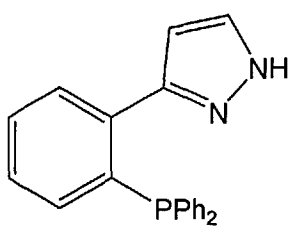


Figure 4.5. Proposed N,P hybrid ligand, Hpz^{phos}.

The interest in this species stems from (i) the potential hemilability of the parent complex, (ii) the ease of derivatisation by chalcogenation of the phosphine moiety thus giving rise to new N,P=O, N,P=S and N,P=Se ligands and (iii) the scope for further functionalisation by reaction at the N–H moiety. This last feature is particularly enticing as it may enable modifications of the steric or electronic properties of the ligand, which could be used to tune the ligand's coordination behaviour towards a metal centre. This functionalisation has been explored in Chapter 5 for the synthesis of a range of novel tris- and tetrakis-pyrazolylborate ligands.

A structurally similar ligand bearing the same triphenylphosphine unit, in this case attached to the pyrazolyl ring via the nitrogen atom (1-position) has recently been reported and has been shown to be active in the nickel catalysed oligomerisation of ethylene.[19] Furthermore, a bis(pyrazol-1-yl)methane ligand bearing diphenylphosphine groups directly attached to the pyrazole rings, rather than through a phenylene-linker, has also been described in the literature.[20] This N,P ligand is also closely related to diphenyl(2-(2'-pyridyl)phenyl) phosphine in which a pyridyl unit

replaces the pyrazolyl ring. This has been used as a ligand in various catalytic processes.[21-23] In addition, the coordination behaviour of a range of N,P,[24-26] ligands is well established in the literature and to a lesser extent, the chemistry of N,P=O[27-34] and N,P=S ligands[35-39] thus highlighting the ongoing interest in this field of chemistry.

The work presented in the following sections describes the formation of the N,P ligand and its N,O and N,S derivatives and their coordination chemistry towards palladium(II). The application of the N,P ligand in palladium-catalysed carbonylation reactions is also investigated.

4.2.2 Proposed Synthetic Pathway

The synthesis of acetophenone bearing a diphenylphosphine substituent in the 2-position has been described in the literature.[40] It was envisaged that this could act as the aromatic acetyl compound for conversion to the corresponding pyrazole in two steps as depicted in Figure 4.6.

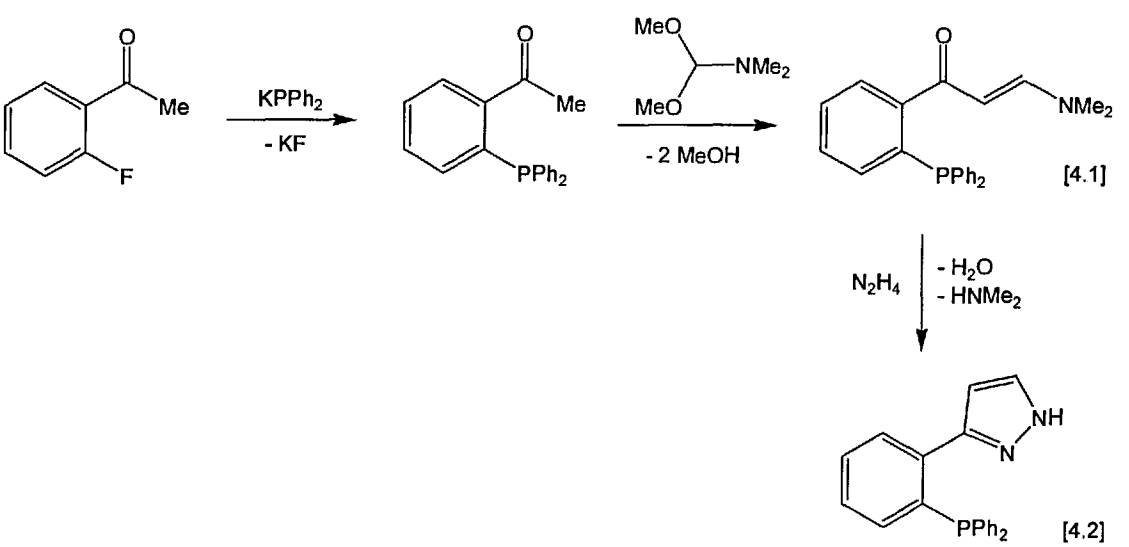


Figure 4.6. Proposed synthesis of the N,P ligand, Hpz^{phos} (**4.2**).

4.2.3 Synthesis of Enone (4.1)

2-Diphenylphosphino acetophenone was synthesised in one step from a refluxing solution of potassium diphenylphosphide and 2-fluoroacetophenone in THF.[40] After

characterisation by ^{1}H and $^{31}P\{^{1}H\}$ NMR spectroscopy and mass spectrometry this compound was converted to the 'masked' β-keto aldehyde (**4.1**) by reaction with refluxing dimethylformamide dimethylacetal (Figure 4.6). This reaction proceeded cleanly to give 1-(2'-diphenylphosphino)phenyl-3-dimethylamino-2-propene-1-one (**4.1**), as an orange solid in excellent yield (92 %). Mass spectrometry (EI) shows the molecular ion at 359 m/z as expected. ^{1}H and $^{31}P\{^{1}H\}$ NMR spectroscopic data for this compound are summarised in Figure 4.7. The ^{1}H assignments were aided by the ^{1}H COSY NMR spectrum.

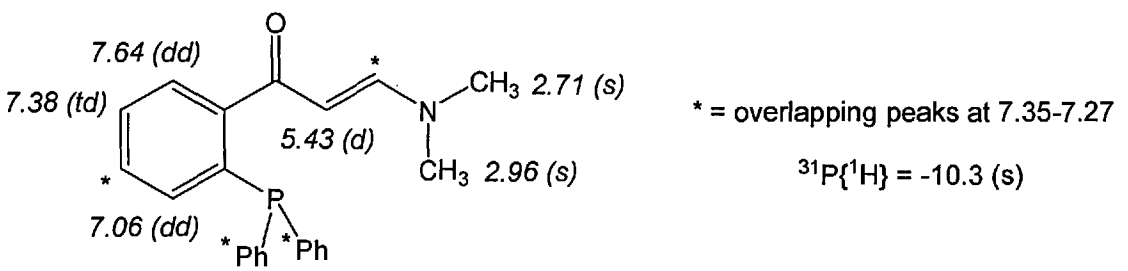


Figure 4.7. Summary of ^{1}H and $^{31}P\{^{1}H\}$ NMR data for masked β-keto aldehyde **4.1**.

$^{31}P\{^{1}H\}$ NMR spectroscopy provides a useful means to follow the progress of these reactions. Here a single peak at -10.3 ppm indicates that no other phosphorus-containing products have been formed. The purity of this species was further confirmed by elemental analysis.

4.2.4 Synthesis of Hpz^{phos} (4.2)

Reaction of **4.1** with hydrazine hydrate in refluxing ethanol (Figure 4.6) gave the desired pyrazole **4.2** in high yield (91 %) after recrystallisation. Formation of the desired species was initially provided by mass spectrometry (EI) showing the molecular ion at 328 m/z. ^{1}H NMR assignments based on analysis of the ^{1}H COSY spectrum are summarised in Table 4.1 alongside the $^{31}P\{^{1}H\}$ NMR and IR data. Upon formation of the pyrazolyl ligand, a broad NH proton is now present on the ^{1}H NMR spectrum at 10.57 ppm. The protons found in the 4-pyrazolyl and 5-pyrazolyl positions are found at 6.34 and 7.48 ppm, respectively. $^{31}P\{^{1}H\}$ NMR shows a singlet at -11.4 ppm corresponding to the new species.

4.2.5 Synthesis of $Hpz^{phos(O)}$ (4.3)

The corresponding phosphine oxide species **4.3** was synthesised by reaction of **4.2** with a slight excess of hydrogen peroxide in DCM (Figure 4.8). This reaction proceeded quickly (< 5 minutes) and quantitatively as judged by $^{31}P\{^{1}H\}$ NMR of the reaction solution. However, losses incurred during work-up led to only a moderate yield of the isolated product **4.3** (63 %).

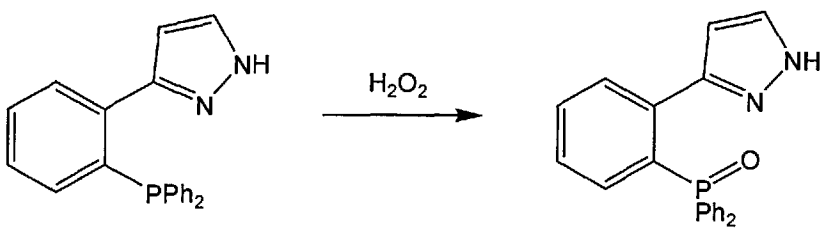


Figure 4.8. Synthesis of the N,O ligand, $Hpz^{phos(O)}$ (**4.3**).

This N,O ligand **4.3** was characterised by ^{1}H and $^{31}P\{^{1}H\}$ NMR spectroscopy (Table 4.1). The $^{31}P\{^{1}H\}$ NMR of the resultant solid shows a singlet at 35.8 ppm. This large downfield shift from the starting material reflects the oxidation of the phosphine moiety whereby it has become considerably deshielded.

Slow diffusion of pentane into a chloroform solution of **4.3** produced single crystals suitable for X-ray analysis. The solid-state structure (Figure 4.9) shows that the molecule dimerises in the solid state via intermolecular hydrogen bonding between adjacent molecules.

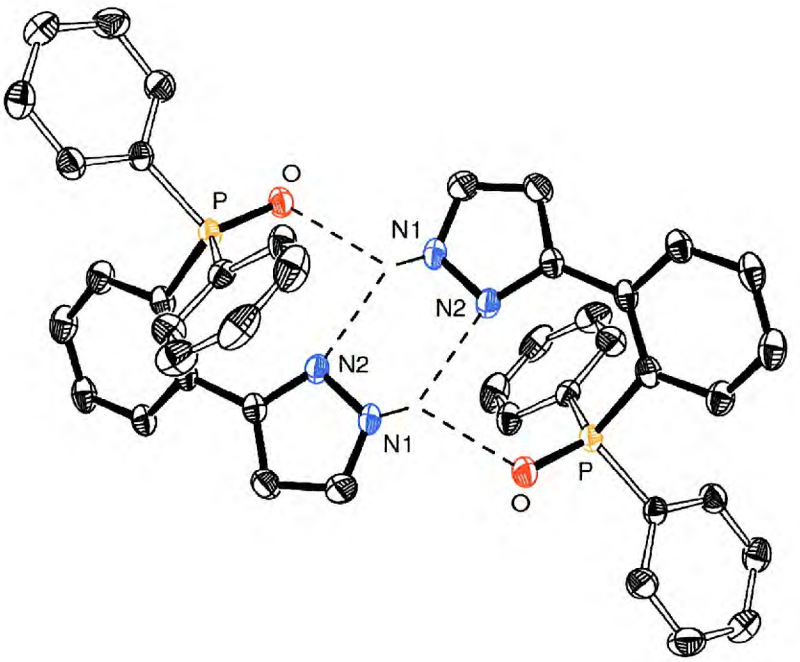


Figure 4.9. Molecular structure of $Hpz^{phos(O)}$ **(4.3)** (50% probability ellipsoids).

It is interesting to note that in the solid state the hydrogen bond from the pyrazole N–H donor is shared equally between two acceptors on the opposing molecule – the unprotonated pyrazole nitrogen and the oxygen atom of the P=O moiety. The N–H···O hydrogen bonds have N···O, H···O (Å), and N–H···O (°) of 2.91, 2.54 and 133 respectively; the N–H···N hydrogen bonds have N···N, H···N (Å), and N–H···N (°) of 2.94, 2.22 and 141 respectively. This dimerisation may also exist in solution as the N–H in the ^{1}H NMR spectrum is found far downfield at 13.24 ppm, whereas the parent complex **4.2** (containing no P=O group) shows the corresponding N–H peak at 10.57 ppm (Table 4.1). This is likely to be the result of reduced electron density around the N–H hydrogen, due to the sharing of its electron density with both the pyrazole nitrogen and the oxygen atom.

4.2.6 Synthesis of $Hpz^{phos(S)}$ (4.4)

In a similar reaction to the oxidation step, the corresponding phosphine sulphide **4.4** was formed by reaction of **4.2** with elemental sulphur (Figure 4.10).

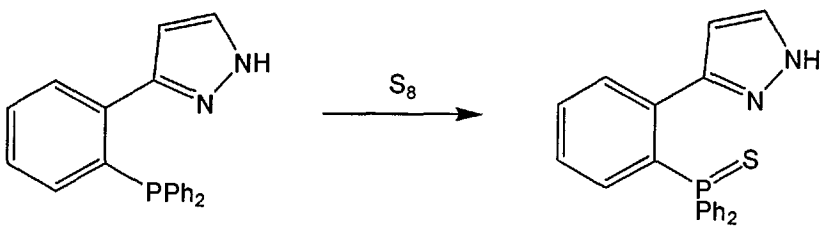


Figure 4.10. Synthesis of the N,S ligand, $Hpz^{phos(S)}$ **(4.4).**

This reaction proceeded in good yield (76 %) to produce the N,S ligand **4.4** as confirmed by NMR and IR spectroscopy (Table 4.1). Again, a large downfield shift in the $^{31}P\{^{1}H\}$ NMR is observed (43.3 ppm). Hydrogen bonding in the solution state may also be present in this species as evidenced by the downfield position of the N–H hydrogen in the ^{1}H NMR spectrum (12.54 ppm).

4.2.7 Summary

Three potentially bidentate, mixed-donor ligands based on a triphenylphosphine unit bearing a pyrazole group in the *ortho* position of one phenyl ring have been synthesised. All three ligands were isolated as air-stable, white solids in good yields and were fully characterised (Table 4.1). The numbering scheme used to identify the various phenyl and pyrazolyl proton positions is shown in Figure 4.11.

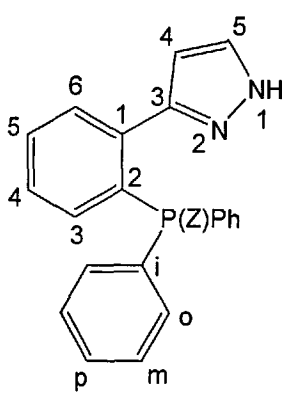


Figure 4.11. Numbering scheme used to describe the ^{1}H environments in ligands **4.2-4.4.**

Table 4.1. IR, ^{1}H and $^{31}P\{^{1}H\}$ NMR data for the three ligands **4.2-4.4**

Ligand	$^{31}P\{^{1}H\}$ NMR[a] δ/ppm	^{1}H NMR[a] δ/ppm								IR[b] ν/cm^{-1}
	P	*NH*	*5-pz*	*4-pz*	*3-Ph*	*4-Ph*	*5-Ph*	*6-Ph*	*Ph-H*	*NH*
4.2 Hpz^{phos}	- 11.4	10.57	7.48 (d)	6.34 (m)	7.03 (ddd)	overlap with Ph-H at 7.30	7.42 (ddd)	7.60 (dd)	7.26-7.37 (m)	3187
4.3 $Hpz^{phos(O)}$	35.8	13.24	7.32 (d)	6.25 (br s)	7.14 (ddd)	7.30 (m)	overlap with Ph-H at 7.61	7.78 (ddd)	7.38-7.64 (m)	3186
4.4 $Hpz^{phos(S)}$	43.3	12.54	7.17 (d)	6.08 (br s)	7.18 (dd)	7.37 (m)	overlap at 7.57 (m)		7.82 (m) & 7.37-7.44 (m)	3220

(a) Recorded in $CDCl_3$ solution; (b) Recorded as KBr disc.

In each ligand the 6-Ph proton is found furthest downfield in the ^{1}H NMR spectrum due to its close proximity to the electron withdrawing pyrazolyl ring. Conversely, the 3-Ph proton is furthest upfield of all the phenyl protons. The 4-pz proton occurs characteristically upfield of the other aromatic protons at around 6 ppm. This is due to weaker ring currents in the pyrazolyl ring compared to the phenyl rings. The 5-pz proton, however, is always observed further downfield (amongst the phenyl protons) due to its close proximity to the electron-withdrawing nitrogen atom.

4.2.8 Coincidental Research

Coincidentally during the course of this research, **4.2** was independently published,[41] albeit by a slightly different synthetic route. In this work, Thiel *et al.* described the synthesis of triphenylphosphine ligands bearing pyrazole in the *ortho* or *meta* position of one of the three phenyl rings. The *ortho* derivative is **4.2**. The pyrazoles were synthesised from diphenylphosphino acetophenones using the same two steps described above (dimethylformamide dimethylacetal then hydrazine). The significant difference in approach came from the synthesis of the diphenylphosphino acetophenones (Figure 4.12).

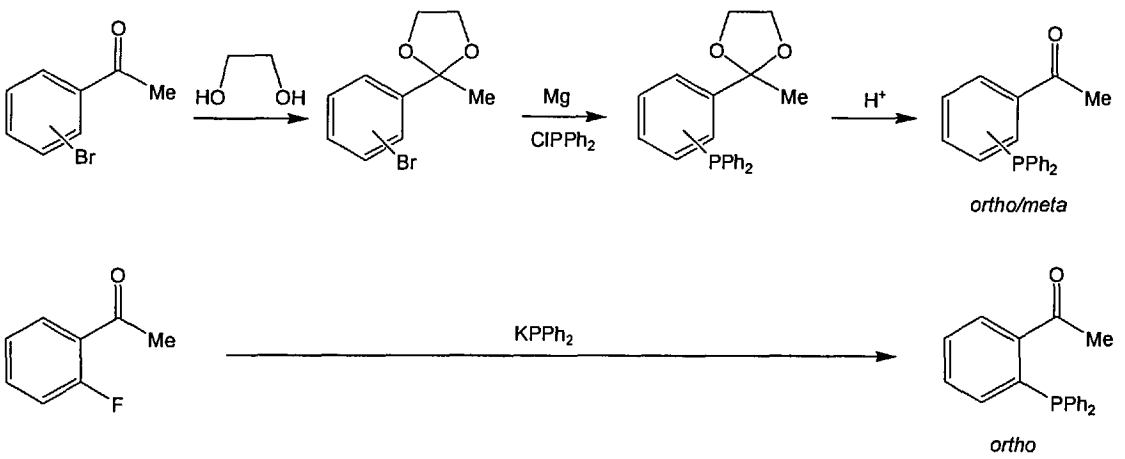


Figure 4.12. Synthetic pathways to phosphinated acetophenones.

Thiel *et al.* used a three-step procedure starting from bromoacetophenone to form the *ortho* and *meta* products in 'good' yield. In this report, an alternative one-step synthesis from $KPPh_2$ and 2-fluoroacetophenone was used to synthesise the *ortho* derivative in excellent yield. While the latter approach is favourable for the synthesis of the *ortho* derivative, it would not be applicable to the synthesis of the *meta* product due to the poor reactivity of 3-fluoroacetophenone towards $KPPh_2$.

4.3 Palladium(II) Coordination Chemistry of Hpz^{phos} (4.2)

Having formed three hybrid ligands consisting of N,P, N,O and N,S donor moieties it was decided to investigate their coordination chemistry towards palladium(II) in the solid and solution state. This was hoped to gain an insight into the behaviour of these ligands and similar compounds during their role in catalytic transformations.

The reactions performed with the N,P ligand **4.2** towards palladium(II) are summarised in Figure 4.13. These reactions examined the variation in coordination behaviour of the ligand depending on the ligand-to-palladium ratio. Replacement of the chloride anions with perchlorate anions was also performed to examine the effect of the counter-anion on the resultant complex.

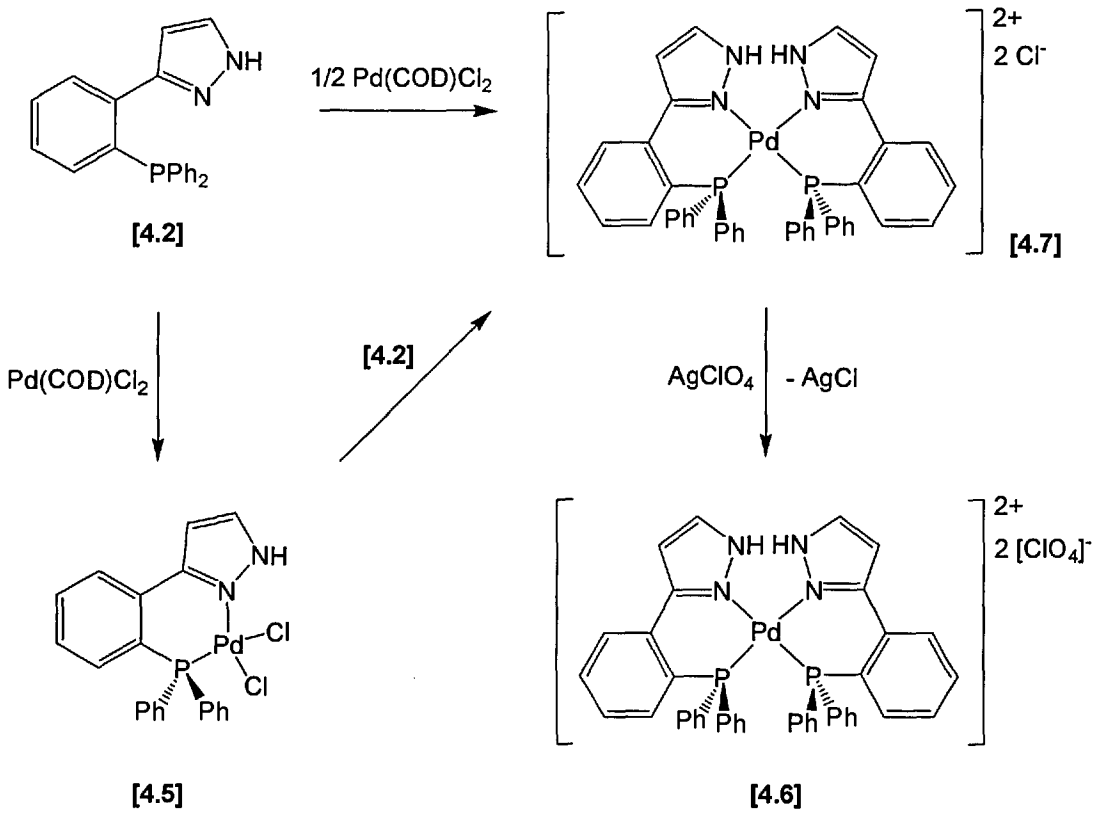


Figure 4.13. Summary of reactions of Hpz^{phos} (**4.2**) with palladium(II) species.

4.3.1 Synthesis of Mono-Chelate (4.5)

Addition of **4.2** in dichloromethane to $Pd(COD)Cl_2$ in a 1:1 molar ratio gave a yellow precipitate (**4.5**) that could be crystallised by slow diffusion of pentane into a chloroform solution of the complex. This complex was analysed by NMR spectroscopy (Table 4.5) and X-ray crystallography (Figure 4.14) and was found to be identical to the complex independently synthesised by Thiel *et al.*[41] by the similar reaction of **4.2** with $Pd(PhCN)_2Cl_2$. In this complex, a single ligand unit chelates to the palladium in via the N and P donor groups with the remaining two coordination sites occupied by chloro ligands to form a $[Pd(Hpz^{phos}\text{-}\kappa^2N,P)Cl_2]$ complex. Selected bond lengths and angles are given in Table 4.2.

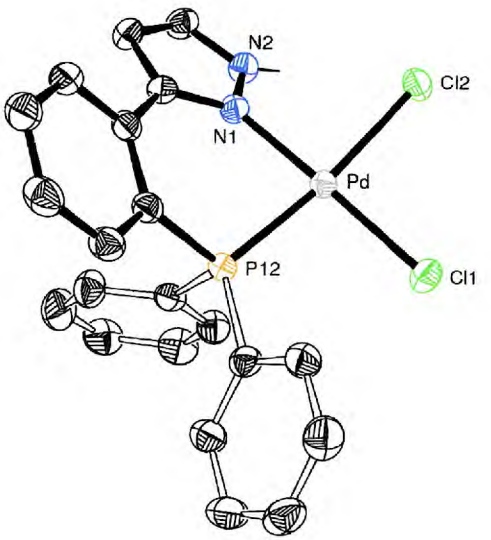


Figure 4.14. Molecular structure of [Pd(Hpz^{phos})Cl_2] (**4.5**) (50% probability ellipsoids).

Table 4.2. Selected bond lengths (Å) and angles (°) for **4.5**

Pd–N(1)	2.0249(17)	Pd–Cl(1)	2.2888(6)
Pd–P(12)	2.2277(6)	Pd–Cl(2)	2.3718(6)
N(2)–N(1)	1.348(2)		
N(1)–Pd–Cl(1)	176.22(5)	P(12)–Pd–Cl(2)	172.244(19)
N(1)–Pd–Cl(2)	89.55(5)	P(12)–Pd–Cl(1)	95.29(2)
N(1)–Pd–P(12)	84.60(5)	Cl(2)–Pd–Cl(1)	90.89(2)

4.3.2 Synthesis of Bis-Chelate (4.6)

Upon increasing the ligand-to-metal ratio from 1:1 to 2:1, it was observed that addition of Pd(COD)Cl_2 to **4.2** gave a different product in solution. This was evidenced by the $^{31}P\{^1H\}$ NMR spectrum of the reaction solution (taken after one hour of stirring) which contained a major peak at 31.8 ppm, corresponding to the new species, and an additional smaller peak at 25.7 ppm corresponding to traces of the 1:1 complex **4.5**. Complex **4.6** was isolated as a yellow solid by precipitation from a dichloromethane solution with hexane.

The $^{31}P\{^1H\}$ NMR spectrum of **4.6** showed one singlet at 31.8 ppm (*c.f.* free N,P ligand **4.2** at -11.4 ppm) indicating the coordination of the two N,P ligands to the palladium centre in chemically equivalent environments. The N–H hydrogen of the pyrazole ring was found to be significantly shifted downfield in the ^1H NMR

spectrum to 14.86 ppm compared to the free N,P ligand (δ = 10.57 ppm), suggesting coordination of the adjacent nitrogen atom of the pyrazole ring to the metal centre (Table 4.5). The bis-ligated nature of **4.6** was confirmed by ESI mass spectrometry which showed a molecular ion peak at 761 m/z corresponding to $[Pd(Hpz^{phos})_2 - H]^+$. For structural confirmation crystals suitable for X-ray diffraction were grown by slow diffusion of pentane into a chloroform solution of the complex.

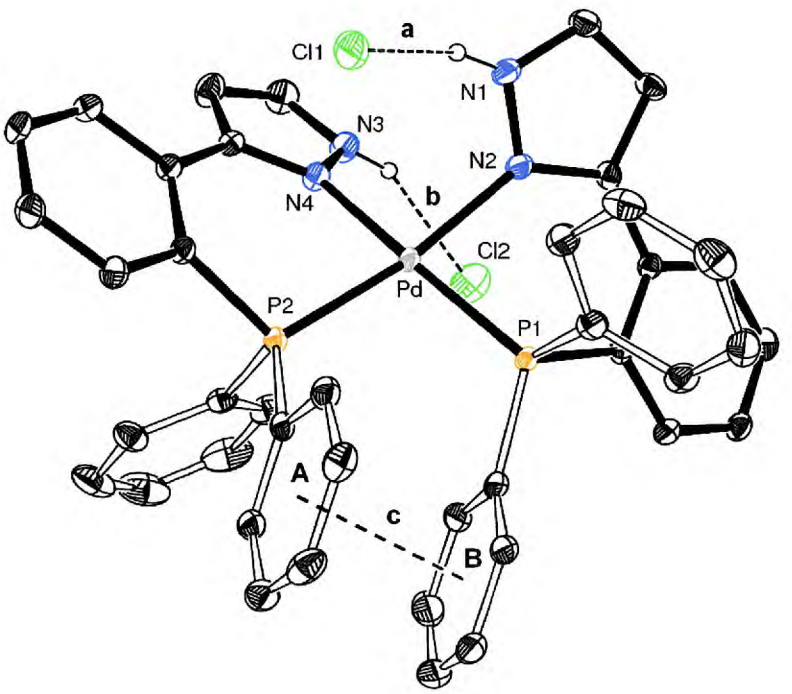


Figure 4.15. Molecular structure of $[Pd(Hpz^{phos})_2]Cl_2$ (**4.6**) (30% probability ellipsoids).

The solid state structure of **4.6** (Figure 4.15) shows the palladium to have a distorted square planar geometry with the two N,P ligands chelating in a *cis* fashion resulting in a dicationic species in which two chloride anions balance the charge. The N–H hydrogen atoms are linked to the chloride anions by N–H···Cl hydrogen bonds. The N–H···Cl hydrogen bonds have N···Cl, H···Cl (Å), and N–H···Cl (°) of (**a**) 3.21, 2.51, 145 and (**b**) 3.01, 2.21, 152 respectively. Selected bond lengths and angles are shown in Table 4.3.

Table 4.3. Selected bond lengths (Å) and angles (°) for **4.6**

Pd–N(2)	2.072(4)	Pd–P(1)	2.2565(13)
Pd–N(4)	2.074(4)	Pd–P(2)	2.2541(13)
N(2)–N(1)	1.360(6)	N(4)–N(3)	1.344(6)
N(2)–Pd–P(1)	83.86(12)	N(4)–Pd–N(2)	92.77(16)
N(2)–Pd–P(2)	168.33(12)	P(1)–Pd–N(4)	169.39(12)
P(1)–Pd–P(2)	101.57(5)	N(4)–Pd–P(2)	83.63(12)

Within each ligand the linked phenyl and pyrazolyl rings are distinctly twisted with respect to each other, the torsion angles for the C–C bond between them being *ca.* 20 and 26° for the N(4) and N(2) ligands respectively. The two {Pd,P,N} coordination planes are twisted with respect to each other by *ca.* 15°, a distortion that may in part be due to a π-π stacking interaction (**c**) between pendant phenyl rings on adjacent ligands. The π-π stacking interaction has centroid···centroid and mean interplanar separations of *ca.* 3.57 and 3.18 Å respectively, the two rings being inclined by *ca.* 7°. The presence of these interactions in solution may be indicated by the ambient temperature ^{1}H NMR spectrum which shows some significantly broadened peaks in the aromatic region. Following this observation, variable temperature spectra were recorded upon cooling the solution to 223 K (aromatic region shown in Figure 4.16).

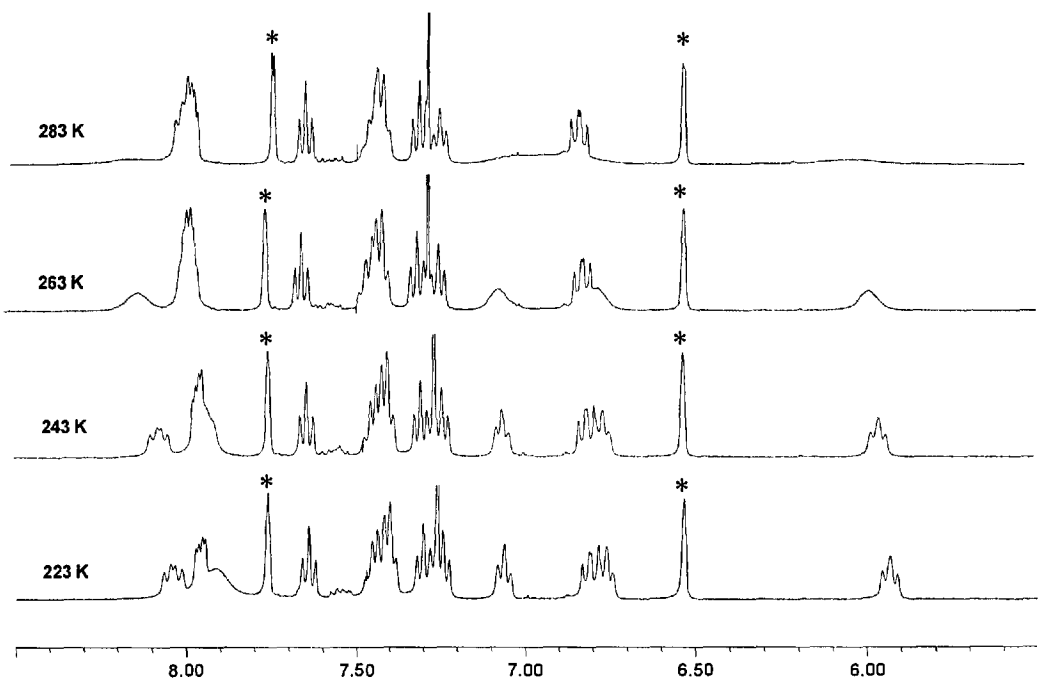


Figure 4.16. Variable temperature (283 K to 223 K) ^{1}H NMR spectra of **4.6**. * marks the 4- and 5-pz protons.

At 223 K, the spectrum consists of sharp peaks and as the temperature is increased, some of these peaks coalesce forming broad signals. It is apparent that not all of the aromatic hydrogens are involved in fluxional behaviour as some resonances are temperature-independent. From the COSY ^{1}H NMR spectrum recorded at 223 K it has been possible to assign the peaks in these spectra; the non-fluxional hydrogens have been assigned as those attached to the pyrazolyl and phenyl rings which comprise the backbone of the ligand. The remaining hydrogens, which all display fluxional behaviour, are those which are present in the diphenylphosphine moiety of the ligand-metal complex. This low temperature phenomenon has been ascribed to hindered rotation about the P–Ph bonds, stabilised by π-π stacking of phenyl rings from opposing ligand moieties. This results in hydrogens occupying different spatial positions and hence unique chemical environments for periods of time comparable to the NMR timescale. These hydrogens are therefore observed as separate resonances while at higher temperatures, the energy barrier to rotation is overcome and these peaks coalesce.

It was also possible to form **4.6** by a stepwise process by first forming and isolating the 1:1 complex **4.5** and then reacting this with a further one equivalent of the N,P ligand (**4.2**) (shown in Figure 4.13). The formation of the bis-chelate species **4.6** is noteworthy as it has been previously reported that it has only been possible to isolate the mono-chelate species **4.5**, even when using a large excess of N,P ligand in the reaction with $Pd(PhCN)_2Cl_2$.[41]

4.3.3 Synthesis of Perchlorate Bis-Chelate (4.7)

Exchange of the chloride counter-anions in **4.6** for perchlorate anions was achieved by addition of two equivalents of silver perchlorate, with the driving force for this reaction being the precipitation of silver chloride (Figure 4.13). The $^{31}P\{^{1}H\}$ NMR of the yellow solid product **4.7** shows a single peak with chemical shift 34.1 ppm (*c.f.* **4.6** at 31.6 ppm) and the N–H in the ^{1}H NMR spectrum is found at 13.42 ppm (Table 4.5). The ^{1}H NMR shows broad peaks corresponding to the diphenylphosphine hydrogens. These broad peaks split into sharp resonances at low temperatures as seen previously for complex **4.6** (Figure 4.17).

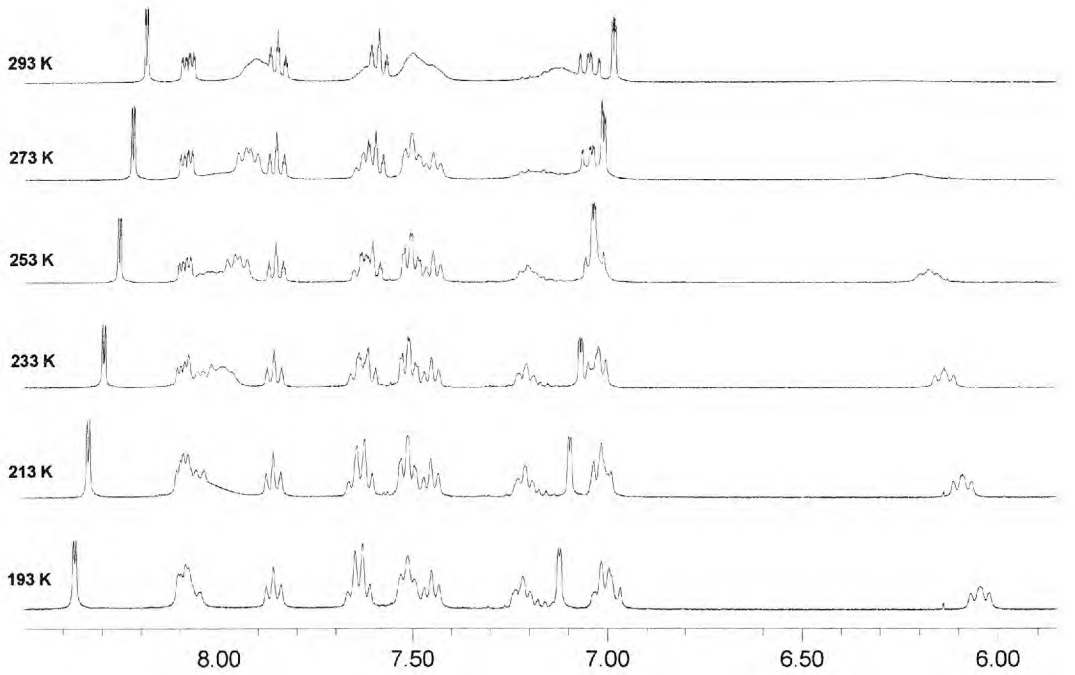


Figure 4.17. Variable temperature (293 K to 193 K) ^{1}H NMR spectra of **4.7**

Layering of hexane above a solution of **4.7** in dichloromethane yielded single crystals suitable for X-ray analysis.

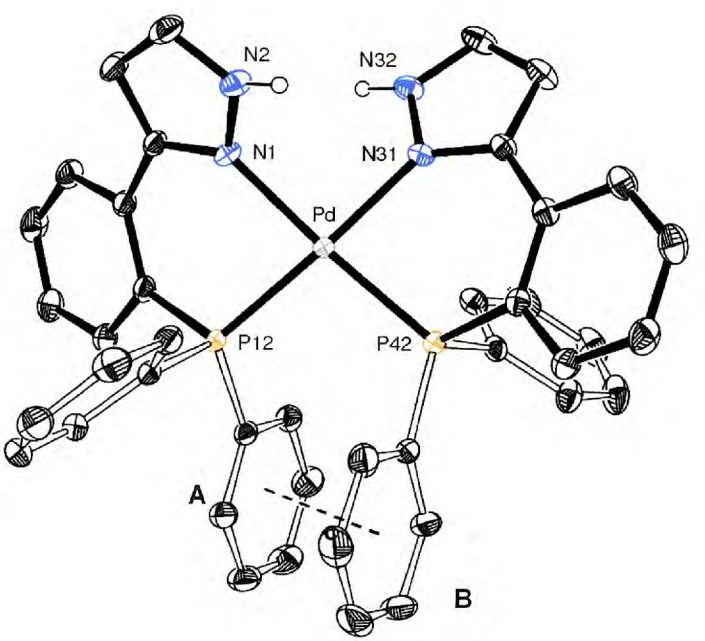


Figure 4.18. Molecular structure of the cation in $[Pd(Hpz^{phos})_2][ClO_4]_2$ (**4.7**) (30% probability ellipsoids).

The solid state structure (Figure 4.18) shows the palladium to have a distorted square planar geometry with the two N,P ligands chelating in a *cis* fashion. The most acute angles at the metal are associated with the bites of the two N,P ligands. A summary of bond lengths and angles is given in Table 4.4. The two N,P ligands have similar conformations such that the complex has approximate C_2 symmetry (Figure 4.19).

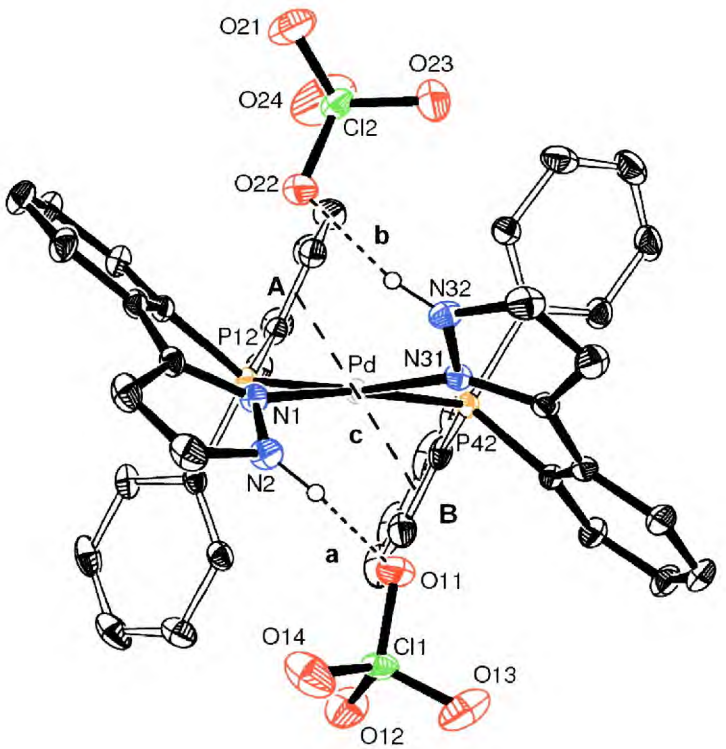


Figure 4.19. Molecular structure of **4.7** viewed along the molecular C_2 axis.

As seen for complex **4.6**, a π-π stacking interaction between pendant phenyl rings on adjacent ligands is observed (**c** in Figure 4.18 and Figure 4.19), and may be responsible for the twisting of the two {Pd,P,N} coordination planes with respect to each other (by *ca.* 14°). The π-π stacking interaction has centroid···centroid and mean interplanar separations of ca. 3.89 and 3.25 Å respectively, the two rings being inclined by ca. 2°. Within each ligand the linked phenyl and pyrazolyl rings are distinctly twisted with respect to each other, the torsion angles for the C–C bond between them being *ca.* 25 and 26° for the N(1) and N(31) ligands respectively. Each of the six membered C_3NPPd chelate rings has a distorted boat conformation. The N–H hydrogen atoms are linked to the perchlorate anions by N–H···O hydrogen bonds (**a**

and **b** in Figure 4.19). The N–H···O hydrogen bonds have N···O, H···O (Å), and N–H···O (°) of **a)** 2.871(3), 2.10, 143; **b)** 2.781(3), 1.90, 165 respectively.

Table 4.4. Selected bond lengths (Å) and angles (°) for **4.7**

Pd–N(1)	2.0738(17)	Pd–P(12)	2.2614(6)
Pd–N(31)	2.0763(17)	Pd–P(42)	2.2545(6)
N(1)–N(2)	1.357(3)	N(31)–N(32)	1.352(2)
N(1)–Pd–P(12)	85.68(5)	N(1)–Pd–N(31)	91.73(7)
N(1)–Pd–P(42)	170.37(5)	P(12)–Pd–N(31)	169.37(5)
P(12)–Pd–P(42)	99.39(2)	N(31)–Pd–P(42)	84.71(5)

4.3.4 Summary

NMR and IR spectroscopic data for complexes **4.5-4.7** are summarised in Table 4.5. Chelation of the N,P ligand has been observed in each complex in the solid state. The behaviour of these species in solution is of particular interest as palladium complexes are in solution during homogeneous catalysis. Coordination of the phosphorus is observed for each species as reflected by the downfield chemical shifts relative to the free N,P ligand. This was expected as phosphorus is known to have a high affinity for palladium, and as such acts as the anchor group in these reactions.

Table 4.5. IR, ^{1}H and $^{31}P\{H\}$ NMR data for the complexes **4.5 – 4.7**

Complex	$^{31}P\{^{1}H\}$ NMR[a] δ/ppm	^{1}H NMR[a] δ/ppm								IR[b] ν/cm^{-1}
	P	*NH*	*5-pz*	*4-pz*	*3-Ph*	*4-Ph*	*5-Ph*	*6-Ph*	*Ph-H*	*NH*
4.5 $[Pd(Hpz^{phos})Cl_2]$	25.6	13.14 (s)	7.65 (dd)	6.86 (dd)	7.05 (ddd)	7.42 (m)	7.70 (dd)	7.90 (ddd)	7.4-7.7 (m)	3230
4.6 $[Pd(Hpz^{phos})_2]Cl_2$	31.6	14.86 (s)	7.72 (d)	6.50 (d)	6.82 (dd)	7.28 (m)	7.63 (dd)	7.97 (m)	—[c]	~3290[d]
4.7[e] $[Pd(Hpz^{phos})_2][ClO_4]_2$	34.1	13.42 (s)	8.19 (dd)	6.99 (dd)	7.05 (ddd)	7.59 (dd)	7.85 (dd)	8.08 (ddd)	—[c]	3302[f]

(a) Recorded as $CDCl_3$ solution at 293 K unless indicated otherwise; (b) Recorded as KBr disc unless indicated otherwise; (c) Temperature dependent – see discussion; (d) Partially obscured by residual H_2O in disc; (e) NMRs recorded in d^6-acetone; (f) Recorded as nujol mull.

The coordination behaviour of the pyrazolyl donor groups was more difficult to forecast. This is because nitrogen donors are harder than the phosphines and are

therefore expected to show a lower affinity towards palladium. In complex **4.6**, one might expect two possible structures in solution: (i) a bis-chelated [Pd(Hpz^{phos}-κ^2*N,P*)$_2$]Cl$_2$ species in which the chlorides are not coordinated to the palladium (as seen in the solid state structure) or (ii) a bis-monodentate adduct, [Pd(Hpz^{phos}-κ*P*)$_2$Cl$_2$], in which the two ligands coordinate in a monodentate fashion via the phosphine groups with the two chloro ligands also bound to the metal. Chelation of the ligand might be preferred because of the formation of unstrained six-membered rings which is thermodynamically favoured. Recently, however, Miller *et al.* reported a similar ligand, bearing a pyridyl instead of a pyrazolyl donor moiety and found that chelation was not observed in solution or the solid state.[42]

The downfield shift of the NH proton (14.86 ppm) in **4.6** suggests that the adjacent nitrogen atom is coordinated to the palladium in solution. If the pyrazole unit was coordinating and dissociating rapidly in solution then one might expect the 4- and 5-pyrazolyl protons to broaden and/or shift during the VT experiments. However, these peaks, marked with * in Figure 4.16, remain static. Furthermore, the broadening of the phenyl peaks in the ^{1}H NMR spectrum of **4.6** was attributed to an interaction between two phenyl rings from separate ligand units. This can only occur as a result of chelation of both N,P ligands. Further proof that chelation of the N,P ligand in **4.6** occurs in solution can be made by comparison to the perchloro complex **4.7**. In the latter species, the chlorides have been replaced by non-coordinating perchlorate anions. As such, it is highly likely that chelation occurs at all times, leaving the perchlorate anions unbound. Given that the NMR data for **4.6** and **4.7** are so similar, it further suggests that both compounds experience chelation of both N,P ligand units in solution.

In summary, depending on the ligand-to-metal molar ratio employed in the reactions of palladium(II) with the N,P ligand **4.2**, either the 1:1 mono-chelate, [Pd(Hpz^{phos}-κ^2*N,P*)Cl$_2$] (**4.5**), or the 2:1 bis-chelate, [Pd(Hpz^{phos}-κ^2*N,P*)$_2$]Cl$_2$ (**4.6**), is obtained. Complex **4.6** contains two six-membered chelate rings in which the chlorides have been displaced from the inner coordination sphere of the palladium. Exchange of the chloride anions in **4.6** for perchlorate anions can be achieved using AgClO$_4$ to give [Pd(Hpz^{phos}-κ^2*N,P*)$_2$][ClO$_4$]$_2$ **4.7**.

4.4 Palladium(II) Coordination Chemistry of $Hpz^{phos(O)}$ (4.3)

The N,O ligand **4.3** displays different coordination behaviour to the N,P ligand **4.2** since the 'soft' phosphine group is now replaced by a 'hard' phosphine oxide donor that has a lower affinity towards palladium(II). Formation of a chelate ring is now entropically disfavoured due to the increased size of the potential chelate ring – now seven-membered as opposed to six-membered for the complexes described above. The reactions performed between **4.3** and $Pd(COD)Cl_2$ are outlined in Figure 4.20.

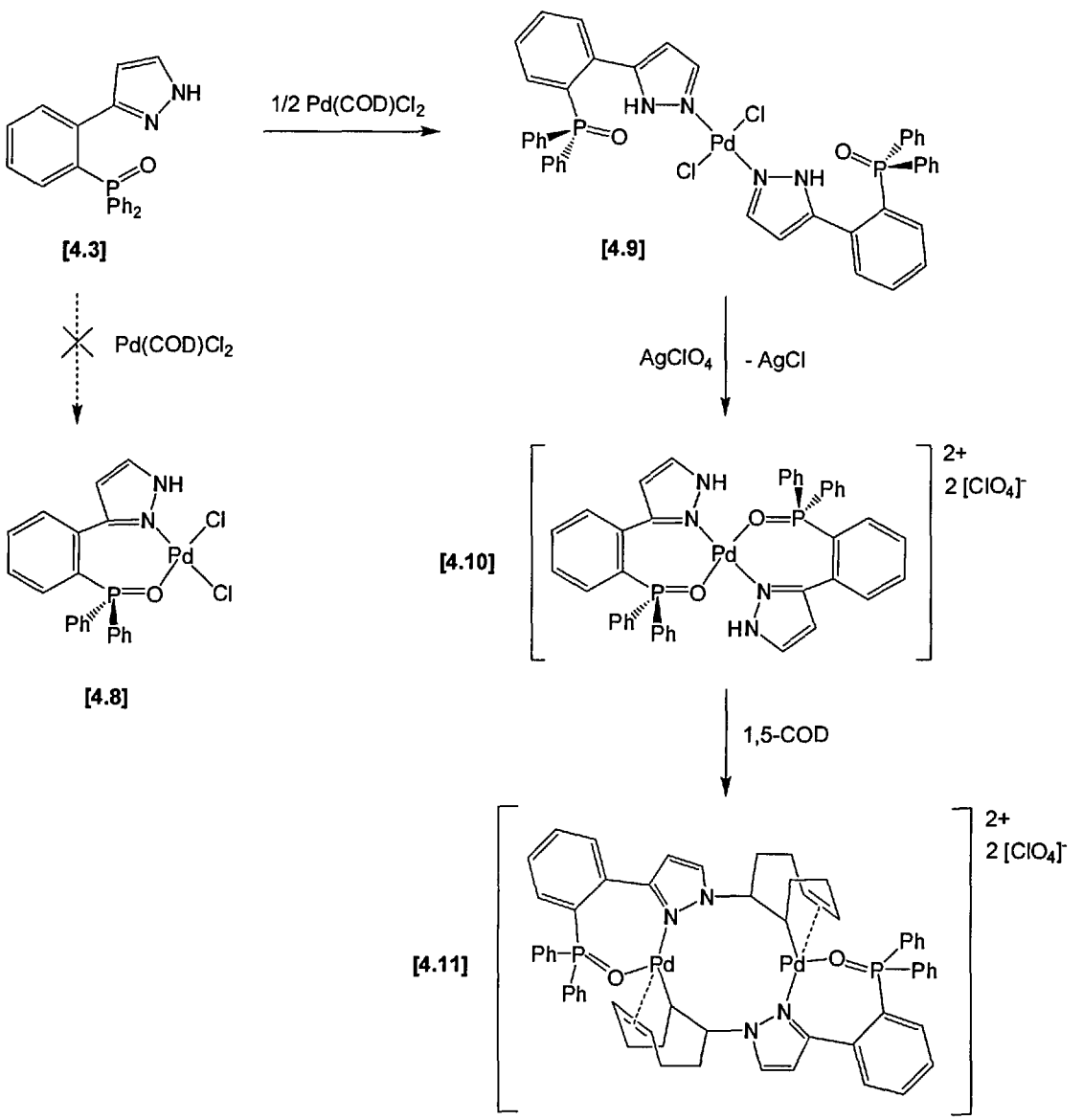


Figure 4.20. Summary of reactions of $Hpz^{phos(O)}$ (**4.3**) with palladium(II) species.

4.4.1 Attempted Synthesis of Mono-Chelate (4.8)

The reactivity of the N,O ligand **4.3** was first examined by performing a 1:1 reaction with $Pd(COD)Cl_2$ in an attempt to synthesise the mono-chelate $[Pd(Hpz^{phos(O)}\text{-}\kappa^2N,O)Cl_2]$ (**4.8**). However, even when using forcing conditions (extended reaction times, reflux, and large excess of palladium) formation of a monodentate species **4.9** (discussed below) was observed with a ^{31}P chemical shift of 33.0 ppm, almost unchanged from the starting material. This indicated that the oxide group is not coordinated to the palladium as a significant downfield shift is expected to occur as a result of the inductive deshielding effect upon the phosphorus atom. No traces of a N,O chelate species were observed by $^{31}P\{^1H\}$ NMR spectroscopy.

4.4.2 Synthesis of Bis-Adduct (4.9)

The formation of **4.9** was subsequently examined by addition of a dichloromethane solution of $Pd(COD)Cl_2$ to two equivalents of **4.3**. The $^{31}P\{^1H\}$ NMR spectrum of the reaction solution was recorded after stirring at room temperature for one hour, with the chemical shift of the predominant species occurring at 33.0 ppm (*c.f.* free ligand at 35.8 ppm). The product, **4.9**, was isolated by addition of hexane to the reaction solution and the $^{31}P\{^1H\}$ and ^1H NMR spectra were recorded of the resultant yellow solid (Table 4.8). The downfield position of the N–H proton in the ^1H NMR spectrum (13.51 ppm) suggests coordination of the pyrazolyl ring has occurred, in a similar fashion to the N,P complexes described above. As such, it was hypothesised that a 2:1 ligand-to-metal complex $[Pd(Hpz^{phos(O)}\text{-}\kappa N)_2Cl_2]$ had formed with the two ligands binding through their pyrazole nitrogens only and with the remaining coordination sites around the palladium centre being occupied by two chloro ligands. This stoichiometry was supported by FAB (+ve) mass spectral data showing a palladium isotope pattern at 869 m/z corresponding to $[Pd(Hpz^{phos(O)})_2Cl_2]^+$. To confirm this structure, crystals were grown by slow diffusion of pentane into a chloroform solution of **4.9** and were subsequently analysed by X-ray crystallography.

The solid state structure of **4.9** (Figure 4.21) shows the palladium to have a square planar geometry with the two N,O ligands bound in a monodentate fashion via Pd–N bonds. In contrast to the N,P complex **4.6,** the two ligands are coordinated in a *trans* fashion with two chloro ligands occupying the remaining two sites around the

palladium. Within each ligand the linked phenyl and pyrazolyl rings are distinctly twisted with respect to each other, the torsion angle for the C–C bond between them being *ca.* 39°. This distortion may be caused by the molecule adopting a conformation that facilitates intramolecular N–H···O hydrogen bonding between the N(1)-H donor and the O(1) acceptor. The intramolecular N–H···O hydrogen bonds (dashed lines in Figure 4.21) have N···O, H···O (Å), and N–H···O (°) of 2.69, 1.92 and 144 respectively. A summary of bond lengths and angles is given in Table 4.6.

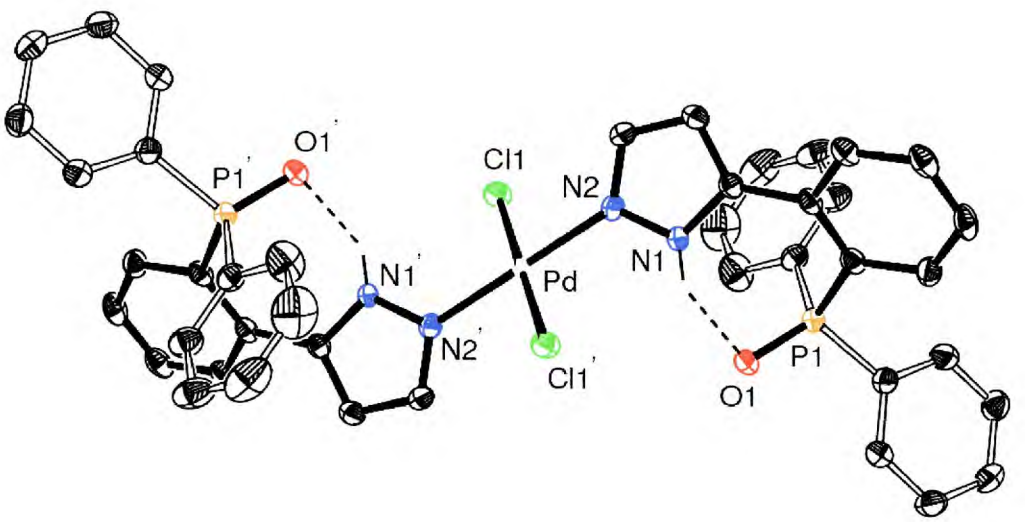


Figure 4.21. Molecular structure of [Pd(Hpz$^{phos(O)}$)Cl_2] (**4.9**) (50% probability ellipsoids).

Table 4.6. Selected bond lengths (Å) and angles (°) for **4.9**

Pd–N(2)	1.999(2)	Pd–Cl(1)	2.2995(7)
N(1)–N(2)	1.348(3)	P(1)-O(1)	1.496(2)
N(2)–Pd–Cl(1)	89.19(7)	N(2)–Pd–N(2')	180
N(2')–Pd–Cl(1)	90.81(7)	Cl(1')-Pd-Cl(1)	180

The combination of the hard oxide donor in **4.3** and the increased size of the potential chelate ring (now seven-membered) disfavours chelation, in contrast to the behaviour of the N,P ligand **4.2**. Since the ligands do not chelate, the *trans* form is observed as steric interactions between the two ligands are minimised. This structure further differs from the uncoordinated N,O ligand **4.3** and the N,P complexes **4.5-4.7** in that the N–H hydrogen has 'swapped' the nitrogen atom to which it is bonded, and

consequently, coordination to palladium now occurs through the nitrogen in the 1'-position (Figure 4.22).

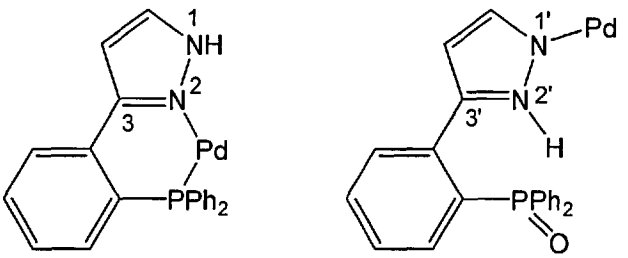


Figure 4.22. Variable bonding modes of **4.2** (left) and **4.3** (right).

This coordination mode in **4.9** is presumed to result from the monodentate behaviour of the N,O ligand which permits the fluxional N–H hydrogen to reside on the nitrogen atom that produces the most energetically favourable configuration in the resultant complex, *i.e.* where steric interactions between the ligand moieties and the metal are minimised. This is achieved by coordination at the 1'-position, thus leaving the bulky triphenylphosphine oxide moiety on the 'other side' of the pyrazolyl ring, pointing away from the metal. This bonding mode has previously been observed for a palladium(II) complex of a 3-substituted pyrazole ligand.[43] Further stabilisation for this form is also achieved by the formation of intramolecular N–H···O hydrogen bonds.

The lack of formation of a seven-membered chelate has been observed previously with another N,P=O ligand towards palladium(II).[34] Although formation of a seven-membered chelate has been observed in the palladium(II) complexes of N,N[44] and N,P ligands,[45] it is disfavoured in the case of oxygen donors due to the lower affinity of these donor groups towards palladium. In contrast, chelation of six-membered N,P=O ligands around palladium has been observed previously,[29] although in one case it required an excess of palladium over ligand and heating at reflux for several hours.[33]

4.4.3 Synthesis of Perchlorate Bis-Chelate (4.10)

It was anticipated that by adding two equivalents of silver perchlorate to a solution of **4.9**, coordination of the oxide groups could be encouraged by removal of the chloro ligands. This was hoped to form a bis-chelate complex of the formula $[Pd(Hpz^{phos(O)}\text{-}\kappa^2\textit{N,O})_2][ClO_4]_2$. This reaction was performed accordingly and after stirring the reaction solution at room temperature for 30 minutes, the $^{31}P\{^1H\}$ NMR spectrum revealed a mixture in which the predominant species occurred at 52.9 ppm. This species was subsequently isolated as a yellow powder by addition of hexane to the reaction mixture and recrystallisation from hot MeOH. The $^{31}P\{^1H\}$ NMR spectrum showed a singlet at 53.8 ppm enabling tentative assignment of this complex as the bis-chelated species **4.10**, as its $^{31}P\{^1H\}$ chemical shift closely resembled that of a similarly coordinated N,P=O species.[29]

In order to confirm the structure of **4.10**, X-ray analysis was performed on a single crystal grown by slow diffusion of pentane into a chloroform solution of the complex. Indeed, the solid state structure (Figure 4.23) shows the palladium to have a square planar geometry with two N,O ligands chelating in a *trans* fashion. Each of the seven membered C_3NPOPd chelate rings has a distorted boat conformation. As a consequence of chelation, the linked phenyl and pyrazolyl rings within each ligand are distinctly twisted with respect to each other, the torsion angle for the C–C bond between them being *ca.* 50°. This is the first structurally characterised example of a N,P=O hybrid ligand chelating at a palladium(II) centre.[46] Selected bond length and angles are given in Table 4.7.

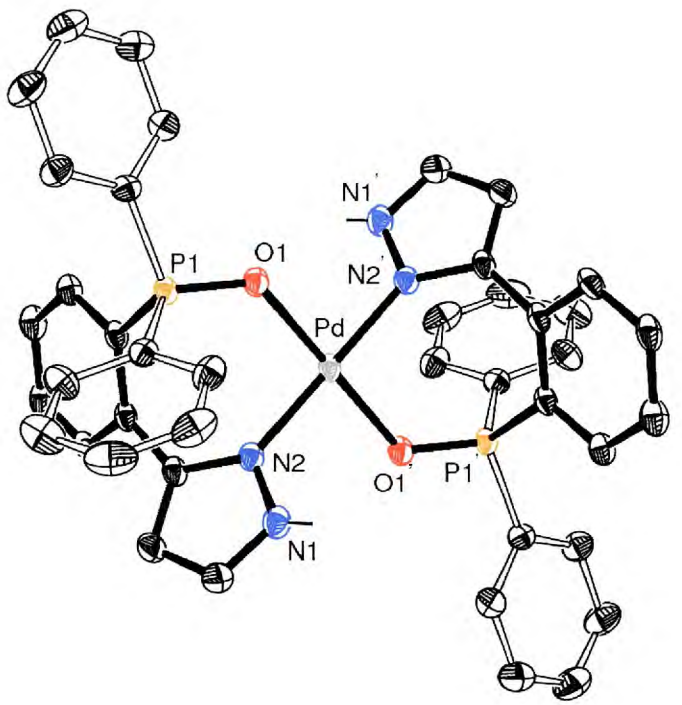


Figure 4.23. Molecular structure of the cation in $[Pd(Hpz^{phos(O)})_2][ClO_4]_2$ (**4.10**) (30 % probability ellipsoids).

Table 4.7. Selected bond lengths (Å) and angles (°) for **4.10**

Pd–N(2)	2.008(4)	Pd–O(1)	2.009(3)
N(1)–N(2)	1.339(7)	P(1)–O(1)	1.526(4)
N(2)–Pd–O(1)	92.89(16)	N(2')–Pd–O(1)	87.11(16)
N(2)–Pd–N(2')	180	O(1)–Pd–O(1')	180

This structure reveals that the N–H hydrogen of the N,O ligand has reverted back to the 1-position of the pyrazole ring (Figure 4.23). This makes available the nitrogen in the 2-position for coordination to the metal and thus allows formation of the seven-membered chelate. Tautomerisation of this kind is required for chelation as when the ligand coordinates via the nitrogen in the 1'-position (as in **4.8**), the rigidity of the ligand prevents the oxide group from approaching the palladium centre.

4.4.4 Synthesis of COD-Insertion Product (4.11)

During an attempted repeat synthesis of **4.10** in which silver perchlorate was added to a solution of the bis-adduct **4.9** made *in situ* from $Pd(COD)Cl_2$ and **4.3**, it was noticed

that upon prolonged stirring of the reaction mixture, the $^{31}P\{^{1}H\}$ NMR began to change as shown in Figure 4.24.

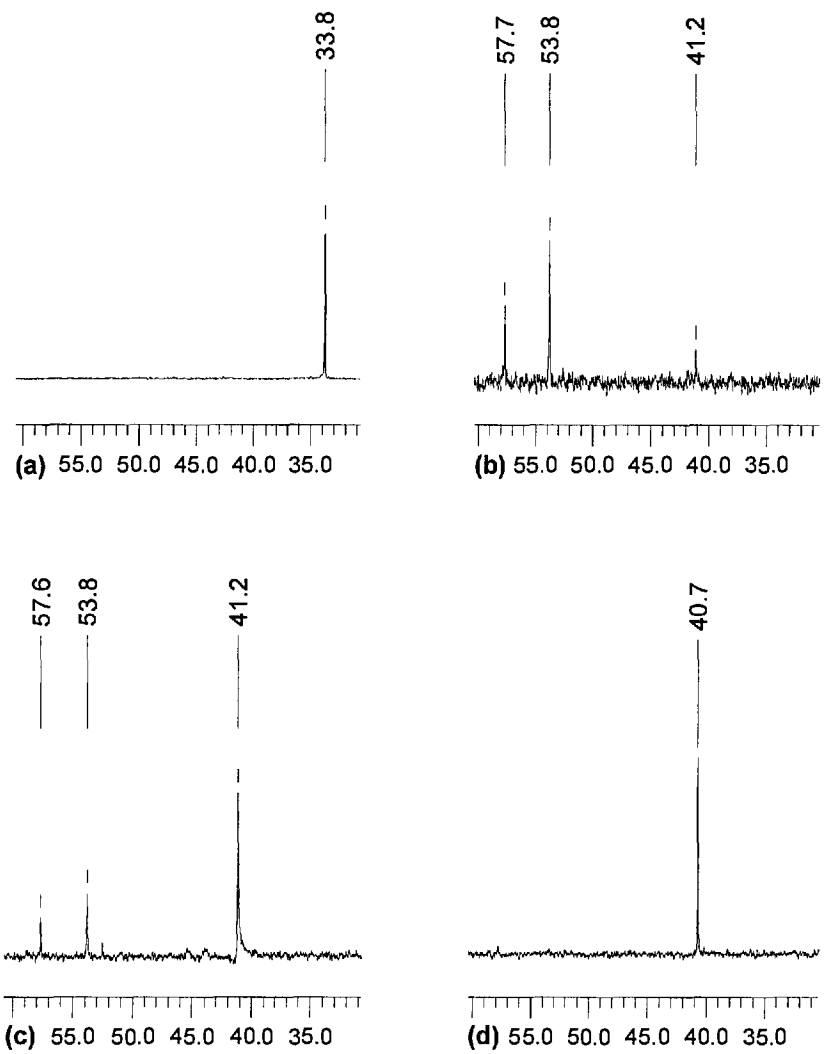


Figure 4.24. $^{31}P\{^{1}H\}$ NMR spectra recorded: (a) before addition of $AgClO_4$ and after stirring for: (b) 12 hrs; (c) 2 weeks and (d) after w/u.

Prior to addition of $AgClO_4$ (**a**) the peak corresponding to the bis-adduct is seen at 33.8 ppm. Upon addition of the $AgClO_4$ (**b**), this peak disappears and three new species appear, with the major species being the bis-chelate **4.10** at 53.8 ppm. Upon prolonged stirring (**c**), this peak diminishes in size as the peak at 41.1 ppm becomes progressively intense. After two weeks stirring at room temperature, the solvent was removed from the reaction mixture and the product isolated and recrystallised from boiling methanol to give a white powder in which the $^{31}P\{^{1}H\}$ NMR spectrum (**d**) showed only one species.

The ^{1}H NMR spectrum of this product (Figure 4.25) was found to be much less straightforward than the $^{31}P\{^{1}H\}$ NMR. As well as the phenyl peaks seen downfield at around 7 ppm, a new series of peaks each with a relative integral of 1H were found further upfield, corresponding to a total of 12 proton environments.

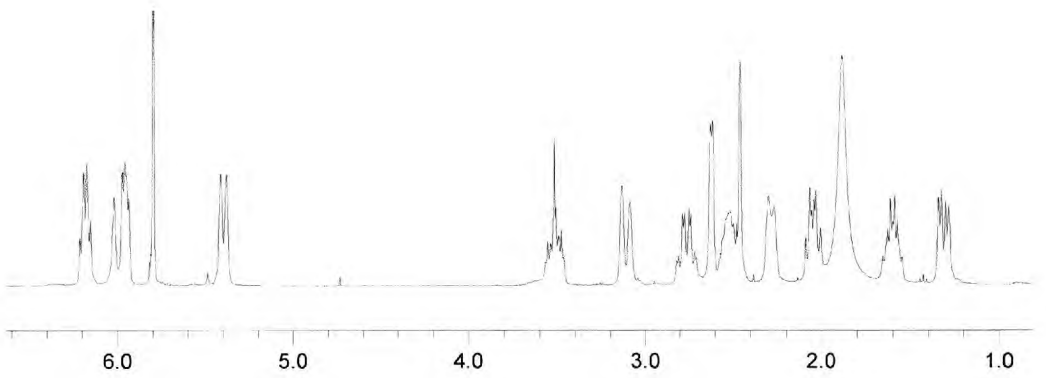


Figure 4.25. Upfield region of ^{1}H NMR spectrum of **4.11**.

To elucidate the structure of this species, the crystal structure of this complex was sought. Fortunately single crystals formed in the NMR tube and were analysed by X-ray crystallography to produce the structure shown in Figure 4.26. Unfortunately, due to some areas of unassignable electron density, this structure was only partially refined and is therefore unsuitable for publication. However, alongside mass spectral, NMR and elemental analysis it has proved entirely suitable for structural confirmation.

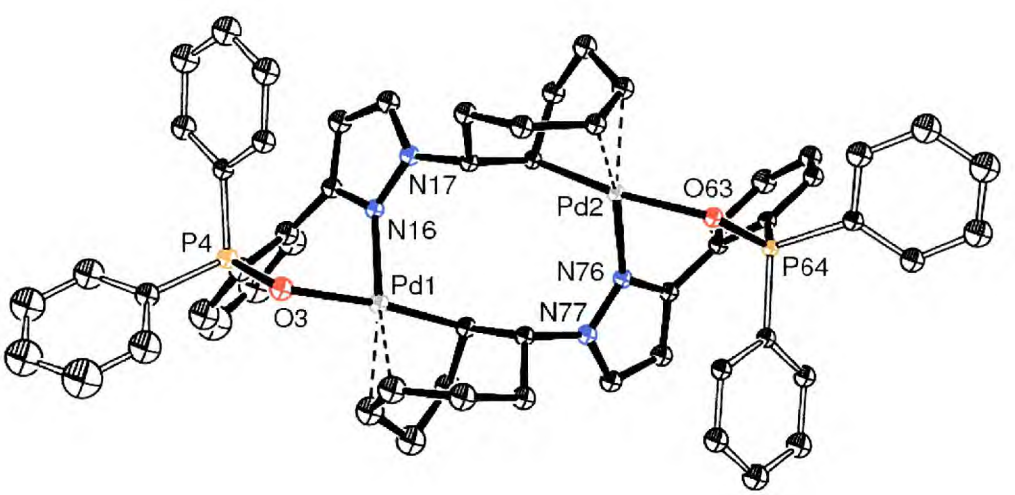


Figure 4.26. Molecular structure of the cation in $[Pd_2(pz^{phos(O)})_2(COD)_2][ClO_4]_2$ (**4.11**).

As can be seen in Figure 4.26, a bridged species has formed incorporating two palladium centres, two N,O ligand units and two molecules of 1,5-cyclooctadiene (COD). One of the double bonds of the COD molecule, which had been displaced from the $Pd(COD)Cl_2$ starting material at the beginning of the reaction, has inserted into a Pd–pyrazole bond, while the pyrazolyl donor group and the appended P=O group bind to a second palladium centre. This species carries an overall +2 charge which is balanced by two non-coordinating perchlorate anions. The ^1H NMR has been fully assigned with reference to the ^1H COSY NMR and accounts for all the COD protons thus supporting this structure.

The mechanism for the formation of this complex is not clear, but it may well proceed through dissociation of one N,O ligand from the bis-chelate **4.10** (Figure 4.27). The N-H proton of the coordinated ligand will be acidic as a consequence of coordination of the adjacent nitrogen. Deprotonation of the NH unit, perhaps by an uncoordinated N,O ligand, would form a negatively charged, palladium-bound pyrazolate ligand. Here, there are two possible paths that could be followed. Path A shows the pyrazolate attacking the COD which in turn forms a bond to palladium in a separate molecule. This process could then occur again, this time in an intramolecular ring-closing reaction to form the observed species **4.11**. Path B shows the formation of a resonance-stabilised 6-membered bis(μ-pyrazolato-*N,N'*)bridged species from two deprotonated Pd(N,O) moeties. This might be the unknown species seen in the $^{31}P\{^1H\}$ NMRs at 57.7 ppm. Two COD molecules would then be able to insert into the Pd-pyrazole bonds to form the thermodynamic product, **4.11**.

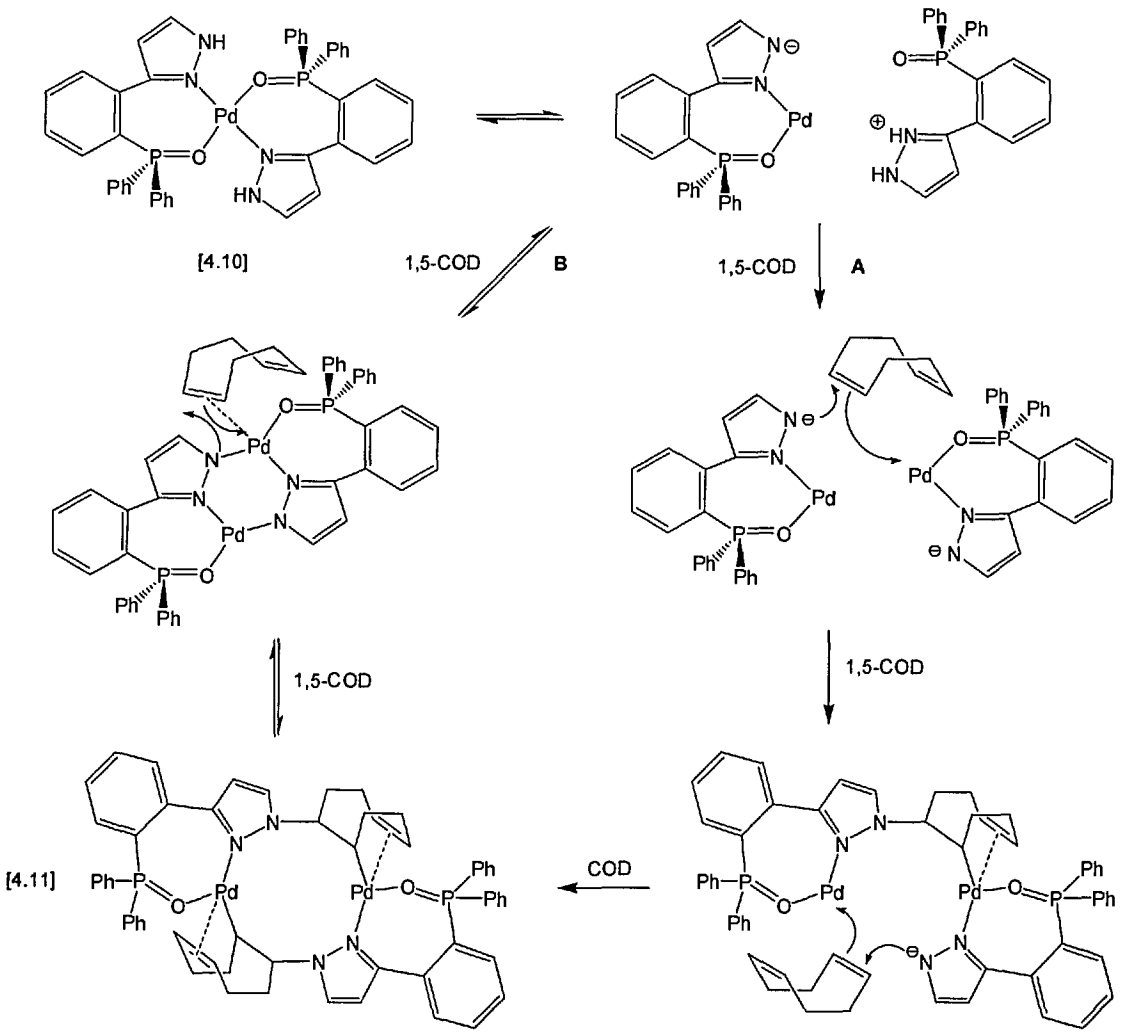


Figure 4.27. Proposed mechanisms for the formation of **4.11**.

Attack of a pyrazolate ion on cyclooctadiene has been observed previously when simple pyrazoles have been reacted with $Pd(COD)Cl_2$ in the presence of sodium methoxide.[47] It is noteworthy that none of these species have been characterised by X-ray crystallography.

4.4.5 Summary

NMR and IR spectroscopic data for complexes **4.9-4.11** are summarised in Table 4.8

Table 4.8. IR, ^{1}H and $^{31}P\{^{1}H\}$ NMR data for the complexes **4.9-4.11**

Complex	$^{31}P\{^{1}H\}$ NMR[a] δ/ppm	^{1}H NMR[a] δ/ppm								IR ν/cm^{-1}
	P	*NH*	*5-pz*	*4-pz*	*3-Ph*	*4-Ph*	*5-Ph*	*6-Ph*	*Ph-H*	*NH*
4.9 $[Pd(Hpz^{phos(O)})_2Cl_2]$	32.7	13.51 (s)	7.81 (dd)	6.19 (dd)	7.22 (dd)	7.37 (dd)	7.61 (dd)	7.57 (dd)	7.74 (m), 7.53 (m), 7.47 (m)	3196[b]
4.10 $[Pd(Hpz^{phos(O)})_2][ClO_4]_2$	53.8	12.34 (s)	7.31 (d)	6.02 (m)	overlap at ~7.4 (m)		8.12 (dd)	8.27 (dd)	7.6-7.9 (m)	3686[c]
4.11 $[Pd_2(COD)_2(pz^{phos(O)})_2][ClO_4]_2$	40.7	—	7.48 (d)	5.80 (d)	7.37 (m)	7.53 (dd)	7.84 (dd)	7.68 (m)	7.62 (m), 7.34 (m)	—[d]

(a) Recorded as $CDCl_3$ solution at 293 K; (b) Recorded as nujol mull; (c) Recorded as CH_2Cl_2 solution; (d) Recorded as KBr disc.

The N,O ligand **4.3** displays an interesting and varied coordination chemistry towards palladium that differs greatly from the reactions of the N,P derivative. Reaction of the **4.3** with palladium(II) forms the bis-adduct species $[Pd(Hpz^{phos(O)}\text{-}\kappa N)_2Cl_2]$ **4.9** regardless of the metal-to-ligand ratio or the order of addition of reactants. Unlike the N,P bis-chelate **4.6**, the N,O ligands in complex **4.9** bind in a monodentate fashion through the N donor atom of the pyrazole rings. This is because the phosphine donor moieties have been replaced by oxide donors which have a far lower affinity towards palladium. Chelation of this N,O ligand can be enforced by removal of the chloro ligands in **4.9** using $AgClO_4$. This forms the kinetic product, the bis-chelate $[Pd(Hpz^{phos(O)}\text{-}\kappa^2 N,O)_2][ClO_4]_2$ **4.10**, containing entropically unfavourable 7-membered chelate rings. If however, this compound is not isolated from the reaction mixture, it can react with cyclooctadiene in solution over extended time periods to form the bridged species **4.11**.

4.5 Palladium(II) Coordination Chemistry of $Hpz^{phos(S)}$ (4.4)

As with the N,O donor ligand **4.3**, the N,S donor ligand **4.4** must form an entropically unfavourable seven-membered ring if it is to chelate. Despite this similarity, the N,S ligand is expected to display contrasting reactivity to **4.3** as the S-donor groups are

considerably 'softer' than the corresponding O-donors. The reactions between **4.4** and $Pd(COD)Cl_2$ have been performed with varying ligand-to-metal ratios and extraction of the chloride ions with silver perchlorate has again been performed. These reactions are summarised in Figure 4.28.

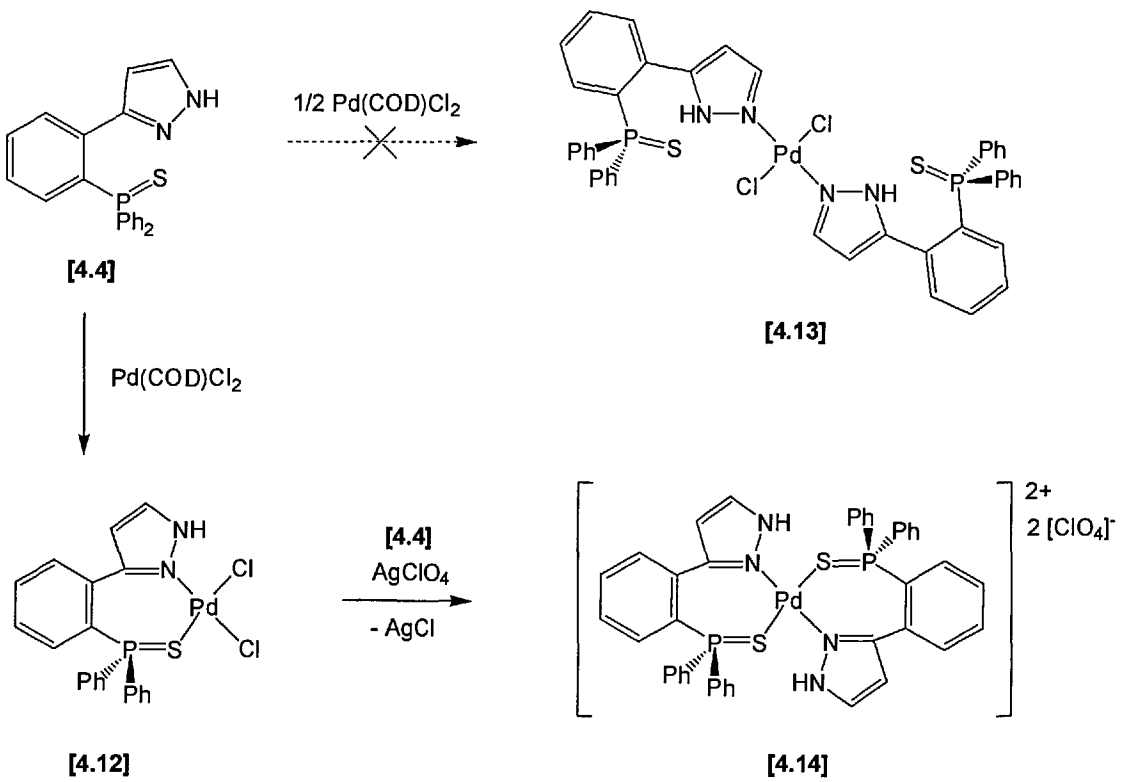


Figure 4.28. Summary of reactions of $Hpz^{phos(S)}$ (**4.4**) with palladium(II) species.

4.5.1 Synthesis of Mono-Chelate (4.12)

The reactivity of the N,S ligand **4.4** was initially investigated by an equimolar reaction between **4.3** and $Pd(COD)Cl_2$. Addition of a solution of **4.4** in DCM to a solution of $Pd(COD)Cl_2$ caused a yellow/orange solid to precipitate. This product was found to be insoluble in common organic solvents with the exception of DMSO. $^{31}P\{^1H\}$ NMR spectroscopy of a d_6-DMSO solution revealed a single peak at 43.3 ppm, although the ^1H NMR spectrum was found to be less straightforward, with the aromatic region showing the presence of some impurities. Due to the coordinating nature of DMSO it was not possible to say for certain whether the P=S moiety was coordinated to the palladium or not, based on $^{31}P\{^1H\}$ NMR data alone. Elemental analysis on this solid revealed a good match with the calculated values for the 1:1

complex, $Pd(Hpz^{phos(S)})Cl_2$ (**4.12** in Figure 4.28). It was therefore assumed that the mono-chelate, $[Pd(Hpz^{phos(S)}\text{-}\kappa^2N,S)Cl_2]$, had formed in order to satisfy the tetra-coordination preference of the palladium(II) centre.

4.5.2 Attempted Synthesis of Bis-Adduct (4.13)

This reaction was performed by increasing the ligand-to-metal ratio to 2:1. Dropwise addition of $Pd(COD)Cl_2$ to a solution of **4.4** caused a yellow solid to precipitate. This solid was again found to possess very low solubility, thus hindering characterisation and purification. Elemental analysis was performed on this sample to elucidate the stoichiometry of the resultant species. These results revealed a very poor match with the calculated values for the 2:1 bis-adduct $[Pd(Hpz^{phos(S)})_2Cl_2]$ (**4.13** in Figure 4.28). They did, however, provide a good match with the 1:1 mono-chelate **4.12** seen previously. This suggests that the palladium is unwilling to coordinate to two N,S ligand moieties, perhaps due to the high stability of the mono-chelated species.

4.5.3 Synthesis of Perchlorate Bis-Chelate (4.14)

The above reaction was repeated, again causing a yellow solid to precipitate. It was hoped that subsequent addition of silver perchlorate to this reaction mixture (along with the unreacted one equivalent of ligand which remains in solution), would encourage both ligand units to bind to the palladium to form the bis-chelated species $[Pd(Hpz^{phos(S)}\text{-}\kappa^2N,S)_2]^{2+}$ (**4.14** in Figure 4.28). This reaction was performed accordingly and immediately after the addition of $AgClO_4$ to the reaction mixture, $^{31}P\{^1H\}$ NMR of the reaction solution revealed a mixture of four species with chemical shifts around 44 ppm. Upon stirring of this mixture overnight, the yellow solid had redissolved, while a fine powder, assumed to be silver chloride had formed in the flask. Filtration and removal of the solvent produced a solid that, once again possessed very poor solubility. Mass spectrometry showed peaks at 927 and 825 m/z, corresponding to the ions $[Pd(Hpz^{phos(S)})_2ClO_4]^+$ and $[Pd(Hpz^{phos(S)})_2]^+$, respectively. This indicated that the bis-chelate species **4.14** had indeed formed.

By chance, crystals formed in the NMR tube that had been used to record the $^{31}P\{^1H\}$ spectrum. These crystals, however, were twinned and displayed some areas of

unassignable electron density. The (non-publishable) structure was adequate for structural confirmation, and supports the mass spectral predictions.

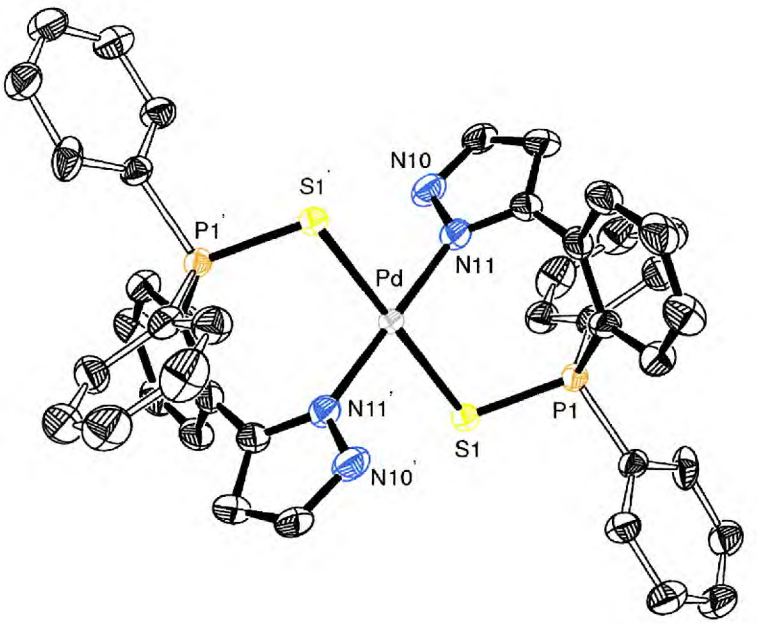


Figure 4.29. Molecular structure of the cation in $[Pd(Hpz^{phos(S)})_2][ClO_4]_2$ (**4.14**).

In this structure (Figure 4.29), the two N,S ligand moieties chelate to the palladium centre in a *trans* arrangement. This is a dicationic complex in which the charge is balanced by two non-coordinating perchlorate anions. This echoes the coordination behaviour of the related N,O ligand in complex **4.10**. Comparison of these bis-chelated species, **4.10** and **4.14**, finds that they adopt very similar solid-state structures. In both cases, each seven-membered $C_3NPS(O)Pd$ chelate ring has a distorted boat conformation and the linked phenyl and pyrazolyl rings within each ligand are distinctly twisted with respect to each other, as a consequence of chelation.

4.5.4 Summary

The reactions of the N,S ligand **4.4** have been less straightforward than the N,P and N,O derivates **4.2** and **4.3**, respectively. This is in mainly due to low solubility of the resultant species which has hindered their characterisation and purification. This low solubility might result from the formation of extensively bridged species in solution and the solid state. The bridging unit is proposed to be the bidentate ligand which

contains N- and S-donor moieties, both of which have a high affinity towards palladium. In this respect, the N,S ligand can be compared to the N,P ligand which also contains two donor groups which coordinate readily to palladium. However, the size of the potential chelate ring with the N,S ligand (seven-membered) compared to the N,P ligand (six-membered) might explain their contrasting behaviour. It could be that because chelation is entropically disfavoured, the N,S ligand bridges between palladium centres to form a complex of the formula $[Pd(\mu\text{-}Hpz^{phos(S)})Cl_2]_n$ in a manner shown in Figure 4.30. In this example, the ligand-to-metal ratio of 1:1 for **4.12** fits with the experimental observations.

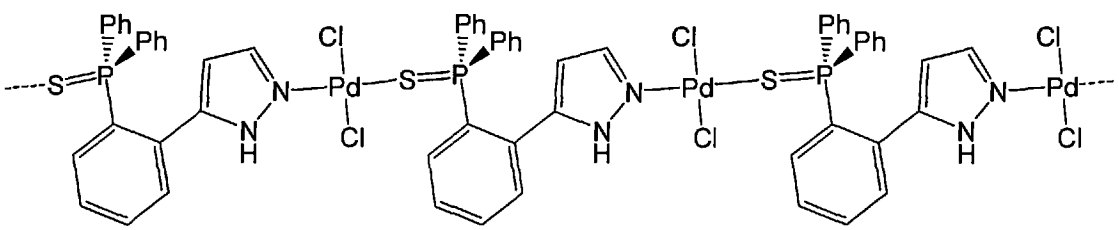


Figure 4.30. Proposed bridged species $[Pd(\mu\text{-}Hpz^{phos(S)})Cl_2]_n$ (**4.12**).

The inability to form the 2:1 bis-adduct **4.13** is however slightly surprising and may be caused by the low solubility and high stability of the 1:1 bridged species which, once formed, precipitates out of solution and becomes unreactive. However, abstraction of the chloride ions using silver perchlorate can force chelation via the thermodynamic driving force of silver chloride precipitation. Here we find that the bis-chelate structure **4.14** forms, although this reaction does not proceed cleanly and it cannot be said for certain that this is the major product.

4.6 Summary of Palladium Chemistry

Relatively simple ligand tuning has been employed to demonstrate the variable coordination behaviour of the N,P ligand **4.2** and the related N,O and N,S ligands, **4.3** and **4.4** towards palladium(II). This tuning effect has demonstrated the potential hemilability of these species – while the N,P ligand favoured chelation in all cases, the N,O ligand acted as a monodentate N-donor that could be forced into a bidentate chelating mode by abstraction of the chloro ligands. Conversely the N,S donor was

unwilling to bond in a monodentate fashion in all instances, preferring to chelate to the palladium in a 1:1 metal-to-ligand ratio.

4.7 Applications in Catalysis

4.7.1 Carbonylation Reactions

The N,P ligand **4.2** has been applied to palladium(0)-catalysed carbonylation reactions of the type described in Chapter 3. In these reactions, a two mole % loading of palladium-ligand complex was used to catalyse the coupling of benzylamine and iodobenzene under an atmosphere of CO to produce *N*-benzylbenzamide (Figure 4.31).[48] These reactions were performed in order to compare the performance of the palladium complexes of **4.2** against a range of existing phosphine ligands. In each case, the extent of amide formation was monitored by GC analysis after 10 minutes and after two hours. The results of these carbonylation reactions are summarised in Table 4.9.

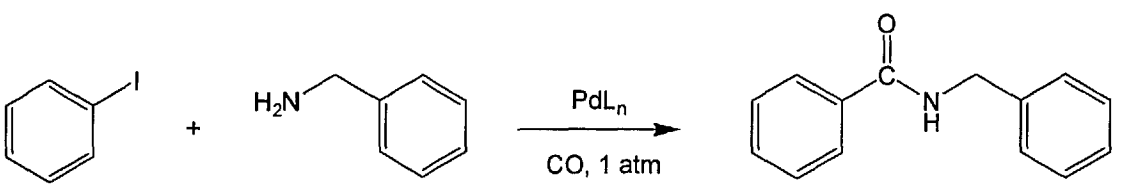


Figure 4.31. Palladium-catalysed carbonylation reaction to form *N*-benzylbenzamide.

Table 4.9. Amide yields from palladium-catalysed carbonylation reactions

Experiment number	Catalyst	Amide Yield /% [a]	
		10 minutes	120 minutes
1	$Pd(PPh_3)_4$	5	67
2	$Pd(dppp)Cl_2$ [b]	9	81
3	$Pd(Hpz^{phos})Cl_2$ (**4.5**)	<1	7
4	$Pd(OAc)_2 + Hpz^{phos}$ (**4.2**)	<1	31
5	$[Pd(Hpz^{phos})_2][ClO_4]_2$ (**4.7**)	<1	<1
6	$Pd(OAc)_2 + 2(Hpz^{phos})$ (**4.2**)	<1	<1

(a) average of two runs; (b) dppp = 1,3-bis(diphenylphosphino)propane.

From Table 4.9 it can be seen that $Pd(dppp)Cl_2$ was the most successful catalytic species (expt. 2). This complex gave the highest yield of all the compounds tested after 10 minutes, and by 120 minutes, an amide yield of 81 % had been achieved. As such, this catalyst was chosen for the carbonylation reactions reported in Chapter 3. The palladium(0) species, $Pd(PPh_3)_4$ (expt. 1) performed well, with a 67 % yield after 120 minutes. In this case though, the yields obtained after 10 minutes fall short of those obtained by $Pd(dppp)Cl_2$.

In comparison, the yields obtained using various complexes of Hpz^{phos} (**4.2**) varied from negligible to poor depending on the ligand-to-palladium ratio. The best results were obtained using an *in situ* generated catalytic species from $Pd(OAc)_2$ and **4.2** (expt. 4) yielding 31 % of the amide after two hours. This is considerably more effective than the preformed 1:1 complex (**4.5**) which gave only 7 % yield after 120 minutes (expt. 3), suggesting that the choice of anion/co-ligand is important in these reactions. As expected, the reactions performed using a 2:1 ratio of **4.2** to palladium resulted in negligible yields of amide for both the preformed and *in situ* generated palladium species (expts. 5 and 6). This is likely to result from the chelating nature of the two ligand moieties which has been previously observed in solution and the solid-state. This effectively blocks access to any reactive substrates at the palladium centre, thus rendering the catalytic centre inactive.

4.7.2 Heck Reaction

Since reporting their synthesis of **4.2**, Thiel *et al.*[49] have investigated the use of this ligand (and other derivatives of varying substitution patterns) in the palladium-catalysed Heck reaction. The reaction performed was the coupling of bromobenzene with styrene as shown in Figure 4.32.

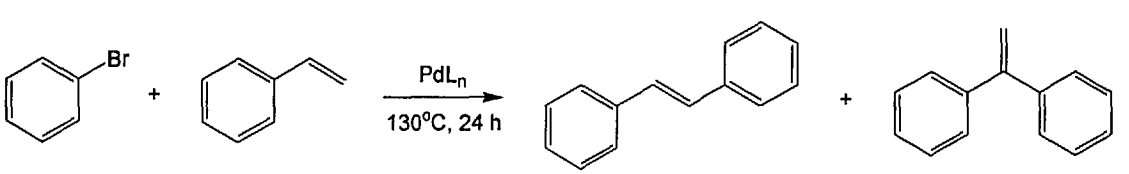


Figure 4.32. Palladium-catalysed Heck reaction.

Among the ligands investigated, **4.2** displayed the highest activities for the coupling of bromobenzene with styrene in the presence of $Pd(OAc)_2$. Here, an *in situ* generated catalytic species was formed from a 1:1 mixture of $Pd(OAc)_2$ and **4.2**. This reaction proceeded with a 96 % conversion of bromobenzene and a high ratio of *trans*-stilbene to 1,1-diphenylethylene. The preformed palladium-ligand complex $[Pd(Hpz^{phos})Cl_2]$ **4.5** displayed slightly poorer activity, with a 74 % conversion of bromobenzene after 24 hrs. Using the *in situ* generated $Pd(OAc)_2$/**4.2** species in the presence of one equivalent of nBu$_4$NI as the additive, unreactive 4-chloroacetophenone was able to undergo Heck coupling with styrene.

4.8 Future Work

4.8.1 Ligand Fine-Tuning

The NH moiety of the hybrid ligands **4.2–4.4** allows further functionalisation reactions to be performed, which may allow fine-tuning of the ligand's behaviour. Since the NH moiety can sit very close to the active site of the catalyst (as shown for the palladium complexes above) it is possible that introduction of a chiral unit at this site could result in a species capable of stereo-controlled catalysis (Figure 4.33 – A). Alternatively, by incorporation of bulky groups at this position, the affinity of the adjacent pyrazolyl N-donor towards a metal centre could be reduced (Figure 4.33 – B). This may be beneficial as it was found that the N,P ligand **4.2** remained chelated in solution, thus potentially blocking access for small molecule substrates. Substitution with appropriate functionalities may also provide access to reactions in different reaction media, such as aqueous or fluorous phase reactions (Figure 4.33 – C).

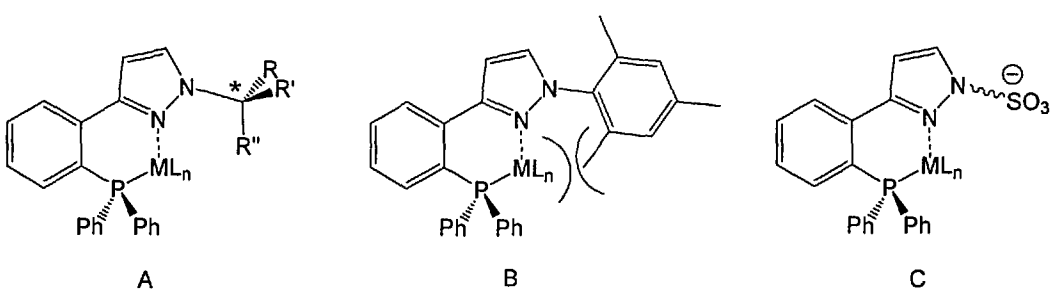


Figure 4.33. Proposed modifications of Hpz^{phos} (**4.2**) to impart: (A) chirality; (B) reduced coordination potential; (C) water solubility.

4.8.2 Supramolecular Chemistry

By exploiting the reactivity of the NH unit towards alkyl halides it may be possible to combine two or more ligand moieties around a central bridging unit. For example, by reacting **4.2** with dibrominated electrophiles one might expect to form a tetradentate [P,N,N,P] ligand (Figure 4.34). Compounds of this type are of interest as they may form supramolecular networks in the solid-state.

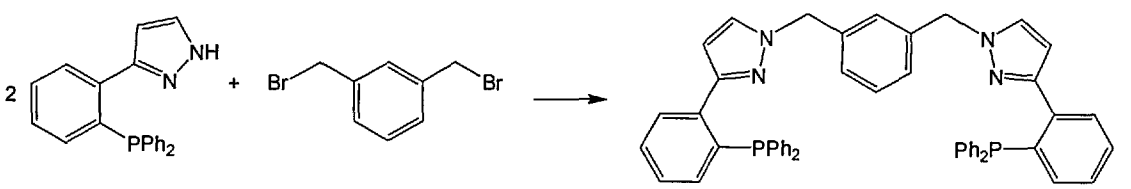


Figure 4.34. Proposed formation of tetradentate [P,N,N,P] ligand.

These reactions are currently being investigated[50] and the above ligand has been synthesised via a modified route to that shown in Figure 4.34. Initial studies into the reactivity of the [P,N,N,P] ligand towards silver(I) have revealed the formation of a discrete molecular complex in the solid-state, as shown in Figure 4.35. It is hoped that modification of the position and number of substituents, can allow supramolecular networks to be synthesised.

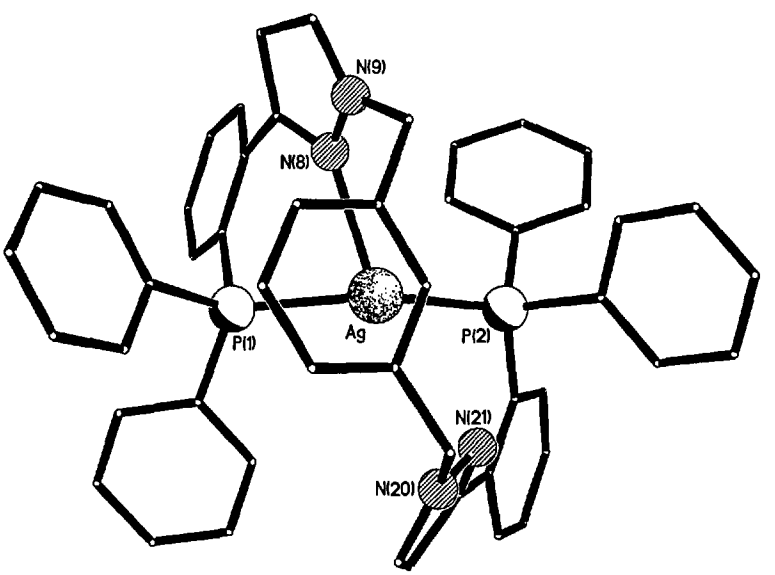


Figure 4.35. Solid state structure of the $Ag[P,N,N,P]^+$ cation.

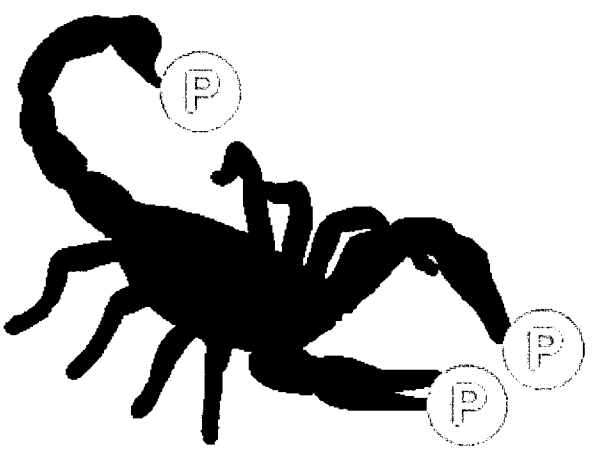
4.9 References

1. P. Braunstein and F. Naud, *Angew. Chem., Int. Ed.*, 2001, **40**, 680.
2. A. D. Burrows, *Science Progress*, 2002, **85**, 199.
3. C. S. Slone, D. A. Weinberger and C. A. Mirkin, *Prog. Inorg. Chem.*, 1999, **48**, 233.
4. A. M. Allgeier and C. A. Mirkin, *Angew. Chem., Int. Ed.*, 1998, **37**, 894.
5. D. A. Weinberger, T. B. Higgins, C. A. Mirkin, L. M. Liable-Sands and A. L. Rheingold, *Angew. Chem., Int. Ed.*, 1999, **38**, 2565.
6. H. Werner, M. Schulz and B. Windmuller, *Organometallics*, 1995, **14**, 3659.
7. G. P. C. M. Dekker, A. Buijs, C. J. Elsevier, K. Vrieze, P. W. N. M. van Leeuwen, W. J. J. Smeets, A. J. Spek, Y. F. Wang and C. H. Stam, *Organometallics*, 1992, **11**, 1937.
8. P. L. Arnold, A. J. Blake and C. Wilson, *Chem. Eur. J.*, 2005, **11**, 6095.
9. M. Bressan, F. Morandini and P. Rigo, *J. Organomet. Chem.*, 1983, **247**, c8.
10. S. Park, D. Hedden and D. M. Roundhill, *Organometallics*, 1986, **5**, 2151.
11. E. Lindner, B. Keppleler, H. A. Mayer, K. Gierling, R. Fawzi and M. Steimann, *J. Organomet. Chem.*, 1996, **526**, 175.
12. D. Sellmann, A. Fetz, M. Moll and F. Knoch, *J. Organomet. Chem.*, 1988, **355**, 495.
13. S. E. Angell, C. W. Rogers, Y. Zhang, M. O. Wolf and W. E. Jones Jr, *Coord. Chem. Rev.*, 2006, **250**, 1829.
14. K. R. Dunbar, *Comm. Inorg. Chem.*, 1992, **13**, 313.
15. J. I. Dulebohn, S. C. Haefner, K. A. Berglund and K. R. Dunbar, *Chem. Mater.*, 1992, **4**, 506.
16. J. R. Dilworth and N. Wheatley, *Coord. Chem. Rev.*, 2000, **199**, 89.
17. R. Fusco, in *The Chemistry of Heterocyclic Compounds: Pyrazoles, Pyrazolines, Pyrazolidines, Indazoles and Condensed Rings*, ed. R. H. Wiley, Wiley, New York, 1967, pp. 1-174.
18. A. Pleier, H. Glas, P. Sirsch and W. R. Thiel, *Synthesis*, 2001, **1**, 55.
19. A. Mukherjee, U. Subramanyam, V. G. Puranik, T. P. Mohandas and A. Sarkar, *Eur. J. Inorg. Chem.*, 2005, 1254.
20. A. Otero, F. Carrillo-Hermosilla, P. Terreros, T. Exposito, S. Rojas, J. Fernandez-Baeza, A. Antinolo and I. Lopez-Solera, *Eur. J. Inorg. Chem.*, 2003, 3233.
21. J. M. Takacs, S. D. Schroder, J. Han, M. Gifford, X. Jiang, T. Saleh, S. Vayalakkada and A. H. Yap, *Org. Lett.*, 2003, **5**, 3595.
22. A. Gsponer and G. Consiglio, *Helv. Chim. Acta*, 2003, **86**, 2170.
23. G. Consiglio and A. Gsponer, *Polym. Mater. Sci. Eng.*, 2002, **87**, 78.
24. D. B. Douglas, Y. Gong, L. Zakharov, J. A. Golen and A. L. Rheingold, *J. Am. Chem. Soc.*, 2006, **128**, 438.
25. K. S. Coleman, M. L. H. Green, S. I. Pascu, N. H. Rees, A. R. Cowley and L. H. Rees, *J. Chem. Soc., Dalton Trans.*, 2001, 3384.
26. P. Espinet and K. Soulantica, *Coord. Chem. Rev.*, 1999, **193**, 499.
27. P. Guillame and M. Postel, *Inorg. Chim. Acta*, 1995, **233**, 109.
28. F. E. Wood, M. M. Olmstead, J. P. Farr and A. L. Balch, *Inorg. Chim. Acta*, 1985, **97**, 77.
29. G. Minghetti, S. Stoccoro, M. A. Cinellu, A. Zucca, M. Manassero and M. Sansoni, *J. Chem. Soc., Dalton Trans.*, 1998, 4119.

30. G. Minghetti, A. Doppiu, S. Stoccoro, A. Zucca, M. A. Cinellu, M. Manassero and M. Sansoni, *Eur. J. Inorg. Chem.*, 2002, 431.
31. L. Prodi, M. Montalti, N. Zaccheroni, G. Pickart, L. Charbonniere and R. Ziessel, *New. J. Chem.*, 2003, **27**, 134.
32. L. Tusek-Bozic, A. Furlani, V. Scarcia, E. De Clercq and J. Balzarini, *J. Inorg. Biochem.*, 1998, **72**, 201.
33. L. Tusek-Bozic, I. Matijasic, G. Bocelli, G. Calestani, A. Furlani, V. Scarcia and A. Papaioannou, *J. Chem. Soc., Dalton Trans.*, 1991, 195.
34. L. Tusek-Bozic, P. Sgarabotto, A. Furlani, V. Scarcia and A. Papaioannou, *Inorg. Chim. Acta*, 1991, **185**, 229.
35. D. Wechsler, R. McDonald, M. J. Ferguson and M. Stradiotto, *Inorg. Chem.*, 2006, **45**, 4562.
36. D. Wechsler, A. Myers, R. McDonald, M. J. Ferguson and M. Stradiotto, *Chem. Commun.*, 2004, 2446.
37. X. Gan, E. N. Duesler, S. Parveen and R. T. Paine, *Dalton Trans.*, 2003, 4704.
38. S. M. Aucott, A. M. Z. Slawin and D. J. Woolins, *J. Chem. Soc., Dalton Trans.*, 2001, 2279.
39. G. G. Talanova, A. N. Kozachkova, K. B. Yatsimirskii, M. I. Kabachnik, T. A. Mastryukova, I. M. Aladzheva and O. V. Bikhovaskaya, *J. Coord. Chem.*, 1996, **39**, 1.
40. S. J. Coote, G. J. Dawson, C. G. Frost and J. M. J. Williams, *Synlett*, 1993, 509.
41. Y. Sun, A. Hienzsch, J. Grasser, E. Herdtweck and W. R. Thiel, *J. Organomet. Chem.*, 2006, **691**, 291.
42. D. A. Clarke, P. W. Miller, N. J. Long and A. J. P. White, *Dalton Trans.*, 2007, 4556.
43. M. C. Torralba, M. Cano, J. A. Campo, J. V. Heras, E. Pinilla and M. R. Torres, *Inorg. Chem. Comm.*, 2002, **5**, 887.
44. C. Navarro-Ranniger, J. M. Perez, F. Zamora, V. M. Gonzalez, J. R. Masaguer and C. Alonso, *J. Inorg. Biochem.*, 1993, **52**, 37.
45. S. Stoccoro, G. Chelucci, A. Zucca, M. A. Cinellu, G. Minghetti and M. Manassero, *J. Chem. Soc., Dalton Trans.*, 1996, 1295.
46. *Search on CSD version 5.28 (January 2007).*
47. F. Bonati and H. C. Clark, *Can. J. Chem.*, 1978, **56**, 2513.
48. *Lucy Jennings is gratefully acknowledged for performing the catalyst test reactions at Imperial College London.*
49. Y. Sun and W. R. Thiel, *Inorg. Chim. Acta*, 2006, **359**, 4807.
50. M. Lui, N. J. Long, S. Kealey and P. W. Miller, *Research in progress, Imperial College, London.*

CHAPTER 5

NEW SCORPIONATE LIGANDS CONTAINING APPENDED DONOR GROUPS



5. New Scorpionate Ligands Containing Appended Donor Groups

5.1 Introduction

Over the last 15 years, a new branch of scorpionate chemistry has emerged in which extra coordinating groups have been attached to the pyrazolyl rings of the poly(pyrazolyl)borate ligand core. Most commonly, the appended donor groups are bound via a linker unit to the 3-position of the pyrazolyl rings, thus creating a species in which each 'arm' of the ligand is capable of bidentate coordination via the pyrazolyl nitrogen and the appended donor site. The presence of extra donor sites in the bis-, tris- and tetrakis-pyrazolylborate ligands has created a number of species which are capable of varied coordination behaviour compared to the unmodified ligands.

The first poly(pyrazolyl)borate ligand of this type, Tp^{py}, was synthesised by Ward *et al.* in 1994.[1] In this species 2-pyridyl groups are bound to the 3-position of the pyrazole rings of a tris(pyrazolyl)borate core to give a potentially hexadentate N_6 donor ligand capable of coordination via three pyrazolyl and three pyridyl nitrogen donors (Figure 5.1).

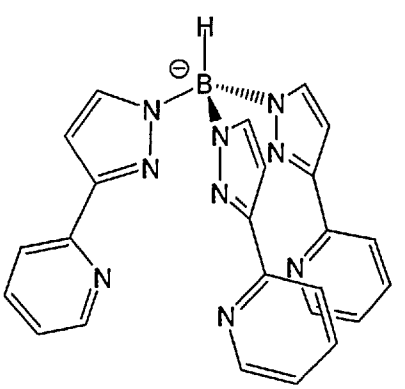


Figure 5.1. The first donor-appended scorpionate ligand, Tp^{py}.

Molecular modelling studies on the cavity size within this ligand revealed a good match with second/third row transition metals and lanthanide ions. These reactions were duly examined, for example, the 1 : 1 reaction of $K[Tp^{py}]$ with europium(III) nitrate produced a complex of the formula $[Eu(Tp^{py})(NO_3)_2]$ in which the metal is 10

coordinate as a result of hexadentate coordination to the N_6 donor podand and two bidentate nitrate ligands (Figure 5.2).[2]

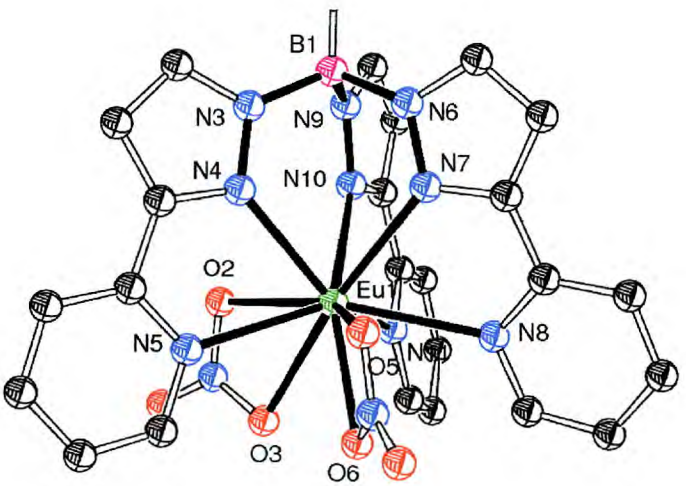


Figure 5.2. Molecular structure of the complex $[Eu(Tp^{py})(NO_3)_2]$.

Since this discovery, functionalised poly(pyrazolyl)borate ligands containing pyridyl,[2, 3] bipyridyl,[4] anisyl,[5, 6] thioanisyl,[7] pyrazinyl,[8] carboxamide,[9] ether,[10] furyl,[11] thienyl,[12] and carboxyl[13] appendages have been synthesised. The appended donor groups do not necessarily exhibit coordination to the chosen metal ion, often as a consequence of a mismatch in compatibility between the donor group and the metal (for example hard donor versus soft acceptor or a geometric constraint).

5.1.1 Potentially Hemilabile Scorpionates

Throughout this research, scorpionate ligands have been employed due to their ability to stabilise copper carbonyl species (as described in Chapter 2) prior to the subsequent decarbonylation reaction via irreversible ligand substitution. A further improvement in the field of controlled CO trapping/release could be the use of a modified Tp ligand which is able to bind CO strongly yet undergo reversible decarbonylation upon stimulation from an external source. UV-triggered decarbonylation of a copper carbonyl species, $[Cu(TMPA)CO]^+$, has recently been reported in the literature by Karlin *et al.*[14] In this process it is believed that metal to ligand charge transfer upon irradiation forms a transient copper(II) species which is unable to support the carbonyl

ligand. In this process it is believed that solvent molecules coordinate to the metal upon loss of the carbonyl.

It might be possible to apply UV-triggered decarbonylation to tris(pyrazolyl)borate-supported copper(I) carbonyls of the type described in Chapter 2. These investigations are currently being performed by Long *et al.*[15] A potentially-reversible carbonylation system could employ a donor-appended scorpionate ligand, whereby chelation of the appended donor group could stabilise the copper centre in the absence of the carbonyl ligand (Figure 5.3).

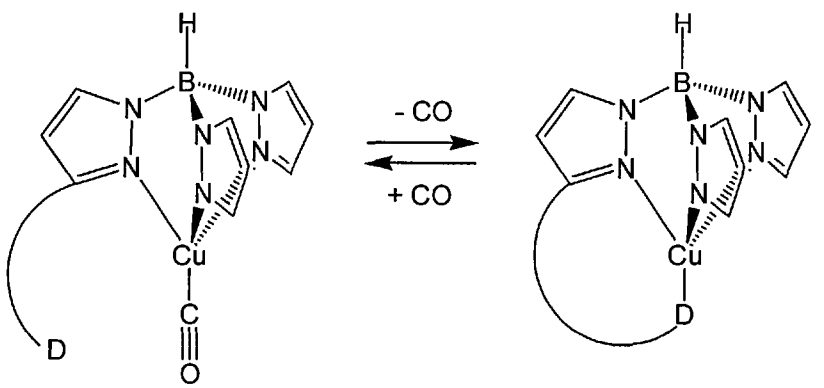


Figure 5.3. Proposed hemilabile Tp ligand stabilising a copper complex in the absence of CO.

The choice of appended donor group and the length and flexibility of the linker unit are likely to be important factors in the effectiveness of such a system. If the competing donor moiety binds too favourably to the copper then it may be impossible to bind the CO. On the other hand, if the donor group has little affinity towards the copper centre, decarbonylation may not be facilitated. Research into the strength of copper-ligand bonds finds the relative binding strength to be ranked in the following order: R-C≡N < CO < PR_3. Scorpionates bearing donor groups at both ends of this scale have been studied, and are described in the following sections.

5.2 Nitrogen-Appended Scorpionates

A good starting point for a potentially reversible system would be a Tp ligand bearing nitrile appendages, but no such species has been reported in the literature. However, Tp^{py} as reported by Ward *et al.*[1] bearing 2-pyridyl donor groups may provide a

suitable substitute for the nitrile species. The $K[Tp^{py}]$ ligand (**5.1**) was synthesised by reaction of KBH_4 with 3(5)-(2'-pyridyl)pyrazole according to the literature procedure[1] and characterised by ^1H and ^{11}B NMR and IR spectroscopy as summarised in Table 5.1.

5.2.1 Synthesis of $Cu_4[Tp^{py}]_4$ (5.2)

Before examining the copper carbonyl chemistry of this ligand, the reactivity of the Tp^{py} ligand with copper(I) chloride in the absence of CO was examined. Ward *et al.*[16] have performed similar studies including the 1:1 reaction of $K[Tp^{py}]$ with $[Cu(MeCN)_4]PF_6$. This yielded a brown solid of the formula $[Cu_3(Tp^{py})_2][PF_6]$. The solid-state structure of this species determined by X-ray crystallography shows a trimetallic species in which the ligand adopts a bridging mode whereby each bidentate arm coordinates to a different copper centre. Unfortunately, no NMR data was provided for this complex.

To follow on from this work and to investigate the reactions of these species with CO, the reaction of an alternative copper(I) source, CuCl, with $K[Tp^{py}]$ was performed in DCM solution under an atmosphere of nitrogen. This yielded an orange solution that was filtered and concentrated to dryness to give an orange powder (**5.2**). Elemental analysis of **5.2** provided an excellent match with the calculated values for a 1:1 $Cu:Tp^{py}$ complex, $[Cu_n(Tp^{py})_n]$ and a poor match with $[Cu_3(Tp^{py})_2][Cl]$, which might have been expected to form based on the formation of $[Cu_3(Tp^{py})_2][PF_6]$ as discussed above. The choice of anion clearly plays an important role in the outcome of this reaction and the absence of the chloride anion in complex **5.2** is proposed to result from the favourable thermodynamic driving force of KCl precipitation.

Attempts to elucidate the solid-state structure of $[Cu_n(Tp^{py})_n]$ (**5.2**) by X-ray analysis were made, but no suitable crystals were obtained. The ^1H NMR spectrum of this complex shows significant broadening at room temperature (Table 5.1) which prompted variable temperature NMR studies. These were performed upon cooling of a CD_2Cl_2 solution of **5.2** and resulted in the broad peaks splitting and becoming sharper as the temperature was lowered (Figure 5.4).

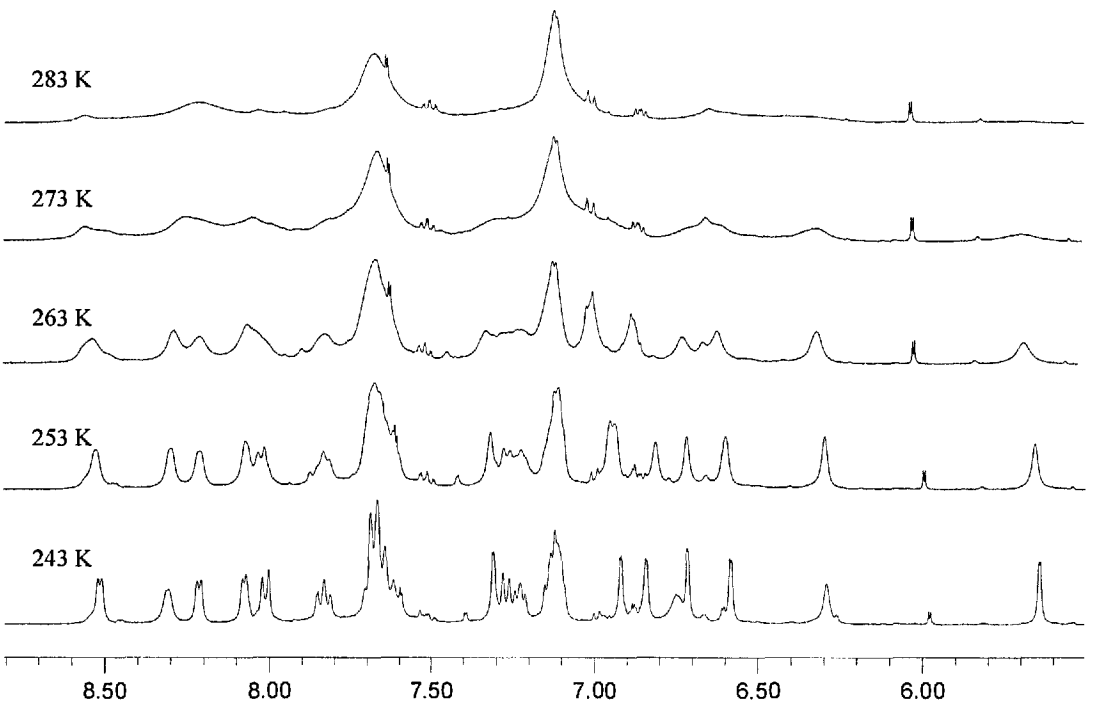
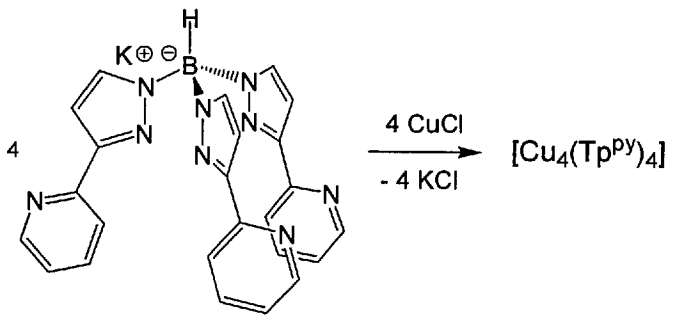


Figure 5.4. Variable temperature ^{1}H NMR spectrum of $[Cu_4(Tp^{py})_4]$ (**5.2**).

At 243 K (-30°C), a complicated spectrum was obtained in which the aromatic protons produce a total relative integral of 24. To elucidate the composition of this solution-species, the proton environments of the Tp^{py} ligand were considered. Uncoordinated Tp^{py} contains three bidentate arms, each containing six distinct chemical environments, to give a total of 18 protons. Given that 24 protons (or a multiple, thereof) are observed on the ^{1}H NMR spectrum, the presence of a mononuclear species in solution could be ruled out. If, however, there were four non-equivalent Tp^{py} moieties present in solution (*e.g.* $[Cu_4(Tp^{py})_A(Tp^{py})_B(Tp^{py})_C(Tp^{py})_D]$) then a total of 72 protons would be present (Figure 5.5).



[5.1] [5.2]

Figure 5.5. Synthesis of $[Cu_4(Tp^{py})_4]$.

In this case the three arms of each Tp ligand are equivalent and therefore result in six separate resonances, each with an integral of 3. Since there are four non-equivalent Tp^{py} moieties present in solution ($[Tp^{py}]_{A\text{-}D}$), a total of 24 separate resonances would be expected and this is indeed observed. These chemical environments have been successfully assigned for the ^1H NMR spectrum recorded at 243 K, with the aid of the ^1H COSY spectrum and are shown in Figure 5.6.

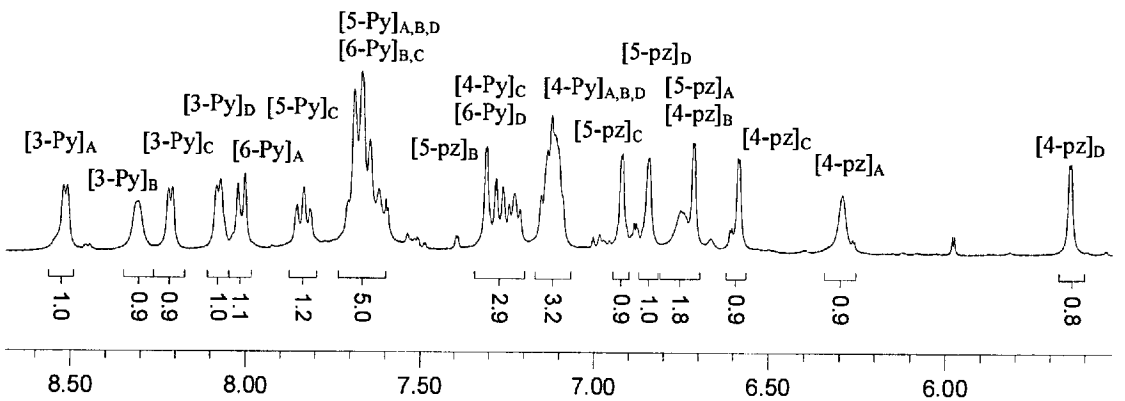


Figure 5.6. ^1H NMR spectrum of $[Cu_4(Tp^{py})_4]$ (**5.2**) at 243 K.

ESI mass spectrometry was performed on a sample of **5.2** and showed the highest significant cluster to be centred at 1079 m/z, corresponding to a trinuclear species, $[Cu_3(Tp^{py})_2]^+$. The nonappearance of a $[Cu_4(Tp^{py})_n]^+$ species is thought to result from fragmentation of this species within the spectrometer.

The predisposition of **5.2** to form a tetranuclear $[Cu_4(Tp^{py})_4]$ species in solution most likely results from the inability of the pyridyl donor groups to chelate to the copper centre due to the strained nature of the potential five-membered chelate ring. Instead, tetracoordination at each copper centre is thought to be achieved by formation of a tetranuclear species in which the ligand arms are able to bridge between separate copper centres. Without a crystal structure, however, the exact nature of this bonding remains unknown.

The broadening of the room temperature ^{1}H NMR spectrum of **5.2** may result from the fluxional behaviour of the bidentate ligand arms. Due to the mismatch in geometry of the Tp^{py} ligand and the tetrahedral requirements of the copper centre, it thought that at room temperature the bidentate arms rapidly interchange in solution between coordinating and non-coordinating modes at the different copper centres. This results in an average of these signals being observed in the ^{1}H NMR spectrum.

5.2.2 Synthesis of Cu[Tp^{py}]CO (5.3)

i. IR studies

Carbonylation of $[Cu_4(Tp^{py})_4]$ (**5.2**) was performed by bubbling CO through a DCM solution of **5.2** and was conveniently monitored by solution IR spectroscopy. After five minutes, the IR spectrum was found to contain a sharp peak at 2081 cm^{-1} (spectrum **A** in Figure 5.7). This value is within the range commonly seen for terminal carbonyl adducts of the formula $Cu[Tp^x]CO$. It an attempt to isolate the solid carbonyl, $Cu[Tp^{py}]CO$ (**5.3**), the solution was concentrated *in vacuo*, however, the carbonyl stretch was found to weaken in the process. This prompted further studies into the decarbonylation of the carbonyl by application of brief vacuum/nitrogen cycles.

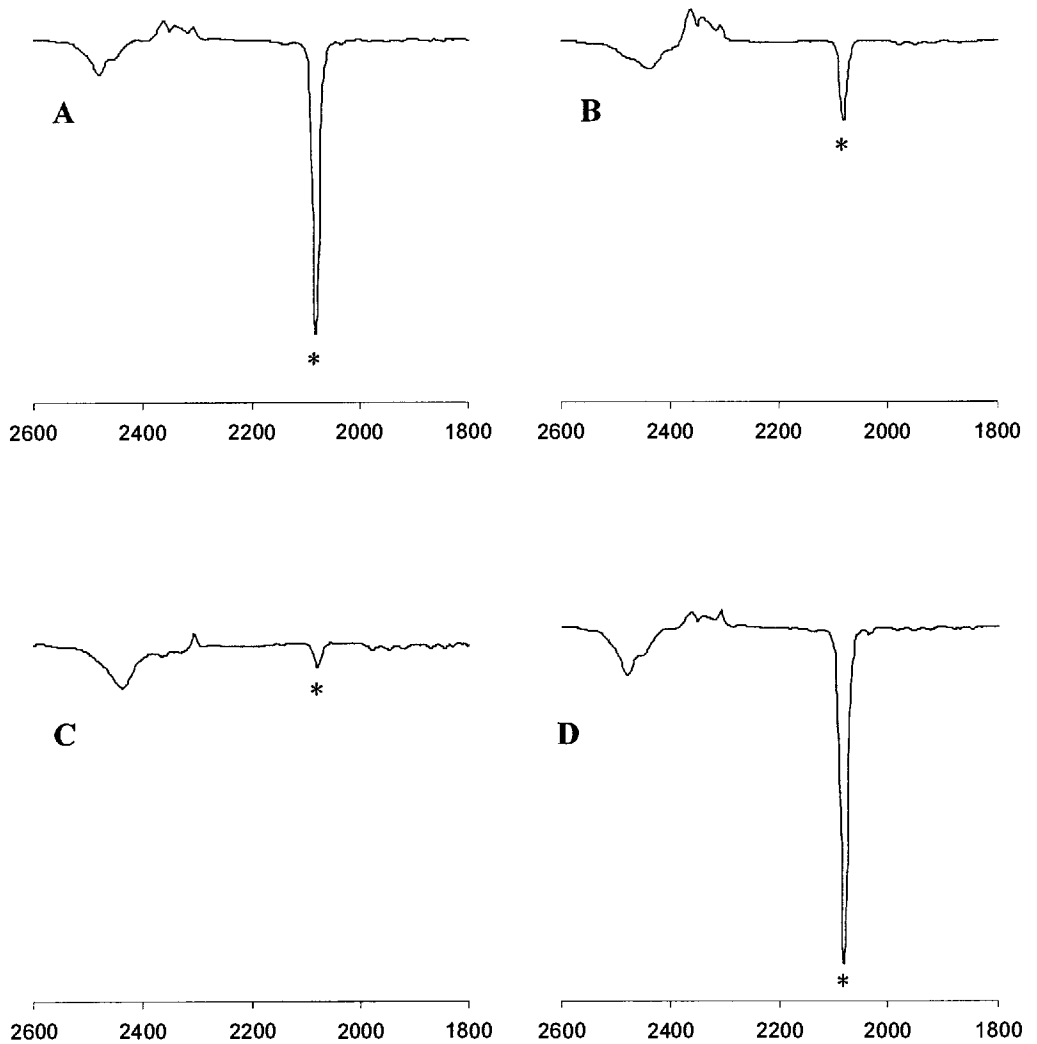


Figure 5.7. IR spectra of a solution of $[Cu_4(Tp^{py})_4]$ **(5.2)** in DCM after: (A) five minutes bubbling CO; (B) three vacuum/N_2 cycles; (C) six vacuum/N_2 cycles and (D) five minutes bubbling CO.

As shown in Figure 5.7, after three vacuum/nitrogen cycles, the CO stretch at 2081 cm^{-1} became significantly weakened (spectrum **B**) and was almost completely removed after another three vacuum/nitrogen cycles (spectrum **C**). To examine the reversibility of this process, CO was again bubbled through the solution for five minutes, causing the strong carbonyl stretch to reappear (spectrum **D**).

The reversibility of this carbonylation process suggests that the tetrameric carbonyl-free complex **5.2** is quite easily dissociated, as in the presence of CO the complex is proposed to fragment to form a mononuclear carbonyl species **5.3** as shown in Figure 5.8.

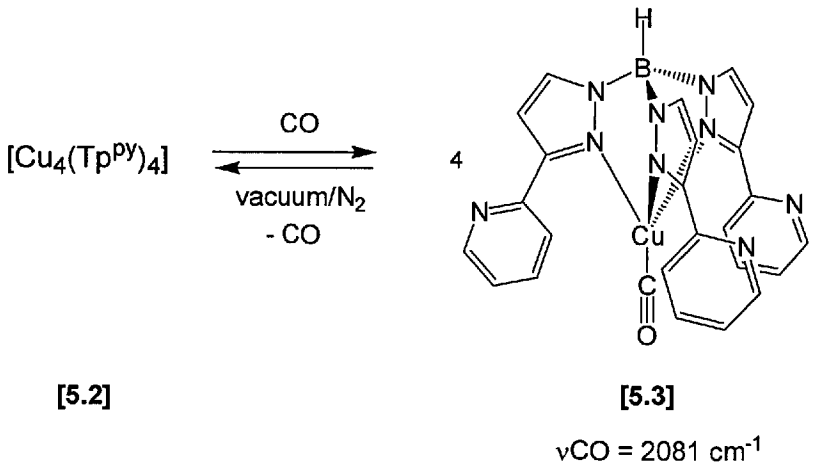


Figure 5.8. Proposed scheme of reversible carbonylation of $[Cu_4(Tp^{py})_4]$ (**5.2**) to form $[Cu(Tp^{py})CO]$ (**5.3**).

ii. NMR studies

To record the ^1H NMR spectrum of the carbonyl adduct, **5.3**, a CD_2Cl_2 solution of **5.2** was first prepared under an atmosphere of nitrogen to produce an orange solution. The nitrogen supply was then swapped for CO and three vacuum/CO cycles were performed, causing the solution to become pale yellow, at which point the room temperature ^1H NMR spectrum was recorded. This revealed a remarkable difference in appearance to the broadened spectrum observed for the carbonyl-free species, **5.2**. Upon formation of the carbonyl complex, **5.3**, a relatively simple spectrum shown in Figure 5.9 is obtained. With the aid of the ^1H COSY spectrum, these peaks have been assigned as shown in Figure 5.9 and summarised in Table 5.1.

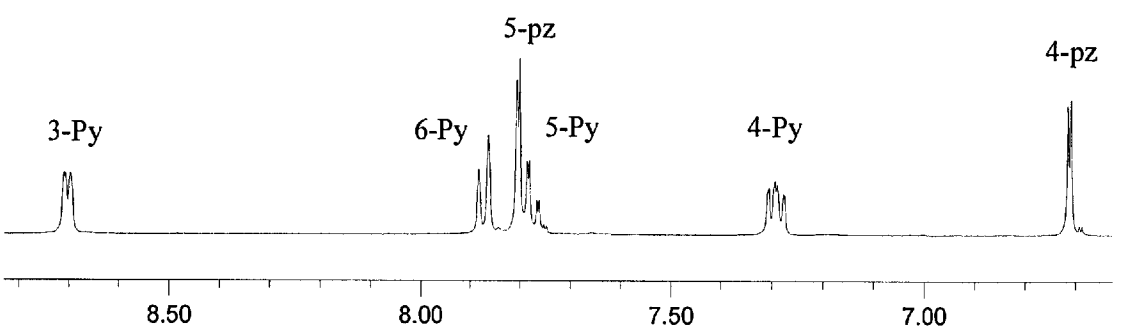


Figure 5.9. ^1H NMR spectrum of $[Cu(Tp^{py})CO]$ (**5.3**) at 300 K.

In **5.3**, the three ligand arms appear equivalent with the six different aromatic protons easily identified. The 3-pyridyl proton is found furthest downfield at 8.70 ppm while the 4-pyrazolyl proton is found characteristically upfield of all the other aromatic resonances at 6.71 ppm. The equivalence of the three ligand arms further supports the hypothesis based on IR data that a C_3 symmetric species has formed in which the three pyrazolyl rings bind to the copper along with a terminal carbonyl ligand as proposed in Figure 5.8.

5.2.3 Summary

Selected NMR and IR spectroscopic data for the complexes of Tp^{py} are summarised in Table 5.1. The numbering scheme used to assign the chemical environments is shown in Figure 5.10. This numbering scheme also applies to the detailed assignments made in the experimental section (Chapter 7).

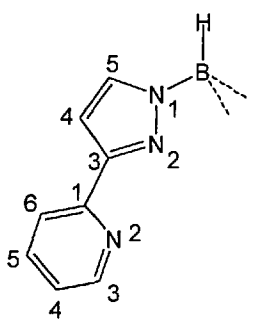


Figure 5.10. Numbering scheme used to describe chemical environments in Tp^{py} complexes.

Table 5.1. IR and ^1H and ^{11}B NMR data for complexes **5.1** - **5.3**

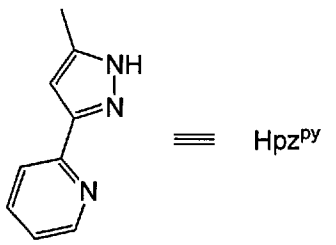
Complex	^{11}B NMR[a] δ/ppm	^1H NMR[a] δ/ppm							IR[b] ν/cm^{-1}	
	B	*5-pz*	*4-pz*	*3-Py*	*4-Py*	*5-Py*	*6-Py*	*BH*	*CO*	*BH*
5.1 $K[Tp^{py}]$[c]	-1.4	7.75 (d)	6.67 (d)	8.56 (ddd)	7.16 (ddd)	7.72 (m)	7.79 (ddd)	4.90 (m)	—	2446
5.2 $Cu_4[Tp^{py}]_4$	—[d]	7.12 (br)	6.48 (br)	8.23 (br)	7.12 (br)	7.78 (br)		4.63 (br)	—	2430
5.3 $Cu[Tp^{py}]CO$	—[d]	7.80 (d)	6.71 (d)	8.70 (d)	7.29 (ddd)	7.77 (m)	7.87 (d)	4.64 (m)	2081[e]	2479[e]

(a) Recorded as CD_2Cl_2 solution at 293 K unless indicated otherwise; (b) Recorded as KBr disc unless indicated otherwise; (c) d_6-acetone solution; (d) Not recorded; (e) CH_2Cl_2 solution.

The reversible carbonylation of Cu[Tp^{py}]CO can be contrasted with the behaviour of the Cu[Tp^{x}]CO species encountered in Chapter 2 (Tp^{x} = Tp, Tp* or $Tp^{Ph,SMe}$). The latter complexes were found to be stable to decarbonylation *in vacuo* as evidenced by the characterisation of these solids after vacuum drying. This difference in reactivity cannot be attributed to a particularly weak Cu–CO bond in **5.3** as solution IR spectroscopy of this species shows νCO to be similar to the corresponding stretches of the Cu[Tp^{x}]CO complexes. This difference in solution behaviour is believed to be caused by the presence of the appended donor groups in **5.3** (the three pyridyl arms) which are able to stabilise the CO-free species by formation of a tetranuclear species where each copper centre is able to maintain its preferred tetracoordinate geometry.

A similar trend in CO reactivity has been observed previously for the TACN macrocycle discussed in Chapter 1. Here it was found that the irreversible carbonylation of the $[Cu(TACN)]^{+}$ complex[17] could be rendered reversible upon use of a TACN ligand bearing a -CH_2Py donor arm,[18] although in this case a mononuclear CO-free species was able to form due to the increased flexibility of the -CH_2Py unit.

The behaviour of copper(I) with Tp^{py} is strikingly similar to the reactivity of copper(I) with the individual Tp arms as reported by Stavropoulos *et al.*[19] In this case, it was found that reaction of copper(I) with the deprotonated pyridyl-appended pyrazole, pz^{py}, yielded a tetrameric species $[Cu_4(pz^{py})_4]$. This yellow-orange species was shown to undergo reversible carbonylation in toluene solution to form a light yellow solution consisting of the trimeric carbonyl species, $[Cu(pz^{py})CO]_3$ (Figure 5.11). This similarity in reactivity is not surprising given that in each case the copper is able to bond to the same donor groups (pyridyl and pyrazolyl) albeit from different parent ligands.



≡ Hpz^{py}

Hpz^{py} + $[Cu(MeCN)_4][PF_6]$ $\xrightarrow{base}$ $[Cu_4(pz^{py})_4]$ $\underset{vacuum}{\overset{CO}{\rightleftharpoons}}$ $[CuCO(pz^{py})]_3$

Figure 5.11. Summary of copper(I) carbonyl chemistry of pz^{py}.

5.3 Phosphine-Appended $T_k$ps

5.3.1 Background

To date a great deal of attention has been paid towards the development of new phosphine-containing hybrid ligands due to their widespread use in catalysis.[20] Similarly, since their conception in the late 1960s, a large amount of research has been focused on the many poly(pyrazolyl)borate 'scorpionate' ligands[21, 22] and their second generation analogues containing extra coordinating groups bound to the pyrazolyl rings of the ligand core. It is therefore somewhat surprising to find that these two fields have not overlapped and that out of all of the functionalised scorpionate ligands produced to date, the most common appendages contain nitrogen,[3, 4, 8] sulphur[7, 12] and oxygen[5, 6, 9-11, 13] donors, and that no phosphine donor scorpionates have been reported.

A Tp ligand containing a phosphine moiety attached via a linker to the ligand backbone would provide an interesting analogue to the Tp^{py} species described above as phosphine donors represent the other end of the copper(I)–ligand affinity scale. It would therefore be worthwhile to study the reactivity of such a ligand towards copper(I) and CO in a similar way to the 'first generation' Tp systems described in Chapter 2. A ligand of this kind could provide a template for future reactions examining reversible CO fixation by $Cu[Tp^x]$ species.

The potentially favourable hemilabile properties of a Tp ligand bearing phosphine donor appendages might also find applications in catalysis. In such a species, the tripodal array of pyrazolyl donors would have an anchor effect of binding a metal ion firmly in place. Meanwhile, coordination of the appended phosphine donor moiety could stabilise the complex, but upon temporary dissociation a vacant site would be created to allow binding of a reactive substrate. The dissociation of a labile group occurs in a range of catalytic processes and the Tp-stabilised complex, $RuTp(PPh_3)_2H$,[23-25] is one such example, whereby the phosphine ligand dissociates initially to make way for substrate binding.

The likely reason for the absence of any phosphine-appended scorpionates in the literature is the hitherto limited availability of phosphorus-containing pyrazoles. In Chapter 4, however, a new synthetic pathway was described for the formation of the triphenylphosphine-appended pyrazole, Hpz^{phos} (**4.2**). This species, along with its phosphine oxide (**4.3**) and phosphine sulphide (**4.4**) derivatives, was studied for potentially hemilabile behaviour with palladium(II). The interest in these ligands stems from their hemilabile behaviour coupled with their ease of derivatisation by substitution at the pyrazole N–H moiety, thus allowing further ligand modifications to fine-tune electronic and steric properties. By exploiting the reactivity of the N–H bond towards metal borohydrides, the conversion of these pyrazoles into novel phosphine-containing scorpionate ligands was proposed, as outlined in Figure 5.12.

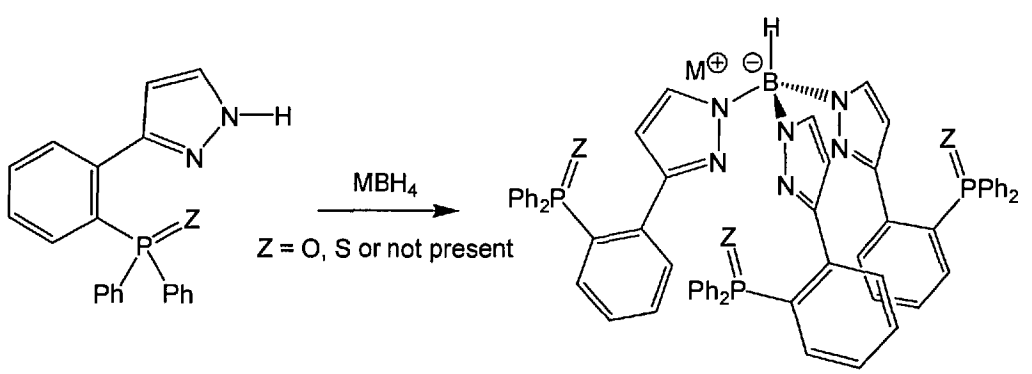


Figure 5.12. Proposed synthesis of novel phosphine-containing scorpionates.

These reactions were duly performed and are discussed in the following sections. The millimolar quantities of reagents employed in these reactions meant that it was

difficult to reliably measure the volume of H_2 gas evolved and consequently it was not possible to follow the progress of the reactions in this manner. To prevent oxidation of the phosphine moiety, the reaction between the phosphine-appended pyrazoles and potassium borohydride were performed under a nitrogen atmosphere. Since it was not possible to follow these reactions by gas evolution, it proved difficult to isolate the desired Tp species without obtaining contamination from either the bis- or tetrakis-pyrazolated species. For this reason, the syntheses of tetrakis(pyrazolyl)borates were performed by reacting an excess of pyrazole with potassium borohydride at elevated temperatures (>200°C).

The proposed T_kp ligands contain four potentially bidentate donor arms connected to a central boron atom. Due to the tetrahedral arrangement at this centre and the rigidity of the ligand arms, it is impossible for all four arms to chelate to one metal centre. In any complexation reactions, the fourth ligand arm should be essentially inert, such that the reactivity of the T_kp ligand will closely resemble that of the theoretical corresponding Tp species.

5.3.2 Synthesis of K[T_kp^{phos}] (5.4)

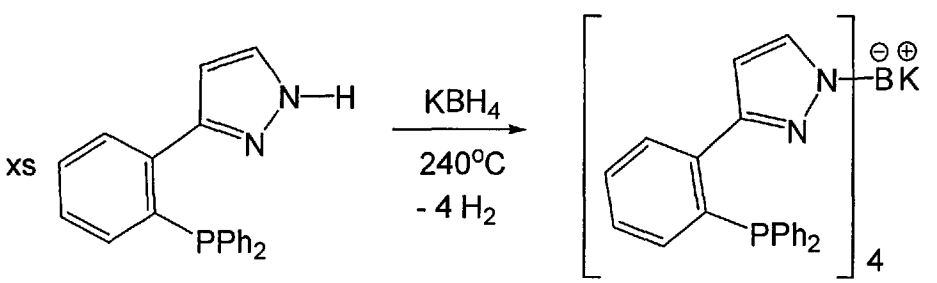


Figure 5.13. Synthesis of phosphine-appended scorpionate ligand K[T_kp^{phos}] (**5.4**).

Reaction of the pyrazole Hpz^{phos} (**4.2**) with potassium borohydride was performed as shown in Figure 5.13. The crude product was obtained as an off-white powder and initial evidence for the formation of the desired species was provided by ESI(-ve) mass spectrometry which showed the required $[T_kp]^-$ anion at 1319 m/z. ^{1}H-Coupled ^{11}B NMR spectroscopy revealed a singlet at 0.9 ppm, further indicating that the tetra-substituted species **5.4** had indeed formed, as formation of the Bp or Tp species would

be evidenced by B–H coupling to produce a triplet or a doublet, respectively. ^{1}H NMR analysis, however, revealed the presence of significant amounts of unreacted pyrazole (**4.2**). Recrystallisations were attempted on this sample, but an improvement in purity was not achieved as both the starting material and the product were found to possess very similar solubilities. It was possible for the ^{1}H environments in **5.4** to be identified and these are summarised in Table 5.2.

Upon conversion of the pyrazole **4.2** into the corresponding T_kp ligand **5.4**, both the pyrazolyl protons are seen to move upfield in the ^{1}H NMR. This reflects an increase in shielding of these environments upon formation of the negatively charged species. The $^{31}P\{^{1}H\}$ chemical shift does not change considerably, perhaps due to the significant separation between the phosphorus atom and the reactive nitrogen moiety.

5.3.3 Synthesis of Zn[T_kp^{phos}]OAc (5.5)

In an attempt to isolate and structurally characterise a complex of T_kp^{phos}, the crude product **5.4** was reacted with $Zn(OAc)_2$ in a 1:1 ratio in order to synthesise Zn[T_kp^{phos}]OAc (**5.5**). This reaction produced a white powder containing the Zn[T_kp^{phos}]$^{+}$ cation as evidenced by mass spectrometry. However, attempts to grow single crystals suitable for X-ray analysis were unsuccessful.

5.3.4 Summary

Selected NMR spectroscopic data for the pyrazole starting material and the new T_kp ligand are summarised in Table 5.2 using the numbering scheme outlined in Figure 5.14. This numbering scheme also applies to the detailed assignments made in the experimental section (Chapter 7).

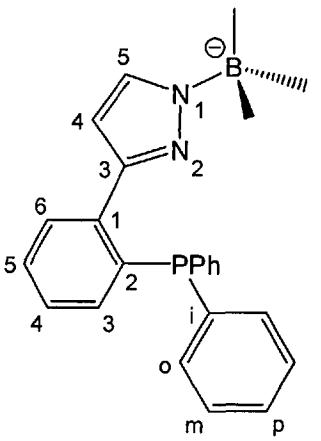


Figure 5.14. Numbering scheme used to describe chemical environments in T_kp^{phos}.

Table 5.2. Selected ^1H, ^{11}B and $^{31}P\{^1H\}$ NMR data for **4.2** and **5.4**

Compound	$^{31}P\{^1H\}$ NMR[a] δ/ppm	^{11}B NMR[a] δ/ppm	^1H NMR[a] δ/ppm						
	P	*B*	*5-pz*	*4-pz*	*3-Ph*	*4-Ph*	*5-Ph*	*6-Ph*	*Ph-H*
4.2 Hpz^{phos}	- 11.4 (s)	—	7.48 (d)	6.34 (m)	7.03 (ddd)	overlap with Ph-H at 7.30	7.42 (ddd)	7.60 (dd)	7.26-7.37 (m)
5.4 $K[T_kp^{phos}]$	-10.0 (s)	0.9 (s)	7.06 (d)	6.06 (d)	6.87 (dd)	overlap with Ph-H		7.57 (dd)	7.10-7.35 (m)

(a) Recorded in $CDCl_3$ solution at 298 K.

It was encouraging to find that the phosphine moiety remained intact during the high temperatures of the ligand-forming reaction and that no side reactions were observed at the phosphorus lone-pair. The presence of a reactive phosphine moiety has proved problematic when attempts have been made to alkylate the N–H moiety, so its tolerance towards the borohydride ion was in doubt. Unfortunately, difficulties in separating the ligand from excess starting material have prevented any further investigations into this species. However, a more successful approach to the synthesis of phosphine-appended Tp ligands is discussed in sections 5.6 and 5.7.

5.4 Phosphine Oxide-Appended $T_k$ps

5.4.1 Synthesis of $K[T_kp^{phos(O)}]$ (5.6)

The reactivity of the phosphine oxide-appended pyrazole, $Hpz^{phos(O)}$ (**4.3**), was similarly investigated, this time with greater success. The reaction of potassium borohydride with an excess of **4.3** was performed according to the scheme shown in Figure 5.15. This reaction was performed by heating at a high temperature (260°C) and under an inert atmosphere to avoid any possible degradation of the reagents. After two hours heating, the product was purified by recrystallisation from hot THF and isolated as a white, air-stable solid in moderate yield (56 %).

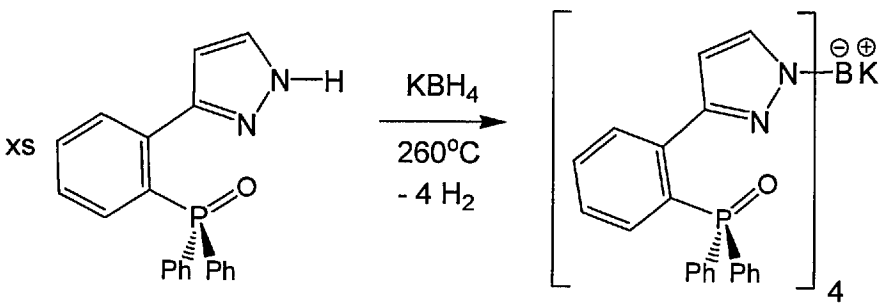


Figure 5.15. Synthesis of phosphine oxide-appended scorpionate ligand $K[T_kp^{phos(O)}]$ (**5.6**).

Evidence for the formation of a new species (**5.6**) was given by $^{31}P\{^1H\}$ NMR spectroscopy, showing a sharp singlet at 30.9 ppm (*cf.* starting material at 35.8 ppm). Crucially, ^1H-coupled ^{11}B NMR spectroscopy showed a sharp singlet at 0.7 ppm, indicating that no B–H bonds remain. This was supported by negative ion ESI mass spectrometry, in which the $[T_kp^{phos(O)}]^-$ anion was observed at 1383 m/z as expected. IR and ^1H, $^{31}P\{^1H\}$ and ^{11}B NMR spectroscopic data for this species is summarised in Table 5.5. Judging from ^1H and $^{13}C\{^1H\}$ NMR data the ligand was found to be pure with no contamination from the pyrazole starting material or any unwanted products. The ^{31}P and pyrazolyl proton resonances shift upfield upon T_kp formation. This may result from increased electron density within the negatively charged species **5.6** compared to the neutral starting material **4.3**.

5.4.2 Synthesis of Tl[$T_kp^{phos(O)}$] (5.7)

In an attempt to structurally characterise this new T_kp ligand, the corresponding thallium complex was synthesised by reaction of **5.6** with thallous nitrate in THF/water. Whereas precipitation of the thallium complex is usually observed when this reaction is performed with Tp ligands,[21] in this case precipitation was not observed, most likely as a result of the increased solubility of this species imparted by the fourth pyrazolyl arm. To isolate this complex, the solution was extracted into DCM, filtered and concentrated to dryness to give an analytically pure sample of Tl[$T_kp^{phos(O)}$] (**5.7**) in good yield (70 %).

^1H and $^{31}P\{^1H\}$ NMR spectroscopic data for **5.7** are summarised in Table 5.5. The $^{31}P\{^1H\}$ NMR spectrum shows a singlet at 30.3 ppm, virtually unmoved from the starting material **5.6** indicating similar solution behaviour in both species. If the phosphine oxide arms were to coordinate to the thallium ion in solution it is thought that splitting of the phosphine resonance in the $^{31}P\{^1H\}$ NMR spectrum would be observed due to ^2J coupling to $^{203/205}Tl$ (both ^{203}Tl and ^{205}Tl are spin ½ with near-identical gyromagnetic ratios). Since a singlet was observed, it suggests that the phosphine oxide arms do not encapsulate the thallium ion. This proposal can be extended to the potassium complex as a nearly identical ^{31}P chemical shift is observed in this species. Crystals of **5.7** suitable for X-ray crystallography were obtained by slow diffusion of pentane vapour into a chloroform solution of this complex.

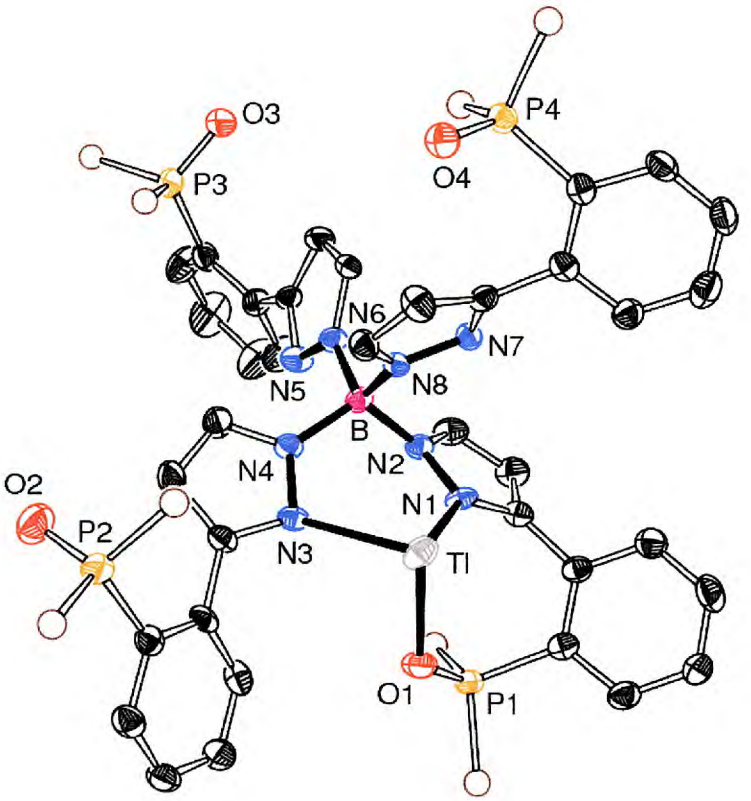


Figure 5.16. Molecular structure of Tl[Tkp$^{phos(O)}$] (**5.7**) (50 % probability ellipsoids). Phenyl groups are represented as points for clarity.

The solid-state structure of **5.7** (Figure 5.16) matches the proposed structure for the T_kp ligand. However, the binding mode of this ligand with thallium appears to be quite unusual. In contrast to most other Tl[Tp] and Tl[T_kp] derivatives where three of the pyrazolyl arms bind to the metal, here in **5.7** only two of the arms coordinate. This mode of coordination has only previously been seen in a handful of related thallium structures.[3, 26-29] The third coordination site at the thallium in **5.7** is occupied by the phosphine oxide donor attached to one of the bound pyrazolyl arms, making this arm bidentate. Only one of the literature examples cited above has an extra donor on the pyrazolyl arms (3-pyridyl groups), and in this case the extra donor is used to bind to a different metal atom, generating a polymer.[3] Thus the $T_kp^{phos(O)}$ bonding mode seen here is the first example of its type. The metal has a hemidirected coordination geometry,[30] the three donors occupying the facial sites of a pseudo-octahedron. The *ca.* 0.05 Å disparity between the Tl–N bond lengths (Table 5.3) is not related to the

bidentate coordination of one of the pyrazolyl arms as this pattern of bonding is also seen in each of the related literature examples cited above.[26-29]

Table 5.3. Selected bond lengths (Å) and angles (°) for $Tl[T_kp^{phos(O)}]$ (**5.7**)

Tl–O(1)	2.541(2)	Tl–N(1)	2.536(3)
Tl–N(3)	2.587(3)	B–N(2)	1.547(4)
B–N(4)	1.561(5)	B–N(6)	1.513(5)
B–N(8)	1.524(5)		
O(1)–Tl–N(1)	74.78(8)	O(1)–Tl–N(3)	83.30(9)
N(1)–Tl–N(3)	75.72(9)	N(2)–B–N(4)	113.2(3)
N(2)–B–N(6)	109.1(3)	N(2)–B–N(8)	107.3(3)
N(4)–B–N(6)	107.7(3)	N(4)–B–N(8)	108.5(3)
N(6)–B–N(8)	111.1(3)		

This unusual κ^3-N_2,O coordination behaviour may be attributed to steric interactions between the fourth pyrazolyl unit and the 5-H substituents of the other pyrazolyl rings (Figure 5.17).

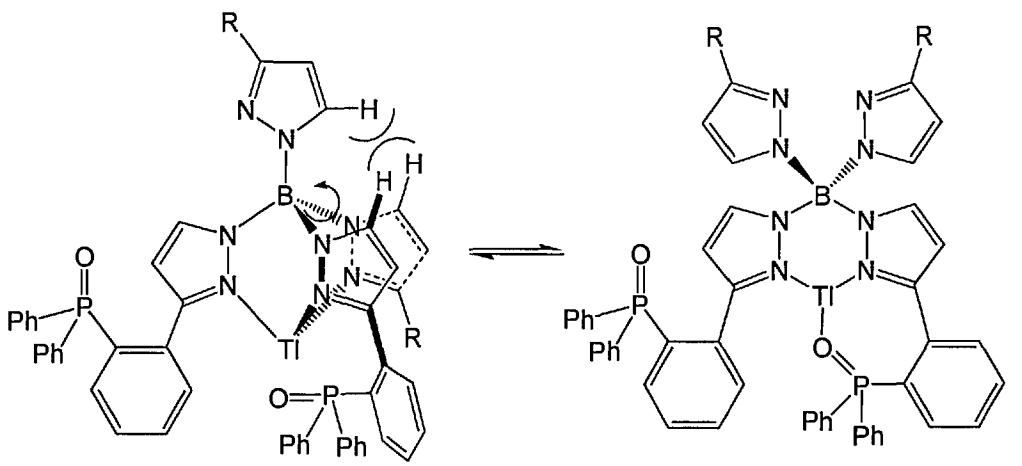


Figure 5.17. Steric clash (left) resulting in an unusual bonding mode (right) in $Tl[T_kp^{phos(O)}]$ (**5.7**). R = 2-($POPh_2$)Ph.

These interactions can be minimised by rotation of one of the B–N bonds which, in turn, impedes coordination of that pyrazolyl unit. In this case, the thallium may still achieve coordinative saturation by bonding to one of the phosphine oxide moieties which has been brought into close proximity to the metal as a consequence of coordination of the remaining pyrazolyl units. Interchange of the coordinating ligand

arms is proposed to occur rapidly in solution as the non-coordinating and coordinating arms are indistinguishable on the room temperature ^{1}H and $^{31}P\{^{1}H\}$ NMR spectra.

5.4.3 Synthesis of Cu[$T_kp^{phos(O)}$]CO (5.8)

The reactivity of the $T_kp^{phos(O)}$ ligand towards copper(I) carbonyls was examined by reaction of **5.6** with CuCl under an atmosphere of CO as shown in Figure 5.18.

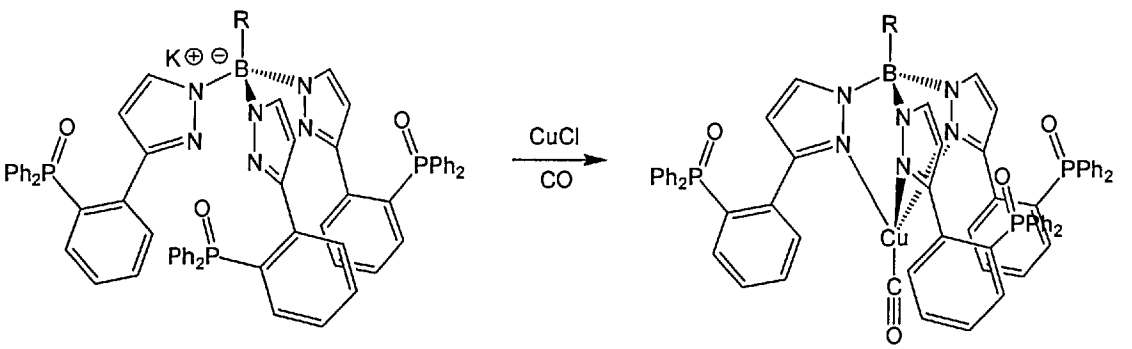


Figure 5.18. Synthesis of Cu[$T_kp^{phos(O)}$]CO (**5.8**). R = 2-($POPh_2$)Ph.

Upon addition of the DCM solvent to the solid reagents, a pale green solution was formed. After stirring for 30 minutes a pale precipitate, presumed to be KCl, had formed. The first indication of the formation of the desired carbonyl was provided by solution IR spectroscopy which showed a sharp stretch at 2083 cm^{-1}. Filtration under an atmosphere of CO followed by removal of the solvent under vacuum gave a faint green solid. Solid-state IR spectroscopy revealed a strong absorption at 2075 cm^{-1} indicating that the Cu–CO bond had remained intact during the application of the vacuum. This is in contrast to the Cu[Tp^{py}]CO species (**5.3**) which was found to reversibly undergo decarbonylation upon application of a vacuum.

Mass spectrometry did not show the presence of the carbonyl, most likely as a result of decarbonylation within the spectrometer. The most intense peak was found at 1447 m/z corresponding to Cu[$T_kp^{phos(O)}$]$^{+}$. ^{1}H, ^{11}B and $^{31}P\{^{1}H\}$ NMR spectra were recorded for this sample and are summarised in Table 5.5. The $^{31}P\{^{1}H\}$ NMR spectrum shows a singlet at 31.0 ppm, virtually identical to the starting material **5.6**. This indicates that the phosphine oxide moiety is not interacting with the copper(I) centre in solution as a downfield shift would be observed. The non-coordinating

nature of these P=O units is expected as the carbonyl ligand occupies the fourth coordination site of the copper. In the ^{1}H NMR spectrum, the 5-pz proton at 6.92 ppm is most significantly shifted upon formation of the copper carbonyl compared to the starting material at 6.49 ppm. This downfield shift is most likely caused by the coordination of the pyrazolyl donors causing the electron density in the ring system to be reduced. As with the thallium complex **5.7**, rapid interchange of the coordinating arms is predicted to occur in solution such that the non-coordinating arm and the coordinating arms are indistinguishable on the NMR timescale.

5.4.4 Synthesis of [Eu($T_kp^{phos(O)}$)NO_3][NO_3] (5.9)

The $T_kp^{phos(O)}$ ligand is a potential N_3,O_3 donor consisting of three bidentate N,O arms (excluding the fourth pyrazolyl arm which cannot coordinate at the same centre due to structural rigidity). In an attempt to achieve full κ^6 chelation it was decided to examine the coordination chemistry of this ligand towards lanthanide ions due to their comparable size to the ligand cavity. Given that lanthanide ions have a high affinity towards hard donors like oxygen and are capable of high coordination numbers, it was envisaged that chelation of the ligand could be achieved.

The reaction of K[$T_kp^{phos(O)}$] (**5.6**) with one equivalent of $Eu(NO_3)_3.5H_2O$ was performed as shown in Figure 5.19. Although europium can accommodate high coordination numbers, it was not known whether the nitrate anions would coordinate directly to the metal because of the bulky nature of the ligand and the large size of the potential chelate rings (seven-membered).

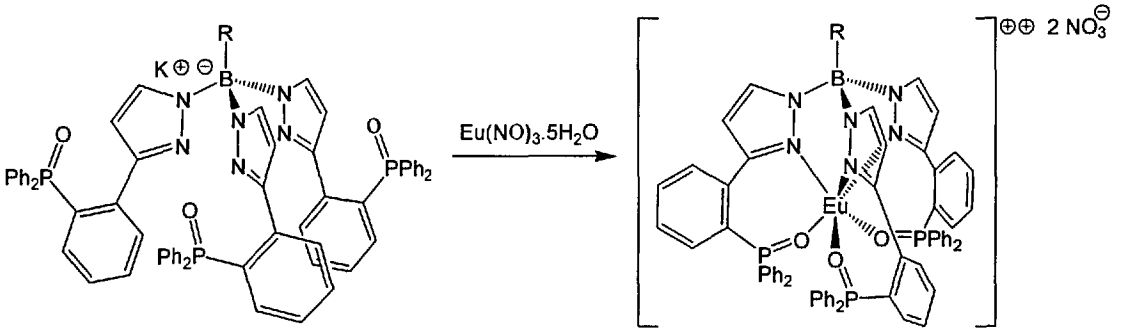


Figure 5.19. Synthesis of Eu[$T_kp^{phos(O)}$](NO_3)$_2$ (**5.9**). R = 2-($POPh_2$)Ph.

Performing this reaction in the minimum amount of methanol yielded a clear solution, which did not result in any precipitation of product after continued stirring, perhaps as a result of the non-coordinating ligand arm imparting increased solubility. $^{31}P\{^{1}H\}$ NMR spectroscopy of the reaction solution showed a major species at 34.2 ppm and a minor species at 31.6 ppm (*cf.* **5.6** at 30.9 ppm); the former was tentatively ascribed as the resonance of the three coordinated bidentate N,O arms and the latter from the fourth uncoordinated arm, pointing away from the metal. Complexation was supported by ESI mass spectrometry (m/z = 1581) which suggested the formation of an Eu : T_kp : NO_3 complex in a 1 : 1 : 1 ratio ($[Eu(T_kp^{phos(O)})NO_2]^+$ = 1581). The product (**5.9**) was isolated as a white powder by extraction into CH_2Cl_2, filtration through celite and concentration to dryness. The paramagnetic nature of the europium(III) centre causes significant broadening in the ^{1}H NMR spectrum making this technique of little diagnostic value.

Single crystals suitable for X-ray analysis were obtained by slow diffusion of pentane vapour into a chloroform solution of **5.9**. The crystal structure of this species (Figure 5.20) shows that the europium is eight-coordinate as a consequence of binding to the hexadentate N_3,O_3 podand and one bidentate nitrate group. This results in a cationic species, $[Eu(T_kp^{phos(O)})NO_3]^+$, with the charge balanced by a non-coordinating nitrate anion. This is in contrast to the europium complex of the hexadentate N_6 donor, $Tp^{py},^{2}$ which is able to accommodate the hexadentate ligand and both nitrates to form a neutrally charged 10-coordinate species. The reason for the difference lies in the size of the chelate rings which are five-membered in $[Eu(Tp^{py})(NO_3)_2]$ (with *N,N'* bite angles of *ca.* 62.2°), and seven-membered here in $[Eu(T_kp^{phos(O)})NO_3]^+$ (with *N,O* bite angles of *ca.* 72.9°), and thus the space remaining for nitrate coordination is reduced in $[Eu(T_kp^{phos(O)})NO_3]^+$ *cf.* $[Eu(Tp^{py})(NO_3)_2]$. Selected bond lengths and angles for **5.9** are shown in Table 5.4.

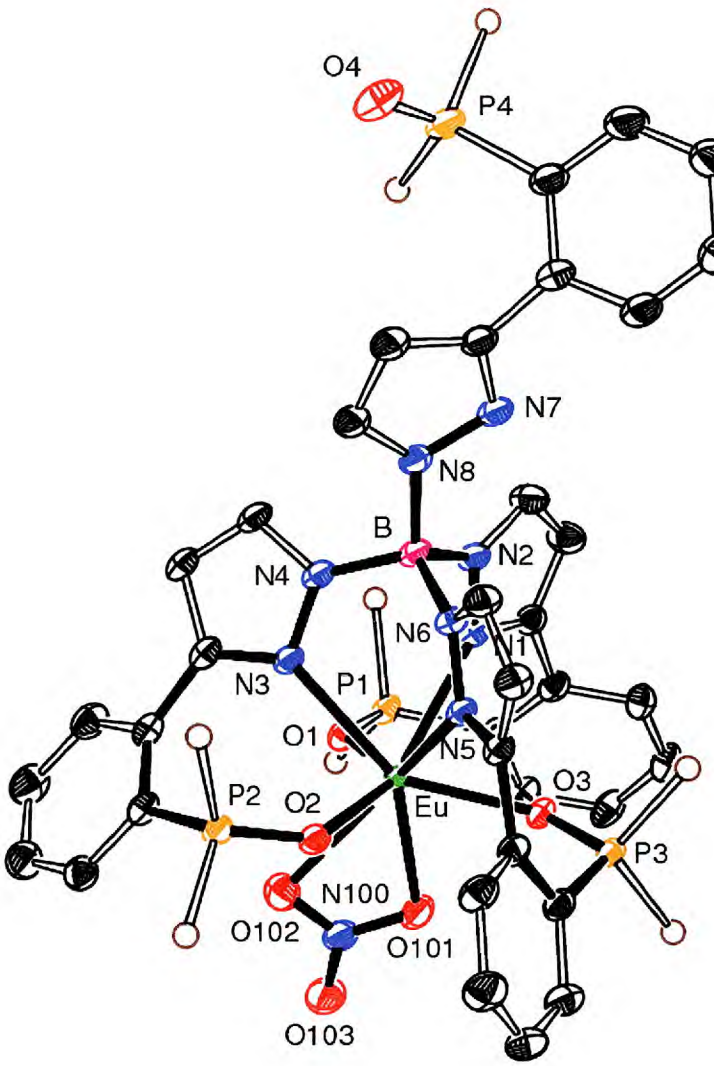


Figure 5.20. Molecular structure of $[Eu(T_kp^{phos(O)})NO_3][NO_3]$ (**5.9**) (30 % probability ellipsoids). Phenyl groups are represented as points for clarity.

Table 5.4. Selected bond lengths (Å) and angles (°) for $[Eu(T_kp^{phos(O)})NO_3][NO_3]$ (**5.9**)

Eu–O(1)	2.303(2)	Eu–O(2)	2.299(2)
Eu–O(3)	2.2710(19)	Eu–N(1)	2.608(2)
Eu–N(3)	2.529(2)	Eu–N(5)	2.546(2)
Eu–O(101)	2.442(2)	Eu–O(102)	2.664(3)
O(1)–Eu–O(2)	126.32(7)	O(1)–Eu–O(3)	116.45(7)
O(1)–Eu–N(1)	72.79(8)	O(1)–Eu–N(3)	79.81(7)
O(1)–Eu–N(5)	139.99(7)	O(2)–Eu–O(3)	113.58(7)
O(2)–Eu–N(1)	139.12(7)	O(2)–Eu–N(3)	73.34(7)
O(2)–Eu–N(5)	73.40(7)	O(3)–Eu–N(1)	75.96(7)
O(3)–Eu–N(3)	141.16(8)	O(3)–Eu–N(5)	72.55(7)
N(1)–Eu–N(3)	76.19(7)	N(1)–Eu–N(5)	72.26(7)
N(3)–Eu–N(5)	73.51(7)		

5.4.5 Summary

A new N,O donor scorpionate ligand, $T_kp^{phos(O)}$, bearing phosphine oxide donor groups appended to the 3-position of the T_kp core has been synthesised and structurally characterised in coordination to Tl(I) and Eu(III). In coordination with thallium an unexpected κ^3-N_2,O species was isolated while complete κ^6-N_3,O_3 chelation was achieved by coordination to europium. Formation of the copper carbonyl complex was successful although reversible decarbonylation was not observed. ^1H, $^{31}P\{^1H\}$ and ^{11}B NMR spectroscopic data for the pyrazole, $Hpz^{phos(O)}$ (**4.3**), and the complexes of $T_kp^{phos(O)}$ are summarised in Table 5.5. The same numbering scheme used to describe the T_kp^{phos} complexes (Figure 5.14) is applied here. Values of coupling constants are provided in the experimental section (Chapter 7).

Table 5.5. Selected ^1H, ^{11}B and $^{31}P\{^1H\}$ NMR data for **4.3** and **5.6 - 5.9**

Compound	$^{31}P\{^1H\}$ NMR[a] δ/ppm	^{11}B NMR[a] δ/ppm	^1H NMR[a] δ/ppm						
	P	*B*	*5-pz*	*4-pz*	*3-Ph*	*4-Ph*	*5-Ph*	*6-Ph*	*Ph-H*
4.3 $Hpz^{phos(O)}$	35.8 (s)	—	7.32 (d)	6.25 (br s)	7.14 (ddd)	7.30 (m)	overlap with Ph-H at 7.61	7.78 (ddd)	7.38-7.64
5.6 $K[T_kp^{phos(O)}]$	30.9 (s)	0.7 (s)	6.49 (d)	6.03 (d)	7.19 (dd)	7.27 (m)	7.55 (d)	7.68 (dd)	7.62, 7.43 & 7.33
5.7 $Tl[T_kp^{phos(O)}]$	30.3 (s)	0.3 (s)	6.87 (s)	5.98 (s)	7.20 – 7.30 (m)		overlap with Ph-H at 7.57	8.00 (dd)	7.65, 7.57 & 7.40
5.8 $Cu[T_kp^{phos(O)}]$ CO	31.0 (s)	0.4 (s)	6.92 (s)	6.07 (s)	overlap with Ph-H at 7.34		overlap with Ph-H at 7.63	7.89 (m)	7.63, 7.49 & 7.34
5.9 $[Eu(T_kp^{phos(O)})NO_3][NO_3]$	37.1 (s), -11.3 (s)	-12.9 (s)	—[b]						

(a) Recorded in $CDCl_3$ solution at 298 K; (b) paramagnetically broadened.

5.5 Phosphine Sulphide-Appended $T_k$ps

5.5.1 Synthesis of K[$T_k p^{phos(S)}$] (5.10)

Following the successful formation of the phosphine oxide-appended T_kp ligand, the synthesis of the phosphine sulphide-appended T_kp was subsequently investigated. Here, the reaction of potassium borohydride with an excess of $Hpz^{phos(S)}$ (**4.4**) was performed according to the equation in Figure 5.21.

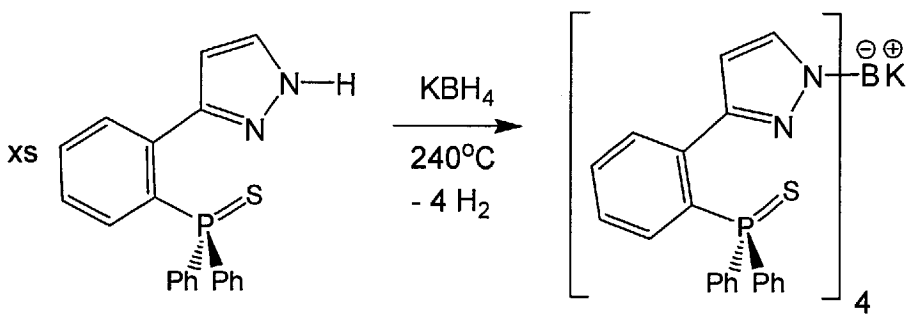


Figure 5.21. Synthesis of phosphine oxide-appended scorpionate ligand K[$T_k p^{phos(S)}$] (**5.10**).

This melt reaction yielded a hard yellow solid to which ethanol was added in an attempt to dissolve the solid before purification. It was found that the pyrazole, which had sublimed around the walls of the flask, dissolved in the ethanol while an off white solid remained undissolved. This crude product was collected by filtration and in good yield (87 %) and recrystallised from boiling ethanol in poorer yield (43 %) due to insufficient precipitation despite prolonged cooling. ESI mass spectrometry confirmed the presence of the desired anion at 1447 m/z with no evidence of the corresponding Bp or Tp species.

^{1}H, ^{11}B and ^{31}P{^{1}H} NMR spectra were recorded for this sample and are summarised in Table 5.6. The ^{11}B NMR spectrum shows a singlet at 0.6 ppm confirming the presence of the T_kp species. ^{1}H NMR spectroscopy followed the same trends in T_kp formation as **5.4** and **5.6**, in that the 5-pyrazolyl proton moves upfield relative to the pyrazole starting material. The ^{31}P{^{1}H} chemical shift (43.3 ppm) is identical to the metal-free pyrazole starting material. This contrasts with the *ca.* 5 ppm upfield shift upon T_kp formation in **5.6**. This difference might be caused by the less electronegative

sulphur atom which is less able to attract the electron density towards the phosphine moiety.

5.5.2 Synthesis of Tl[$T_kp^{phos(S)}$] (5.11)

The potassium salt was converted into the corresponding thallium complex, K[$T_kp^{phos(S)}$] (**5.11**), by reaction with thallous nitrate. This reaction proceeded in moderate yield (61 %) to give a white powder which was characterised by ^1H, ^{11}B and $^{31}P\{^1H\}$ NMR spectroscopy (Table 5.6) and elemental analysis. As with the corresponding $T_kp^{phos(O)}$ species, the ^{31}P resonance is barely shifted with respect to the starting material and no coupling to thallium is evident, suggesting that the P=S moieties are not involved in coordination to the thallium centre in solution. The solid state structure of this species was sought for comparison to the unusual N_2,O coordination mode of $T_kp^{phos(O)}$ in **5.7**. However, attempts to obtain single crystals for X-ray analysis were unsuccessful with powders being formed.

5.5.3 Summary

A new ligand, $T_kp^{phos(S)}$, bearing phosphine sulphide donor groups appended to the 3-position of the T_kp core has been synthesised and characterised in coordination with K^+ and Tl^+ ions. ^1H, $^{31}P\{^1H\}$ and ^{11}B NMR spectroscopic data for the pyrazole, $Hpz^{phos(S)}$ (**4.4**), and the complexes of $T_kp^{phos(S)}$ are summarised in Table 5.6. The same numbering scheme used to describe the T_kp^{phos} and $T_kp^{phos(O)}$ complexes (Figure 5.14) is applied here. Values of coupling constants are provided in the experimental section (Chapter 7).

Table 5.6. Selected ^{1}H, ^{11}B and $^{31}P\{^{1}H\}$ NMR data for **4.4**, **5.10** and **5.11**

Compound	$^{31}P\{^{1}H\}$ NMR[a] δ/ppm	^{11}B NMR[a] δ/ppm	^{1}H NMR[a] δ/ppm						
	P	*B*	*5-pz*	*4-pz*	*3-Ph*	*4-Ph*	*5-Ph*	*6-Ph*	*Ph-H*
4.4 $Hpz^{phos(S)}$	43.3	—	7.17 (d)	6.08 (br s)	7.18 (dd)	7.37 (m)	overlap at 7.57 (m)		7.82 & 7.37-7.44
5.10 $K[T_kp^{phos(S)}]$	43.3	0.6	6.69 (d)	6.00 (d)	7.24 (ddd)	7.27 (m)	7.51 (m)	7.66 (dd)	7.82, 7.42 & 7.36
5.11 $Tl[T_kp^{phos(S)}]$	42.3	0.7	6.65 (d)	6.21 (d)	7.21 (dd)	7.29 (m)	7.54 (dd)	7.71 (dd)	7.81, 7.45 & 7.38

(a) Recorded in $CDCl_3$ solution at 298 K.

5.6 Phosphine-Appended Bulky Pyrazoles

5.6.1 Introduction

The syntheses discussed so far have yielded T_kp ligands due to difficulties in obtaining the preferred Tp species without contamination of the corresponding Bp and T_kp species. However, as discussed in Chapter 2, introduction of a substituent in the 5-pyrazolyl position provides a steric block which prevents the reaction progressing past the tris-pyrazolated stage. As such, it was hoped that by placing a methyl group in the 5-position of the pyrazole ring, the synthesis of a novel phosphine-appended scorpionate ligand 'ScorpoPhos' could be achieved (Figure 5.22). This species is particularly appealing due to its potential applications in homogeneous catalysis.

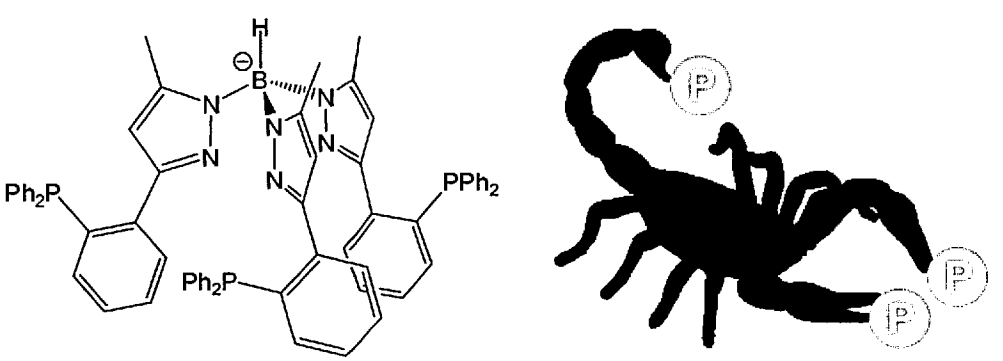


Figure 5.22. Proposed phosphine-appended Tp ligand 'ScorpoPhos'.

5.6.2 Synthesis of Enone (5.12)

Previously the synthesis of the pyrazole-precursor (enone **4.1**) was performed by reaction of 2-diphenylphosphino-acetophenone with dimethylformamide dimethylacetal. It was hoped that the methyl group could be incorporated at this stage by using a methylated derivative of this reagent. This compound, dimethylacetamide dimethylacetal (DMA-DMA), was found to be a commercially available liquid reagent. The reactivity of this species was unknown but it was hoped that the analogous reaction with 2-diphenylphosphino-acetophenone would form the methylated pyrazole-precursor as shown in Figure 5.23. Due to the increased cost of this reagent, this reaction was performed using a slight excess of DMA-DMA dissolved in toluene, rather than using a large excess as both reagent and solvent.

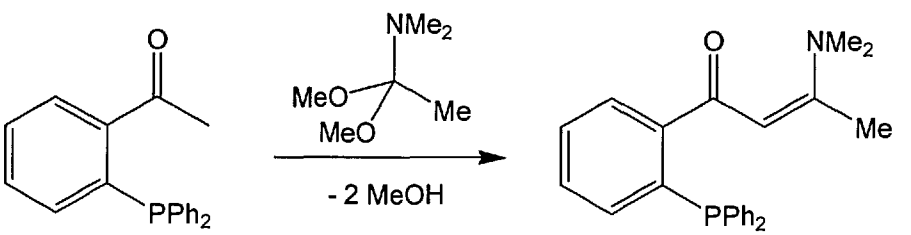


Figure 5.23. Synthesis of pyrazole-precursor (**5.12**).

$^{31}P\{^{1}H\}$ NMR was used to follow the progress of this reaction and it was found that after two days heating at 110°C, the peak corresponding to the starting material at -2.6 ppm had been replaced by a peak at -11.6 ppm. This was presumed to be the desired product as its chemical shift closely resembles that of the related species **4.1** which occurs at -10.3 ppm. This product (**5.12**) was isolated as a red powder and ESI mass spectrometry confirmed the presence of the desired molecular ion at 374 m/z. The purity was further confirmed by ^{1}H, $^{31}P\{^{1}H\}$ and $^{13}C\{^{1}H\}$NMR spectroscopy and elemental analysis. The NMR data are summarised in Figure 5.24 and Table 5.7.

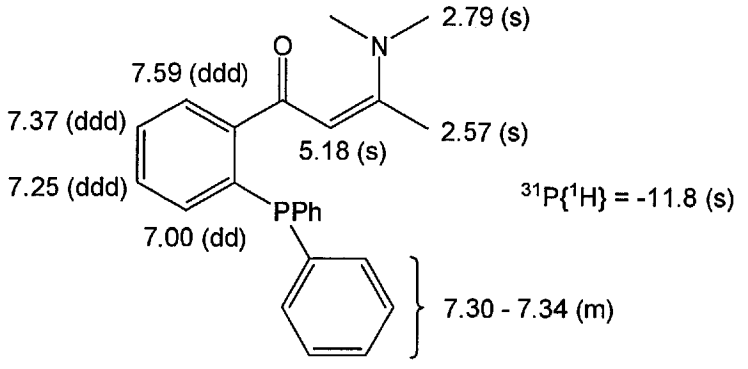


Figure 5.24. ^{1}H and ^{31}P chemical shifts for **5.12** (all values in ppm).

5.6.3 Synthesis of $Hpz^{phos,Me}$ (5.13)

Reaction of **5.12** with an excess of hydrazine hydrate was performed in order to form the desired pyrazole (**5.13**) as shown in Figure 5.25. This reaction was performed by refluxing in ethanol, under an atmosphere of nitrogen for two hours.

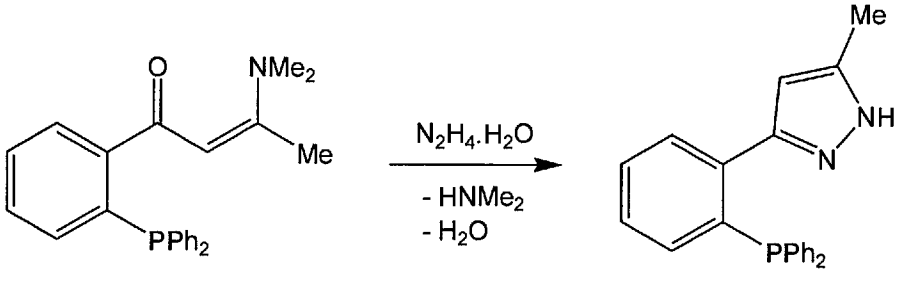


Figure 5.25. Synthesis of pyrazole, $Hpz^{phos,Me}$ (**5.13**).

This reaction proved successful, with the product being isolated as a pure solid in good yield (88 %) after flash chromatography. ESI mass spectrometry confirmed the presence of the desired molecular ion at 343 m/z. ^{1}H, $^{13}C\{^{1}H\}$ and $^{31}P\{^{1}H\}$ NMR spectra were recorded and full assignments have been made. These are summarised in Table 5.7. Notably, on formation of the pyrazole, a broad singlet at 10.31 ppm appears in the ^{1}H NMR spectrum due to the NH proton. The 4-pyrazolyl proton is found characteristically upfield of all the other aromatic protons at 6.09 ppm, while the methyl group is observed at 2.24 ppm.

5.6.4 Synthesis of $Hpz^{phos(O),Me}$ (5.14)

The corresponding phosphine oxide species (**5.14**) was synthesised by performing the above reaction in air with an extended reaction time of 12 hours (Figure 5.26).

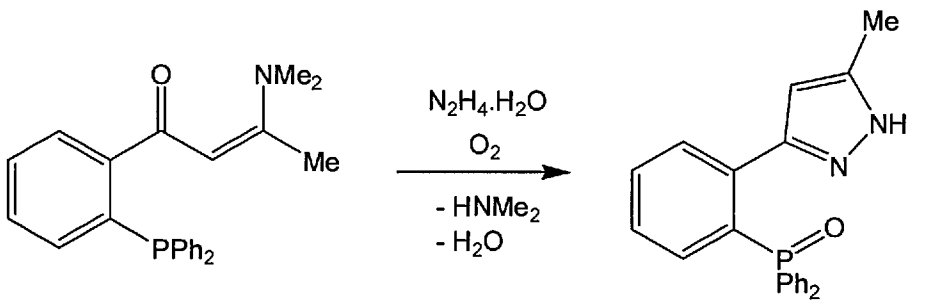


Figure 5.26. Synthesis of pyrazole, $Hpz^{phos(O),Me}$ (**5.14**).

An off-white solid was collected in 78 % yield and $^{31}P\{^{1}H\}$ NMR spectroscopy showed no trace of **5.13**, with a sharp singlet being observed at 35.6 ppm. This closely resembles the chemical shift of the corresponding non-methylated species, **4.3**, which occurs at 35.8 ppm. This was confirmed as the desired phosphine oxide by ESI mass spectrometry (m/z = 359) and found to be pure based on ^{1}H and $^{13}C\{^{1}H\}$ NMR spectroscopy and elemental analysis. ^{1}H and $^{31}P\{^{1}H\}$ chemical shifts are summarised in Table 5.7. Here in **5.14** the NH proton is found further downfield than in **5.13**, possibly as a result of inter- or intra-molecular hydrogen bonding between the NH proton and the oxygen lone pair on the P=O unit.

5.6.5 Summary

Two new 3,5-disubstituted pyrazoles bearing a methyl substituent and either a triphenylphosphine or triphenylphosphine oxide moiety attached to the pyrazole ring have been successfully synthesised in two steps from 2-diphenylphosphino acetophenone. These pyrazoles open up the possibility of forming new donor-appended Tp ligands. ^{1}H and $^{31}P\{^{1}H\}$ NMR and IR spectroscopic data for the enone **5.12** and the pyrazoles, **5.13** and **5.14**, are summarised in Table 5.7. Values of coupling constants are provided in the experimental section (Chapter 7).

Table 5.7. Selected ^{1}H and $^{31}P\{^{1}H\}$ NMR data for **5.12 - 5.14**

Compound	$^{31}P\{^{1}H\}$ NMR[a] δ/ppm	^{1}H NMR[a] δ/ppm								IR[b] ν/cm^{-1}
	P	*NH*	*Me*	*4-pz*	*3-Ph*	*4-Ph*	*5-Ph*	*6-Ph*	*Ph-H*	*NH*
5.12 enone	-11.8 (s)	—	2.57 (s)	—	7.00 (dd)	7.25 (ddd)	7.37 (ddd)	7.59 (ddd)	7.30 – 7.34	—
5.13 $Hpz^{phos,Me}$	-11.7 (s)	10.31 (s)	2.24 (s)	6.09 (s)	7.03 (dd)	overlap with Ph-H	7.40 (ddd)	7.59 (dd)	7.25 – 7.38	3051
5.14 $Hpz^{phos(O),Me}$	35.6 (s)	12.88 (s)	2.15 (s)	6.04 (s)	7.15 (dd)	7.29 (m)	overlap with Ph-H	7.71 (dd)	7.58 – 7.68, 7.53 & 7.43	3205

(a) Recorded in $CDCl_3$ solution at 298 K; (b) Recorded as KBr disc.

5.7 Phosphine-Appended Tps

5.7.1 Synthesis of K[Tp^{phos,Me}] (5.15)

Conversion of $Hpz^{phos,Me}$ (**5.13**) into the corresponding Tp ligand was carried out by reaction of **5.13** with potassium borohydride as shown in Figure 5.27. This reaction was performed by heating the melt at 220°C for five hours.

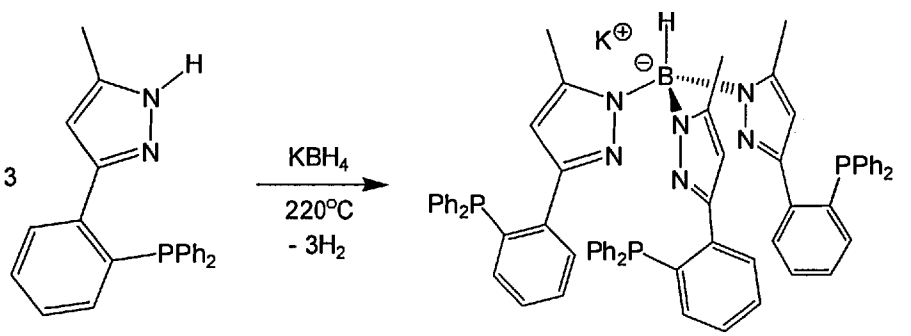


Figure 5.27. Synthesis of phosphine-appended scorpionate ligand K[Tp^{phos,Me}] (**5.15**).

The product, potassium tris(3-[2-(diphenylphosphino)phenyl] 5-methyl pyrazolyl) borate, K[Tp^{phos,Me}] (**5.15**) was obtained in reasonable yield (64 %) after recrystallisation from DCM/hexane. Evidence of the formation of the desired species was provided by negative ion ESI mass spectrometry in which the [Tp^{phos,Me}]$^-$ ion was observed at 1035 m/z and further characterised by ^{1}H, $^{31}P\{^{1}H\}$, $^{11}B\{^{1}H\}$, $^{13}C\{^{1}H\}$ NMR and IR spectroscopy. Selected NMR data for **5.15** are summarised in Table 5.11. Upon formation of the Tp ligand, the methyl resonance moves slightly upfield

relative to the starting material (**5.13**). The $^{31}P\{^{1}H\}$ NMR spectrum suggests that the phosphine units are not involved in coordination to the potassium ion in solution as the chemical shift is identical to that of the metal-free pyrazole starting material at -11.7 ppm.

Unlike the phosphine-appended T_kp ligand (**5.4**) discussed previously, it was pleasing to find that this material could be purified in good yield by a simple recrystallisation. This $Tp^{phos,Me}$ ligand contains three potentially bidentate N,P donor arms and its reactivity towards copper was explored to see if CO binding would occur. Further studies were performed in order to explore the coordination chemistry of this ligand towards a range of metals varying in size, coordination number and acceptor properties.

5.7.2 Synthesis of Tl[$Tp^{phos,Me}$] (5.16)

In an attempt to structurally characterise the $Tp^{phos,Me}$ ligand, the corresponding thallium complex was synthesised via an equimolar reaction of **5.15** with thallous nitrate. This reaction proceeded cleanly and in good yield (70 %) and crystals suitable for X-ray analysis were obtained by slow evaporation of an acetone solution.

The solid-state structure of **5.16** revealed the presence of five crystallographically independent complexes of the same formula, one of which (**5.16-A**) is shown in Figure 5.28 (see Appendix - Chapter 8 for details of the others).

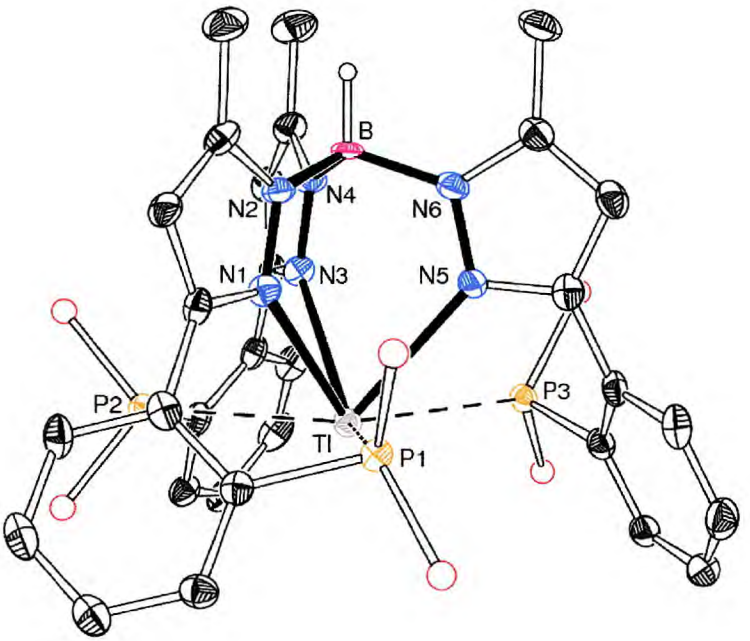


Figure 5.28. Molecular structure of **5.16-A**, one of the five crystallographically independent complexes present in the crystals of **5.16** (30 % probability ellipsoids). Phenyl groups are represented as points for clarity.

In each case the metal centre is encapsulated in an approximately C_3 symmetric manner by all six available donor atoms with Tl–N and Tl–P distances of *ca.* 2.64 and 3.29 Å respectively (Table 5.8). In each complex the metal lies in the plane of the three phosphorus atoms, the mean deviation across the five complexes being ca. 0.12 Å. The Tl–P interactions at *ca.* 3.29 Å are beyond the length of a formal coordination bond. They most likely result from coordination of the N_3 pyazolyl array which is able to satisfy the coordination requirements of the thallium centre. In doing so, the phosphine arms are brought into close proximity of the metal whereupon they can weakly coordinate at the remaining vacant sites in order to confer increased stability upon the complex.

Table 5.8. Selected bond lengths (Å) and angles (°) for **5.16-A**.

Tl–N(1)	2.643(3)	Tl–N(3)	2.678(3)
Tl–N(5)	2.637(3)	Tl–P(1)	3.2274(9)
Tl–P(2)	3.2122(9)	Tl–P(3)	3.2488(9)
Tl···B	3.812(4)	Tl···[N_3] (a)	1.988
N(1)–Tl–N(3)	68.87(9)	N(1)–Tl–N(5)	70.03(9)
N(3)–Tl–N(5)	71.00(10)		

(a) This is the deviation of the thallium centre from the plane of the three coordinated nitrogen atoms.

Despite the length of Tl–P interaction, this contact is also present in solution at room temperature as evidenced by $^{31}P\{^{1}H\}$ NMR spectroscopy (Figure 5.29). Here, coupling of the three equivalent ^{31}P nuclei with ^{203}Tl (I = 1/2, abundance = 30 % γ = 15.54) and ^{205}Tl (I = 1/2, abundance = 70 %, γ = 15.69) produces an overlapping pair of doublets centred at -3.1 ppm (^{1}J = 1253 Hz), suggesting that the thallium remains encapsulated by the podand ligand in solution. The ^{1}H, $^{31}P\{^{1}H\}$ and ^{11}B NMR data for this complex are summarised in Table 5.11.

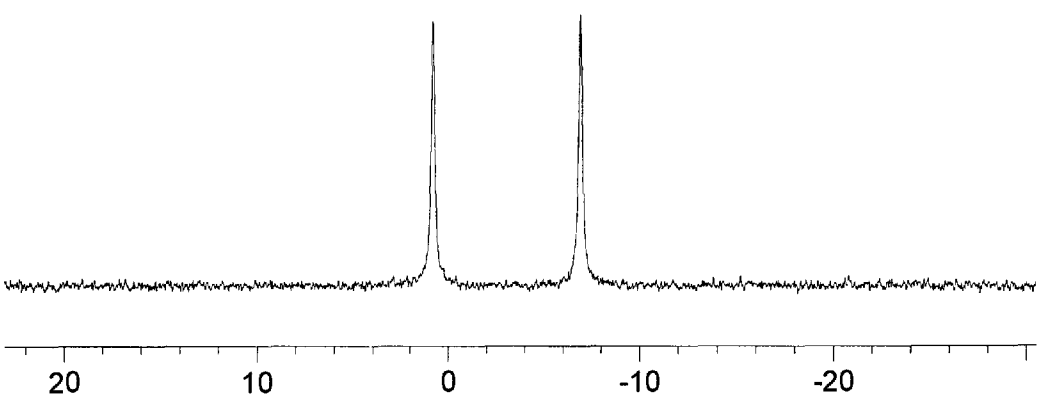


Figure 5.29. $^{31}P\{^{1}H\}$ NMR spectrum of Tl[$Tp^{phos,Me}$] (**5.16**).

There are few examples of thallium(I)-phosphine complexes in the literature due to the mismatch of hard metal and soft donor. Of these species, reported $J_{P\text{-}Tl}$ coupling constants lie in the 4000-6000 Hz range for complexes of the formula Tl[$PhB(CH_2PR_2)_3$][31, 32] and Tl[$Ph_2(CH_2PR_2)_2$],[33] while a Tl[PNP] complex[34] has been reported to display a $J_{P\text{-}Tl}$ coupling constant of 2385 Hz. These resonances are all centred between 20 and 133 ppm. In comparison, the ^{31}P resonance of **5.16** has the lowest coupling constant (1253 Hz) and occurs furthest upfield (-3.1 ppm) of all the P–Tl(I) species. The upfield chemical shift most likely arises as a result of the N_3

pyrazolyl donor array which imparts increased electron density on the thallium, while the low coupling constant is believed to result from the weak nature of the Tl–P interaction similarly observed in the solid state.

5.7.3 Synthesis of Cu[Tp^{phos,Me}] (5.17)

To explore the reactivity of this ligand towards copper and CO, the reaction of K[Tp^{phos,Me}] with CuCl was performed under an atmosphere of CO. Mononuclear copper(I) complexes of Tp ligands are well known (see Chapter 2), with the copper achieving coordinative saturation by binding to the tripodal array of pyrazolyl donors and a second monodentate ligand to form a tetrahedral complex. As discussed previously, phosphine ligands have a greater affinity towards copper than CO, so in the case of Tp^{phos,Me}, it was thought that a single ligand unit might be able to stabilise the copper centre via coordination of the three pyrazolyl units plus coordination of one of the appended phosphine groups (top structure - Figure 5.30). However, this N_3,P bonding mode would require distortion of the tetrahedral copper in order to accommodate the phosphine moiety. As such, preferential coordination of the CO ligand (bottom structure - Figure 5.30) or formation of a bridging species (with or without CO coordination) could not be ruled out.

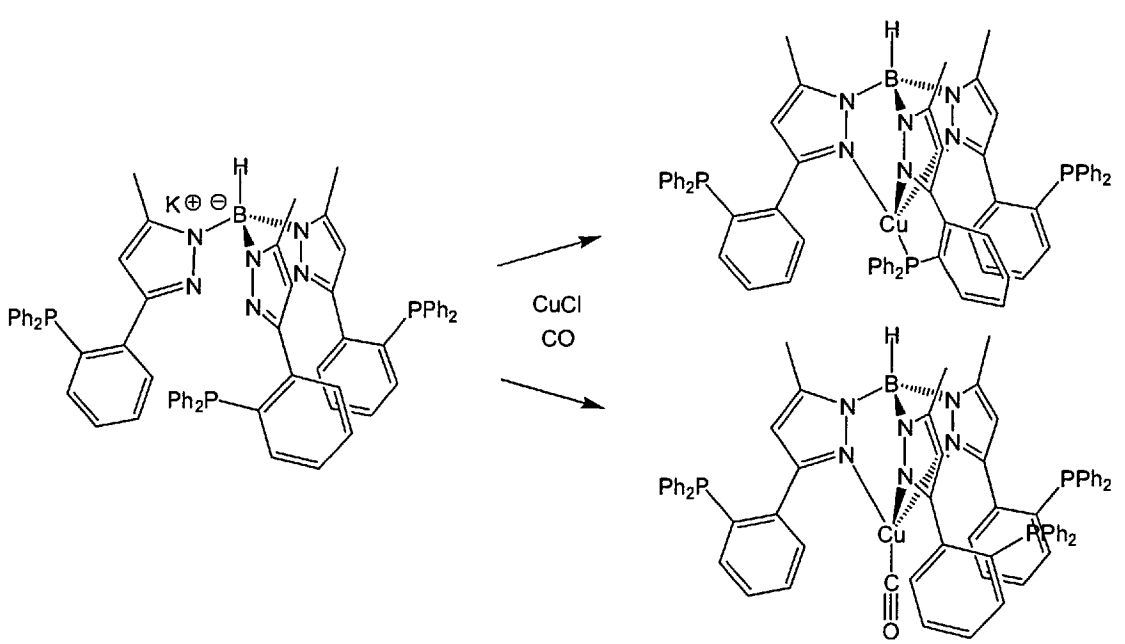


Figure 5.30. Possible products of reaction between **5.15** and CuCl under a CO atmosphere.

Accordingly, the reaction between $K[Tp^{phos,Me}]$ and CuCl was performed in THF under an atmosphere of CO. $^{31}P\{^{1}H\}$ NMR spectroscopy of the resultant yellow solution showed a sharp singlet at -9.0 ppm (*cf.* **5.15** at -11.7 ppm), indicating formation of a new species. Solution IR spectroscopy did not show any signs of a carbonyl absorption in the 2000-2100 cm^{-1} region, suggesting that the carbonyl complex had not formed at all. Subsequent filtration and removal of the solvent gave a faint yellow powder (**5.17**) which ESI(+ve) mass spectrometry showed to contain a species at 1099 m/z, corresponding to $Cu[Tp^{phos,Me}]^{+}$. This ruled out the formation of a multinuclear species but could not be used to discount CO coordination as carbonyl loss has previously been found occur to in the mass spectrometer. Elemental analysis, however, revealed an excellent match with the calculated values for the $Cu[Tp^{phos,Me}]$ adduct, which, in conjunction with the IR data, indicates that the carbonyl was not bound.

The room temperature ^{1}H, ^{11}B and $^{31}P\{^{1}H\}$ NMR data for this complex are summarised in Table 5.11. The downfield shift of the single peak in the $^{31}P\{^{1}H\}$ NMR (-7.4 ppm) relative to the starting material (**5.15** at -11.7 ppm) prompted further studies to probe the solution behaviour of this complex. Variable temperature $^{31}P\{^{1}H\}$ NMR studies were performed upon cooling of a CD_2Cl_2 solution of the complex down to 183 K (Figure 5.31).

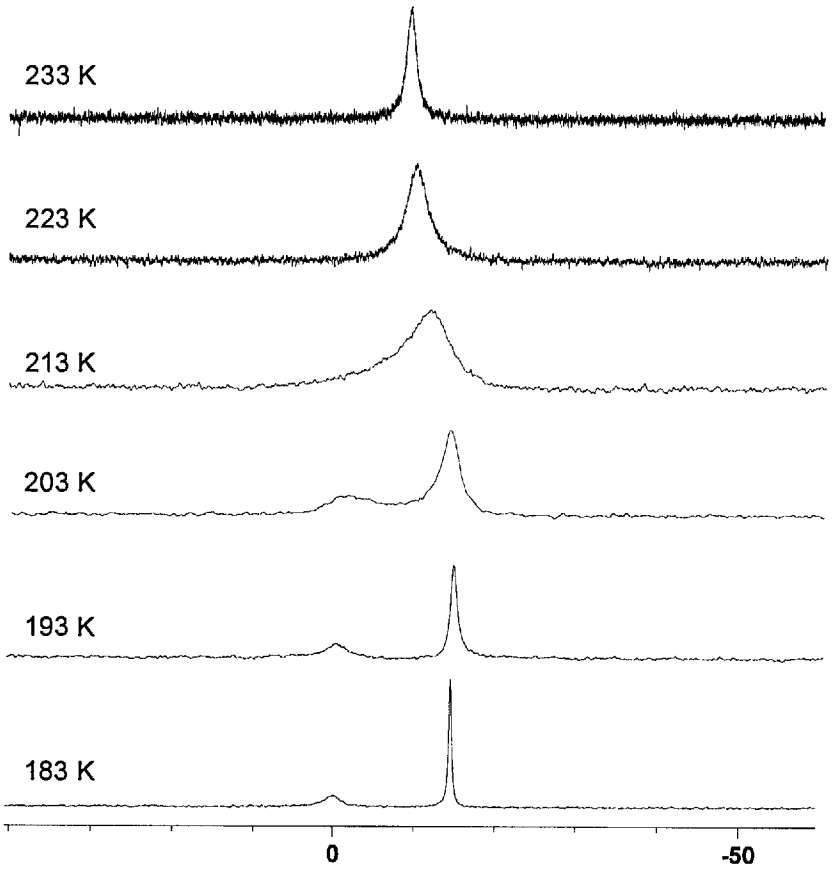


Figure 5.31. Variable temperature $^{31}P\{^{1}H\}$ NMR spectrum of Cu[$Tp^{phos,Me}$] **5.17**.

At approximately 213 K (-60°C) decoalescence of the single peak becomes apparent, and when the temperature is lowered to 183 K (-90°C) two separate peaks are observed at -14.6 ppm and 0.0 ppm with relative intergals of approximately 2 to 1, respectively. The chemical shift and integral of these peaks suggest a mononuclear complex in which the downfield resonance is that of a single copper-bound phosphine moiety, while the upfield resonance is attributed to the two remaining phosphine moieties which are unbound in solution. Due to the approaching freezing point of the solvent (- 95°C), the temperature could not be lowered any further in these studies.

To elucidate the absolute structure of this complex, crystals suitable for X-ray crystallography were obtained by recrystallisation from warm acetone. The resultant crystal structure supports the predicted low temperature solution behaviour. As shown in Figure 5.32, the ligand coordinates in a κ^4-N_3,P fashion via three pyrazolyl donors and one phosphine group with a Cu–P(1) separation of 2.1745(6) Å (*cf. ca.* 3.29 Å in the thallium complex **5.16**) to form a distorted tetrahedron around the copper.

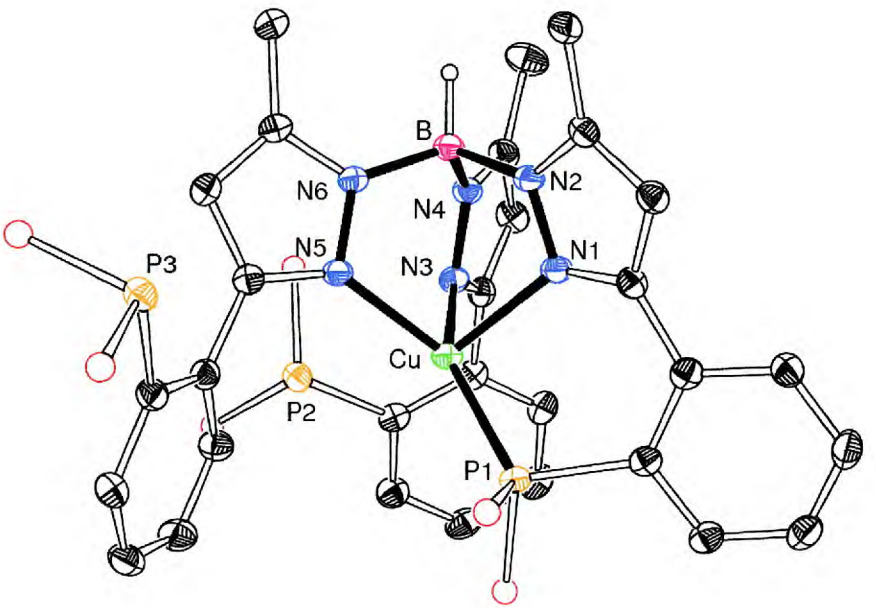


Figure 5.32. Molecular structure of Cu[Tp^{phos,Me}] (**5.17**) (30 % probability ellipsoids). Phenyl groups are represented as points for clarity.

Excluding the PPh_2 units, the rest of the complex retains approximate C_3 symmetry, and the metal is, as expected, much closer to the boron centre [Cu···B 3.025(2) Å *cf. ca.* 3.79 Å for the Tl···B separations in **5.16**]. Chelation of one bidentate arm to the copper forms a favourable six-membered [$CuNC_3P$] ring, with this coordinated phosphorus being observed as the downfield resonance in the low temperature $^{31}P\{^1H\}$ NMR spectrum. At room temperature, however, the phosphine moieties are so rapidly interchanging by random association and dissociation that an average signal is observed on the $^{31}P\{^1H\}$ NMR spectrum. Selected bond lengths and angles for this complex are shown in Table 5.9.

Table 5.9. Selected bond lengths (Å) and angles (°) for Cu[Tp^{phos,Me}] (**5.17**)

Cu–N(1)	2.0987(16)	Cu–N(3)	2.0872(16)
Cu–N(5)	2.0733(16)	Cu–P(1)	2.1745(6)
Cu···P(2)	3.7767(7)	Cu···P(3)	5.7297(7)
Cu···B	3.025(2)	Cu···[N_3] (a)	1.187
N(3)–Cu–N(5)	89.88(6)	N(1)–Cu–N(5)	96.04(6)
N(1)–Cu–N(3)	86.11(6)	N(1)–Cu–P(1)	90.37(5)
N(3)–Cu–P(1)	139.14(5)	N(5)–Cu–P(1)	130.95(5)

(a) This is the deviation of the copper centre from the plane of the three coordinated nitrogen atoms.

5.7.4 Synthesis of [Ru(Tp^{phos,Me})]Cl (5.18)

To further explore the coordination chemistry of the Tp^{phos,Me} ligand, attempts were made to achieve full hexadentate N_3,P_3 coordination with a suitable metal. Ruthenium(II) was chosen as a good candidate as it is known to bind to N,P ligands and is capable of forming N_3,P_3 complexes, for example, by coordination to three bidentate N,P ligands,[35, 36] or a tridentate P_3 ligand and three monodentate N-donors.[37, 38] Ruthenium, being a second row transition element, is larger than the first row element, copper, encountered previously. This larger metal was hoped to allow the podand ligand to bind via all three PPh_2 units with minimal steric encumbrance.

A Tp-ruthenium(II) complex, [TpRuCl(PPh_3)$_2$], has been previously been synthesised by Alcock *et al.*[39] by the reaction of $RuCl_2(PPh_3)_3$ with KTp* in DCM. $RuCl_2(PPh_3)_3$ was not chosen as the starting material for the corresponding reaction of K[Tp^{phos,Me}] (**5.15**) because of fears that the PPh_3 groups would remain coordinated to the ruthenium thus blocking access of the appended $-PPh_2$ units of the Tp^{phos,Me} ligand. Instead, a ruthenium(II) salt containing weakly coordinating ligands was sought in the hope that they would be easily displaced by the competing ligand. $RuCl_2(DMSO)_4$, as reported by Wilkinson *et al.*,[40] was proposed as a suitable starting material as the DMSO ligands are readily displaced by other ligands. The reaction between K[Tp^{phos,Me}] and $RuCl_2(DMSO)_4$ was performed in a 1:1 molar ratio as shown in Figure 5.33.

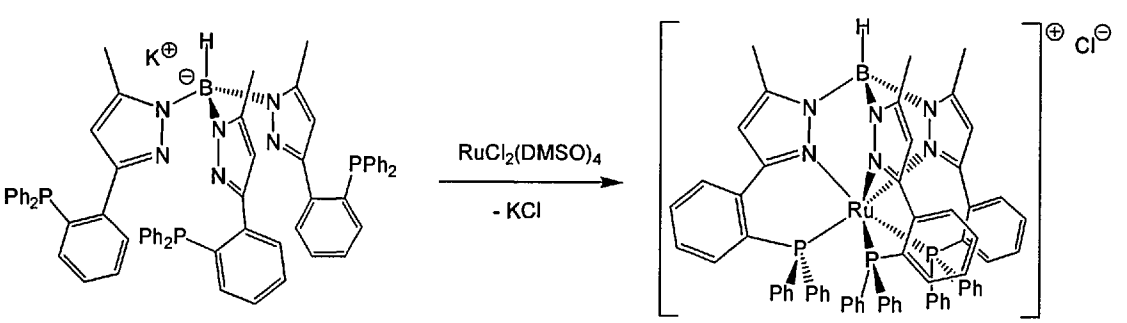


Figure 5.33. Synthesis of Ru[Tp^{phos,Me}]Cl (**5.18**)

This reaction yielded a yellow solid (**5.18**) which was found to be pure by ^{1}H and ^{31}P{^{1}H} NMR spectroscopy (Table 5.11). The methyl group in the 5-pyrazolyl position is found slightly further downfield (2.28 ppm) in this complex compared to

the starting material **5.15** at 2.13 ppm. This follows the trend observed for the previous complexes suggesting the N_3 donor moiety is coordinated to the ruthenium. The $^{31}P\{^1H\}$ NMR spectrum shows a singlet at -11.7 ppm, identical to the starting material (**5.15**), which indicates that the phosphine moieties are not coordinated in solution.

In order to ascertain the solid-state structure of this complex, single crystals were obtained by diffusion of pentane vapour into a chloroform solution and subsequently analysed by X-ray crystallography. The resultant structure (Figure 5.34) reveals that in the solid-state, the $Tp^{phos,Me}$ podand binds in a hexadentate N_3,P_3 fashion to an octahedral ruthenium centre. This results in a monocationic species of which the charge is balanced by one non-coordinating chloride anion. Chelation of each bidentate arm to the ruthenium forms three six-membered [$RuNC_3P$] ring with Ru–N and Ru–P distances of *ca.* 2.11 and 2.35 Å respectively (Table 5.10). Each arm is orientated in the same manner as a result of crystallographic C_3 symmetry.

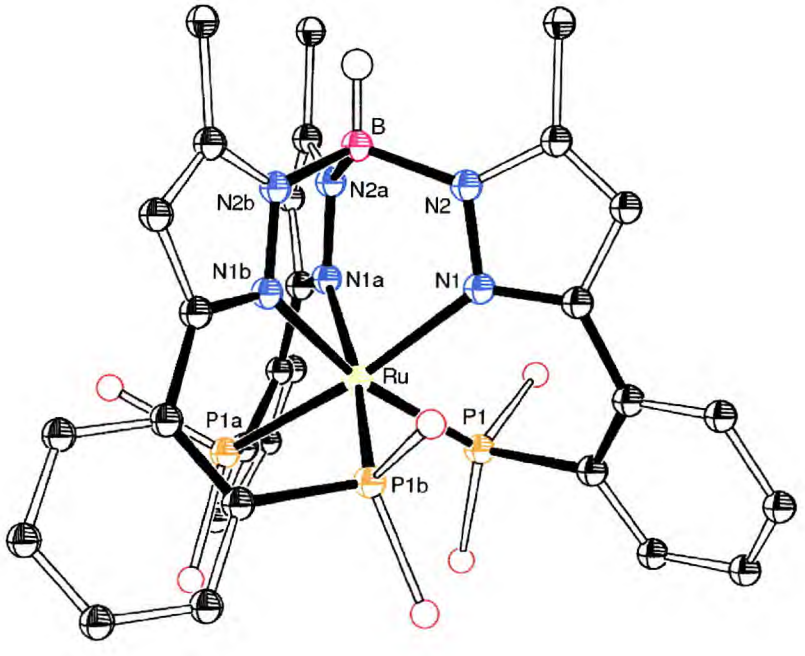


Figure 5.34. Molecular structure of the cation in [Ru($Tp^{phos,Me}$)]Cl (**5.18**). Phenyl groups are represented as points for clarity.

Table 5.10. Selected bond lengths (Å) and angles (°) for [Ru($Tp^{phos,Me}$)]Cl (**5.18**)

Ru–N(1)	2.110(7)	Ru–P(1)	2.351(2)
B–N(2)	1.593(11)	N(1)–N(2)	1.383(11)
Ru··B	3.175	Ru···[N_3] ([a])	1.272
N(1)–Ru–N(1a)	87.4(3)	N(1)–Ru–P(1)	80.1(2)
N(1)–Ru–P(1a)	167.5(2)	N(1)–Ru–P(1b)	92.98(19)
P(1)–Ru–P(1a)	99.42(8)	N(2)–B–N(2a)	109.4(8)

(a) This is the deviation of the ruthenium centre from the plane of the three coordinated nitrogen atoms.

The successful N_3,P_3 chelation of the $Tp^{phos,Me}$ ligand to ruthenium can be compared with the N_3,P bonding mode observed in the copper(I) species. In each case the ligand is able to fulfil the coordination requirements of the metal by coordination of the N_3 moiety plus the required number of phosphine units. This highlights the flexibility and versatility of this ligand in satisfying the specific coordination requirements of the metal.

5.7.5 Synthesis of Zn[$Tp^{phos,Me}$]OAc (5.19)

In order to probe the behaviour of the $Tp^{phos,Me}$ ligand towards a metal which commonly does not display coordination to phosphines, the reaction of K[$Tp^{phos,Me}$] with $Zn(OAc)_2$ was studied. In this case, an acetate anion is expected to coordinate to zinc along with the N_3 donor array of the scorpionate thus forming the complex depicted in Figure 5.35.

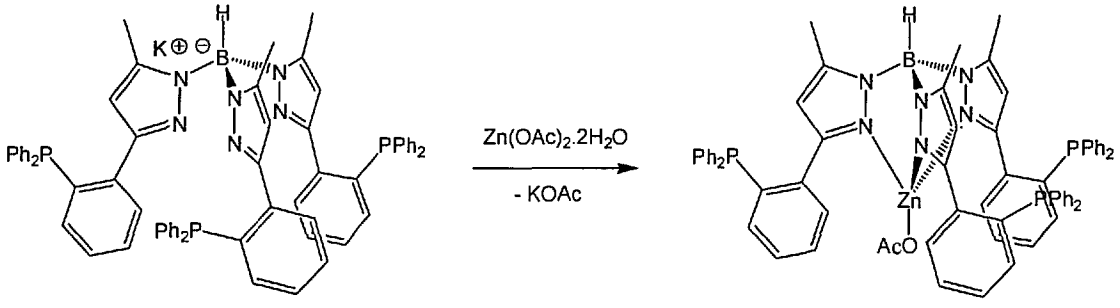


Figure 5.35. Synthesis of Zn[$Tp^{phos,Me}$]OAc (**5.19**)

This reaction yielded a white powder (**5.19**) in good yield (90 %). Elemental analysis revealed an excellent match with the predicted values for a complex of the formula Zn[$Tp^{phos,Me}$]OAc. The ^1H and $^{31}P\{^1H\}$ NMR data are summarised in Table 5.11. The

unshifted ^{31}P resonance upon formation of the zinc complex indicates that the phosphine groups are non-coordinating in solution. The ^{1}H NMR shows a broad singlet corresponding to the methyl group of the acetate ligand at 1.34 ppm.

Although no single crystals were obtained for this complex, the structure can be estimated with reference to the IR spectrum. The behaviour of the acetate moiety can vary between uncoordinated (ionic), unidentate, asymmetrical bidentate and symmetrical bidentate. From the IR spectrum of **5.19**, ν_a(COO) is found at 1630 cm^{-1}, while ν_s(COO) could not be distinguished amongst a series of strong absorptions between 1300 and 1500 cm^{-1}. However, the high value of ν_a(COO) suggests either a unidentate or asymmetric bidentate coordination mode.[41] Furthermore, the related complex, Zn[$Tp^{SMe,Ph}$]OAc, has been structurally characterised and shown to display an asymmetrically bound bidentate acetate anion (see section 5.9.2). This 5-coordinate complex displays a ν_a(COO) of 1636 cm^{-1} suggesting that the same coordination mode may be found in **5.19**.

5.7.6 Summary

A new tris(pyrazolyl)borate ligand bearing phosphine donor groups appended to the 3-position of the pyrazolyl rings has been synthesised and the hemilabile behaviour of this tris-N,P ligand in coordination with K^+, Tl^+ and Cu^+, Ru^{2+} and Zn^{2+} ions has been investigated. The solution behaviour of the phosphine units is conveniently monitored using ^{31}P NMR spectroscopy which can be performed on aliquots of the reaction solution. This allows for observation of the progress of a reaction or to explore the dynamic behaviour of the ligand arms in the isolated complex. ^{1}H, ^{11}B and $^{31}P\{^{1}H\}$ NMR spectroscopic data for the pyrazole **5.13** and the complexes of $Tp^{phos,Me}$ are summarised in Table 5.11. Values of coupling constants are provided in the experimental section (Chapter 7).

Table 5.11. Selected ^{1}H, ^{11}B and $^{31}P\{^{1}H\}$ NMR data for **5.13** and **5.15 - 5.19**

Compound	$^{31}P\{^{1}H\}$ NMR[a] δ/ppm	^{11}B NMR[a] δ/ppm	^{1}H NMR[a] δ/ppm						
	P	*BH*	*Me*	*4-pz*	*3-Ph*	*4-Ph*	*5-Ph*	*6-Ph*	*Ph-H*
5.13 $Hpz^{phos,Me}$	-11.7 (s)	—	2.24 (s)	6.09 (s)	7.03 (dd)	overlap with Ph-H	7.40 (ddd)	7.59 (dd)	7.25 – 7.38
5.15 $K[Tp^{phos,Me}]$	-11.7 (s)	-5.1 (s)[b]	2.13 (s)	6.15 (s)	6.89 (dd)	overlap with Ph-H	7.33 (ddd)	7.72 (dd)	7.10 – 7.20, 7.04 & 6.94
5.16 $Tl[Tp^{phos,Me}]$	-3.1 (d)	-5.1 (s)[b]	2.26 (s)	5.62 (s)	6.82 (m)	overlap with Ph-H		7.54 (m)	7.23, 7.10 – 7.20 & 6.97
5.17 $Cu[Tp^{phos,Me}]$	-7.4 (s)[c]	-5.4 (s-br)[c]	2.31 (s)	5.98 (s)	overlap with Ph-H	7.11 (ddd)	overlap with Ph-H	7.94 (d)	7.18, 7.06 & 6.95
5.18 $Ru[Tp^{phos,Me}]$ Cl	-11.7 (s)	—d	2.28 (s)	6.10 (s)	7.01 (dd)	overlap with Ph-H	7.41 (ddd)	7.57 (dd)	7.28 – 7.38
5.19 $Zn[Tp^{phos,Me}]$ OAc	-11.4 (s)	—d	2.32 (s)	5.75 (s)	6.78 (dd)	overlap with Ph-H at 7.14	overlap with Ph-H at 7.21	7.67 (dd)	7.21, 7.14 & 7.01

(a) Recorded in $CDCl_3$ solution at 298 K; (b) ^{1}H-decoupled spectrum; (c) CD_2Cl_2 solution; (d) not recorded.

Solution and solid-state studies have revealed that the appended phosphine moieties are able to stabilise a metal centre depending on the coordination requirements of the metal employed. With copper, a fluxional process of phosphorus coordination/dissociation at the fourth coordination site of the metal has been identified by variable temperature NMR studies which could provide an opportunity for future substrate binding. It is noteworthy that the competing carbonyl ligand was not able to gain access to the copper centre due to preferred chelation of one phosphine moiety.

Transition-metal catalysed reactions might be successful using this stabilising ligand. For example, $[RuTp(PPh_3)_2Cl]$, catalysed transformations could be similarly explored using the $[Ru(Tp^{phos,Me})]^{+}$ complex (**5.18**). This is discussed in the Future Work section.

5.8 Summary of Scorpionate Chemistry

A range of N, O, S and P donor-appended scorpionates have been synthesised and their coordination chemistry towards a variety of metals has been explored. This has revealed a range of coordination modes in the solid-state including κ^3-N_2,O in $Tl[T_kp^{phos(O)}]$ (**5.7**), κ^6-N_3,O_3 in $[Eu(T_kp^{phos(O)})NO_3]NO_3$ (**5.9**), κ^4-N_3,P in $Cu[Tp^{phos,Me}]$ (**5.17**) and κ^6-N_3,P_3 in $[Ru(Tp^{phos,Me})]Cl$ (**5.18**). In some instances, solution phase behaviour could be monitored using $^{31}P\{^1H\}$ NMR spectroscopy which in the case of $Tl[Tp^{phos,Me}]$ (**5.16**) revealed encapsulation of the thallium ion as evidenced by P-Tl coupling, while fluxional ligand association/dissociation was observed in $Cu[Tp^{phos,Me}]$ (**5.17**).

The reactions of three N, O and P donor-appended scorpionate ligands towards copper and CO has been investigated and shown to display varied behaviour depending on the affinity of the donor group towards copper. The progress of these reactions is summarised in Figure 5.36. It was found that the phosphine oxide-appended scorpionate $T_kp^{phos(O)}$ would undergo carbonylation to form **5.8** which was stable to vacuum decomposition. Conversely the phosphine-appended donor $Tp^{phos,Me}$ would not bond to the carbonyl ligand, preferring to form a chelate complex, **5.17**. The pyridyl-appended scorpionate was found to display intermediate reactivity. In this case the carbonyl complex **5.3** was able to undergo reversible decarbonylation by application of a vacuum/nitrogen cycles.

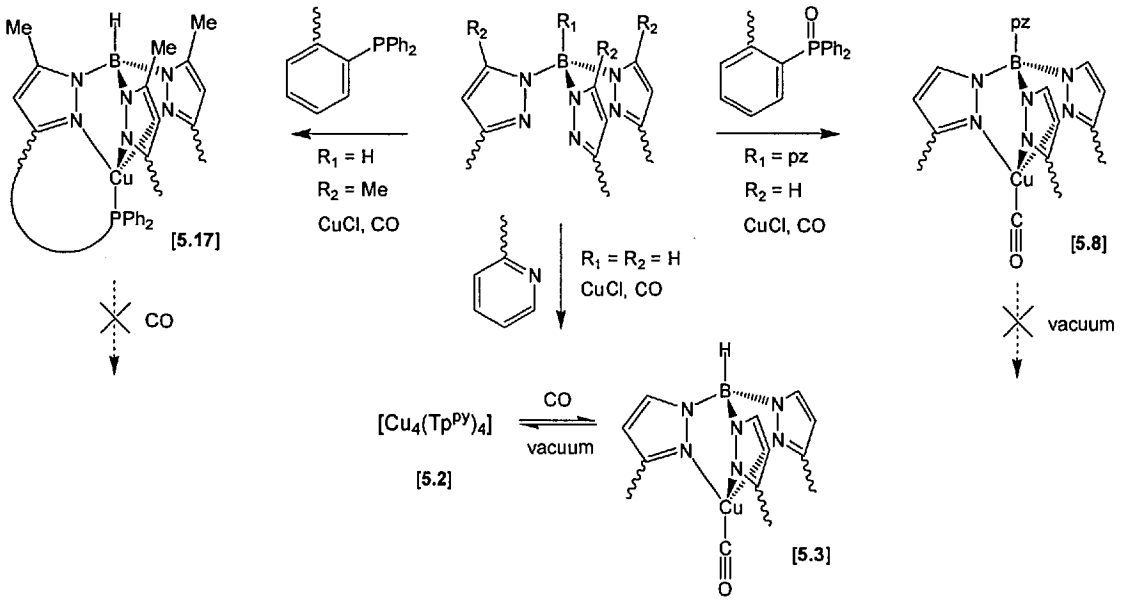


Figure 5.36. Summary of reactions of donor-appended scorpionates with copper and CO.

From these reactions it is now possible to assert that phosphine oxides bind very unfavourably to copper(I) centres and that pyridyl ligands bind slightly less favourably than CO. As such, the ligand affinity scale can be extended as follows: $R_3P{=}O$ < R-C≡N ≈ pyridyl < CO < PR_3. This demonstrates how simple ligand modifications (*e.g.* oxidation of the phosphine moiety) can have a significant impact on the behaviour of the resultant ligand.

5.9 Future Work

5.9.1 Donor Scorpionates in Catalysis

Scorpionate-supported metal complexes have been used to catalyse a range of reactions. Most commonly, scorpionate complexes of rhodium(I) and iridium(I) have been studied for their role in C–H bond activation. Heteroleptic metal complexes containing both a Tp ligand and one or more phosphine ligands have been shown to be catalytically active. For example, the commercially available complex, $[TpRuCl(PPh_3)_2]$[39] (Strem Chemicals), has been used to catalyse the regioselective cyclisation of α,ω-alkynoic acids to yield endocyclic enol lactones,[23] the reaction of terminal alkynes with hydrazines to give nitriles[24] and the dimerisation of terminal alkynes to give disubstituted butenynes.[25] Furthermore, a Tp/PPh_3 supported

rhodium(I) complex, [TpRh(PPh_3)$_2$], has recently been shown to be active in the hydrothiolation of alkynes with aliphatic thiols.[42]

In these catalytic reactions, dissociation of the triphenylphosphine ligand is thought to occur initially to allow substrate binding. In an analogous fashion, dissociation of the phosphine groups in the Tp/phosphine hybrid ligand, $Tp^{phos,Me}$, has been shown to occur at copper in Cu[$Tp^{phos,Me}$] (**5.17**) and is thought to explain the upfield ^{31}P chemical shift in Ru[$Tp^{phos,Me}$]Cl (**5.18**). As such, $Tp^{phos,Me}$ may prove effective as a catalyst for these and similar reactions as it contains PPh_3 moieties tethered to the Tp ligand backbone.

5.9.2 Coordination Chemistry of 'Crowned Scorpionates'

The preceding sections have examined the coordination chemistry of scorpionates containing appended donors attached to the 3-pyrazolyl positions. Conversely, the $Tp^{Ph,SMe}$ ligand introduced in Chapter 2, contains potential donor groups (-SMe) attached to the 5-position of the pyrazolyl rings. Upon coordination of a metal at the tridentate array of pyrazolyl N-donors (as in the CuCO species, **2.12**), the three methylthio groups become arranged in a pseudo-macrocyclic manner. Since the lone pairs point inwards in the solid state it suggests that minimal conformational changes would need to occur for a metal to coordinate here.

This S_3 donor array compares favourably to the 9S3 macrocycle which also adopts an endo-dentate conformation in its free form and does not have to undergo any conformational change upon metal coordination. This is believed to explain its improved reactivity over the 12S3 macrocycle which adopts an exo-dentate conformation in the free form which necessitates substantial rearrangement to permit tridentate ligation.[43] The 'crowned scropionate' $Tp^{Ph,SMe}$ (Figure 5.37) may open up an interesting field of coordination chemistry whereby coordination of a second metal could be achieved at the crown thioether-like moiety.

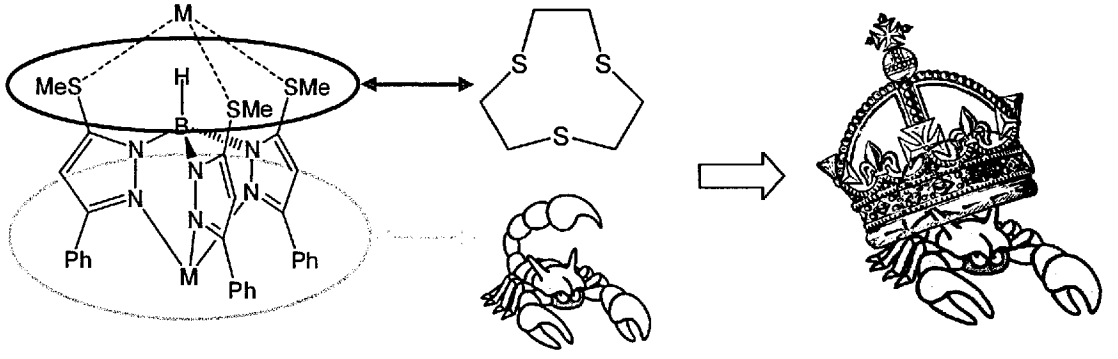
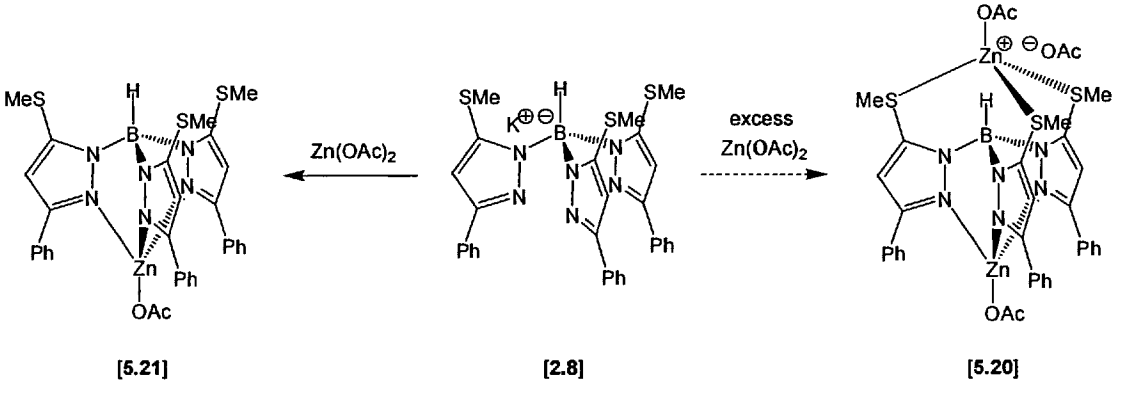


Figure 5.37. 'Crowned scorpionate', $Tp^{Ph,SMe}$.

Surprisingly there is only one other scorpionate ligand reported in the literature containing donor groups tethered to the 5-pyrazolyl position. In this example, Parkin *et al.*[44] report the synthesis of $Tp^{CF3,Tn}$ in which thienyl groups are located in the 5-pyrazolyl position of the Tp backbone. The coordination chemistry at this potential donor site, however, has not been explored. The absence of any other 5-pyrazolyl donor species is a result of steric factors which govern the regiochemistry of scorpionate ligands whereby the largest substituent in a 3,5-disubstituted pyrazole ends up in the 3-position of the resultant Tp ligand. Since the donor moiety is usually the largest substituent of the pyrazole precursor, this group invariably ends up in the 3-position.

Preliminary studies were performed into the potential coordination of metals to both the N_3 and S_3 donor arrays. Zinc was chosen as it is known to bind favourably to crown thioethers and to conventional Tp ligands. As such, a large excess of zinc acetate was reacted with $K[Tp^{Ph,SMe}]$ as depicted in Figure 5.38.



[5.21] [2.8] [5.20]

Figure 5.38. Proposed formation of zinc-'crowned scorpionate' (**5.20**).

This reaction yielded a white powder which was isolated and subsequently recrystallised for X-ray analysis. However, the resultant structure (**5.21** in Figures 5.38 and 5.39) revealed that one zinc centre had been coordinated by the pyrazolyl array, while the S donor moieties remained unbound. Bond lengths and angles for **5.21** are summarised in Table 5.12. This complex could be used as a template for future coordination reactions at the S_3 moiety. This might be advantageous as the zinc complex is air stable in solution and is also diamagnetic, thus allowing NMR spectroscopic characterisation.

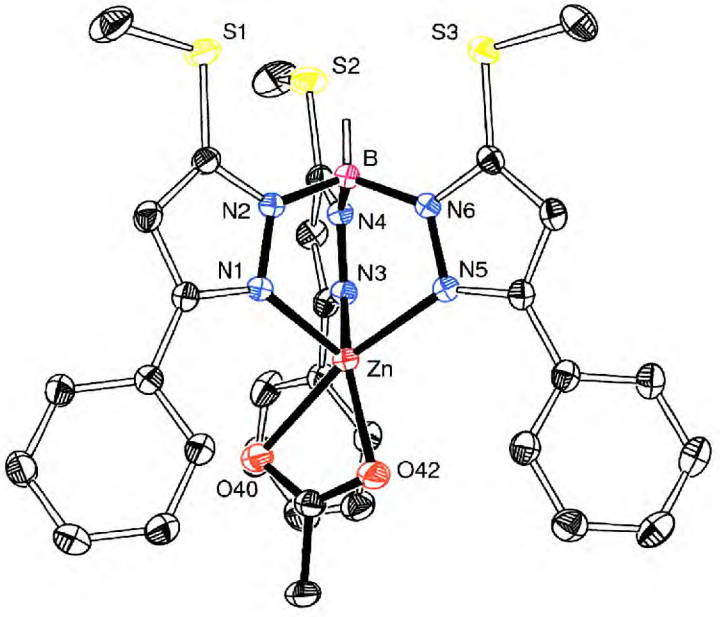


Figure 5.39. Molecular structure of Zn[$Tp^{Ph,SMe}$]OAc (**5.21**) (50 % probability ellipsoids).

Table 5.12. Selected bond lengths (Å) and angles (°) for Zn[$Tp^{Ph,SMe}$]OAc (**5.21**)

Zn–N(1)	2.0590(11)	Zn–N(3)	2.0395(11)
Zn–N(5)	2.1044(11)	Zn–O(40)	2.3320(10)
Zn–O(42)	1.9605(10)	B–N(2)	1.5438(19)
B–N(4)	1.5537(18)	B–N(6)	1.5452(18)
Zn··B	3.017	Zn···[N_3] ([a])	1.142
N(3)–Zn–N(5)	89.78(5)	N(3)–Zn–N(1)	95.30(4)
N(1)–Zn–N(5)	92.05(4)	O(42)–Zn–O(40)	60.47(4)
O(42)–Zn–N(3)	131.22(5)	O(42)–Zn–N(1)	128.11(5)
O(42)–Zn–N(5)	107.32(4)	O(40)–Zn–N(1)	97.34(4)
O(40)–Zn–N(3)	97.30(4)	O(40)–Zn–N(5)	167.64(4)

(a) This is the deviation of the zinc centre from the plane of the three coordinated nitrogen atoms.

By judicious metal choice it is hoped that future coordination of the crown unit can be achieved. Soft metals which are known to have a high affinity towards sulphur-containing macrocycles such as tungsten might prove effective. It is though that interaction of the S_3 crown unit in Cu[$Tp^{Ph,SMe}$]CO with another metal might have an effect on the carbonyl stretching frequency, νCO, which could lead to sensing applications.

5.9.3 Supramolecular Chemistry of T_kp Ligands

The tetrakis(pyrazolyl)borates, T_kp^{phos}, $T_kp^{phos(O)}$ and $T_kp^{phos(S)}$ described previously contain four bidentate arms each capable of chelation to metal centres. In their reactions, discrete molecular complexes were formed, usually by coordination of three arms to the same metal centre. However, by altering the reaction conditions (*e.g.* concentration, metal type, ligand-to-metal ratio) it might be possible to achieve coordination of the fourth pyrazolyl arm whereby supramolecular networks would be formed (Figure 5.40).

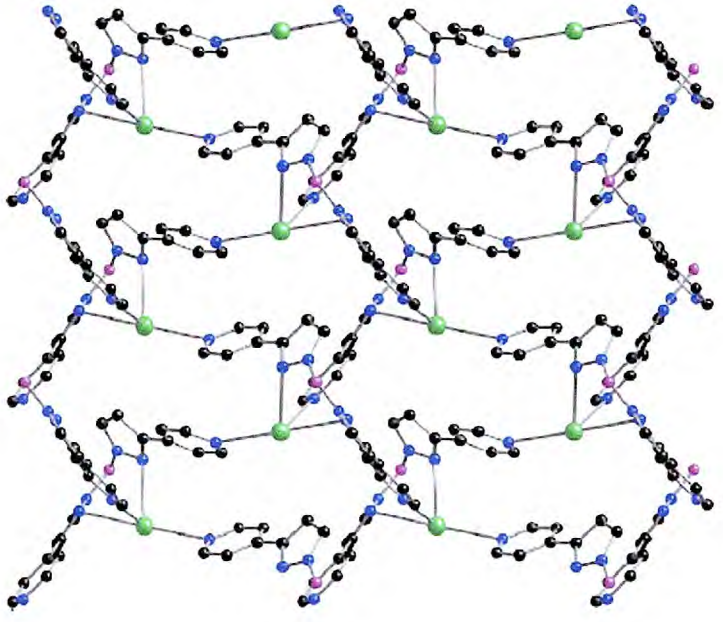


Figure 5.40. Example of a supramolecular coordination polymer derived from a T_kp ligand (Tl[T_kp^{4py}]).[3]

5.9.4 Novel Nitrogen-Donor Scorpionates

Given that reversible carbonylation has been observed with the pyridyl-substituted Tp complex, Cu[Tp^{py}]CO, the synthesis of new nitrogen appended scorpionates ligands is of interest. In this case, chelation of the pyridyl arms was not observed due to strain in the five-membered chelate ring. An extension of this work would be to create an amine-appended derivative of the phosphine-appended species $Tp^{phos,Me}$ as this displayed chelation of a donor arm to copper through a less-strained six-membered ring. By using a similar synthetic pathway it might be possible to synthesise the anilinyl-substituted species, $Tp^{Ani,Me}$ (Figure 5.41) in two steps from 2-(*N,N*-dimethylamino)acetophenone. In this nitrogen-substituted derivative, the donor groups would be expected to display a lower affinity towards the copper than the phosphine donor groups of $Tp^{phos,Me}$.

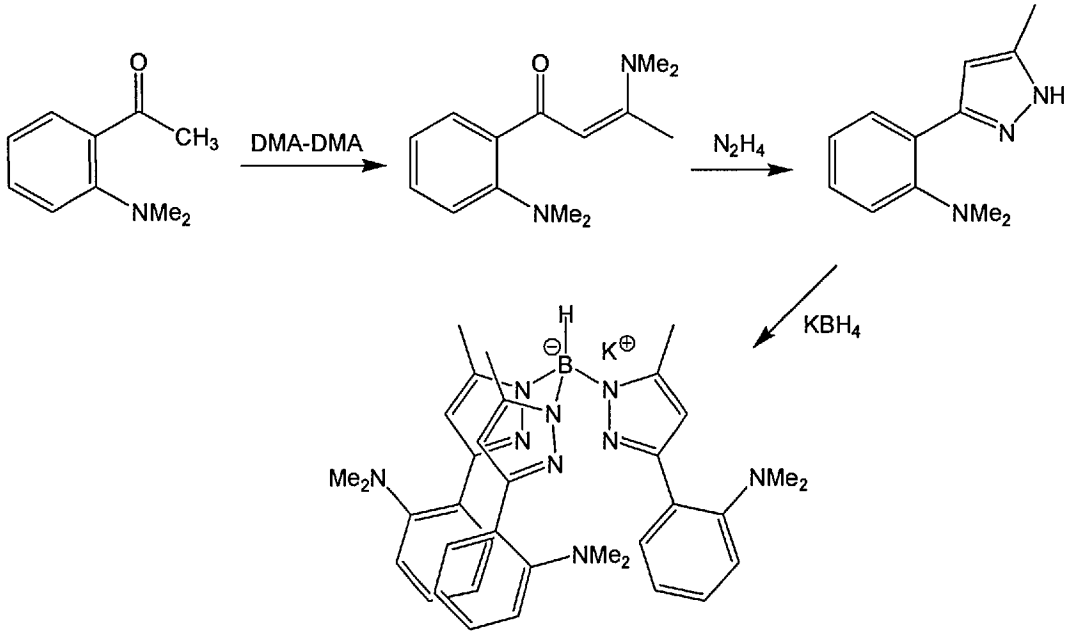


Figure 5.41. Proposed synthesis of new N_6 donor ligand, K[$Tp^{Ani,Me}$].

5.10 References

1. A. J. Amoroso, A. M. Cargill Thompson, J. C. Jeffery, P. L. Jones, J. A. McCleverty and M. D. Ward, *J. Chem. Soc., Chem. Commun.*, 1994, 2751.
2. P. L. Jones, A. J. Amoroso, J. C. Jeffery, J. A. McCleverty, E. Psillakis, L. H. Rees and M. D. Ward, *Inorg. Chem.*, 1997, **36**, 10.

3. H. Adams, S. R. Batten, G. M. Davies, M. B. Duriska, J. C. Jeffery, P. Jensen, J. Lu, G. R. Motson, S. J. Coles, M. B. Hursthouse and M. D. Ward, *Dalton Trans.*, 2005, 1910.
4. J. S. Fleming, E. Psillakis, S. M. Couchman, J. C. Jeffery, J. A. McCleverty and M. D. Ward, *J. Chem. Soc., Dalton Trans.*, 1998, 537.
5. A. L. Rheingold, B. S. Haggerty, L. M. Liable-Sands and S. Trofimenko, *Inorg. Chem.*, 1999, **38**, 6306.
6. P. L. Jones, K. L. V. Mann, J. C. Jeffery, J. A. McCleverty and M. D. Ward, *Polyhedron*, 1997, **16**, 2435.
7. E. R. Humphrey, K. L. V. Mann, Z. R. Reeves, A. Behrendt, J. C. Jeffery, J. A. McCleverty and M. D. Ward, *New. J. Chem.*, 1999, **23**, 417.
8. K. L. V. Mann, J. C. Jeffery, J. A. McCleverty and M. D. Ward, *Polyhedron*, 1999, **18**, 721.
9. A. L. Rheingold, C. D. Incarvito and S. Trofimenko, *J. Chem. Soc., Dalton Trans.*, 2000, 1233.
10. M. H. Chisholm, J. C. Gallucci and G. Yaman, *Chem. Commun.*, 2006, 1872.
11. J. A. Maldonado Calvo and H. Vahrenkamp, *Inorg. Chim. Acta*, 2006, **359**, 4079.
12. J. Kisala, A. Bialonska, Z. Ciunik, S. Kurek and S. Wolowiec, *Polyhedron*, 2006, **25**, 3222.
13. G. Bandoli, A. Dolmella, G. G. Lobbia, G. Papini, M. Pellei and C. Santini, *Inorg. Chim. Acta*, 2006, **359**, 4036.
14. D. V. Scaltrito, H. C. Fry, B. M. Showalter, D. W. Thompson, H. C. Liang, C. X. Zhang, R. M. Kretzer, E. Kim, J. P. Toscano, K. D. Karlin and G. J. Meyer, *Inorg. Chem.*, 2001, **40**, 4514.
15. C. Child, P. W. Miller, S. Kealey and N. J. Long, *Research in progress, Imperial College, London.*
16. P. L. Jones, J. C. Jeffery, J. P. Maher, J. A. McCleverty, P. H. Rieger and M. D. Ward, *Inorg. Chem.*, 1997, **36**, 3088.
17. P. Chaudhuri and K. Oder, *J. Organomet. Chem.*, 1989, **367**, 249-258.
18. L. M. Berreau, J. A. Halfen, V. G. Young and W. B. Tolman, *Inorg. Chim. Acta*, 2000, **297**, 115-128.
19. K. Singh, J. R. Long and P. Stavropoulos, *Inorg. Chem.*, 1998, **37**, 1073.
20. P. Braunstein and F. Naud, *Angew. Chem., Int. Ed.*, 2001, **40**, 680.
21. S. Trofimenko, *Scorpionates: The Coordination Chemistry of Polypyrazolylborate Ligands*, Imperial College Press, London, 1999.
22. J. A. McCleverty and T. J. Meyer, *Comprehensive Coordination Chemistry II - From Biotechnology to Nanotechnology*, Elsevier, 2003.
23. M. Jimenez-Tenorio, M. C. Puerta, P. Valerga, F. J. Moreno-Dorado, F. M. Guerra and G. M. Massanet, *Chem. Commun.*, 2001, 2324.
24. Y. Fukumoto, T. Dohi, H. Masaoka, N. Chatani and S. Murai, *Organometallics*, 2002, **21**, 3845.
25. C. Slugovc, K. Mereiter, E. Zobetz, R. Schmid and K. Kirchner, *Organometallics*, 1996, **15**, 5275.
26. S. Guo, J. W. Bats, M. Bolte and M. Wagner, *J. Chem. Soc., Dalton Trans.*, 2001, 3572.
27. C. Janiak, L. Braun and F. Girgsdies, *J. Chem. Soc., Dalton Trans.*, 1999, 3133.
28. J. L. Kisko, T. Hascall, C. Kimblin and G. Parkin, *J. Chem. Soc., Dalton Trans.*, 1999, 1929.

29. F. Jakle, K. Polborn and M. Wagner, *Chem. Ber.*, 1996, **129**, 603.
30. L. Shimoni-Livny, J. P. Glusker and C. W. Bock, *Inorg. Chem.*, 1998, **37**, 1853.
31. I. R. Shapiro, D. M. Jenkins, J. Christopher Thomas, M. W. Day and J. C. Peters, *Chem. Commun.*, 2001, 2152.
32. T. A. Betley and J. C. Peters, *Inorg. Chem.*, 2003, **42**, 5074.
33. J. C. Thomas and J. C. Peters, *Inorg. Chem.*, 2003, **42**, 5055.
34. J. C. DeMott, F. Basuli, U. J. Kilgore, B. M. Foxman, J. C. Huffman, O. V. Ozerov and D. J. Mindiola, *Inorg. Chem.*, 2007, **46**, 6271.
35. G. Espino, F. Jalon, M. Maestro, B. R. Manzano, M. Perez-Manrique and A. C. Bacigalupe, *Eur. J. Inorg. Chem.*, 2004, 2542.
36. T. Suzuki, T. Kuchiyama, S. Kishi, S. Kaizaki, H. D. Takagi and M. Kato, *Inorg. Chem.*, 2003, **42**, 785.
37. A. Albinati, Q. Jiang, H. Ruegger and L. M. Venanzi, *Inorg. Chem.*, 1993, **32**, 4940.
38. C. Bianchini, V. Dal Santo, A. Meli, W. Oberhauser, R. Psaro and F. Vizza, *Organometallics*, 2000, **19**, 2433.
39. N. W. Alcock, I. D. Burns, K. S. Claire and A. F. Hill, *Inorg. Chem.*, 1992, **31**, 2906.
40. I. P. Evans, A. Spencer and G. Wilkinson, *J. Chem. Soc., Dalton Trans.*, 1973, 204.
41. K. Nakamoto, *Infrared and Raman Spectra of Inorganic and Coordination Compounds. Part B: Applications in Coordination, Organometallic and Bioinorganic Chemistry*, 5th edn., Wiley, New York, 1992.
42. L. R. Fraser, J. Bird, Q. Wu, C. Cao, B. O. Patrick and J. A. Love, *Organometallics*, 2007, **26**, 5602.
43. S. R. Cooper, *Acc. Chem. Res.*, 1988, **21**, 141.
44. R. Han, P. Ghosh, P. J. Desrosiers, S. Trofimenko and G. Parkin, *J. Chem. Soc., Dalton Trans.*, 1997, 3713.

CHAPTER 6

CONCLUSION

6. Conclusion

In this research, solutions to the problems associated with the low solubility and low concentration of ^{11}CO encountered in PET radiolabelling experiments were sought in order to expand the scope [^{11}C]carbonylation reactions. Carbonylation reactions provide access to an array of biologically-active functional groups and the development of new methodologies that facilitate the synthesis of ^{11}C-labelled compounds in this manner are highly sought after. The long-standing literature precedent of copper(I) solutions being able to reversibly bind to CO was used as the basis for these investigations. Starting with the copper(I)-scorpionate complex CuTp*CO, that provided the first ever structurally characterised copper(I) carbonyl, a system was designed that could solubilise ^{11}CO by the formation of this species from a solution of CuCl and KTp*. This was found to trap unlabelled CO efficiently when using a concentrated gas stream. Decarbonylation of this species was achieved by addition of triphenylphosphine in an irreversible ligand exchange process to form CuTp*PPh_3. The disappearance of νCO from the solution IR spectrum indicated that decarbonylation was complete within two minutes of triphenylphosphine addition.

The application of this CO-trapping system to the hot-cell proved successful with initial experiments performed using a ^{11}CO preconcentration step resulting in a trapping efficiency of 96 %. This led to further experiments in which the preconcentration step was removed, and the CuTp* solution was still able to trap ^{11}CO from within the nitrogen-rich gas stream with extremely high efficiency. This compares favourably to previous reports in which trapping efficiencies of 10 % and under have been observed using ordinary solvent systems.

The subsequent release of CO from solution and its use in palladium-catalysed carbonylation reactions between aryl-halides and benzylamine has been found to be effective for the synthesis of amides. These reactions have been performed using unlabelled CO via two different methods. Small-scale reactions were performed by infusing a solution of CuTp*CO and a solution of the cross-coupling reagents into the channels of a microfluidic chip. 'Bulk-scale' reactions were similarly performed by injection of the cross-coupling reagents into a sealed Schlenk flask containing a solution of CuTp*CO. Both systems gave access to series of amides with a range of

yields dependent on the reaction time and the particular substrate involved. Electron-poor aryl-halides resulted in the highest yields and this was attributed to their increased rate of oxidative addition to the palladium centre during the catalytic cycle.

This system was adapted to the conditions of the hot-cell to perform carbonylation reactions with ^{11}CO. The bulk reactions were mimicked in the radiolaboratory using sealed sample vials as the reaction vessels instead of Schlenk flasks. In these reactions, the ^{11}CO trapping process was followed by injection of the cross-coupling reagents into the sample vial before being heated for 10 minutes. Once complete, ^{11}C-labelled amides were detected by radio HPLC indicating the viability of this system for further radiolabelling experiments.

In addition to the radiolabelling experiments, a new series of ligands based on the pyrazolyl donor moiety was developed. These ligands contained a triphenylphosphine appendage in the 3-pyrazolyl position, forming a potentially bidentate species. The reason for synthesising these compounds was two-fold; (i) because of their potential application as ligands in palladium-catalysed carbonylation reactions and (ii) because of their potential conversion to new donor-appended scorpionate ligands, which may themselves find applications in reversible CO binding with copper(I).

The pyrazolyl-based, N,P donor ligand, Hpz^{phos}, was synthesised along with the related N,O and N,S derivatives ($Hpz^{phos(O)}$ and $Hpz^{phos(S)}$, respectively) and their coordination chemistry with palladium(II) was investigated.[1] This revealed a range of coordination modes depending on the affinity of the donor group towards palladium. In all cases, coordination of the pyrazolyl N-donor moiety was observed. The N,P ligand, Hpz^{phos}, was shown to chelate at all times, and no 'hemilabile' behaviour was observed. This species displayed moderate activity in the palladium-catalysed carbonylation reaction between benzylamine and iodobenzene to produce *N*-benzylbenzamide. The N,O and N,S ligands displayed more varied coordination behaviour. In the case of the N,O ligand, $Hpz^{phos(O)}$, the oxide moiety did not display coordination to the palladium centre unless forced to do so by addition of silver perchlorate. This formed a bis-chelate complex which unexpectedly converted to a new species over longer periods due to reaction with cyclooctadiene present in solution.

These pyrazolyl ligands were converted into the corresponding tetrakis(pyrazolyl)borate ligands by reaction with potassium borohydride. This gave access to a new series of phosphorus-containing scorpionate ligands capable of up-to hexadentate coordination. Their coordination chemistry was examined with a range of metals, with particular attention paid towards their reactivity with copper(I) and CO. The N_4,O_4 ligand $T_kp^{phos(O)}$ was structurally characterised as the thallium(I) salt and the europium(III) κ^6 complex.[2] The copper carbonyl species, $Cu[T_kp^{phos(O)}]CO$, was found to resist decarbonylation in solution upon application of a vacuum. This reactivity contrasted with that of the known ligand, Tp^{py}. The copper(I) carbonyl chemistry of this species was examined for the first time and it was found that $Cu[Tp^{py}]CO$ could be reversibly carbonylated by application of vacuum/nitrogen cycles.

The desire to form a tris(pyrazolyl)borate ligand with phosphine appendages led to a new synthetic approach being sought for the formation of a phosphine-appended pyrazole containing a methyl group at the 5-pyrazolyl position. This species, $Hpz^{phos,Me}$, was synthesised accordingly and reacted with potassium borohydride. Here, steric effects prevented the formation of the tetrakis(pyrazolyl)borate species and the resultant N_3,P_3 ligand, $Tp^{phos,Me}$ was structurally characterised with thallium(I), copper(I) and ruthenium(II). The copper complex $Cu[Tp^{phos,Me}]$ was shown to be inert towards CO, a property that was explained by its solid state structure and low temperature NMR behaviour that showed that one of the appended phosphine groups was able to chelate to the copper centre thus satisfying the coordination preference of the metal.[3]

The interest into the use of Tp ligands for CO trapping led to the synthesis of a novel Tp ligand containing methylthio groups attached directly to the pyrazolyl ligand core. This species, $Tp^{Ph,SMe}$, provides the first example of a heteroatom-substituted Tp ligand (with the exception of the halogenated compounds) and is hoped to open up a new field of scorpionate chemistry in which Tp ligands containing direct substitution of N, O, P, and S atoms on the pyrazolyl rings are synthesised for their potentially-advantageous electronic and coordinating properties.

Overall, the objectives described at the beginning of this research have been successfully accomplished which has led to a significant amount of additional research which could be performed to further develop the fields of [^{11}C]carbonylation and scorpionate chemistry. The positive results achieved for the ^{11}CO trapping and carbonylation reactions create a range of potential follow-up reactions which could be performed in order to optimise the process. Subsequent investigations into the use of this system for carbonylation reactions to produce other CO-containing functionalities, such as esters and ketones, could then be performed. The versatile coordination chemistry of the new donor-appended scorpionates shows that they are capable of stabilising metal complexes depending on the specific coordination requirements of the metal. As well as extending the range of metal being studied (*e.g.* group II metals) the potential application of these species, particularly the phosphine-appended Tp, could be examined within the field of homogeneous catalysis.

6.1 References

1. S. Kealey, N. J. Long, P. W. Miller, A. J. P. White, P. B. Hitchcock and A. D. Gee, *Dalton Trans.*, 2007, 2823.
2. S. Kealey, N. J. Long, A. J. P. White and A. D. Gee, *Dalton Trans.*, 2007, 4763.
3. S. Kealey, N. J. Long, P. W. Miller, A. J. P. White and A. D. Gee, *Dalton Trans.*, 2008, 2677.

CHAPTER 7

EXPERIMENTAL

7. Experimental

7.1 Synthesis of Ligands and Complexes

All manipulations of air/moisture sensitive compounds were performed on a conventional vacuum/nitrogen/carbon monoxide line using standard Schlenk techniques. All solvents were distilled over standard drying agents, under an atmosphere of nitrogen, directly prior to use. Chromatographic separations were carried out on Kiesegel 60 silica gel. ^{1}H, ^{11}B, $^{19}F\{^{1}H\}$ and $^{31}P\{^{1}H\}$ NMR spectra were collected on a Jeol EX 270 MHz or Bruker AV-400 spectrometer. $^{13}C\{^{1}H\}$, HMQC and 2D spectra were recorded on a Bruker DRX-400 or AV-500 spectrometer. VT ^{1}H and $^{31}P\{^{1}H\}$ NMR spectra were recorded by Dick Shepherd and Peter Haycock on a Bruker DRX-400 spectrometer at the Department of Chemistry, Imperial College, London. Chemical shifts are reported in parts per million using the residual proton impurities in the solvents. d_2-Dichloromethane, d_1-chloroform and d_6-acetone were dried over 4 Å molecular sieves and stored under nitrogen. Pseudo-triplets resulting from near-identical *J*-value coupling to two chemically inequivalent protons are labelled as dd and are recognised by the inclusion of two identical *J*-values. Mass spectra were recorded on a Micromass Autospec Q spectrometer by Mr. J. Barton and Mr. G. Tucker of the Department of Chemistry, Imperial College. Identification of characteristic isotope patterns was used to confirm the assignments, where appropriate. Infrared absorption spectra were collected either as KBr discs, nujol mulls or THF solutions using a Perkin Elmer RX FT-IR spectometer. Elemental analyses were performed by Stephen Boyer at the London Metropolitan University. All reagents were purchased from Aldrich Chemical Company, Alfa Aesar, Fisher Chemicals, Strem Chemicals Inc. or Fluorochem and used without further purification unless stated otherwise.

7.1.1 Experimental Procedures for Chapter 2

For the synthesis of the poly(pyrazolyl)borates, unless otherwise stated, the progress of the reaction was followed by measuring the volume of H_2 gas evolved via the displacement of water from a container by the gas. Copper(I) chloride was recrystallised from concentrated HCl and distilled water and stored under nitrogen. $[Cu(MeCN)_4]PF_6$ was prepared as reported previously.[1]

Potassium hydrotris(pyrazol-1-yl)borate, *KTp* (2.1)

KBH_4 (2.700 g, 50 mmol) and pyrazole (13.620 g, 200 mmol) were heated to 90°C with stirring, causing the pyrazole to melt and H_2 gas to evolve slowly. The temperature was then raised to 125°C causing H_2 to evolve more quickly. When 1.75 l (70 mmol) of H_2 had been evolved the temperature was raised to 190°C and the reaction continued until 3.75 l (150 mmol) of H_2 had been evolved. The melt was poured into ethanol (20 ml, 0°C) and the ethanol removed to leave a thick white slurry, which was dried *in vacuo* to give a white solid. This solid was ground to a fine powder and the unreacted pyrazole was removed by vacuum sublimation at 80°C to give KTp as a white powder (10.89 g, 43 mmol, 86%) which was recrystallised from hot anisole, and washed with toluene then ether (8.43 g, 33 mmol, 67%). Anal. (%) calc. (found) for $C_9H_{10}BKN_6$: C, 42.9 (42.9); H, 4.00 (3.92); N, 33.3 (33.2). IR (KBr disc), ν_{max}/cm^{-1} = 2437 (BH). ^1H NMR (+25°C, D_2O, 270 MHz): δ = 7.66 [d ($^3J_{HH}$ = 1.1 Hz), 3H, 5-pz], 7.40 [d ($^3J_{HH}$ = 1.6 Hz), 3H, 3-pz], 6.33 [m, 3H, 4-pz]. ^{11}B NMR (+25°C, D_2O, 270 MHz): δ = -2.4 [d ($^1J_{BH}$ = 101 Hz), BH].

Potassium hydrotris(3,5-dimethyl(pyrazol-1-yl))borate, *KTp (2.2)**

KBH_4 (1.079 g, 20.0 mmol) and 3,5-dimethylpyrazole (9.613 g, 100.0 mmol) were slowly heated to 210°C causing H_2 to evolve. After 3 hrs, 1.5 l (60.0 mmol) of H_2 had been evolved and the melt was poured into ethanol (10 ml, 0°C) and the ethanol removed using a rotavap to leave a white solid which was further dried on the vacuum line. This solid was ground to a fine powder and the unreacted 3-5-dimethylpyrazole was removed by vacuum sublimation at 110°C. The remaining solid was dissolved in acetone (80 ml) and filtered. Removal of the acetone gave a white solid which was trituration with ether (5 ml) followed by filtration and air drying to give KTp* as a white solid (5.140 g, 13.3 mmol, 77%). Anal. (%) calc. (found) for $C_{15}H_{22}BKN_6$: C, 53.6 (53.5); H, 6.59 (6.53); N, 25.0 (24.9). IR (KBr disc): ν_{max}/cm^{-1} = 2438 (BH). ^1H NMR (+ 25°C, d_6-acetone, 270 MHz): δ = 5.53 [s, 3H, 4-pz], 2.17 [s, 9H, 5-CH_3], 2.01 [s, 9H, 3-CH_3]. ^{11}B NMR (+25°C, d_6-acetone, 270 MHz): δ = -7.9 [d ($^1J_{BH}$ = 101 Hz), BH].

Potassium dihydrobis(pyrazolyl)borate, *KBp* (2.3)

A finely ground mixture of KBH_4 (2.020 g, 37.4 mmol) and pyrazole (10.200 g, 149.8 mmol) were heated to 90°C with stirring, causing the pyrazole to melt and H_2 gas to

evolve slowly. The temperature was then raised to 120°C and the reaction continued until 1.9 l (75 mmol) of H_2 had been evolved. The melt was poured into stirred toluene (25 ml), filtered whilst hot and washed with toluene (3 x 5 ml) then hexane (2 x 10 ml) and air dried (3.570 g, 19.2 mmol, 51 %). Recrystallisation twice from anisole gave KBp as a white powder. To obtain an analytically pure sample the solid was dissolved in the minimum amount of ethanol and filtered to remove some insoluble material. The filtrate was concentrated to dryness and the resultant powder was stirred in ether and collected by filtration and dried *in vacuo*. Anal. (%) calc. (found) for $C_6H_8BKN_4$: C, 38.7 (39.1); H, 4.33 (4.05); N, 30.1 (30.2). IR (KBr disc), ν_{max}/cm^{-1} = 2433, 2402 (BH). ^{1}H NMR (+25°C, D_2O, 270 MHz): δ = 7.67 [d ($^3J_{HH}$ = 2.1 Hz), 2H, 5-pz], 7.53 [d ($^3J_{HH}$ = 1.8 Hz), 2H, 3-pz], 6.24 [dd ($^3J_{HH}$ = 1.9 Hz, $^3J_{HH}$ = 1.9 Hz), 2H, 4-pz], 3.67 [m(br), BH_2]. ^{11}B NMR (+25°C, 500 MHz, D_2O): δ = -5.3 [t ($^1J_{BH}$ = 89 Hz), BH_2].

Potassium dihydrobis(3,5-dimethyl(pyrazol-1-yl))borate, *KBp (2.4)**

KBH_4 (2.230 g, 41.3 mmol) and 3,5-dimethylpyrazole (11.900 g, 123.9 mmol) were heated to 160°C until 2.07 l (82.6 mmol) of H_2 was collected. The melt was poured into ethanol (25 ml, 0°C) and the ethanol removed using a rotavap to leave a white solid which was further dried *in vacuo*. The solid was ground to a fine powder and the unreacted 3-5-dimethylpyrazole was removed by vacuum sublimation at 110°C. The crude product was found to contain some KTp* impurities which were removed by Soxhlet extraction in ether followed by recrystallisation from hot anisole. Washing with hexane and drying *in vacuo* gave KBp* as a white solid (4.360 g, 18.0 mmol, 44%). Elemental analysis was performed on a further purified sample obtained by recrystallisation from boiling toluene, washing with hexane and drying *in vacuo*. Anal. (%) calc. (found) for $C_{10}H_{16}BKN_4$: C, 49.6 (49.7); H, 6.66 (6.60); N, 23.1 (23.2). IR (d_6-acetone), ν_{max}/cm^{-1} = 2592 (BH). ^{1}H NMR (+25°C, d_6-acetone, 270 MHz): δ = 5.49 [s, 2H, pz-H], 2.22 [s, 6H, 5-CH_3] 2.02 [s, 6H, 3-CH_3]. ^{11}B NMR (+25°C, d_6-acetone, 270 MHz): δ = -12.2 [t ($^1J_{BH}$ = 95 Hz), BH_2].

Attempted synthesis of 3,5-diethoxy pyrazole, *Hpz^{2OEt}* (2.5)

A solution of hydrazine hydrate (4.9 ml, 100.0 mmol) in water (5 ml) was added dropwise to a stirred solution of diethylmalonate (15.2 ml, 100.0 mmol) in ethanol (5 ml) at 0°C. After stirring for 1 hr, a white solid had precipitated which was collected

by filtration and dried *in vacuo*. The solid was found to be insoluble in all common organic solvents. Recrystallisation was achieved using a mixture of water and ethanol to give a white solid (3.88 g). MS(EI): m/z = 132 $[C_3H_8N_4O_2]^+$ (indicating formation of dihydrazide). Anal. (%) calc. for pyrazole ($C_7H_{12}N_2O_2$): C, 53.8; H, 7.74; N, 17.9; for dihydrazide ($C_3H_8N_4O_2$. 0.7 H_2O): C, 24.9; H, 6.55; N, 38.7; found: C, 25.2; H, 6.84; N, 38.3.

3,3-Bis(methylthio)phenyl-2-propen-1-one (2.6)

Acetophenone (4.8 ml, 41.0 mmol) was added dropwise to a mechanically stirred solution of potassium *tert*-butoxide (9.650 g, 86.0 mmol) in THF (200 ml) to form a cloudy white mixture. Carbon disulphide (2.6 ml, 43.1 mmol) was added dropwise over a period of 30 mins, immediately forming an orange suspension which became extremely viscous during the addition. Iodomethane (5.4 ml, 86.10 mmol) was added dropwise over 1 hr and the mixture was stirred for 12 hrs then poured into ice-cold water (400 ml) and the mixture transferred into a round bottomed flask and the THF removed by rotary evaporation. To the resultant mixture was added CH_2Cl_2 (200 ml) and the organic layer was separated and the aqueous layer was washed with CH_2Cl_2 (2 x 100 ml). The combined organic washings were dried over $MgSO_4$ and concentrated to dryness to give an orange oil. Recrystallisation from hot ethanol produced a yellow solid (4.646 g, 20.7 mmol, 51 %). ^{1}H NMR (+25°C, $CDCl_3$, 400 MHz): δ = 7.94 [m, 2H, 2,6-Ph], 7.49 [m, 3H, 3,4,5-Ph], 6.79 [s, 1H, COCH], 2.58 [s, 3H, SCH_3], 2.55 [s, 3H, SCH_3].

3(5)-Phenyl-5(3)-methylthiopyrazole, $Hpz^{Ph,SMe}$ (2.7)

2.6 (4.49 g, 20.0 mmol) and hydrazine hydrate (0.97 ml, 20.0 mmol) in ethanol (50 ml) were heated at reflux for 12 hrs. Removal of the solvent gave a thick yellow oil which was triturated with pentane (40 ml) in an ultrasonic bath to give an off-white powder containing some lumps of solid. The solid was collected by filtration and dissolved in ether and concentrated to dryness to give a uniform off-white powder which was purified by reprecipitation from benzene/hexane. The resultant white powder was collected by filtration, washed with hexane and dried *in vacuo* (3.060 g, 16.1 mmol, 80 %). Anal. (%) calc. (found) for $C_{10}H_{10}N_2S$: C, 63.1 (63.2); H, 5.30 (5.36); N, 14.7 (14.8). ^{1}H NMR (+25°C, $CDCl_3$, 400 MHz): δ = 10.93 [s(br), 1H, NH], 7.67 [d ($^3J_{HH}$ = 7.3 Hz), 2H, *o*-Ph], 7.43 [dd ($^3J_{HH}$ = 7.3 Hz, $^3J_{HH}$ = 7.3 Hz), 2H,

m-Ph], 7.37 [m, 1H, *p*-Ph], 6.57 [s, 1H, 4-pz], 2.55 [s, 3H, CH_3]. MS(EI), *m/z* = 190 $[M]^+$.

Potassium hydrotris(3-phenyl,5-methylthio(pyrazol-1-yl))borate, *K[Tp^{Ph,SMe}]* (2.8)

A finely ground mixture of **2.7** (3.00 g, 15.8 mmol) and KBH_4 (0.17 g, 3.2 mmol) was heated to 90°C causing a melt to form. The temperature was gradually increased to 220°C and stirring at this temperature for 2 hrs caused a white solid to precipitate. After cooling, ethanol (20 ml) was added and the solid broken up with a spatula and sonicated to produce a white powder which was collected by filtration, purified by precipitation from THF/hexane and dried *in vacuo* (1.305 g, 2.1 mmol, 66 %). IR (KBr disc), ν_{max}/cm^{-1} = 2448 (BH). ^1H NMR (+25°C, d_6-acetone, 400 MHz): δ = 7.75 [d ($^3J_{HH}$ = 7.1 Hz), 6H, *o*-Ph], 7.22 [dd ($^3J_{HH}$ = 7.2 Hz, $^3J_{HH}$ = 7.2 Hz), 6H, *m*-Ph], 7.16 [m, 3H, *p*-Ph], 6.55 [s, 3H, 4-pz], 5.43 [m(br), 1H, BH], 2.34 [s, 9H, CH_3]. $^{13}C\{^1H\}$ NMR (+25°C, d_6-acetone, 126 MHz), δ = 151.8 [s, 3-pz], 144.3 [s, 5-pz], 136.1 [s, *i*-Ph], 129.1 [s, *m*-Ph], 127.2 [s, *p*-Ph], 126.0 [s, *o*-Ph], 103.4 [s, 4-pz], 17.5 [s, CH_3]. ^{11}B NMR (+25°C, d_6-acetone, 128 MHz), δ = -5.6 [s(br), BH]. MS(ESI -ve), *m/z* = 579 $[Tp^{Ph,SMe}]^-$.

Thallium hydrotris(3-phenyl,5-methylthio(pyrazol-1-yl))borate, *Tl[Tp^{Ph,SMe}]* (2.9)

A solution of $TlNO_3$ (0.103 g, 0.39 mmol) in water (15 ml) was added to a stirred solution of **2.8** (200 mg, 0.32 mmol) in THF (10 ml) causing the immediate precipitation of a white solid. This was collected by filtration, washed with methanol (10ml) and dried *in vacuo* to give a white powder (0.213 g, 0.27 mmol, 84 %). Single crystals suitable for X-ray analysis were grown by vapour diffusion of pentane into a chloroform solution of this complex. Anal. (%) calc. (found) for $C_{30}H_{28}BN_6S_3Tl$: C, 46.0 (46.0); H, 3.60 (3.50); N 10.7 (10.7). IR (nujol): ν_{max}/cm^{-1} = 2498 (BH). ^1H NMR (+25°C, $CDCl_3$, 400 MHz): δ = 7.61 [d ($^3J_{HH}$ = 7.0 Hz), 6H, *o*-Ph], 7.41 [dd ($^3J_{HH}$ = 7.3 Hz, $^3J_{HH}$ = 7.3 Hz), 6H, *m*-Ph], 7.35 [t ($^3J_{HH}$ = 7.3 Hz), 3H, *p*-Ph], 6.37 [s, 3H, 4-pz], 5.41 [m(br), 1H, BH], 2.56 [s, 9H, CH_3]. $^1H\{^{11}B\}$(+57°C, $CDCl_3$, 400 MHz): As above except broad BH multiplet becomes a sharper singlet at 5.41 ppm. $^{13}C\{^1H\}$ NMR (+25°C, $CDCl_3$, 101 MHz), δ = 153.1 [s, 3-pz], 145.7 [s, 5-pz], 133.5 [s, *i*-Ph], 128.8 [s, *m*-Ph], 127.9 [s, *p*-Ph], 126.9 [d ($^4J_{CTl}$ = 108.2 Hz), *o*-Ph], 103.1 [s, 4-pz],

17.2 [s, CH_3]. ^{11}B NMR (+25°C, $CDCl_3$, 400 MHz): δ = -6.9 [s(br)]. MS(ESI -ve): *m/z* = 579 [$Tp^{Ph,SMe}$]$^-$.

Copper(I)hydrotris(pyrazol-1-yl)borate carbonyl, *CuTpCO* (2.10)

CO saturated THF (10 ml) was added to CuCl (0.099 g, 1.00 mmol) and KTp (**2.1**) (0.252 g, 1.00 mmol) and CO was bubbled through the stirred suspension for 1 hr. Filtration and removal of the solvent gave Cu(Tp)CO as a white powder (0.287 g, 0.94 mmol, 94 %). IR (KBr disc): ν_{max}/cm^{-1} = 2071 (CO), 2462 (BH). ^1H NMR (+25°C, d_6-acetone, 270 MHz): δ = 7.71 [m, 6H, 3,5-pz], 6.18 [dd ($^3J_{HH}$ = 1.9 Hz, $^3J_{HH}$ = 1.9 Hz), 3H, 4-pz], 4.53 [m(br), BH]. $^{11}B\{^1H\}$ NMR (+25°C, d_6-acetone, 270 MHz): δ = -5.0 [s].

Copper(I)hydrotris(3,5-dimethyl(pyrazol-1-yl))borate carbonyl, *CuTp*CO* (2.11)

CO saturated THF (10 ml) was added to CuCl (0.099 g, 1.00 mmol) and KTp* (**2.2**) (0.336 g, 1.00 mmol) and CO was bubbled through the stirred suspension for 2 hrs. Filtration and removal of the solvent gave a mixture of Cu(Tp*)CO and KTp* as judged by NMR. Extraction of the solid into ether (dry, CO saturated) (60 ml) gave a clear solution and some insoluble white solid (unreacted KTp*). Filtration followed by concentration of the filtrate gave a white solid. Anal. (%) calc. (found) for $C_{16}H_{22}BCuN_6O$: C, 49.4 (49.6); H, 5.70 (5.79); N, 21.6 (21.8). IR (THF): ν_{max}/cm^{-1} = 2064 (CO), 2517 (BH). IR (KBr disc): ν_{max}/cm^{-1} = 2060 (CO), 2500 (BH). ^1H NMR (+25°C, CD_2Cl_2, 270 MHz): δ = 5.76 [s, 3H, 4-pz], 4.55 [m(br), 1H, BH], 2.33 [s, 9H, 3-CH_3], 2.28 [s, 9H, 5-CH_3]. ^{11}B NMR (+25°C, d_6-acetone, 270 MHz): δ = -10.9 [d ($^1J_{BH}$ = 101 Hz)].

CuTp*^{13}CO (2.11-^{13}C)

THF (5 ml) was added to a Schlenk flask containing CuCl (0.033 g, 0.33 mmol) and KTp* (**2.2**) (0.111 g, 0.33 mmol). The flask was sealed and ^{13}CO was bubbled through the suspension for 1 min. 0.5 ml of solution was removed for IR studies and the remainder was concentrated to dryness to give a white solid that was extracted into CD_2Cl_2 and filtered straight into an NMR tube under an atmosphere of nitrogen. IR (THF): ν_{max}/cm^{-1} = 2516 (BH), 2017 (^{13}CO); IR (KBr disc): ν_{max}/cm^{-1} = 2500 (BH of CuTp*CO), 2483 (BH of KTp*), 2012 (^{13}CO). ^{13}C NMR (+25°C, CD_2Cl_2, 400

MHz): δ = 177.3 [m, CuTp*CO], 148.0 [s, 5-pz], 144.4 [s, 3-pz], 104.5 [s, 4-pz], 13.8 [s, 3-CH_3], 12.5 [s, 5-CH_3].

Copper(I)hydrotris(3-phenyl,5-thiomethyl(pyrazol-1-yl))borate carbonyl, *Cu[Tp^{Ph,SMe}]CO* (2.12)

CO was bubbled through a suspension of K[Tp^{Ph,SMe}] (**2.8**) (0.100 g, 0.16 mmol) and copper chloride (0.016 g, 0.16 mmol) in THF for 30 mins. THF solution IR spectroscopy indicated formation of the carbonyl adduct (ν(CO) = 2081 cm^{-1}). The suspension was allowed to settle and filtered to give a clear, colourless filtrate which was concentrated to dryness to produce a white powder (0.064 g, 0.10 mmol, 60 %). Anal. (%) calc. (found) for $C_{31}H_{28}BCuN_6OS_3$: C, 55.5 (55.4); H, 4.21 (4.30); N 12.5 (12.4). IR (KBr disc): ν_{max}/cm^{-1} = 2500 (BH), 2087 (CO). ^{1}H NMR (+25°C, CD_2Cl_2, 400 MHz): δ = 7.69 [d ($^3J_{HH}$ = 6.8 Hz), 6H, *o*-Ph], 7.43 [m, 9H, *m,p*-Ph], 6.32 [s, 3H, 4-pz], 5.19 [m(br), 1H, BH], 2.59 [s, 9H, CH_3]. ^{11}B NMR (+25°C, CD_2Cl_2, 400 MHz): δ = -9.1 [s(br), BH]. MS(ESI +ve): *m/z* = 581 [Tp^{Ph,SMe}]$^+$, 684 [Cu(Tp^{Ph,SMe})CO + 14]$^+$.

Cu[Tp^{Ph,SMe}]^{13}CO (2.12-^{13}C)

CD_2Cl_2 and CH_2Cl_2 was added to an NMR tube containing K[Tp^{Ph,SMe}] (**2.8**) (0.037 g, 0.06 mmol) and CuCl (0.006 g, 0.06 mmol). ^{13}CO was bubbled through the suspension for 1 min. Single crystals suitable for X-ray analysis were grown by slow evaporation of this solution. ^{13}C{^{1}H} NMR (+25°C, CD_2Cl_2, 400 MHz): δ = 174.8 [s(br), CO], 153.0 [s, 3-pz], 144.8 [s, 5-pz], 133.4 [s, *i*-Ph], 128.3 [s, *m,p*-Ph], 127.6 [s, *o*-Ph], 103.4 [s, 4-pz], 17.0 [s, CH_3].

Rapid carbonylation reaction

d_6-Acetone (0.5 ml) was added to an NMR tube (capped with a suba seal) containing KTp* (**2.2**) (0.020 g, 0.06 mmol) and CuCl (0.006 g, 0.06 mmol). ^{13}CO was bubbled through the suspension for 1 min. ^{1}H NMR (+25°C, d_6-acetone, 400 MHz): δ = 5.75 [s, CuTp*CO 4-pz], 5.55 [s, KTp* 4-pz], 2.34 [s, CuTp*CO CH_3], 2.25 [s, CuTp*CO CH_3], 2.19 [s, KTp* CH_3], 2.03 [s, KTp* CH_3].

Decarbonylation of CuTp*CO - IR study

Under an atmosphere of nitrogen, PPh_3 (0.078 g, 0.30 mmol) was added to a CH_2Cl_2 solution of CuTp*CO generated *in situ* from KTp* (0.050 g, 0.15 mmol), $[Cu(MeCN)_4]PF_6$ (0.055 g, 0.15 mmol) and CO. Solution IR spectroscpoy after 2 mins stirring showed no carbonyl absorption.

Copper(I)hydrotris(3,5-dimethyl(pyrazol-1-yl))borate triphenylphosphine, *CuTp*PPh$_3$* (2.13)

PPh_3 (0.042 g, 0.16 mmol) in THF (4 ml) was added to a solution of CuTp*CO (**2.11**) (0.062 g, 0.16 mmol) in THF (4 ml) causing effervescence of CO gas to occur immediately and the solution was stirred for 30 mins at room temperature. IR (THF): ν_{max}/cm^{-1} = 2507 (BH), ν(CO) not observed. The THF was removed on the vacuum line to give a white solid. Anal. (%) calc. (found) for $C_{33}H_{37}BCuN_6P$: C, 63.6 (63.5); H, 5.99 (5.98); N, 13.5 (13.4). ^1H NMR (270 MHz, d^6-acetone, 25°C): δ = 7.68 [m, 9H, *m,p*-Ph], 7.37 [m, 6H, *o*-Ph-H], 5.63 [s, 3H, 4-pz], 2.38 [s, 9H, CH_3], 1.68 [s, 9H, CH_3]. $^{31}P\{^1H\}$ NMR (+25°C, d_6-acetone, 270 MHz): δ = +29.6 [s].

Decarbonylation of Cu[Tp^{Ph,SMe}]CO - IR study

Under an atmosphere of nitrogen, PPh_3 (0.080 g, 0.31 mmol) was added to a CH_2Cl_2 solution of Cu[Tp^{Ph,SMe}]CO generated *in situ* from K[Tp^{Ph,SMe}] (0.100 g, 0.16 mmol), $[Cu(MeCN)_4]PF_6$ (0.060 g, 0.16 mmol) and CO. Solution IR spectra were recorded after 2 mins stirring (νCO = 2084m) and after a further 8 mins stirring (νCO = 2084w).

7.1.2 Experimental Procedures for Chapter 3

Carbon monoxide trapping reaction performed with ^{11}CO – 'hot chemistry'

See description in Chapter 3.

Carbonylative cross-coupling reactions performed with ^{12}CO – 'cold chemistry' in microfluidic device

A solution of CuTp*CO (**2.11**) (0.194 g, 0.50 mmol) in THF (7.5 ml) was loaded into a syringe and connected to a microfluidic chip (path length = 5 ml, total volume = 75 μl). Another syringe was fillled with $Pd(dppp)Cl_2$ (0.006 g, 0.01 mmol), aryl-halide

(0.50 mmol) and triphenylphosphine (0.132 g, 0.50 mmol) in benzylamine (7.5 ml, excess) and connected to the chip. Both syringes were attached to syringe pumps and the reagents were infused in the chip at 85°C at a flow rate of 6 µl /min for each syringe. After 80 mins, 0.96 ml of liquid had been collected from the chip. All samples were studied by GC analysis using a phenyl ether standard of known concentration.

Carbonylative cross-coupling reactions performed with ^{12}CO – 'cold chemistry' in Schlenk apparatus

A solution of $Pd(dppp)Cl_2$ (0.012 g, 0.02 mmol), aryl-halide (1.00 mmol) and triphenylphosphine (0.289 g, 1.00 mmol) in benzylamine (5.0 ml, excess) was added to a saturated solution of CuTp*CO (**2.11**) (0.194 g, 1.00 mmol) in THF (15 ml) in a Schlenk flask. The flask was immediately sealed and the solution heated at 85°C with stirring for either 90 mins or 20 mins. Standard acidic work-up (layering between acidified reaction solution and CH_2Cl_2, separation of the organic layer, washing with water, drying over $MgSO_4$) was followed by GC analysis using a phenyl ether standard of known concentration.

Carbonylative cross-coupling reactions performed with ^{11}CO – 'hot chemistry' in glass vial

See description in Chapter 3.

7.1.3 Experimental Procedures for Chapter 4

2'-(Diphenyphosphino)acetophenone[2] was prepared as reported previously.

Ligand Syntheses

1-(2'-Diphenylphosphino)phenyl-3-dimethylamino-2-propene-1-one (4.1)

Using a variation of a literature procedure,[3] 2'-(diphenyphosphino)acetophenone (12.350 g, 40.6 mmol) and *N,N*-dimethylformamide dimethylacetal (25 ml, excess) were heated at 120°C for 12 hrs over which time the yellow solution turned deep brown. After cooling to room temperature, the excess *N,N*-dimethylformamide dimethyl acetal was removed *in vacuo* to leave a dark orange solid which was broken up and stirred in pentane (100 ml) and filtered to produce an orange solid which was

dried *in vacuo* (13.482 g, 37.5 mmol, 92 %). Analysis was carried out on a sample recrystallised from CH_2Cl_2/hexane. Anal. (%) calc. (found) for $C_{23}H_{22}NOP$: C, 76.9 (76.8); H, 6.17 (6.03); N, 3.90 (3.83). IR (KBr disc): ν_{max}/cm^{-1} = 1637 (CO). ^1H NMR (+ 25°C, $CDCl_3$, 400 MHz): δ = 7.64 [dd ($^3J_{HH}$ = 6.9 Hz, $^4J_{HH}$ = 3.8 Hz), 1H, 6-Ph], 7.38 (ddd ($^3J_{HH}$ = 7.7 Hz, $^3J_{HH}$ = 7.6 Hz, $^4J_{HH}$ = 1.2 Hz), 1H, 5-Ph), 7.27-7.35 [m, 11H, 4-Ph + *o,m,p*-Ph + $CHNMe_2$], 7.06 [dd ($^3J_{HH}$ = 7.3 Hz, $^4J_{HH}$ = 3.5 Hz), 1H, 3-Ph], 5.43 [d ($^3J_{HH}$ = 12.6 Hz), 1H, COCH], 2.96 [s, 3H, NCH_3], 2.71 [s, 3H, NCH_3]; $^{31}P\{^1H\}$ NMR (+25°C, $CDCl_3$, 162.05 MHz), δ = -10.3 [s]. MS(EI): *m/z* = 359 $[M]^+$.

3-[2-(Diphenylphosphino)phenyl]pyrazole, *Hpz^{phos}* (4.2)

Hydrazine hydrate (10 ml, excess) was added dropwise to a solution of **4.1** (12.000 g, 33.4 mmol) in hot ethanol (150 ml) and stirred under reflux for 3 hrs. Removal of the solvent gave an orange solid to which was added water (50 ml) and the solid was collected by filtration. The aqueous washings were extracted into $CHCl_3$ (200 ml) and the organic fraction was separated and used to dissolve the solid. Drying ($MgSO_4$), filtration and concentration followed by recrystallisation from $CHCl_3$/hexane gave a colourless solid (9.930 g, 30.2 mmol, 91%). Anal. (%) calc. (found) for $C_{21}H_{17}N_2P$: C, 76.8 (77.0); H, 5.22 (5.00); N, 8.53 (8.35). IR (KBr disc): ν_{max}/cm^{-1} = 3187 (NH). ^1H NMR (+25°C, $CDCl_3$, 500 MHz): δ = 10.57 [s, 1H, NH], 7.60 [dd ($^3J_{HH}$ = 7.1 Hz, $^4J_{HH}$ = 3.7 Hz), 1H, 6-Ph], 7.48 [d ($^3J_{HH}$ = 2.0 Hz), 1H, 5-pz], 7.42 [ddd ($^3J_{HH}$ = 7.7 Hz, $^3J_{HH}$ = 7.6 Hz, $^4J_{HH}$ = 1.3 Hz), 1H, 5-Ph], 7.33-7.37 [m, 6H, *m,p*-Ph], 7.26-7.31 [m, 5H, *o*-Ph + 4-Ph], 7.03 [ddd ($^3J_{HP}$ = 7.8 Hz, $^3J_{HH}$ = 4.2 Hz, $^4J_{HH}$ = 1.1 Hz), 1H, 3-Ph], 6.34 [m, 1H, 4-pz]. $^{13}C\{^1H\}$ NMR (+ 25°C, $CDCl_3$, 500 MHz): δ = 146.9 [s, 3-pz], 140.0 [s, 5-pz], 137.1 [d, ($^1J_{CP}$ = 10.6 Hz), *i*-Ph], 136.1 [d ($^2J_{CP}$ = 17.3 Hz), 1-Ph], 134.3 [s, 3-Ph], 133.9 [d, ($^2J_{CP}$ = 19.7 Hz), *o*-Ph], 131.8 [s, 2-Ph], 130.0 [d ($^3J_{CP}$ = 5.5 Hz), 6-Ph], 128.9 [s, 4-Ph], 128.8 [s, 5-Ph], 128.6 [d ($^3J_{CP}$ = 7.6 Hz), *m*-Ph], 128.3 [s, *p*-Ph], 106.5 [s, 4-pz]. $^{31}P\{^1H\}$ NMR (+25°C, $CDCl_3$, 162.05 MHz): δ = -11.4 [s]. MS(EI): *m/z* = 328 $[M]^+$.

3-[2-(Diphenylphosphinoyl)phenyl]pyrazole, *Hpz$^{phos(O)}$* (4.3)

A solution of Hpz^{phos} (**4.2**) (0.300 g, 0.91 mmol) and H_2O_2 (27.5 % in H_2O, 135 μL, 1.10 mmol) in CH_2Cl_2 (30 ml) was stirred for 1 hr after which time H_2O (40 ml) was added and the organic layer separated, dried ($MgSO_4$) and concentrated to dryness to give a colourless solid (0.201 g, 0.58 mmol, 63 %). Crystals suitable for X-ray studies

were grown by slow diffusion of pentane in a chloroform solution of this complex. Anal. (%) calc. (found) for $C_{21}H_{17}N_2OP$: C, 73.3 (73.1); H, 4.98 (5.01); N, 8.14 (8.02). IR (nujol): ν_{max}/cm^{-1} = 3186 (NH). ^1H NMR (+25°C, $CDCl_3$, 500 MHz): δ = 13.24 [s, 1H, NH], 7.78 [ddd ($^3J_{HH}$ = 7.8 Hz, $^4J_{HH}$ = 4.2 Hz, $^5J_{HH}$ = 1.0 Hz), 1H, 6-Ph], 7.61 [m, 5H, *o*-Ph + 5-Ph], 7.50 [m, 2H, *p*-Ph], 7.41 [m, 4H, *m*-Ph], 7.32 [d ($^3J_{HH}$ = 1.8 Hz), 1H, 5-pz], 7.30 [m, 1H, 4-Ph], 7.14 [ddd ($^3J_{HP}$ = 14.6 Hz, $^3J_{HH}$ = 7.8 Hz, $^4J_{HH}$ = 1.1 Hz), 1H, 3-Ph], 6.25 [s, 1H, 4-pz]. $^{13}C\{^1H\}$ NMR (+25°C, $CDCl_3$, 500 MHz): δ = 141.8 [s, 3-pz], 139.7 [s, 5-pz], 134.9 [d ($^2J_{CP}$ = 8.0 Hz), 1-Ph], 134.1 [d ($^2J_{CP}$ = 12.1 Hz), 3-Ph], 132.7 [s, 5-Ph], 132.2 [s, *p*-Ph], 131.7 [d ($^2J_{CP}$ = 9.8 Hz), *o*-Ph], 131.3 [d ($^3J_{CP}$ = 9.6 Hz), 6-Ph], 130.4 [d ($^1J_{CP}$ = 106.4 Hz), *i*-Ph], 130.0 [d ($^1J_{CP}$ = 99.2 Hz), 2-Ph], 128.6 [d ($^3J_{CP}$ = 12.4 Hz), *m*-Ph], 127.3 [d ($^3J_{CP}$ = 12.4 Hz), 4-Ph], 105.3 [s, 4-pz]. $^{31}P\{^1H\}$ NMR (+25°C, $CDCl_3$, 162 MHz): δ = +35.8 [s]. MS(EI): *m/z* = 344 $[M]^+$.

3-[2-(Diphenylphosphinothioyl)phenyl]pyrazole, *Hpz$^{phos(S)}$* (4.4)

A solution of Hpz^{phos} (**4.2**) (0.300 g, 0.91 mmol) and S_8 (0.044 g, 0.17 mmol) in CH_2Cl_2 (15 ml) was stirred for 1 hr and then reduced in volume to 5 ml and hexane added dropwise. The resultant off-white precipitate was collected by filtration, washed with hexane and dried *in vacuo* (0.250 g, 0.69 mmol, 76 %). Anal. (%) calc. (found) for $C_{21}H_{17}N_2PS$: C, 70.0 (70.1); H, 4.75 (4.83); N, 7.77 (7.66). IR (KBr disc): ν_{max}/cm^{-1} = 3220 (NH). ^1H NMR (+25°C, $CDCl_3$, 500 MHz): δ = 12.54 [s, 1H, NH], 7.82 [dd ($^3J_{HH}$ = 13.6 Hz, $^4J_{HH}$ = 7.1 Hz), 4H, o-Ph], 7.57 [m, 2H, 6-Ph & 5-Ph], 7.44 [m, 2H, *p*-Ph], 7.37 [m, 4H, *m*-Ph], 7.37 [m, 1H, 4-Ph], 7.18 [dd ($^3J_{HP}$ = 14.9 Hz, $^3J_{HH}$ = 8.0 Hz), 1H, 3-Ph], 7.17 [d ($^3J_{HH}$ = 1.8 Hz), 1H, 5-pz], 6.08 [s, 1H, 4-pz]. $^{13}C\{^1H\}$ NMR (+25°C, $CDCl_3$, 500 MHz): δ = 139.7 [s, 3-pz], 139.3 [s, 5-pz], 133.4 [d ($^2J_{CP}$ = 11.2 Hz), 3-Ph], 133.2 [s, *i*-Ph], 132.6 [s, 2-Ph], 132.4 [d ($^3J_{CP}$ = 9.8 Hz), 6-Ph], 132.0 [d ($^2J_{CP}$ = 10.7 Hz), *o*-Ph], 131.9 [s, 5-Ph], 131.7 [s, *p*-Ph], 130.7 [s, 1-Ph], 128.4 [d ($^3J_{CP}$ = 12.7 Hz), *m*-Ph], 128.1 [d ($^3J_{CP}$ = 12.3 Hz), 4-Ph], 105.9 [s, 4-pz]. $^{31}P\{^1H\}$ NMR (+25°C, $CDCl_3$, 162 MHz): δ = +43.3 [s]. MS(EI): *m/z* = 360 $[M]^+$.

Complex Syntheses

Caution! - Synthesis of palladium perchlorate complexes - Although we did not observe any explosive behaviour with the perchlorate compounds described below, all

metal perchlorates must be treated as potentially explosive species and appropriate safety measures must be taken. See for example reference [4].

[Pd(Hpz^{phos})Cl$_2$] (4.5)

Hpz^{phos} (**4.2**) (0.330 g, 1.00 mmol) in CH_2Cl_2 (10 ml) was added dropwise to a stirred solution of Pd(COD)Cl$_2$ (0.290 g, 1.00 mmol) in CH_2Cl_2 (20 ml). The orange solution was stirred for 10 mins causing a yellow solid to precipitate. This was collected by filtration, stirred with hexane (20 ml), filtered and dried *in vacuo* to give a bright yellow solid (0.460 g, 0.91 mmol, 91 %). Yellow needles suitable for X-ray studies were grown by slow diffusion of pentane in a chloroform solution of the complex. Anal. (%) calc. (found) for $C_{21}H_{17}Cl_2N_2PPd$: C, 49.9 (49.8); H, 3.39 (3.33); N, 5.54 (5.42). IR (KBr disc): ν_{max}/cm^{-1} = 3230 (NH). ^{1}H NMR (+25°C, $CDCl_3$, 500 MHz): δ = 13.14 [s, 1H, NH] 7.90 [ddd ($^3J_{HH}$ = 7.9 Hz, $^4J_{HH}$ = 4.4 Hz, $^5J_{HH}$ = 1.0 Hz), 1H, 6-Ph], 7.70 [dddd ($^3J_{HH}$ = 7.9 Hz, $^3J_{HH}$ = 7.9 Hz, $^4J_{HH}$ = 1.5 Hz, $^5J_{HP}$ = 1.5 Hz), 1H, 5-Ph], 7.65 [dd ($^3J_{HH}$ = 2.8 Hz, $^3J_{HH}$ = 1.8 Hz), 1H, 5-pz], 7.61 [m, 4H, *o*-Ph], 7.54 [m, 2H, *p*-Ph], 7.44 [m, 4H, *m*-Ph], 7.42 [m, 1H, 4-Ph], 7.05 [ddd ($^3J_{HP}$ = 10.8 Hz, $^3J_{HH}$ = 7.9 Hz, $^4J_{HH}$ = 1.2 Hz), 1H, 3-Ph], 6.86 [m, 1H, 4-pz]. ^{31}P{^{1}H} NMR (+25°C, $CDCl_3$, 162 MHz): δ = +25.6 [s]. MS(EI): *m/z* = 471 [M-Cl]$^+$.

[Pd(Hpz^{phos})$_2$]Cl$_2$ (4.6)

Pd(COD)Cl$_2$ (0.065 g, 0.23 mmol) in CH_2Cl_2 (15 ml) was added dropwise to a solution of Hpz^{phos} (**4.2**) (0.150 g, 0.46 mmol) in CH_2Cl_2 (15 ml). After stirring overnight, the volume of the solvent was reduced to 10 ml and hexane (10 ml) was added causing a yellow solid to precipitate. This was collected by filtration and dried *in vacuo* (0.150 g, 0.18 mmol, 78 %). Yellow crystals suitable for X-ray studies were grown by slow diffusion of pentane in a chloroform solution of this complex. Anal. (%) calc. (found) for $C_{42}H_{34}Cl_2N_4P_2Pd.2CH_2Cl_2$: C, 52.6 (52.6); H, 3.82 (3.62); N, 5.58 (5.37). IR (KBr disc): ν_{max}/cm^{-1} = 3290 (NH). ^{1}H NMR (-50°C, $CDCl_3$, 400 MHz): δ = 14.54 [s, 1H, NH], 8.05 [dd ($^3J_{HH}$ = 12.8 Hz, $^4J_{HH}$ = 7.9 Hz), 1H, Ph], 7.96 [dd ($^3J_{HH}$ = 7.5 Hz, $^4J_{HH}$ = 3.4 Hz), 1H, 6-Ph], 7.96 [s (br), 2H, Ph], 7.76 [s, 1H, 5-pz], 7.64 [dd, ($^3J_{HH}$ = 7.6 Hz, $^3J_{HH}$ = 7.6 Hz), 1H, 5-Ph], 7.42 [m, 3H, Ph], 7.30 [dd ($^3J_{HH}$ = 7.7 Hz, $^3J_{HH}$ = 7.7 Hz), 1H, 4-Ph], 7.22 [m, 1H, Ph], 7.06 [dd ($^3J_{HH}$ = 7.4 Hz), 1H, Ph], 6.79 [m, 2H, 3-Ph + Ph], 6.53 [s, 1H, 4-pz], 5.94 [dd ($^3J_{HH}$ = 9.0 Hz, $^3J_{HH}$ = 9.0

Hz), 1H, Ph]. $^{31}P\{^{1}H\}$ NMR (+25°C, $CDCl_3$, 162 MHz): δ = +31.6 [s]. MS(ESI): *m/z* = 761 $[Pd(Hpz^{phos})_2]^+$.

Alternative synthesis of $[Pd(Hpz^{phos})_2]Cl_2$ (4.6)

A solution of Hpz^{phos} (**4.2**) (0.032 g, 0.10 mmol) in CH_2Cl_2 (10 ml) was added to a solution of **4.5** (0.050 g, 0.10 mmol) in CH_2Cl_2 (10 ml) and stirred overnight. The solution was concentrated to half the volume and hexane (10 ml) added dropwise causing a yellow solid to precipitate. The solid was collected by filtration and dried *in vacuo* to give **4.6** as evidenced by identical ^{1}H and $^{31}P\{^{1}H\}$ NMR data for both compounds (0.058 g, 0.07 mmol, 70%).

$[Pd(Hpz^{phos})_2][ClO_4]_2$ (4.7)

$Pd(COD)Cl_2$ (0.087 g, 0.30 mmol) in CH_2Cl_2 (5 ml) was added dropwise to a solution of Hpz^{phos} (**4.2**) (0.200 g, 0.61 mmol) in CH_2Cl_2 (20 ml). After stirring for 1 hr, silver perchlorate (0.114 g, 0.64 mmol) was added and the flask stirred overnight in the dark during which time AgCl precipitated. Filtration through celite and concentration of the filtrate to dryness gave a yellow powder which was stirred with hexane (20 ml), filtered and recrystallised from hot methanol to give a yellow solid (0.180 g, 0.19 mmol, 61 %). Single crystals for X-ray analysis were grown in an NMR tube by layering hexane above a CH_2Cl_2 solution of the product. Anal. (%) calc. (found) for $C_{42}H_{34}Cl_2N_4O_8P_2Pd$: C, 52.4 (52.5); H, 3.56 (3.69); N, 5.82 (5.73). IR (nujol): ν_{max}/cm^{-1} = 3302 (NH). ^{1}H NMR (+25°C, d_6-acetone, 400 MHz): δ = 13.42 [s, 1H, NH], 8.19 [dd ($^{3}J_{HH}$ = 2.8 Hz, $^{4}J_{HH}$ = 0.7 Hz), 1H, 5-pz], 8.08 [ddd ($^{3}J_{HH}$ = 7.8 Hz, $^{4}J_{HH}$ = 4.3 Hz, $^{5}J_{HH}$ = 1.2 Hz), 1H, 6-Ph], 7.90 (m (br), 2H, Ph), 7.85 [dd ($^{3}J_{HH}$ = 7.8 Hz, $^{3}J_{HH}$ = 7.8 Hz), 1H, 5-Ph], 7.40-7.70 [m (br), 4H, Ph], 7.59 [dd ($^{3}J_{HH}$ = 8.0 Hz, $^{3}J_{HH}$ = 8.0 Hz), 1H, 4-Ph], 7.08-7.25 [m (br), 2H, Ph], 7.05 [ddd ($^{3}J_{HP}$ = 11.1 Hz, $^{3}J_{HH}$ = 7.9 Hz, $^{4}J_{HH}$ = 0.8 Hz), 1H, 3-Ph], 6.99 [dd ($^{3}J_{HH}$ = 7.8 Hz, $^{3}J_{HH}$ = 1.6 Hz), 1H, 4-pz]. $^{31}P\{^{1}H\}$ NMR (+25°C, d_6-acetone, 162 MHz): δ = +34.1 [s]. MS(FAB +ve), *m/z* = 761 $[Pd(Hpz^{phos})_2]^+$.

Attempted synthesis of $[Pd(Hpz^{phos(O)})Cl_2]$ (4.8)

$Hpz^{phos(O)}$ (**4.3**) (0.030 g, 0.09 mmol) in CH_2Cl_2 (10 ml) was added dropwise to a refluxing solution of $Pd(COD)Cl_2$ (0.030 g, 0.10 mmol) in CH_2Cl_2 (20 ml). The refluxing solution was stirred for 16 hrs and $^{31}P\{^{1}H\}$ NMR of the reaction solution

recorded (+25°C, $CH_2Cl_2/CDCl_3$, 162.05 MHz): δ = +32.8 [s], indicating formation of the bis-adduct **3.9**.

[Pd(Hpz$^{phos(O)}$)$_2$Cl$_2$] (4.9)

$Pd(COD)Cl_2$ (0.021 g, 0.07 mmol) in CH_2Cl_2 (10 ml) was added dropwise to a solution of Hpz$^{phos(O)}$ (**4.3**) (0.050 g, 0.15 mmol) in CH_2Cl_2 (20 ml). After stirring for 2 hrs, half the solvent was evaporated under a stream of N_2 to give a yellow solution to which hexane was added dropwise (5 ml) causing a pale yellow precipitate to form. This was collected by filtration, washed with hexane (5 ml) and dried *in vacuo* to give a pale yellow powder (0.052 g, 0.06 mmol, 83 %). Yellow crystals suitable for X-ray studies were grown by slow diffusion of pentane in a chloroform solution of this complex. Anal. (%) calc. (found) for $C_{42}H_{34}Cl_2N_4O_2P_2Pd$: C, 58.3 (58.2); H, 3.96 (4.00); N, 6.47 (6.39). IR (nujol): ν_{max}/cm^{-1} = 3196 (NH). ^1H NMR (+25°C, $CDCl_3$, 400 MHz), δ = 13.51 [s, 1H, NH], 7.81 [dd ($^3J_{HH}$ = 2.1 Hz), 1H, 5-pz], 7.74 [m, 4H, *o*-Ph], 7.61 [dd ($^3J_{HH}$ = 7.5 Hz, $^3J_{HH}$ = 7.5 Hz), 1H, 5-Ph], 7.57 [dd ($^3J_{HH}$ = 7.6 Hz, $^3J_{HH}$ = 7.6 Hz), 1H, 6-Ph], 7.53 [m, 2H, *p*-Ph], 7.47 [m, 4H, *m*-Ph], 7.37 [dd ($^3J_{HH}$ = 7.5 Hz, $^3J_{HH}$ = 7.5 Hz), 1H, 4-Ph], 7.22 [dd ($^3J_{HP}$ = 14.2 Hz, $^3J_{HH}$ = 7.5 Hz), 1H, 3-Ph], 6.19 [dd ($^3J_{HH}$ = 2.2 Hz), 1H, 4-pz]. $^{31}P\{^1H\}$ NMR (+25°C, $CDCl_3$, 162 MHz): δ = +32.7 [s]. MS(FAB +ve), *m/z* = 869 [Pd(Hpz$^{phos(O)}$)$_2$Cl$_2$]$^+$.

[Pd(Hpz$^{phos(O)}$)$_2$][ClO$_4$]$_2$ (4.10)

$AgClO_4$ (0.025 g, excess) was added to a suspension of **4.9** (0.034 g, 0.04 mmol) in CH_2Cl_2 (5 ml). After stirring overnight, half the solvent was evaporated under a stream of N_2 to give a yellow solution to which hexane was added dropwise (5 ml) causing a yellow precipitate to form. This was collected by filtration, washed with hexane (5 ml) and dried *in vacuo* to give **4.10** as yellow powder (0.024 g, 0.02 mmol, 60 %). Yellow crystals suitable for X-ray studies were grown by slow diffusion of pentane in a chloroform solution of this complex. Anal. (%) calc. (found) for $C_{42}H_{34}Cl_2N_4O_{10}P_2Pd$: C, 50.8 (50.7); H, 3.45 (3.43); N, 5.64 (5.58). IR (CH_2Cl_2 solution): ν_{max}/cm^{-1} = 3686 (NH). ^1H NMR (+25°C, $CDCl_3$, 400 MHz): δ = 12.35 [s, 1H, NH], 8.27 [dd ($^3J_{HH}$ = 7.4 Hz, $^4J_{HH}$ = 4.4 Hz), 1H, 6-Ph], 8.12 [dd ($^3J_{HH}$ = 7.7 Hz, $^3J_{HH}$ = 7.7 Hz), 1H, 5-Ph], 7.60-7.85 [m, 10 H, *o,m,p*-Ph], 7.35-7.50 [m, 2 H, 4,3-Ph], 7.31 [d ($^3J_{HH}$ = 2.0 Hz), 1H, 5-pz], 6.02 [m, 1H, 4-pz]. $^{31}P\{^1H\}$ NMR (+ 25°C, $CDCl_3$, 162 MHz): δ = +53.9 [s]. MS(FAB +ve), *m/z* = 900 [Pd(Hpz$^{phos(O)}$)$_2$ClO$_4$]$^+$.

[Pd-COD-pz$^{phos(O)}$]$_2$[ClO$_4$]$_2$ (4.11)

A solution of Pd(COD)Cl$_2$ (0.041 g, 0.15 mmol) in CH_2Cl_2 (5ml) was added dropwise to a solution of Hpz$^{phos(O)}$ (**4.3**) (0.100 g, 0.29 mmol). After 2 hrs stirring, $AgClO_4$ (0.098 g, 0.44 mmol) was added and the mixture was stirred in the dark for 1 week. MeOH (1 ml) was then added and stirring resumed for 5 days. The mixture was filtered through celite and the solvent removed to give a yellow residue. This was recrystallised from hot MeOH causing a white powder to precipitate. Collection by filtration and drying *in vacuo* yielded a white powder (0.030 g, 0.02 mmol, 32 % from palladium). Anal. (%) calc. (found) for $C_{58}H_{56}Cl_2N_4O_{10}P_2Pd_2$: C, 53.0 (52.9); H, 4.29 (4.35); N, 4.26 (4.14). IR (KBr disc): ν_{max}/cm^{-1} = 2931w, 1630w, 1438m, 1384w, 1088s. ^{1}H NMR (+25°C, $CDCl_3$, 400 MHz): δ = 7.84 [dd ($^3J_{HH}$ = 7.6 Hz, $^3J_{HH}$ = 7.6 Hz), 1H, 5-Ph], 7.68 [m, 1H, 6-Ph], 7.62 [m, 6H, *o,p*-Ph], 7.53 [dd ($^3J_{HH}$ = 6.9 Hz, $^3J_{HH}$ = 6.9 Hz), 1H, 4-Ph], 7.48 [d ($^3J_{HH}$ = 2.5 Hz), 1H, 5-pz], 7.37 [m, 1H, 3-Ph], 7.34 [m, 4H, *m*-Ph], 6.17 [dd (J_{HH} = 15.1 Hz, J_{HH} = 8.5 Hz), 1H, 12-COD], 5.95 [m, 1H, 11-COD], 5.80 [d ($^3J_{HH}$ = 2.5 Hz), 1H, 4-pz], 5.40 [d (J_{HH} = 12.4 Hz), 1H, 10-COD], 3.52 [m, 1H, 9-COD], 3.10 [d (J_{HH} = 17.4 Hz), 1H, 8-COD], 2.76 [dtd (J_{HH} = 13.2 Hz, J_{HH} = 12.9 Hz, J_{HH} = 4.2 Hz), 1H, 7-COD], 2.62 [d (J_{HH} = 4.9 Hz), 1H, 6-COD], 2.52 [m, 1H, 5-COD], 2.28 [d (J_{HH} = 13.7 Hz), 1H, 4-COD], 2.04 [dt (J_{HH} = 13.7 Hz, J_{HH} = 9.4 Hz), 1H, 3-COD], 1.61 [m, 1H, 2-COD], 1.30 [m, 1H, 1-COD]. $^{31}P\{^1H\}$ NMR (+25°C, $CDCl_3$, 162 MHz): δ = +40.7 [s]. MS(ESI +ve): *m/z* = 1169 [(Pd-COD-pz$^{phos(O)}$)$_2$ + 55]$^+$.

[Pd(Hpz$^{phos(S)}$)Cl$_2$] (4.12)

A solution of Hpz$^{phos(S)}$ (**4.4**) (0.060 g, 0.17 mmol) in CH_2Cl_2 (5 ml) was added dropwise to a stirred solution of Pd(COD)Cl$_2$ (0.048 g, 0.17 mmol) in CH_2Cl_2 (5 ml) causing a yellow/orange solid to precipitate. This was collected by filtration, washed with hexane. The pale orange solid was then stirred with ether, collected by filtration and dried *in vacuo*. Anal. (%) calc. (found) for $C_{21}H_{17}Cl_2N_2PPdS$: C, 46.9 (45.4); H, 3.19 (3.36); N, 5.21 (4.49). IR (KBr disc): ν_{max}/cm^{-1} = 3230 (NH). ^{1}H NMR (+25°C, d_6-DMSO, 400 MHz) - not clear in aromatic region due to impurities. Assignable peaks include: δ = 14.19 [s(br), 1H, NH], 6.08 [t (J_{HH} = 2.1 Hz), 4-pz]. $^{31}P\{^1H\}$ NMR (+25°C, d_6-DMSO, 162 MHz): δ = +43.3 [s].

Attempted synthesis of $[Pd(Hpz^{phos(S)})_2Cl_2]$ (4.13)

A solution of $Pd(COD)Cl_2$ (0.032 g, 0.11 mmol) in CH_2Cl_2 (10 ml) was added dropwise to a solution of $Hpz^{phos(S)}$ (**4.4**) (0.080 g, 0.22 mmol) in CH_2Cl_2 (10 ml). Addition of the last few drops caused a yellow solid to precipitate and the mixture was stirred for 16 hrs. Filtration gave a yellow/orange solid which was washed with methanol (5 ml) and pentane (5 ml) and dried in *vacuo.* Attempts to dissolve this solid in common organic solvents were unsuccessful. Anal. (%) calc. for $[Pd(Hpz^{phos(S)})_2Cl_2]$ ($C_{42}H_{34}Cl_2N_4P_2PdS_2$): C, 56.2; H, 3.82; N, 6.24; for $[Pd(Hpz^{phos(S)})Cl_2]$ ($C_{21}H_{17}Cl_2N_2PPdS$): C, 46.9; H, 3.19; N, 5.21; found: C, 47.1; H, 3.04; N, 5.06. IR (KBr disc): ν_{max}/cm^{-1} = 3230 (NH). MS(ESI +ve): *m/z* = 825 $[Pd(Hpz^{phos(S)})_2]^+$, 1008 $[Pd(Hpz^{phos(S)})_2 + 183]^+$.

$[Pd(Hpz^{phos(S)})_2][ClO_4]_2$ (4.14)

A solution of $Pd(COD)Cl_2$ (0.032 g, 0.11 mmol) in CH_2Cl_2 (5 ml) was added dropwise to a solution of $Hpz^{phos(S)}$ (**4.4**) (0.080 g, 0.22 mmol) in CH_2Cl_2 (5 ml) causing a yellow solid to precipitate. $AgClO_4$ (0.075 g, 0.33 mmol) was added and the suspension stirred in the dark for 30 mins. The $^{31}P\{^1H\}$ NMR spectrum was recorded at this point and revealed a mixture of four species at around 44 ppm and upon standing, crystals suitable for X-ray analysis formed in the NMR tube. The solution was stirred for a further 24 hrs during which time the yellow solid redissolved and a fine pale precipitate formed (AgCl). The mixture was filtered, concentrated to approximately half the volume and hexane added dropwise causing a yellow solid to precipitate. The solid was collected by filtration, washed with hexane, then ether and dried *in vacuo*. The low solubility of this solid meant that purification was difficult and further attempts at isolating the pure product failed. MS(ESI +ve): *m/z* = 927 $[Pd(Hpz^{phos(S)})_2ClO_4]^+$, 825 $[Pd(Hpz^{phos(S)})_2]^+$.

Catalyst testing

Carbonylation reactions were performed in a Radley's carousel reactor. A solution of PdL_n (2 mol %) in benzylamine (1 ml) was added to a tube containing benzylamine (4 ml) preheated to 100°C under an atmosphere of CO. Iodobenzene (1.00 mmol) was added and the mixture stirred at 100°C. Yields of amide were monitored after 10 and 120 mins by removal of an aliquot of solution for GC analysis.

7.1.4 Experimental Procedures for Chapter 5

2'-(Diphenyphosphino)acetophenone,[2] Hpz^{py} [3] and $RuCl_2(DMSO)_4$[5] were prepared as reported previously.

$K[Tp^{py}]$ (5.1)

This was synthesised according to the literature procedure[6] and characterised as follows: IR (KBr disc): ν_{max}/cm^{-1} = 2446 (BH). ^1H NMR (+25°C, $CDCl_3$, 400 MHz): δ = 8.56 [ddd ($^3J_{HH}$ = 4.9 Hz, $^4J_{HH}$ = 1.8 Hz, $^5J_{HH}$ = 0.9 Hz), 3H, 3-Py], 7.79 [ddd ($^3J_{HH}$ = 8.0 Hz, $^4J_{HH}$ = 1.0 Hz, $^4J_{HH}$ = 1.0 Hz), 3H, 6-Py], 7.75 [d ($^3J_{HH}$ = 2.3 Hz), 3H, 5-pz], 7.72 [m, 3H, 5-Py], 7.16 [ddd ($^3J_{HH}$ = 7.4 Hz, $^4J_{HH}$ = 4.9 Hz, $^5J_{HH}$ = 1.3 Hz), 3H, 4-Py], 6.67 [d ($^3J_{HH}$ = 4.9 Hz), 3H, 4-pz], 4.90 [m(br), 1H, BH]. ^{11}B NMR (+25°C, $CDCl_3$, 128 MHz): δ = -1.4 [d ($^1J_{BH}$ = 103.1 Hz)]. MS(FAB-ve): *m/z* = 444 $[Tp^{py}]^-$.

$Cu_4(Tp^{py})_4$ (5.2)

CH_2Cl_2 (15 ml) was added to a mixture of $K[Tp^{py}]$ (**5.1**) (0.121 g, 0.25 mmol) and CuCl (0.025 g, 0.25 mmol) to form an orange solution. After stirring for 30 mins, the mixture was allowed to settle, filtered and concentrated *in vacuo* to give an orange powder (0.208 g, 0.20 mmol, 81 %). Anal. (%) calc. (found) for $C_{24}H_{19}BCuN_9$: C, 56.8 (56.7); H, 3.77 (3.73); N, 24.8 (24.9). IR (KBr disc): ν_{max}/cm^{-1} = 2430 (BH). ^1H NMR (+25°C, CD_2Cl_2, 400 MHz): δ = 8.23 [s(br), 3H, 3-Py], 7.68 [m(br), 6H, 5-Py + 6-Py], 7.12 [s(br), 6H, 4-Py + 5-pz], 6.48 [s(br), 3H, 4-pz], 4.63 [m(br), 1H, BH]. MS(ESI +ve): *m/z* = 1016 $[Cu_2(Tp^{py})_2]^+$, 1079 $[Cu_3(Tp^{py})_2]^+$. ^1H NMR (-30°C, CD_2Cl_2, 400 MHz): δ = 8.52 [d ($^3J_{HH}$ = 4.4 Hz), 3H, $(3\text{-Py})_A$], 8.31 [s(br), 3H, $(3\text{-Py})_B$], 8.22 [d ($^3J_{HH}$ = 4.6 Hz), 3H, $(3\text{-Py})_C$], 8.08 [d ($^3J_{HH}$ = 4.0 Hz), 3H, $(3\text{-Py})_D$], 8.01 [d ($^3J_{HH}$ = 8.1 Hz), 3H, $(6\text{-Py})_A$], 7.84 [m, 3H, $(5\text{-Py})_C$], 7.67 [m, 15H, $(5\text{-Py})_{A,B,D}$ + $(6\text{-Py})_{B,C}$], 7.31 [d ($^3J_{HH}$ = 1.7 Hz), 3H, $(5\text{-pz})_B$], 7.27 [d ($^3J_{HH}$ = 8.0 Hz), 3H, $(6\text{-Py})_D$], 7.23 [m, 3H, $(4\text{-Py})_C$], 7.12 [m, 9H, $(4\text{-Py})_{A,B,D}$], 6.92 [d ($^3J_{HH}$ = 1.9 Hz), 3H, $(5\text{-pz})_C$], 6.84 [s, 3H, $(5\text{-pz})_D$], 6.75 [s(br), 3H, $(5\text{-pz})_A$], 6.72 [d ($^3J_{HH}$ = 1.7 Hz), 3H, $(4\text{-pz})_B$], 6.58 [d ($^3J_{HH}$ = 1.9 Hz), 3H, $(4\text{-pz})_C$], 6.29 [s, 3H, $(4\text{-pz})_A$], 5.64 [d ($^3J_{HH}$ = 1.9 Hz), 3H, $(4\text{-pz})_D$], 4.40 [s(br), 4H, $(BH)_{A,B,C,D}$].

Cu[Tp^{py}]CO (5.3)

A solution of **5.2** in CH_2Cl_2 (15 ml) was made *in situ* from CuCl (0.025 g, 0.25 mmol) and K[Tp^{py}] (**5.1**) (0.121 g, 0.25 mmol) under an atmosphere of nitrogen. The orange solution was filtered and CO gas was bubbled through the solution for 5 mins. This caused the solution to become yellow-orange in colour. IR (CH_2Cl_2): ν_{max}/cm^{-1} = 2081s (CO). Successive vacuum/nitrogen cycles caused νCO to become progressively weaker. Bubbling of CO through this solution caused νCO to reappear as a strong absorption. ^{1}H NMR (+25°C, CD_2Cl_2, 400 MHz): δ = 8.70 [d ($^3J_{HH}$ = 4.3 Hz), 3H, 3-Py], 7.87 [d, ($^3J_{HH}$ = 7.9 Hz), 3H, 6-Py], 7.80 [d, ($^3J_{HH}$ = 2.1 Hz), 3H, 5-pz], 7.77 [m, 3H, 5-Py], 7.29 [ddd, ($^3J_{HH}$ = 7.3 Hz, $^3J_{HH}$ = 4.9 Hz, $^4J_{HH}$ = 0.8 Hz), 3H, 4-Py], 6.71 [d ($^3J_{HH}$ = 2.3 Hz, 3H, 4-pz], 4.64 [m(br), 1H, BH].

Potassium tetrakis{3-[2-(diphenylphosphino)phenyl]pyrazol-1-yl}borate, *K[Tkp^{phos}]* (5.4)

A mixture of KBH_4 (0.025 g, 0.46 mmol) and Hpz^{phos} (**4.2**) (0.750 g, 2.28 mmol) was heated gradually to 240°C and heated at this temperature for 2 hrs. The mixture was allowed to cool forming a brown solid which was dissolved in CH_2Cl_2 (10 ml), filtered and concentrated to dryness to give a yellow powder. Attempts to remove the excess starting material from the crude product were unsuccessful and a 4 : 5 molar ratio of Hpz^{phos} : K[Tkp^{phos}] was obtained as judged by NMR spectroscopy. ^{1}H NMR (+25°C, $CDCl_3$, 400 MHz): δ = 7.57 [dd ($^3J_{HH}$ = 7.1 Hz, $^4J_{HH}$ = 3.8 Hz), 4H, 6-Ph], 7.1-7.4 [m, *o,m,p*-Ph, 4,5-Ph of Hpz^{phos}/K(Tkp^{phos})], 7.06 [d ($^3J_{HH}$ = 2.1 Hz), 4H, 5-pz], 6.87 [dd ($^3J_{HH}$ = 7.1 Hz, $^3J_{HH}$ = 4.3 Hz), 1H, 3-Ph], 6.06 [d ($^3J_{HH}$ = 1.6 Hz), 1H, 4-pz]. ^{31}P{^{1}H} NMR (+25°C, $CDCl_3$, 162 MHz): δ = -10.0 [s, K(Tkp^{phos})], -11.7 [s, Hpz^{phos}]. ^{11}B NMR (+25°C, $CDCl_3$, 128 MHz): δ = +0.9 [s]. MS(ESI -ve): *m/z* = 1319 [Tkp^{phos}]$^-$.

Zn[Tkp^{phos}]OAc (5.5)

In an attempt to separate Tkp^{phos} from the mixture of Hpz^{phos} and K[Tkp^{phos}], the reaction with $Zn(OAc)_2.2H_2O$ was attempted as follows. **5.4** (0.100 g, corresponding to 0.083 g of K[Tkp^{phos}], 0.06 mmol) and $Zn(OAc)_2.2H_2O$ (0.013 g, 0.06 mmol) was dissolved in a mixture of CH_2Cl_2 (5 ml) and MeOH (5 ml) and the mixture stirred for 2 hrs. The resultant solution was then concentrated to dryness, extracted into CH_2Cl_2, filtered to remove some insoluble material (KOAc) and concentrated to dryness to

give an off-white solid. ^{1}H and $^{31}P\{^{1}H\}$ NMR spectroscopy revealed a mixture of products and further attempts at purification failed. MS(FAB +ve): *m/z* = 1383 $[Zn(T_kp^{phos})]^+$, 1399 $[Zn(T_kp^{phos}) + O]^+$, 1415 $[Zn(T_kp^{phos}) + 2O]^+$.

Potassium tetrakis{3-[2-(diphenylphosphinoyl)phenyl]pyrazol-1-yl}borate, *K[T$_k$p$^{phos(O)}$]* (5.6)

A finely ground mixture of $Hpz^{phos(O)}$ (**4.3**) (3.000 g, 8.71 mmol) and KBH_4 (0.094 g, 1.74 mmol) was stirred and gradually heated using a heating mantle. At approximately 160°C a pale brown melt had formed which appeared to bubble gently. At 260°C the temperature remained constant and the mixture was stirred for 2 hrs and the melt did not change greatly in appearance and no precipitation was observed. Addition of ethanol (50 ml) gave a brown solution which was filtered and concentrated to dryness to give a pale brown powder. ^{1}H NMR spectroscopy showed the product to be contaminated by some unreacted $Hpz^{phos(O)}$. Recrystallisation of the crude solid from hot THF gave pure $K[T_kp^{phos(O)}]$ as a white solid. (1.405 g, 1.0 mmol, 56 %). IR (KBr disc): ν_{max}/cm^{-1} = 3055m, 1636w, 1590w, 1482s, 1438s, 1426m, 1259w, 1137w, 1192s, 1116s, 1071m. ^{1}H NMR (+25°C, $CDCl_3$, 400 MHz): δ = 7.68 [dd ($^{3}J_{HH}$ = 7.3 Hz, $^{4}J_{HH}$ = 4.0 Hz), 4H, 6-Ph], 7.62 [dd ($^{3}J_{HP}$ = 11.9 Hz, $^{3}J_{HH}$ = 7.2 Hz), 16H, *o*-Ph], 7.55 [dd ($^{3}J_{HH}$ = 7.6 Hz, $^{3}J_{HH}$ = 7.6 Hz), 4H, 5-Ph], 7.43 [t ($^{3}J_{HH}$ = 6.9 Hz), 8H, *p*-Ph], 7.33 [ddd ($^{3}J_{HH}$ = 7.6 Hz, $^{3}J_{HH}$ = 7.4 Hz, $^{4}J_{HH}$ = 2.6 Hz), 16H, *m*-Ph], 7.27 [m, 4H, 4-Ph], 7.19 [dd ($^{3}J_{HP}$ = 14.1 Hz, $^{3}J_{HH}$ = 7.3 Hz), 4H, 3-Ph], 6.49 [d ($^{3}J_{HH}$ = 2.2 Hz), 4H, 5-pz], 6.03 [d ($^{3}J_{HH}$ = 2.2 Hz), 4H, 4-pz]. $^{13}C\{^{1}H\}$ NMR (+25°C, $CDCl_3$, 126 MHz), δ = 152.1 [s, 3-pz], 141.1 [s, 1-Ph], 135.7 [s, 5-pz], 133.9 [d ($^{2}J_{CP}$ = 12.7 Hz), 3-Ph], 133.1 [d ($^{3}J_{CP}$ = 9.9 Hz), 6-Ph], 133.1 [d ($^{1}J_{CP}$ = 133.1 Hz), *i*-Ph], 131.8 [m, *o*-Ph + 4-Ph], 131.4 [s, *p*-Ph], 130.1 [d ($^{1}J_{CP}$ = 103.0 Hz), 2-Ph], 128.2 [d ($^{3}J_{CP}$ = 12.1 Hz), *m*-Ph], 126.6 [d ($^{3}J_{CP}$ = 12.8 Hz), 4-Ph], 107.1 [s, 4-pz]. $^{31}P\{^{1}H\}$ NMR (+25°C, $CDCl_3$, 162 MHz), δ = +30.9 [s]. ^{11}B NMR (+25°C, $CDCl_3$, 128 MHz): δ = +0.7 [s]. MS(ESI -ve): *m/z* = 1383 $[T_kp^{phos(O)}]^-$.

Tl[T$_k$p$^{phos(O)}$] (5.7)

A solution of thallium nitrate (0.034 g, 0.13 mmol) in a mixture of THF (2 ml) and water (2 ml) was added to a solution of $K[T_kp^{phos(O)}]$ (**5.6**) (0.150 g, 0.11 mmol) in a mixture of THF (20 ml) and CH_2Cl_2 (20 ml) and stirred for 1 hr. The solution was extracted into CH_2Cl_2 (80 ml), dried over magnesium sulphate, filtered and

concentrated to dryness *in vacuo* to give Tl[$T_kp^{phos(O)}$] as a white solid (0.120 g, 0.08 mmol, 70 %). Single crystals suitable for X-ray analysis were grown by slow diffusion of pentane vapour into a solution of the product in chloroform. Anal. (%) calc. (found) for $C_{84}H_{64}BN_8O_4P_4Tl$: C, 63.5 (63.4); H, 4.06 (3.97); N, 7.05 (6.96). IR (KBr disc): ν_{max}/cm^{-1} = 3055m, 1636w, 1591w, 1482m, 1438m, 1385w, 1340w, 1260w, 1186s, 1116s, 1071m. ^1H NMR (+25°C, $CDCl_3$, 400 MHz): δ = 8.00 [dd ($^3J_{HH}$ = 7.3 Hz, $^4J_{HH}$ = 4.1 Hz), 4H, 6-Ph], 7.65 [dd ($^3J_{HP}$ = 11.7 Hz, $^3J_{HH}$ = 7.4 Hz), 16H, *o*-Ph], 7.57 [m, 12H, *p*-Ph + 5-Ph], 7.40 [ddd ($^3J_{HH}$ = 7.7 Hz, $^3J_{HH}$ = 7.7 Hz, $^4J_{HH}$ = 2.8 Hz), 16H, *m*-Ph], 7.20-7.30 [m, 6H, 4-Ph + 3-Ph], 6.87 [d ($^3J_{HH}$ = 2.2 Hz), 4H, 5-pz], 5.98 [d ($^3J_{HH}$ = 2.2 Hz), 4H, 4-pz]. $^{31}P\{^1H\}$ NMR (+25°C, $CDCl_3$, 162 MHz): δ = +30.3 [s]. ^{11}B NMR (+25°C, $CDCl_3$, 128 MHz): δ = +0.3 [s]. MS(ESI -ve): *m/z* = 1383 [$T_kp^{phos(O)}$]$^-$.

[$CuT_kp^{phos(O)}$(CO)] (5.8)

CH_2Cl_2 (15 ml) was added to a mixture of K[$T_kp^{phos(O)}$] (**5.6**) (0.100 g, 0.07 mmol) and CuCl (0.007 g, 0.07 mmol) under an atmosphere of CO forming a pale green solution. After stirring for 30 mins a fine precipitate had formed. Filtration, followed by removal of the solvent *in vacuo* produced a very pale green solid (0.065 g, 0.04 mmol, 63 %). IR (KBr disc): ν_{max}/cm^{-1} = 2075 (CO). ^1H NMR (+25°C, $CDCl_3$, 400 MHz): δ = 7.89 [m, 4H, 6-Ph], 7.63 [m, 20H, *o*-Ph + 5-Ph], 7.49 [t ($^3J_{HH}$ = 7.3 Hz), 8H, *p*-Ph], 7.34 [m, 24H, *m*-Ph + 4-Ph + 3-Ph], 6.92 [s(br), 4H, 5-pz], 6.07 [s(br), 4H, 4-pz]. $^{31}P\{^1H\}$ NMR (+25°C, $CDCl_3$, 162 MHz): δ = +31.0 [s]. ^{11}B NMR (+25°C, $CDCl_3$, 128 MHz): δ = +0.4 [s]. MS(ESI +ve): *m/z* = 1447 [Cu($T_kp^{phos(O)}$)]$^+$.

[$EuT_kp^{phos(O)}(NO_3)$][NO_3] (5.9)

A solution of K[$T_kp^{phos(O)}$] (**5.6**) (0.075 g, 0.05 mmol) in methanol (5 ml) was added to a solution of europium(III) nitrate pentahydrate in methanol (2 ml) and stirred for 2 hrs. Despite no precipitation, the $^{31}P\{^1H\}$ NMR of the reaction solution indicated formation of a new species. The solution was concentrated to dryness *in vacuo*, extracted into CH_2Cl_2 (80 ml) leaving some insoluble white solid, filtered through celite and concentrated to dryness *in vacuo* to give a white solid (0.075 g, 0.05 mmol, 90 %). Single crystals suitable for X-ray analysis were grown by slow diffusion of ether vapour into a solution of the product in methanol. Anal. (%) calc. (found) for $C_{84}H_{64}BEuN_{10}O_{10}P_4$: C, 60.8 (60.7); H, 3.89 (3.99); N, 8.44 (8.35). IR (KBr disc):

ν_{max}/cm^{-1} = 2964m, 1636w, 1485m, 1437m, 1384m, 1356w, 1262s, 1177m, 1147s, 1091s, 1025s. $^{31}P\{^{1}H\}$ NMR (+25°C, $CDCl_3$, 162 MHz): δ = +37.1 [s], -11.3 [s(br)]. ^{11}B NMR (+25°C, $CDCl_3$, 128 MHz): δ = -12.9 [s]. MS(ESI +ve): *m/z* = 1581 $[EuT_kp^{phos(O)}\{NO_2\}]^+$.

Potassium tetrakis{3-[2-(diphenylphosphinothioyl)phenyl]pyrazol-1-yl}borate, *K[$T_kp^{phos(S)}$]* (5.10)

A mixture of $Hpz^{phos(S)}$ (**4.4**) (0.475 g, 1.32 mmol) and KBH_4 (0.014 g, 0.26 mmol) was stirred and gradually heated using a heating mantle. At approximately 160-180°C a melt formed and heating was continued until the temperature reached 240°C. The melt was stirred at this temperature for a further 90 mins and then allowed to cool to room temperature. Ethanol (20 ml) was added to the resultant solid causing the pyrazole starting material (some of which had sublimed onto the walls of the flask) to dissolved and an off-white solid to remain undissolved. The solid was collected by filtration and dried *in vacuo*. The solid was recrystallised from hot ethanol to produce a white powder (0.146 g, 0.10 mmol, 38%). IR (KBr disc): ν_{max}/cm^{-1} = 3049m, 2966m, 1631s, 1480s, 1437s, 1384s, 1340w, 1261w, 1186s, 1098s. ^{1}H NMR (+25°C, $CDCl_3$, 400 MHz): δ = 7.82 [dd ($^{3}J_{HP}$ = 13.3 Hz, $^{3}J_{HH}$ = 7.1 Hz), 16H, *o*-Ph], 7.66 [dd ($^{3}J_{HH}$ = 7.2 Hz, $^{4}J_{HH}$ = 4.8 Hz), 4H, 6-Ph], 7.51 [m, 4H, 5-Ph], 7.42 [m, 8H, *p*-Ph], 7.36 [m, 16H, *m*-Ph], 7.27 [m (obscured by residual $CHCl_3$), 4-Ph], 7.24 [ddd ($^{3}J_{HP}$ = 7.7 Hz, $^{3}J_{HH}$ = 7.6 Hz, $^{4}J_{HH}$ = 1.0 Hz), 4H, 3-Ph], 6.69 [d ($^{3}J_{HH}$ = 2.2 Hz), 4H, 5-pz], 6.00 [d ($^{3}J_{HH}$ = 2.2 Hz), 4H, 4-pz]. $^{31}P\{^{1}H\}$ NMR (+25°C, $CDCl_3$, 162 MHz): δ = +43.3 [s]. ^{11}B NMR (+25°C, $CDCl_3$, 128 MHz): δ = +0.6 [s]. MS(ESI -ve): *m/z* = 1447 $[T_kp^{phos(S)}]^-$.

Tl[$T_kp^{phos(S)}$] (5.11)

A solution of thallium nitrate (0.029 g, 0.11 mmol) in water (5 ml) was added to a solution of K[$T_kp^{phos(S)}$] (**5.10**) (0.136 g, 0.09 mmol) in a mixture of THF (5 ml) and stirred for 1 hr, during which time it became cloudy. The mixture was extracted into CH_2Cl_2, dried over $MgSO_4$, filtered and concentrated to dryness to give a thick oil. This was recrystallised from CH_2Cl_2/hexane to give a white powder (0.091 g, 0.05 mmol, 61 %). Anal. (%) calc. (found) for $C_{84}H_{64}BN_8P_4S_4Tl$: C, 61.0 (61.1); H, 3.90 (3.88); N, 6.78 (6.78). ^{1}H NMR (+25°C, $CDCl_3$, 400 MHz): δ = 7.81 [dd ($^{3}J_{HP}$ = 13.3 Hz, $^{3}J_{HH}$ = 7.1 Hz), 16H, *o*-Ph], 7.71 [dd ($^{3}J_{HH}$ = 6.8 Hz, $^{4}J_{HH}$ = 4.8 Hz), 4H, 6-Ph],

7.54 [dd ($^3J_{HH}$ = 7.5 Hz, $^3J_{HH}$ = 7.5 Hz), 4H, 5-Ph], 7.45 [m, 8H, *p*-Ph], 7.38 [m, 16H, *m*-Ph], 7.29 [m (obscured by residual $CHCl_3$), 4-Ph], 7.21 [dd ($^3J_{HP}$ = 14.7 Hz, $^3J_{HH}$ = 7.68 Hz), 4H, 3-Ph], 6.65 [d ($^3J_{HH}$ = 2.2 Hz), 4H, 5-pz], 6.21 [d ($^3J_{HH}$ = 2.0 Hz), 4H, 4-pz]. $^{31}P\{^1H\}$ NMR (+25°C, $CDCl_3$, 162 MHz): δ = +42.3 [s]. ^{11}B NMR (+25°C, $CDCl_3$, 128 MHz): δ = +0.7 [s]. MS(ESI -ve): *m/z* = 1447 $[T_kp^{phos(S)}]^-$.

1-(2'-diphenylphosphino)3-dimethylamino-2-butene-1-one (5.12)

2-(Diphenyphosphino)acetophenone (9.80 g, 32.2 mmol) and *N,N*-dimethylacetamide dimethylacetal (9.4 ml, 64.4 mmol) in toluene (25 ml) were refluxed for 48 hrs. After cooling to room temperature, toluene and remaining *N,N*-dimethylacetamide dimethylacetal were removed *in vacuo* to leave red solid which was triturated with pentane (50 ml), filtered, washed with pentane (40 ml) and dried *in vacuo* to give a red powder (11.102 g, 29.72 mmol, 92%). Anal. (%) calc. (found) for $C_{24}H_{24}NOP$: C, 77.2 (77.2); H, 6.48 (6.50); N, 3.75 (3.70). IR (KBr disc): ν_{max}/cm^{-1} = 1533 (CO). ^1H NMR (+25°C, $CDCl_3$, 400 MHz): δ = 7.59 [ddd ($^3J_{HH}$ = 7.4 Hz, $^4J_{HH}$ = 4.0 Hz, $^5J_{HH}$ = 1.0 Hz), 1H, 6-Ph], 7.37 [ddd ($^3J_{HH}$ = 7.6 Hz, $^3J_{HH}$ = 7.5 Hz, $^4J_{HH}$ = 1.0 Hz), 1H, 5-Ph], 7.30-7.34 [m, 10H, *o,m,p*-Ph], 7.25 [ddd ($^3J_{HH}$ = 7.7 Hz, $^3J_{HH}$ = 7.6 Hz, $^4J_{HH}$ = 1.3 Hz), 1H, 4-Ph], 7.00 [dd ($^3J_{HH}$ = 7.8 Hz, $^4J_{HH}$ = 3.8 Hz), 1H, 3-Ph], 5.18 [s, 1H, COCH], 2.79 [s, 6H, $N(CH_3)_2$], 2.57 [s, 3H, =C-CH_3]. $^{13}C\{^1H\}$ NMR (+25°C, $CDCl_3$, 101 MHz): δ = 191.1 [s, CO], 163.0 [s, =*C*(NMe_2)Me], 151.3 [d ($^2J_{CP}$ = 27.7 Hz), 1-Ph], 138.9 [d ($^1J_{CP}$ = 12.1 Hz), *i*-Ph], 134.5 [s, 3-Ph], 134.2 [d ($^1J_{CP}$ = 17.2 Hz), 2-Ph], 133.8 [d ($^2J_{CP}$ = 19.9 Hz), *o*-Ph], 128.6 [d ($^4J_{CP}$ = 3.1 Hz), 5-Ph], 128.3 [d ($^3J_{CP}$ = 6.9 Hz), *m*-Ph], 128.2 [s, *p*-Ph], 128.0 [s, 4-Ph], 127.3 [d ($^3J_{CP}$ = 5.5 Hz), 6-Ph], 96.9 [s, (OC)H*C*=], 39.7 [s, $N(CH_3)_2$], 16.5 [s, =C-*C*H_3]. $^{31}P\{^1H\}$ NMR (+25°C, $CDCl_3$, 162 MHz): δ = -11.8 [s]. MS(ESI +ve): *m/z* = 374 $[M+H]^+$.

3-[2-(diphenylphosphino)phenyl] 5-methyl pyrazole, *Hpz*^{phos,Me} (5.13)

Hydrazine hydrate (2.3 ml, 6 eq.) was added dropwise to a solution of **5.12** (7.79 g, 20.9 mmol) in hot degassed ethanol (45 ml). The solution was heated at reflux for 2 hrs, allowed to cool and the ethanol removed *in vacuo*. CH_2Cl_2 (100 ml) was added to the resultant solid and the solution dried over $MgSO_4$. Filtration followed by removal of the solvent gave a yellow powder. Purification by flash column chromatography on silica gel (7:1 CH_2Cl_2:ethyl acetate) gave a white powder (6.285 g, 18.36 mmol, 88 %). IR (KBr disc): ν_{max}/cm^{-1} = 3051 (NH). ^1H NMR (+25°C, $CDCl_3$, 400 MHz): δ =

10.31 [s(br), 1H, NH], 7.59 [dd ($^3J_{HH}$ = 7.0 Hz, $^4J_{HH}$ = 4.0 Hz,), 1H, 6-Ph], 7.40 [ddd ($^3J_{HH}$ = 7.5 Hz, $^3J_{HH}$ = 7.5 Hz, $^4J_{HH}$ = 1.1 Hz), 1H, 5-Ph], 7.25-7.38 [m, 11H, *o,m,p*-Ph + 4-Ph], 7.03 [dd ($^3J_{HH}$ = 7.6 Hz, $^4J_{HH}$ = 4.0 Hz), 1H, 3-Ph], 6.09 [s, 1H, 4-pz], 2.24 [s, 3H, CH_3]. $^{13}C\{^1H\}$ NMR (+25°C, $CDCl_3$, 101 MHz): δ = 137.3 [d ($^1J_{CP}$ = 10.7 Hz), *i*-Ph], 135.8 [d ($^1J_{CP}$ = 16.9 Hz), 2-Ph], 134.4 [s, 3-Ph], 133.9 [d ($^2J_{CP}$ = 20.1 Hz), *o*-Ph], 129.8 [d ($^3J_{CP}$ = 5.0 Hz), 6-Ph], 128.9 [s, 5-Ph], 128.7 [s, *p*-Ph], 128.6 [d ($^3J_{CP}$ = 6.6 Hz), *m*-Ph], 128.2 [s, 4-Ph], 106.0 [s, 4-pz], 12.3 [s, CH_3]. $^{31}P\{^1H\}$ NMR (+25°C, $CDCl_3$, 162 MHz): δ = -11.7 [s]. MS(ESI +ve): *m/z* = 343 $[M+H]^+$.

3-[2-(diphenylphosphinoyl)phenyl] 5-methyl pyrazole, *Hpz$^{phos(O),Me}$* (5.14)

Hydrazine hydrate (0.3 ml, 6 eq.) was added dropwise to a solution of **5.12** (0.400 g, 1.10 mmol) in hot ethanol (10 ml). The solution was heated at reflux in air for 12 hrs, allowed to cool and the ethanol removed *in vacuo*. CH_2Cl_2 (20 ml) was added to the resultant solid and the solution dried over $MgSO_4$. Filtration followed by removal of the solvent gave an off-white powder (0.300 g, 0.83 mmol, 78 %). Anal. (%) calc. (found) for $C_{22}H_{19}N_2OP$: C, 73.7 (73.7); H, 5.34 (5.29); N, 7.82 (7.69). IR (KBr disc): ν_{max}/cm^{-1} = 3205 (NH). ^1H NMR (+25°C, $CDCl_3$, 400 MHz): δ = 12.88 [s(br), 1H, NH], 7.71 [dd ($^3J_{HH}$ = 7.4 Hz, $^4J_{HH}$ = 3.7 Hz,), 1H, 6-Ph], 7.58-7.68 [m, 5H, *o*-Ph + 5-Ph], 7.53 [td ($^3J_{HH}$ = 7.3 Hz, $^4J_{HH}$ = 1.3 Hz), 2H, *p*-Ph], 7.43 [ddd ($^3J_{HH}$ = 7.5 Hz, $^3J_{HH}$ = 7.3 Hz, $^4J_{HH}$ = 3.1 Hz), 4H, *m*-Ph], 7.29 [m, 1H, 4-Ph], 7.15 [dd ($^3J_{HP}$ = 14.2 Hz, $^3J_{HH}$ = 8.0 Hz), 1H, 3-Ph], 6.04 [s, 1H, 4-pz], 2.15 [s, 3H, CH_3]. $^{13}C\{^1H\}$ NMR (+25°C, $CDCl_3$, 101 MHz): δ = 148.5 [s, 3-pz], 142.6 [s, 5-pz], 135.2 [d ($^2J_{CP}$ = 6.6 Hz), 1-Ph], 134.1 [d ($^2J_{CP}$ = 12.2 Hz), 3-Ph], 132.6 [s, 5-Ph], 132.0 [s, *p*-Ph], 131.8 [d ($^2J_{CP}$ = 9.8 Hz), *o*-Ph], 131.2 [d ($^3J_{CP}$ = 9.7 Hz), 6-Ph], 130.6 [d ($^1J_{CP}$ = 106.3 Hz), *i*-Ph], 129.9 [d ($^1J_{CP}$ = 99.6 Hz), 2-Ph], 128.5 [d ($^3J_{CP}$ = 12.4 Hz), *m*-Ph], 127.2 [d ($^3J_{CP}$ = 12.4 Hz), *4*-Ph], 105.0 [s, 4-pz], 13.2 [s, CH_3]. $^{31}P\{^1H\}$ NMR (+25°C, $CDCl_3$, 162 MHz): δ = +35.6 [s]. MS(ESI +ve): *m/z* = 359 $[M+H]^+$.

Potassium hydrotris{3-[2-(diphenylphosphino)phenyl] 5-methyl pyrazol-1-yl}borate, *K[Tp^{phos,Me}]* (5.15)

A mixture of $Hpz^{phos,Me}$ (**5.13**) (4.000 g, 11.70 mmol) and KBH_4 (0.158 g, 2.92 mmol) was heated gently to 160°C causing the solid to melt. The temperature was then increased to 200°C causing the melt to bubble as H_2 was produced. After 30 mins of stirring the temperature was further increased to 220°C. After 5 hrs at this

temperature, heating was stopped and the mixture allowed to cool to room temperature, to produce a yellow solid. This was isolated by dissolution in CH_2Cl_2 followed by removal of the solvent by rotary evaporation to give an off-white powder. Recrystallisation from CH_2Cl_2/hexane gave a white powder which was analytically pure (2.017 g, 1.88 mmol, 64 %). Anal. (%) calc. (found) for $C_{66}H_{55}BKN_6P_3$: C, 73.7 (73.8); H, 5.16 (5.22); N, 7.82 (7.90). IR (KBr disc): ν_{max}/cm^{-1} = 2363 (BH). ^1H NMR (+25°C, $CDCl_3$, 400 MHz): δ = 7.72 [dd ($^3J_{HH}$ = 7.1 Hz, $^4J_{HH}$ = 3.9 Hz), 3H, 6-Ph], 7.33 [ddd ($^3J_{HH}$ = 7.8 Hz, $^3J_{HH}$ = 7.6 Hz, $^4J_{HH}$ = 1.0 Hz), 3H, 5-Ph], 7.10-7.20 [m, 9H, 4-Ph + *p*-Ph], 7.04 [dd ($^3J_{HH}$ = 7.2 Hz, $^3J_{HH}$ = 7.2 Hz), 12H, *m*-Ph], 6.94 [dd ($^3J_{HP}$ = 7.1 Hz), $^3J_{HH}$ = 7.1 Hz), 12H, *o*-Ph], 6.89 [dd ($^3J_{HP}$ = 7.1 Hz, $^3J_{HH}$ = 3.6 Hz), 3H, 3-Ph], 6.15 [s, 3H, 4-pz], 4.67 [m(br), 1H, BH], 2.13 [s, 9H, CH_3]. $^1H\{^{11}B\}$ NMR (+25°C, $CDCl_3$, 400 MHz): As above, except broad BH peak at 4.67 ppm becomes significantly sharper. $^{13}C\{^1H\}$ NMR (+25°C, $CDCl_3$, 126 MHz): δ = 150.9 [s, 3-pz], 145.4 [s, 5-pz], 141.0 [d ($^2J_{CP}$ = 25.2 Hz), 1-Ph], 138.9 [d ($^1J_{CP}$ = 13.4 Hz), *i*-Ph], 134.5 [d ($^1J_{CP}$ = 18.8 Hz), 2-Ph], 134.2 [d ($^2J_{CP}$ = 24.3 Hz), 3-Ph], 133.8 [d ($^2J_{CP}$ = 20.3 Hz), *o*-Ph], 129.7 [m, 6-Ph], 128.4 [s, 5-Ph], 128.0 [d ($^3J_{CP}$ = 6.8 Hz), *m*-Ph], 127.9 [s, *p*-Ph], 126.4 [s, 4-Ph], 105.7 [s, 4-pz], 30.9 [s, CH_3]. $^{31}P\{^1H\}$ NMR (+25°C, $CDCl_3$, 162 MHz): δ = -11.7 [s]. $^{11}B\{^1H\}$ NMR (+25°C, $CDCl_3$, 128 MHz): δ = -5.1 [s]. MS(ESI -ve): *m/z* = 1035 [$Tp^{phos,Me}$]$^-$.

Tl[$Tp^{phos,Me}$] (5.16)

A solution of thallium nitrate (0.059 g, 0.22 mmol) in water (2 ml) was added to a solution of K[$Tp^{phos,Me}$] (**5.15**) (0.200 g, 0.19 mmol) in THF (5 ml) and stirred for 30 mins to produce a faintly cloudy solution. The solution was extracted into CH_2Cl_2 (20 ml), washed with water (10 ml) and the organic layer separated, dried over $MgSO_4$, filtered and concentrated to dryness *in vacuo* to give a glassy colourless solid on the walls of the flask. Dissolution in CH_2Cl_2 (2 ml) and hexane (10 ml) followed by slow evaporation of the solvent gave a white powder. Recrystallisation from acetone/hexane gave an analytically pure sample (0.162 g, 0.13 mmol, 70 %). Single crystals suitable for X-ray analysis were grown by slow evaporation of an acetone solution. Anal. (%) calc. (found) for $C_{66}H_{55}BN_6P_3Tl$: C, 63.9 (64.0); H, 4.47 (3.56); N, 6.78 (6.85). IR (KBr disc): ν_{max}/cm^{-1} = 2512 (BH). ^1H NMR (+25°C, $CDCl_3$, 400 MHz): δ = 7.54 [m, 3H, 6-Ph], 7.23 [t ($^3J_{HH}$ = 7.3 Hz), 6H, *p*-Ph], 7.10-7.20 [m, 18H, 4-Ph + 5-Ph + *m*-Ph), 6.97 [dd ($^3J_{HP}$ = 6.8 Hz, $^3J_{HH}$ = 6.8 Hz), 12H, *o*-Ph], 6.82 [m,

3H, 3-Ph], 5.62 [s, 3H, 4-pz], 4.68 [m(br), 1H, BH], 2.26 [s, 9H, CH_3]. $^{31}P\{^1H\}$ NMR (+25°C, $CDCl_3$, 162 MHz): δ = -3.1 [d ($^1J_{PTh}$ = 1253 Hz)]. $^{11}B\{^1H\}$ NMR (+25°C, $CDCl_3$, 128 MHz): δ = -5.1 [s]. MS(ESI -ve): *m/z* = 1035 [$Tp^{phos,Me}$]$^-$.

Cu[$Tp^{phos,Me}$] (5.17)

THF (10 ml) was added to a mixture of K[$Tp^{phos,Me}$] (**5.15**) (0.100 g, 0.09 mmol) and CuCl (0.009 g, 0.09 mmol) immediately forming a yellow solution. $^{31}P\{^1H\}$ NMR spectroscopy of the reaction solution indicated formation of a new species at -9.0 ppm. The solution was filtered and concentrated to dryness *in vacuo* to give a pale yellow solid of analytical purity (0.083 g, 0.08 mmol, 81 %). Recrystallisation from warm acetone yielded colourless single crystals suitable for X-ray analysis. Anal. (%) calc. (found) for $C_{66}H_{55}BCuN_6P_3$: C, 72.1 (72.0); H, 5.04 (5.10); N, 7.64 (7.58). IR (KBr disc): ν_{max}/cm^{-1} = 2509 (BH). ^1H NMR (+25°C, $CDCl_3$, 400 MHz): δ = 7.94 [d ($^3J_{HH}$ = 7.6 Hz), 3H, 6-Ph], 7.18 [m, 9H, 5-Ph + *p*-Ph], 7.11 [ddd ($^3J_{HH}$ = 7.5 Hz, $^3J_{HH}$ = 7.5 Hz, $^4J_{HH}$ = 1.0 Hz), 3H, 4-Ph], 7.06 [dd ($^3J_{HH}$ = 7.5 Hz, $^3J_{HH}$ = 7.5 Hz), 12H, *m*-Ph], 6.95 [m, 15H, 3-Ph + *o*-Ph], 5.98 [s, 3H, 4-pz], 4.79 [m(br), 1H, BH], 2.31 [s, 9H, CH_3]. $^{31}P\{^1H\}$ NMR (+25°C, CD_2Cl_2, 162 MHz): δ = -7.4 [s]. $^{31}P\{^1H\}$ NMR (-90°C, CD_2Cl_2, 162 MHz): δ = -14.64 [s(br), 2P, PPh_2], 0.0 [s, 1P, PPh_2–Cu]. ^{11}B NMR (+25°C, CD_2Cl_2, 128 MHz): δ = -5.4 [s(br)]. MS(ESI +ve): *m/z* = 1099 [Cu($Tp^{phos,Me}$)]$^+$.

[Ru($Tp^{phos,Me}$)]Cl (5.18)

A solution of $RuCl_2(DMSO)_4$ (0.023 g, 0.05 mmol) and K[$Tp^{phos,Me}$] (**5.15**) (0.050 g, 0.05 mmol) in CH_2Cl_2 (7 ml) was stirred for 48 hrs causing a fine off-white precipitate to form. Filtration gave a yellow solution which was concentrated *in vacuo* to give a sticky yellow solid. Extraction into ether (10 ml) gave a yellow solution and some insoluble material which was removed by filtration. Removal of the solvent from the filtrate gave a yellow solid. Single crystals suitable for X-ray analysis were grown by slow diffusion of pentane vapour into a chloroform solution of the product. ^1H NMR (+25°C, $CDCl_3$, 400 MHz): δ =7.57 [dd ($^3J_{HH}$ = 7.3 Hz, $^3J_{HH}$ = 4.5 Hz), 3H, 6-Ph], 7.41 [ddd ($^3J_{HH}$ = 7.6 Hz, $^3J_{HH}$ = 7.5 Hz, $^4J_{HH}$ = 1.2 Hz), 3H, 5-Ph], 7.25-7.38 [m, 33H, 4-Ph + *o,m,p*-Ph], 7.01 [dd ($^3J_{HH}$ = 7.9 Hz, $^4J_{HH}$ = 3.9 Hz), 3H, 3-Ph], 6.10 [s, 3H, 4-pz], 2.28 [s, 9H, CH_3]. $^{31}P\{^1H\}$ NMR (+25°C, $CDCl_3$, 162 MHz): δ = -11.7 [s]. MS(ESI +ve): *m/z* = 1137 [Ru($Tp^{phos,Me}$)]$^+$, 1173 [Ru($Tp^{phos,Me}$)Cl]$^+$.

Zn[Tp^{phos,Me}]OAc (5.19)

$Zn(OAc)_2.2H_2O$ (0.022 g, 0.09 mmol) in MeOH (5 ml) was added to a solution of K[Tp^{phos,Me}] (**5.15**) (0.100 g, 0.09 mmol) in THF (3 ml) and stirred for 60 hrs. The clear solution was concentrated to dryness and the resultant white solid extracted into CH_2Cl_2, filtered through celite and concentrated to dryness to give a white powder which was recrystallised from THF/pentane (0.097 g, 0.08 mmol, 90 %). Anal. (%) calc. (found) for $C_{68}H_{58}BN_6O_2P_3Zn$: C, 70.4 (70.5); H, 5.04 (5.14); N, 7.24 (7.18). IR (KBr disc): ν_{max}/cm^{-1} = 2543 (BH), 1630 (COO). ^1H NMR (+25°C, $CDCl_3$, 400 MHz): δ = 7.67 [dd ($^3J_{HH}$ = 6.8 Hz, $^4J_{HH}$ = 4.0 Hz), 3H, 6-Ph], 7.21 [m, 9H, 5-Ph + *p*-Ph], 7.14 [m, 15H, 4-Ph + *o*-Ph], 7.01 [m, 12H, *m*-Ph], 6.78 [dd ($^3J_{HP}$ = 7.6 Hz, $^3J_{HH}$ = 4.2 Hz), 3H, 3-Ph], 5.75 [s, 3H, 4-pz], 4.74 [m(br), 1H, BH], 2.32 [s, 9H, CH_3], 1.34 [s, 3H, CO_2CH_3]. $^{31}P\{^1H\}$ NMR (+25°C, $CDCl_3$, 162 MHz): δ = -11.4 [s]. MS(ESI +ve): *m/z* = 1100 [Zn(Tp^{phos,Me})]$^+$.

Attempted synthesis of [Zn_2(Tp^{Ph,SMe})$(OAc)_2$][OAc] (5.20)

A solution of K[Tp^{Ph,SMe}] (**2.8**) (0.050 g, 0.08 mmol) in THF (3 ml) was added to a stirred solution of $Zn(OAc)_2.2H_2O$ (0.071 g, 0.32 mmol, 4 eq.) in methanol (3 ml) causing a white solid to precipitate immediately. Addition of CH_2Cl_2 (5 ml) caused the solid to redissolve and the solution was stirred for a further 48 hrs during which time no precipitation was observed. Evaporation of the CH_2Cl_2 under a slow stream of N_2 caused a white solid to precipitate. This solid was collected by filtration and dried *in vacuo* and shown to be identical to **5.21** by NMR (0.042 g, 0.06 mmol, 74 %). MS(ESI +ve): *m/z* = 1335 [(Zn[Tp^{Ph,SMe}])$_2$OAc - 10]$^+$. Single crystals suitable for X-ray analysis were grown by vapour diffusion of pentane into a chloroform solution of this complex.

Zn(Tp^{Ph,SMe})OAc (5.21)

A solution of K[Tp^{Ph,SMe}] (**2.8**) (0.200 g, 0.32 mmol) in THF (10 ml) was added to a stirred solution of $Zn(OAc)_2.2H_2O$ (0.078 g, 0.36 mmol, 1.1 eq.) in methanol (10 ml) causing a white solid to precipitate immediately. This was collected by filtration, washed with THF (5 ml) and dried *in vacuo* (0.198 g, 0.28 mmol, 88 %). Anal. (%) calc. (found) for $C_{32}H_{31}BN_6O_2S_3Zn$: C, 54.6 (54.7); H, 4.44 (4.50); N, 11.9 (12.0). IR (KBr disc): ν_{max}/cm^{-1} = 2506 (BH), 1636 (COO). ^1H NMR (+25°C, $CDCl_3$, 400 MHz): δ = 7.64 [dd ($^3J_{HH}$ = 7.7 Hz, $^4J_{HH}$ = 1.7 Hz), 6H, *o*-Ph], 7.38 [m, 9H, *m,p*-Ph],

6.29 [s, 3H, 4-pz], 5.30 [m(br), 1H, BH], 2.59 [s, 9H, SCH_3], 1.50 [s(br), 3H, CO_2CH_3]. ^{11}B NMR (+25°C, CD_2Cl_2, 128 MHz): δ = -8.9 [s(br)].

7.2 References

1. G. J. Kubas, *Inorg. Synth.*, 1990, **28**, 68.
2. S. J. Coote, G. J. Dawson, C. G. Frost and J. M. J. Williams, *Synlett*, 1993, 509.
3. A.-K. Pleier, H. Glas, M. Grosche, P. Sirsch and W. R. Thiel, *Synthesis*, 2001, **1**, 55.
4. W. C. Wolsey, *J. Chem. Ed.*, 1973, **50**, A335.
5. I. P. Evans, A. Spencer and G. Wilkinson, *J. Chem. Soc., Dalton Trans.*, 1973, 204.
6. A. J. Amoroso, A. M. Cargill Thompson, J. C. Jeffery, P. L. Jones, J. A. McCleverty and M. D. Ward, *J. Chem. Soc., Chem. Commun.*, 1994, 2751.

CHAPTER 8

APPENDIX

8. Appendix

8.1 Crystal Structure Determinations

Diffraction data for all compounds except **4.3, 4.6, 4.9** and **4.10** were collected on an Oxford Diffraction Xcalibur 3 diffractometer and Mo-K α radiation by Dr Andrew J. P. White at the Department of Chemistry, Imperial College London. Diffraction data for compounds **4.3, 4.6, 4.9** and **4.10** were collected on a Brucker KappaCCD diffractometer using crystals coated in oil and cooled in a stream of cold nitrogen gas, and Mo-K α radiation by Dr Peter B. Hitchcock at the University of Sussex.

Table 8.1. Crystal data and structure refinement for $Tl[Tp^{Ph,SMe}]$ (**2.9**)

Identification code	NL0705
Empirical formula	C30 H28 B N6 S3 Tl
Formula weight	783.94
Temperature	173(2) K
Diffractometer, wavelength	OD Xcalibur 3, 0.71073 Å
Crystal system, space group	Monoclinic, P2(1)/c
Unit cell dimensions	a = 12.8755(2) Å α = 90°
	b = 14.4834(2) Å β= 109.588(2)°
	c = 17.3040(3) Å γ = 90°
Volume, Z	3040.12(8) $Å^3$, 4
Density (calculated)	1.713 Mg/m^3
Absorption coefficient	5.550 mm^{-1}
F(000)	1536
Crystal colour / morphology	Colourless platy needles
Crystal size	0.45 x 0.10 x 0.02 mm^3
θ range for data collection	3.70 to 32.43°
Index ranges	-19<=h<=19, -20<=k<=20, -26<=l<=24
Reflns collected / unique	44906 / 10124 [R(int) = 0.0463]
Reflns observed [F>4σ(F)]	7500
Absorption correction	Analytical
Max. and min. transmission	0.892 and 0.344
Refinement method	Full-matrix least-squares on F^2
Data / restraints / parameters	10124 / 1 / 374
Goodness-of-fit on F^2	1.022
Final R indices [F>4σ(F)]	R1 = 0.0226, wR2 = 0.0476
R indices (all data)	R1 = 0.0417, wR2 = 0.0557
Largest diff. peak, hole	1.712, -0.732 $eÅ^{-3}$
Mean and maximum shift/error	0.000 and 0.002

Table 8.2. Crystal data and structure refinement for $Cu[Tp^{Ph,SMe}]CO$ (**2.12**)

Identification code	NL0707
Empirical formula	C31 H28 B Cu N6 O S3
Formula weight	671.12
Temperature	173(2) K
Diffractometer, wavelength	OD Xcalibur 3, 0.71073 Å
Crystal system, space group	Monoclinic, P2(1)/c
Unit cell dimensions	a = 12.8579(3) Å α = 90°
	b = 14.7465(3) Å β = 111.388(3)°
	c = 17.5158(4) Å γ = 90°
Volume, Z	3092.43(12) $Å^3$, 4
Density (calculated)	1.441 Mg/m^3
Absorption coefficient	0.945 mm^{-1}
F(000)	1384
Crystal colour / morphology	Colourless plates
Crystal size	0.22 x 0.19 x 0.02 mm^3
θ range for data collection	3.68 to 32.42°
Index ranges	-19<=h<=18, -21<=k<=21, -25<=l<=24
Reflns collected / unique	42257 / 10320 [R(int) = 0.0786]
Reflns observed [F>4σ(F)]	5760
Absorption correction	Semi-empirical from equivalents
Max. and min. transmission	1.00000 and 0.88639
Refinement method	Full-matrix least-squares on F^2
Data / restraints / parameters	10320 / 1 / 392
Goodness-of-fit on F^2	0.958
Final R indices [F>4σ(F)]	R1 = 0.0606, wR2 = 0.0928
R indices (all data)	R1 = 0.1468, wR2 = 0.1138
Largest diff. peak, hole	1.039, -0.514 $eÅ^{-3}$
Mean and maximum shift/error	0.000 and 0.001

Table 8.3. Crystal data and structure refinement for $Hpz^{phos(O)}$ (**4.3**)

Identification code	aug2206
Empirical formula	C21 H17 N2 O P . (CHCl3)
Formula weight	463.70
Temperature	173(2) K
Wavelength	0.71073 Å
Crystal system	Triclinic
Space group	$P\bar{1}$ (No.2)
Unit cell dimensions	a = 9.9204(3) Å α= 71.592(2)°
	b = 10.2022(3) Å β= 78.246(2)°
	c = 11.5173(3) Å γ = 87.496(1)°
Volume	1082.56(5) $Å^3$
Z	2
Density (calculated)	1.42 Mg/m^3
Absorption coefficient	0.51 mm^{-1}
F(000)	476
Crystal size	0.30 x 0.20 x 0.20 mm^3
Theta range for data collection	3.63 to 25.98°
Index ranges	-12<=h<=12, -12<=k<=12, -14<=l<=14
Reflections collected	15085
Independent reflections	4226 [R(int) = 0.041]
Reflections with I>2sigma(I)	3615
Completeness to theta = 25.98°	99.3 %
Refinement method	Full-matrix least-squares on F^2
Data / restraints / parameters	4226 / 0 / 266
Goodness-of-fit on F^2	1.111
Final R indices [I>2sigma(I)]	R1 = 0.048, wR2 = 0.124
R indices (all data)	R1 = 0.057, wR2 = 0.130
Largest diff. peak and hole	1.04 and -0.65 e.$Å^{-3}$(near solvate)

Table 8.4. Crystal data and structure refinement for $Pd(Hpz^{phos})Cl_2$ (**4.5**)

Identification code	NL0606
Empirical formula	C21 H17 Cl2 N2 P Pd
Formula weight	505.64
Temperature	173(2) K
Diffractometer, wavelength	OD Xcalibur PX Ultra, 1.54248 Å
Crystal system, space group	Monoclinic, P2(1)/n
Unit cell dimensions	a = 9.2136(16) Å α = 90°
	b = 21.296(4) Å β= 101.263(13)°
	c = 10.3831(15) Å γ = 90°
Volume, Z	1998.1(6) $Å^3$, 4
Density (calculated)	1.681 Mg/m^3
Absorption coefficient	10.771 mm^{-1}
F(000)	1008
Crystal colour / morphology	Yellow needles
Crystal size	0.16 x 0.04 x 0.04 mm^3
θ range for data collection	4.15 to 70.97°
Index ranges	-11<=h<=10, -23<=k<=26, -12<=l<=12
Reflns collected / unique	47773 / 3853 [R(int) = 0.0321]
Reflns observed [F>4σ(F)]	3392
Absorption correction	Semi-empirical from equivalents
Max. and min. transmission	1.17103 and 0.48463
Refinement method	Full-matrix least-squares on F^2
Data / restraints / parameters	3853 / 1 / 248
Goodness-of-fit on F^2	1.060
Final R indices [F>4σ(F)]	R1 = 0.0208, wR2 = 0.0556
R indices (all data)	R1 = 0.0238, wR2 = 0.0562
Largest diff. peak, hole	0.742, -0.376 $eÅ^{-3}$
Mean and maximum shift/error	0.000 and 0.002

Table 8.5. Crystal data and structure refinement for $[Pd(Hpz^{phos})_2]Cl_2$ (**4.6**)

Identification code	aug2306
Empirical formula	C42 H34 Cl2 N4 O2 P2 Pd.(CHCl3) . 2(H2O)
Formula weight	1021.37
Temperature	173(2) K
Wavelength	0.71073 Å
Crystal system	Monoclinic
Space group	$P2_1/n$ (No.14)
Unit cell dimensions	a = 14.5729(3) Å α= 90°
	b = 12.3105(1) Å β= 98.680(1)°
	c = 24.1681(4) Å γ = 90°
Volume	4286.09(12) $Å^3$
Z	4
Density (calculated)	1.58 Mg/m^3
Absorption coefficient	0.87 mm^{-1}
F(000)	2072
Crystal size	0.20 x 0.20 x 0.02 mm^3
Theta range for data collection	3.41 to 26.01°
Index ranges	-17<=h<=17, -15<=k<=15, -29<=l<=29
Reflections collected	64821
Independent reflections	8415 [R(int) = 0.080]
Reflections with I>2sigma(I)	6347
Completeness to theta = 26.01°	99.8 %
Tmax. and Tmin.	0.9524 and 0.8732
Refinement method	Full-matrix least-squares on F^2
Data / restraints / parameters	8415 / 0 / 532
Goodness-of-fit on F^2	1.019
Final R indices [I>2sigma(I)]	R1 = 0.058, wR2 = 0.144
R indices (all data)	R1 = 0.084, wR2 = 0.159
Largest diff. peak and hole	2.25 and -1.05 e.$Å^{-3}$ (near CHCl3 solvate)

Table 8.6. Crystal data and structure refinement for $[Pd(Hpz^{phos})_2][ClO_4]_2$ (**4.7**)

Identification code	NL0609
Empirical formula	[C42 H34 N4 P2 Pd](ClO4)2
Formula weight	961.97
Temperature	173(2) K
Diffractometer, wavelength	OD Xcalibur 3, 0.71073 Å
Crystal system, space group	Orthorhombic, Pbca
Unit cell dimensions	a = 13.8787(11) Å α = 90°
	b = 18.264(2) Å β = 90°
	c = 31.8160(14) Å γ = 90°
Volume, Z	8064.7(13) $Å^3$, 8
Density (calculated)	1.585 Mg/m^3
Absorption coefficient	0.732 mm^{-1}
F(000)	3904
Crystal colour / morphology	Yellow plates
Crystal size	0.31 x 0.17 x 0.06 mm^3
θ range for data collection	3.69 to 32.00°
Index ranges	-20<=h<=20, -25<=k<=27, -44<=l<=46
Reflns collected / unique	102703 / 13189 [R(int) = 0.0367]
Reflns observed [F>4σ(F)]	9927
Absorption correction	Semi-empirical from equivalents
Max. and min. transmission	1.06785 and 0.94916
Refinement method	Full-matrix least-squares on F^2
Data / restraints / parameters	13189 / 2 / 540
Goodness-of-fit on F^2	1.037
Final R indices [F>4σ(F)]	R1 = 0.0407, wR2 = 0.0860
R indices (all data)	R1 = 0.0613, wR2 = 0.0915
Largest diff. peak, hole	0.664, -0.833 $eÅ^{-3}$
Mean and maximum shift/error	0.000 and 0.006

Table 8.7. Crystal data and structure refinement for $Pd(Hpz^{phos(O)})_2Cl_2$ (**4.9**)

Identification code	sep106
Empirical formula	C42 H34 Cl2 N4 O2 P2 Pd. 4(CHCl3)
Formula weight	1343.44
Temperature	173(2) K
Wavelength	0.71073 Å
Crystal system	Triclinic
Space group	$P\bar{1}$ (No.2)
Unit cell dimensions	a = 10.1514(3) Å α= 74.004(1)°
	b = 11.8973(3) Å β= 67.062(1)°
	c = 12.9736(3) Å γ = 77.013(2)°
Volume	1374.87(6) $Å^3$
Z	1
Density (calculated)	1.62 Mg/m^3
Absorption coefficient	1.12 mm^{-1}
F(000)	672
Crystal size	0.25 x 0.20 x 0.15 mm^3
Theta range for data collection	3.41 to 25.98°
Index ranges	-12<=h<=12, -14<=k<=14, -15<=l<=15
Reflections collected	18377
Independent reflections	5368 [R(int) = 0.042]
Reflections with I>2sigma(I)	4860
Completeness to theta = 25.98°	99.5 %
Tmax. and Tmin.	0.8502 and 0.7675
Refinement method	Full-matrix least-squares on F^2
Data / restraints / parameters	5368 / 0 / 317
Goodness-of-fit on F^2	0.932
Final R indices [I>2sigma(I)]	R1 = 0.042, wR2 = 0.111
R indices (all data)	R1 = 0.047, wR2 = 0.115
Largest diff. peak and hole	1.26 and -1.11 e.$Å^{-3}$ (near solvate)

Table 8.8. Crystal data and structure refinement for $[Pd(Hpz^{phos(O)})_2][ClO_4]_2$ (**4.10**)

Identification code	sep206
Empirical formula	C42 H34 Cl12 N4 O10 P2 Pd . 4(CHCl3)
Formula weight	1471.44
Temperature	173(2) K
Wavelength	0.71073 Å
Crystal system	Monoclinic
Space group	$P2_1/c$ (No.14)
Unit cell dimensions	a = 8.5748(3) Å α= 90°
	b = 19.1391(7) Å β= 91.343(2)°
	c = 17.7847(6) Å γ = 90°
Volume	2917.92(18) $Å^3$
Z	2
Density (calculated)	1.68 Mg/m^3
Absorption coefficient	1.07 mm^{-1}
F(000)	1472
Crystal size	0.10 x 0.02 x 0.02 mm^3
Theta range for data collection	3.41 to 26.03°
Index ranges	-10<=h<=9, -20<=k<=23, -21<=l<=21
Reflections collected	17925
Independent reflections	5693 [R(int) = 0.052]
Reflections with I>2sigma(I)	3921
Completeness to theta = 26.03°	99.0 %
Tmax. and Tmin.	0.9756 and 0.9003
Refinement method	Full-matrix least-squares on F^2
Data / restraints / parameters	5693 / 30 / 366
Goodness-of-fit on F^2	1.009
Final R indices [I>2sigma(I)]	R1 = 0.060, wR2 = 0.136
R indices (all data)	R1 = 0.098, wR2 = 0.158
Largest diff. peak and hole	1.19 and -0.72 e.$Å^{-3}$(near solvate)

Table 8.9. Crystal data and structure refinement for Tl[$T_kP^{phos(O)}$] (**5.7**)

Identification code	NL0708
Empirical formula	C84 H64 B N8 O4 P4 Tl . 3.5CHCl3 . 0.5C5H12
Formula weight	2042.35
Temperature	173(2) K
Diffractometer, wavelength	OD Xcalibur 3, 0.71073 Å
Crystal system, space group	Triclinic, P-1
Unit cell dimensions	a = 14.6110(3) Å α = 62.012(2)°
	b = 19.0394(3) Å β = 73.056(2)°
	c = 19.8132(4) Å γ = 85.878(2)°
Volume, Z	4642.07(15) $Å^3$, 2
Density (calculated)	1.461 Mg/m^3
Absorption coefficient	2.164 mm^{-1}
F(000)	2052
Crystal colour / morphology	Colourless blocks
Crystal size	0.14 x 0.13 x 0.05 mm^3
θ range for data collection	3.73 to 29.01°
Index ranges	-19<=h<=17, -25<=k<=21, -26<=l<=26
Reflns collected / unique	52575 / 21105 [R(int) = 0.0562]
Reflns observed [F>4σ(F)]	14291
Absorption correction	Analytical
Refinement method	Full-matrix least-squares on F^2
Data / restraints / parameters	21105 / 195 / 1165
Goodness-of-fit on F^2	0.962
Final R indices [F>4σ(F)]	R1 = 0.0430, wR2 = 0.0847
R indices (all data)	R1 = 0.0764, wR2 = 0.0940
Largest diff. peak, hole	1.657, -0.941 $eÅ^{-3}$
Mean and maximum shift/error	0.000 and 0.009

Table 8.10. Crystal data and structure refinement for $[Eu(T_kP^{phos(O)})(NO_3)][NO_3]$ (**5.9**)

Identification code	NL0709
Empirical formula	[C84 H64 N9 O7 P4 B Eu](NO3) . 4MeOH
Formula weight	1788.27
Temperature	173(2) K
Diffractometer, wavelength	OD Xcalibur PX Ultra, 1.54184 Å
Crystal system, space group	Monoclinic, P2(1)/c
Unit cell dimensions	a = 25.0529(2) Å α = 90°
	b = 13.1352(1) Å β = 106.560(1)°
	c = 26.4601(2) Å γ = 90°
Volume, Z	8346.19(11) $Å^3$, 4
Density (calculated)	1.423 Mg/m^3
Absorption coefficient	6.686 mm^{-1}
F(000)	3672
Crystal colour / morphology	Colourless blocks
Crystal size	0.21 x 0.20 x 0.14 mm^3
θ range for data collection	3.45 to 71.37°
Index ranges	-30<=h<=30, -16<=k<=16, -32<=l<=31
Reflns collected / unique	112068 / 16144 [R(int) = 0.0324]
Reflns observed [F>4σ(F)]	14231
Absorption correction	Semi-empirical from equivalents
Max. and min. transmission	1.00000 and 0.67974
Refinement method	Full-matrix least-squares on F^2
Data / restraints / parameters	16144 / 155 / 1093
Goodness-of-fit on F^2	1.057
Final R indices [F>4σ(F)]	R1 = 0.0343, wR2 = 0.0918
R indices (all data)	R1 = 0.0419, wR2 = 0.0986
Largest diff. peak, hole	0.992, -0.646 $eÅ^{-3}$
Mean and maximum shift/error	0.000 and 0.007

Table 8.11. Crystal data and structure refinement for Tl[$Tp^{phos,Me}$] (**5.16**)

Identification code	NL0711
Empirical formula	C66 H55 B N6 P3 Tl
Formula weight	1240.25
Temperature	173(2) K
Diffractometer, wavelength	OD Xcalibur 3, 0.71073 Å
Crystal system, space group	Trigonal, P3
Unit cell dimensions	a = 38.2173(2) Å α = 90°
	b = 38.2173(2) Å β = 90°
	c = 10.39625(8) Å γ = 120°
Volume, Z	13150.1(3) $Å^3$, 9
Density (calculated)	1.410 Mg/m^3
Absorption coefficient	2.891 mm^{-1}
F(000)	5616
Crystal colour / morphology	Colourless tablets
Crystal size	0.30 x 0.26 x 0.06 mm^3
θ range for data collection	3.69 to 31.46°
Index ranges	-54<=h<=55, -54<=k<=55, -15<=l<=14
Reflns collected / unique	173459 / 53602 [R(int) = 0.0461]
Reflns observed [F>4σ(F)]	42785
Absorption correction	Semi-empirical from equivalents
Max. and min. transmission	1.00000 and 0.63061
Refinement method	Full-matrix least-squares on F^2
Data / restraints / parameters	53602 / 1 / 2090
Goodness-of-fit on F^2	1.015
Final R indices [F>4σ(F)]	R1 = 0.0372, wR2 = 0.0632
	R1+ = 0.0397, wR2+ = 0.0707
	R1- = 0.0731, wR2- = 0.1691
R indices (all data)	R1 = 0.0551, wR2 = 0.0696
Absolute structure parameter	x+ = 0.1593(16), x- = 0.8407(16)
	Partial racemic twin
Largest diff. peak, hole	1.384, -1.200 $eÅ^{-3}$
Mean and maximum shift/error	0.000 and 0.004

Table 8.12. Crystal data and structure refinement for $Cu[Tp^{phos,Me}]$ (**5.17**)

Identification code	NL0712
Empirical formula	C66 H55 B Cu N6 P3 . Me2CO
Formula weight	1157.50
Temperature	173(2) K
Diffractometer, wavelength	OD Xcalibur PX Ultra, 1.54184 Å
Crystal system, space group	Triclinic, P-1
Unit cell dimensions	a = 14.4370(7) Å α = 80.770(3)°
	b = 14.6381(4) Å β = 68.299(4)°
	c = 17.2046(7) Å γ = 61.978(4)°
Volume, Z	2981.75(19) $Å^3$, 2
Density (calculated)	1.289 Mg/m^3
Absorption coefficient	1.659 mm^{-1}
F(000)	1208
Crystal colour / morphology	Colourless blocks
Crystal size	0.12 x 0.08 x 0.07 mm^3
θ range for data collection	2.76 to 71.32°
Index ranges	-17<=h<=17, -17<=k<=15, -20<=l<=21
Reflns collected / unique	30433 / 11176 [R(int) = 0.0374]
Reflns observed [F>4σ(F)]	7403
Absorption correction	Semi-empirical from equivalents
Max. and min. transmission	1.00000 and 0.93407
Refinement method	Full-matrix least-squares on F^2
Data / restraints / parameters	11176 / 1 / 739
Goodness-of-fit on F^2	0.895
Final R indices [F>4σ(F)]	R1 = 0.0342, wR2 = 0.0771
R indices (all data)	R1 = 0.0583, wR2 = 0.0815
Largest diff. peak, hole	0.336, -0.315 $eÅ^{-3}$
Mean and maximum shift/error	0.000 and 0.001

Table 8.13. Crystal data and structure refinement for [Ru($Tp^{phos,Me}$)]Cl (**5.18**)

Identification code	NL0801b
Empirical formula	[C66 H55 B N6 P3 Ru](Cl) . 5CHCl3
Formula weight	1769.24
Temperature	173(2) K
Diffractometer, wavelength	OD Xcalibur PX Ultra, 1.54184 Å
Crystal system, space group	Hexagonal, P6(3)
Unit cell dimensions	a = 12.52762(6) Å α = 90°
	b = 12.52762(6) Å β = 90°
	c = 27.4497(2) Å γ = 120°
Volume, Z	3730.82(12) $Å^3$, 2
Density (calculated)	1.575 Mg/m^3
Absorption coefficient	7.960 mm^{-1}
F(000)	1788
Crystal colour / morphology	Yellow hexagonal plates
Crystal size	0.15 x 0.12 x 0.04 mm^3
θ range for data collection	4.38 to 71.51°
Index ranges	-15<=h<=15, -15<=k<=15, -33<=l<=33
Reflns collected / unique	52927 / 4794 [R(int) = 0.0421]
Reflns observed [F>4σ(F)]	4172
Absorption correction	Semi-empirical from equivalents
Max. and min. transmission	1.00000 and 0.57348
Refinement method	Full-matrix least-squares on F^2
Data / restraints / parameters	4794 / 116 / 356
Goodness-of-fit on F^2	1.125
Final R indices [F>4σ(F)]	R1 = 0.0783, wR2 = 0.1966
	R1+ = 0.0822, wR2+ = 0.2047
	R1- = 0.0854, wR2- = 0.2120
R indices (all data)	R1 = 0.0855, wR2 = 0.2001
Absolute structure parameter	x+ = 0.41(2), x- = 0.59(2)
	partial racemic twin
Largest diff. peak, hole	0.865, -0.565 $eÅ^{-3}$
Mean and maximum shift/error	0.000 and 0.002

Table 8.14. Crystal data and structure refinement for $Zn[Tp^{Ph,SMe}]OAc$ (**5.21**)

Identification code	NL0710
Empirical formula	C32 H31 B N6 O2 S3 Zn
Formula weight	703.99
Temperature	173(2) K
Diffractometer, wavelength	OD Xcalibur 3, 0.71073 Å
Crystal system, space group	Monoclinic, P2(1)/c
Unit cell dimensions	a = 12.12155(16) Å α = 90°
	b = 15.80496(17) Å β = 107.9757(14)°
	c = 17.4056(2) Å γ = 90°
Volume, Z	3171.81(12) $Å^3$, 4
Density (calculated)	1.474 Mg/m^3
Absorption coefficient	1.013 mm^{-1}
F(000)	1456
Crystal colour / morphology	Colourless blocks
Crystal size	0.23 x 0.12 x 0.07 mm^3
θ range for data collection	3.76 to 32.50°
Index ranges	-18<=h<=17, -23<=k<=22, -26<=l<=21
Reflns collected / unique	45705 / 10604 [R(int) = 0.0505]
Reflns observed [F>4σ(F)]	7310
Absorption correction	Analytical
Max. and min. transmission	0.937 and 0.826
Refinement method	Full-matrix least-squares on F^2
Data / restraints / parameters	10604 / 1 / 411
Goodness-of-fit on F^2	0.944
Final R indices [F>4σ(F)]	R1 = 0.0318, wR2 = 0.0749
R indices (all data)	R1 = 0.0563, wR2 = 0.0813
Largest diff. peak, hole	0.393, -0.318 $eÅ^{-3}$
Mean and maximum shift/error	0.000 and 0.001

8.2 Crystal Data for Complex 5.16

The structure of **5.16** (which crystallised in the chiral space group *P*3) was found to contain five crystallographically independent complexes, referred to as **5.16-A**, **5.16-B**, **5.16-C**, **5.16-D** and **5.16-E** for the "base" complex, and the ones labelled with primes ('), double primes ("), asterisks (*) and carets (^) respectively. Two of these have C_1 symmetry [**A** and **B**] and three have C_3 symmetry [**C**, **D** and **E**], making a total of three complexes in the asymmetric unit. These are shown in Figures 8.1 to 8.55. (The two complexes that do not have *crystallographic* C_3 symmetry, **A** and **B**, do possess *molecular* C_3 symmetry.)

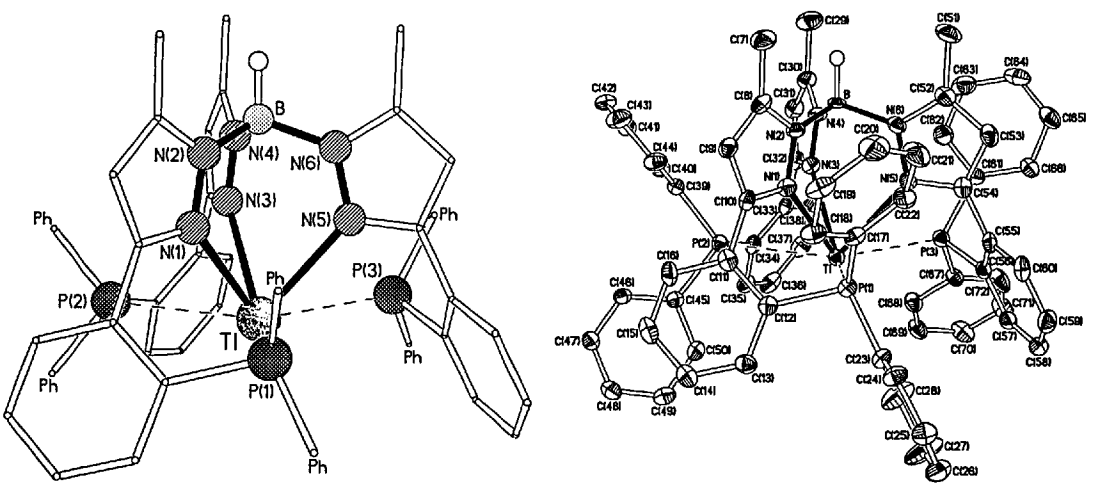


Figure 8.1. The molecular structure of **5.16-A**, one of the five crystallographically independent complexes present in the crystals of **5.16** (30% probability ellipsoids).

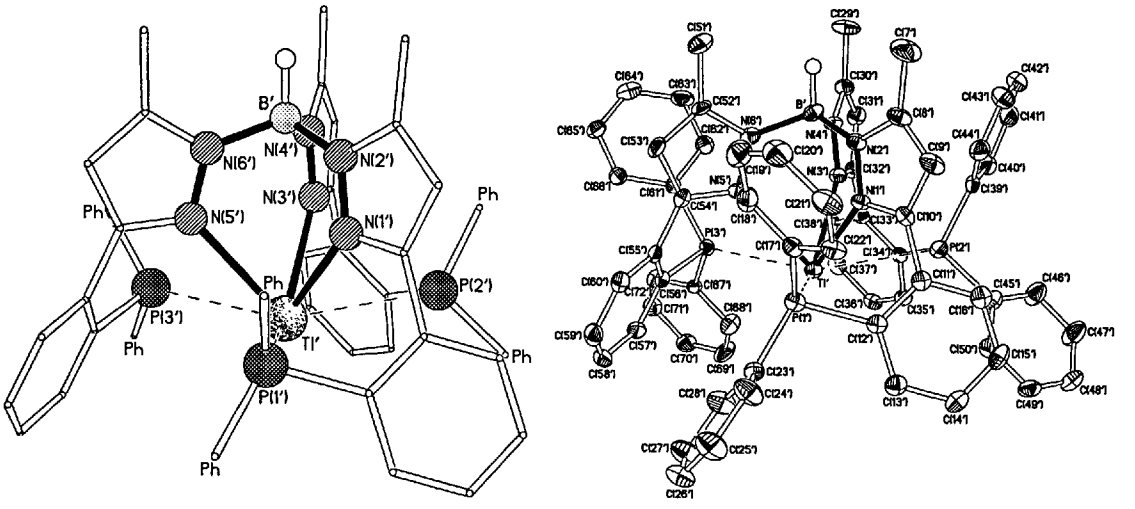


Figure 8.2. The molecular structure of **5.16-B**, one of the five crystallographically independent complexes present in the crystals of **5.16** (30% probability ellipsoids).

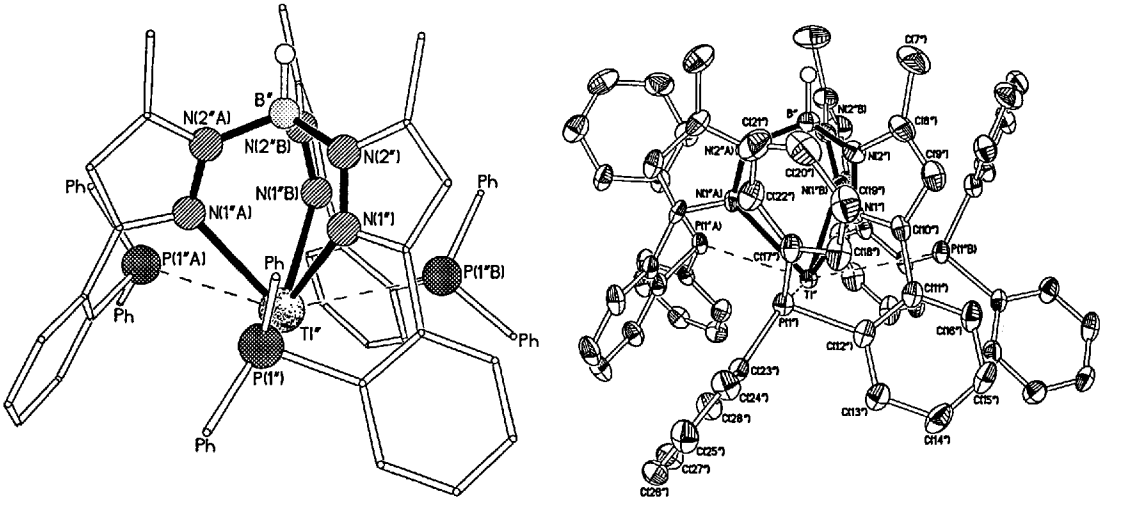


Figure 8.3. The molecular structure of **5.16-C**, one of the five crystallographically independent complexes present in the crystals of **5.16** (30% probability ellipsoids).

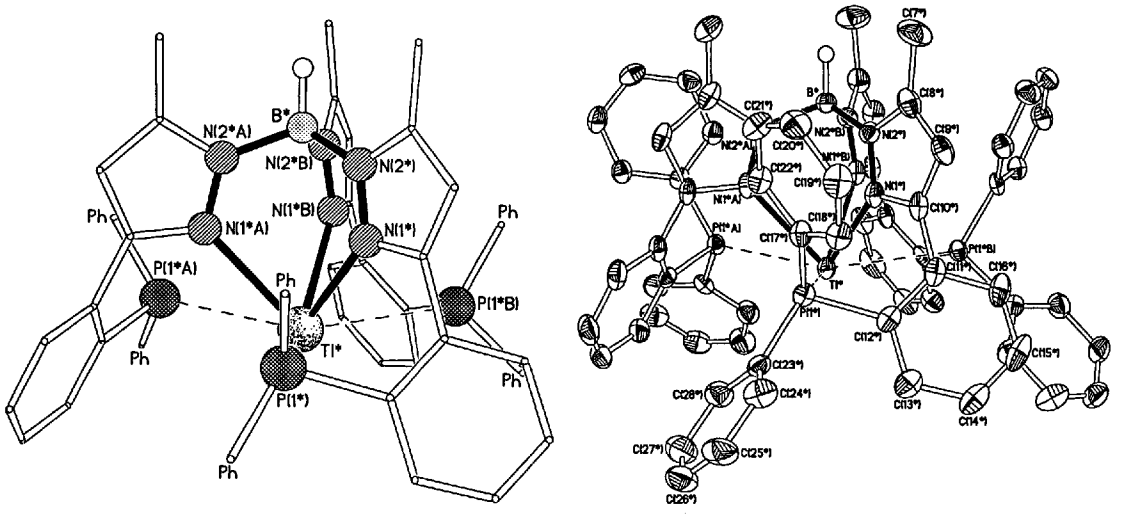


Figure 8.4. The molecular structure of **5.16-D**, one of the five crystallographically independent complexes present in the crystals of **5.16** (30% probability ellipsoids).

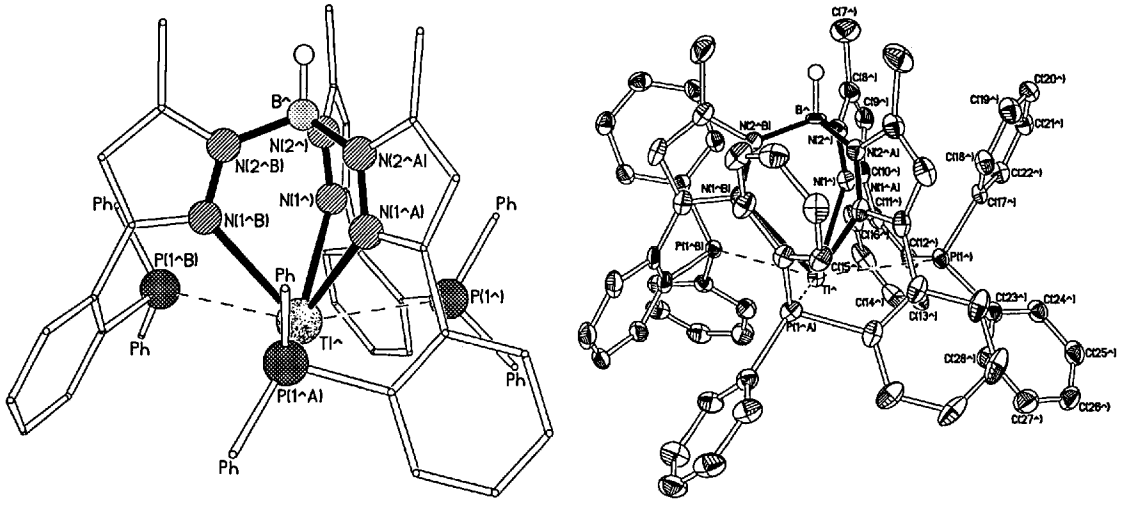


Figure 8.5. The molecular structure of **5.16-E**, one of the five crystallographically independent complexes present in the crystals of **5.16** (30% probability ellipsoids).

Given the twist of each arm of the ligand, the complexes are chiral, and the five independent complexes in the asymmetric unit are not all of the same chirality. Complexes **B**, **C**, **D** and **E** all have the same chirality, which is different to that of **A**, so in total the asymmetric unit contains two complexes of one chirality, and one complex of the other. Additionally, the crystal studied was a partial racemic twin, meaning that in *ca.* 84% of the unit cells in the crystal studied the chiralities are as shown in the figures, whilst in the other 16% all of the chiralities are reversed.

Amongst the five independent complexes present in the structure of **5.16**, molecule **C** stands out with shorter Tl–N and Tl···B separations, longer Tl–P distances, and larger N–Tl–N angles (Table 8.15). Assuming no other deformations, all these differences are consistent with the thallium centre in **C** being occupying a position closer to the N(1),N(3),N(5) plane than in the other four molecules [*ca.* 1.91 Å for **C** *cf.* between 1.96 and 1.99 Å for the others], though the reason for this deformation is unclear.

Table 8.15. Comparative selected bond lengths (Å) and angles (°) for the five crystallographically independent complexes present in the crystals of **5.16**.

	A	**B**	**C** [a]	**D** [a]	**E** [a]
Tl–N(1)	2.643(3)	2.635(3)	2.581(3)	2.631(3)	2.654(3)
Tl–N(3)	2.678(3)	2.621(3)			
Tl–N(5)	2.637(3)	2.643(3)			
Tl–P(1)	3.2274(9)	3.2893(9)	3.4374(10)	3.3169(10)	3.2580(9)
Tl–P(2)	3.2122(9)	3.3475(9)			
Tl–P(3)	3.2488(9)	3.2640(9)			
Tl···B	3.812(4)	3.803(5)	3.730(9)	3.798(9)	3.830(7)
Tl···[N_3] [b]	1.988	1.971	1.905	1.955	1.977
N(1)–Tl–N(3)	68.87(9)	70.85(9)	71.54(11)	70.87(11)	70.60(11)
N(1)–Tl–N(5)	70.03(9)	70.15(9)			
N(3)–Tl–N(5)	71.00(10)	69.31(9)			

(a) The molecule has C_3 symmetry meaning that the Tl–N(3) and Tl–N(5) bonds are symmetry equivalents of the Tl–N(1) bond, the Tl–P(2) and Tl–P(3) bonds are equivalent to the Tl–P(1) bond, and the N(1)–Tl–N(5) and N(3)–Tl–N(5) angles are equivalent to the N(1)–Tl–N(3) angle. (b) This is the deviation of the thallium centre from the plane of the three coordinated nitrogen atoms.

8.3 Publications

Variable coordination behaviour of pyrazole-containing *N*,*P* and *N*,*P*(*O*) ligands towards palladium(II)†

Steven Kealey,[a] Nicholas J. Long,*[a] Philip W. Miller,[a] Andrew J. P. White,[a] Peter B. Hitchcock[b] and Antony Gee[a,c]

Received 16th March 2007, Accepted 12th April 2007
First published as an Advance Article on the web 2nd May 2007
DOI: 10.1039/b704051b

Three bidentate, mixed-donor ligands based on a triphenylphosphine unit bearing a pyrazole group in the *ortho*-position of one phenyl ring have been synthesised; the *N*,*P* ligand [2-(3-pyrazolyl)phenyl]-diphenylphosphine **pzphos** has been synthesised and transformed into new *N*,*P*(*O*) and *N*,*P*(*S*) derivatives, [2-(3-pyrazolyl)phenyl]diphenylphosphine oxide **pzphos(O)** and [2-(3-pyrazolyl)phenyl]-diphenylphosphine sulfide **pzphos(S)**, respectively. The coordination chemistry of **pzphos** and **pzphos(O)** towards palladium(II) has been investigated. Depending on the ligand to metal molar ratio employed in the reactions of palladium(II) with **pzphos**, either the 1 : 1 chelate [Pd(pzphos)Cl_2] **1a** or the 2 : 1 *N*,*P* chelate [Pd(pzphos)$_2$]Cl_2 **1b** was obtained. **1b** contains two six-membered chelate rings in which the chlorides have been displaced from the inner coordination sphere of palladium. Exchange of the chloride anions in **1b** for perchlorate anions was achieved using $AgClO_4$ to give [Pd(pzphos)$_2$][ClO_4]$_2$ **1c**. Reaction of **pzphos(O)** under the same conditions forms the 2 : 1 adduct [Pd(pzphos(O))$_2$$Cl_2$] **2b** regardless of the metal to ligand ratio or the order of addition of reactants. Unlike the *N*,*P* chelate **1b**, the *N*,*P*(*O*) ligands in complex **2b** bind in a monodentate fashion through the N-donor atoms of the pyrazole rings. Abstraction of the chloro ligands in compound **2b** using $AgClO_4$ gave the 2 : 1 *N*,*P*(*O*) chelate [Pd{pzphos(O)}$_2$][ClO_4]$_2$ **2c**, in which entropically unfavourable 7-membered chelate rings are formed. X-Ray diffraction has been used to confirm the solid-state structures of the **pzphos(O)** ligand and the complexes **1b**, **1c**, **2b** and **2c**.

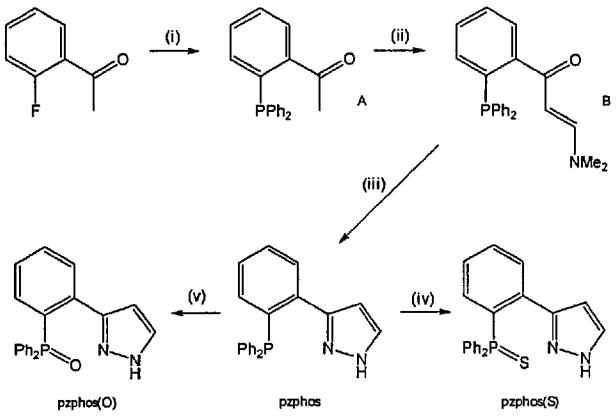
Introduction

Over recent years, considerable attention has been drawn towards the coordination chemistry of hybrid ligands *i.e.* those molecules containing significantly different donor groups. Of particular interest are the metal complexes of hybrid 'hemilabile' ligands,[1,2] containing at least one substitutionally inert donor group plus one or more substitutionally labile donor groups. These ligands, in the presence of a small molecule substrate, can allow the donor group with the lowest affinity towards the metal to dissociate to create a vacant coordination site which is then available to accommodate the new substrate. The 'anchor' effect of the stronger, permanently-bound donor group means that after the substrate has left the coordination sphere of the metal, chelation can again occur to stabilise the metal. These enticing properties of hemilabile ligands has led them to receive much interest in the field of catalysis,[2-11] as well as in small-molecule sensing,[12] functional materials,[3,13,14] and molecular activation.[15-21]

Coincidentally, during the course of our research, the ligand, [2-(3-pyrazolyl)phenyl]diphenylphosphine (**pzphos**), which consists of a triphenylphosphine unit (soft donor) bearing a pyrazole group (hard donor) in the *ortho*-position of one phenyl ring, was independently published,[22,23] albeit by a different synthetic route. Our route is shown in Scheme 1 and we are interested in this family of pyrazole-containing ligands for a number of reasons, namely; (i) the potential hemilability of the parent complex; (ii) the ease of derivatisation by chalcogenation of the phosphine moiety thus giving rise new to *N*,*P*(*O*), *N*,*P*(*S*) and *N*,*P*(*Se*) ligands; (iii) the scope for further functionalisation by alkylation of the N–H moiety. This last feature is particularly appealing as it may enable modifications of the steric or electronic properties of the ligand, which could be used to tune the ligand's coordination behaviour towards a metal centre.

A structurally similar ligand bearing the same triphenylphosphine unit, in this case attached to the pyrazolyl ring *via* the nitrogen atom (1-position) has recently been reported and has been shown to be active in the nickel catalysed oligomerisation of ethylene.[24] Furthermore, a bis(pyrazol-1-yl)methane ligand bearing diphenylphosphine groups directly attached to the pyrazole rings, rather than through a phenyl-linker, has also been described in the literature,[25] thus highlighting the ongoing interest in this field of chemistry. In addition, the coordination behaviour of a range of

[a]*Department of Chemistry, Imperial College London, South Kensington, London, UK SW7 2AZ. E-mail: n.long@imperial.ac.uk; Tel: +44 (0)20 7594 5781*
[b]*Department of Chemistry, School of Life Sciences, University of Sussex, Falmer, Brighton, UK BN1 7QJ*
[c]*GSK Clinical Imaging Centre, Imperial College London, Hammersmith Hospital, Du Cane Road, London, UK W12 0NN*
† Electronic supplementary information (ESI) available: Crystallographic and NMR data. See DOI: 10.1039/b704051b



Scheme 1 Synthesis of **pzphos(O)** and **pzphos(S)**. Reagents and conditions: (i) $KPPh_2$, THF, reflux, 1 h; (ii) *N*,*N*-dimethylformamide dimethyl acetal, EtOH, reflux, 12 h; (iii) $N_2H_4.H_2O$, EtOH, reflux, 3 h; (iv) S_8, CH_2Cl_2, rt, 1 h; (v) H_2O_2, CH_2Cl_2, rt, 1 h.

N,*P* ligands[26–28] is well established in the literature and to a lesser extent, the chemistry of *N*,*P*(*O*) ligands.[29–36] The work presented herein, describes the formation of two chalcogen derivatives of **pzphos** and the coordination chemistry of the *N*,*P* and *N*,*P*(*O*) ligands, **pzphos** and **pzphos(O)**, towards palladium(II).

Results and discussion

Ligand synthesis

The synthesis of the three ligands is outlined in Scheme 1: Ligand precursor **A** was synthesised using a different approach to the three-step synthesis described recently by Sun *et al.*[22] Instead, a facile one step synthesis which involved heating a solution of potassium diphenylphosphide and 2-fluoroacetophenone in THF was used to synthesise **A** rapidly and in high yield.[37] **A** was then converted into the **pzphos** ligand in good yield in two steps. The chalcogen derivatives were synthesised by reaction of **pzphos** with hydrogen peroxide or sulfur to produce the respective phosphine oxide and phosphine sulfide ligands, **pzphos(O)** and **pzphos(S)**. All three ligands were isolated as air-stable, white solids in good yields and were fully characterised. As shown in Table 1, the ^{31}P NMR spectra of the phosphorus(v) species **pzphos(O)** and **pzphos(S)** show characteristic upfield shifted singlets at +35.8 ppm and +43.3 ppm, respectively, compared to the phosphorus(III) parent ligand, **pzphos** at −11.4 ppm.

Slow diffusion of pentane into a chloroform solution of the ligand produced single crystals suitable for X-ray analysis. The solid-state structure of **pzphos(O)** shows that the molecule dimerises in the solid state *via* intermolecular hydrogen bonding between adjacent molecules (Fig. 1). It is interesting to note that the hydrogen bond from the pyrazole N–H donor is shared equally between two acceptors on the opposing molecule: the unprotonated pyrazole nitrogen and the oxygen atom of the P(O) moiety. This dimerisation is also observed in solution as the N–H in the ^1H NMR spectrum is far downfield at 13.24 ppm, whereas the parent complex **pzphos** (containing no P=O group) shows the corresponding N–H peak at 10.57 ppm (Table 1). This is likely to be the result of reduced electron density around the N–H hydrogen, due to the sharing of its electron density with both

Table 1 IR, ^1H and $^{31}P\{^1H\}$ NMR data for the three ligands

Ligand	$^{31}P\{^1H\}$ NMR[a] δ/ppm	^1H NMR[a] δ/ppm								IR[b] ν/cm^{-1}
	P	NH	5-pz	4-pz	3-Ph	4-Ph	5-Ph	6-Ph	Ph-H	NH
pzphos	−11.4	10.57	7.48 (d)	6.34 (m)	7.60 (dd)	7.42 (ddd)	overlap with Ph–H at 7.30	7.03 (ddd)	7.26–7.37 (m)	3187
pzphos(O)	+35.8	13.24	7.32 (d)	6.25 (br s)	7.78 (ddd)	overlap with Ph–H at 7.61	7.30 (m)	7.14 (ddd)	7.38–7.64 (m)	3186
pzphos(S)	+43.3	12.54	7.17 (d)	6.08 (br s)	overlap at 7.57 (m)		7.37 (m)	7.18 (dd)	7.82 (m) & 7.37–7.44 (m)	3220

[a] Recorded in $CDCl_3$ solution. [b] Recorded as KBr disc.

This journal is © The Royal Society of Chemistry 2007

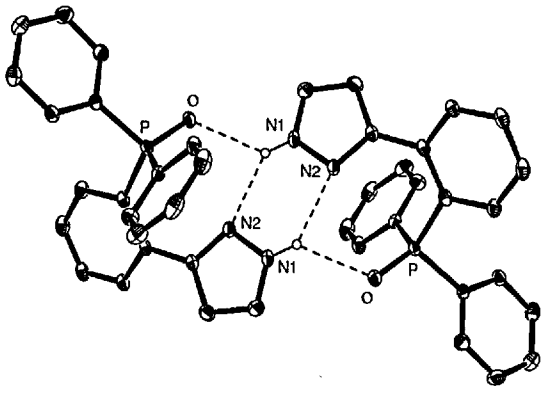


Fig. 1 The molecular structure of **pzphos(O)** (50% probability ellipsoids). The N–H···O hydrogen bonds have N···O, H···O (Å), and N–H···O (°) of 2.91, 2.54 and 133 respectively; the N–H···N hydrogen bonds have N···N, H···N (Å), and N–H···N (°) of 2.94, 2.22 and 141 respectively.

the pyrazole nitrogen *and* the oxygen atom. A similar effect may also be observed with the sulfur derivative, **pzphos(S)**, as evidenced by the downfield position (12.54 ppm) of the corresponding N–H hydrogen in the ^{1}H NMR spectrum.

Coordination chemistry

Reactions of *N,P* ligand, pzphos. The reactions performed with the *N,P* ligand **pzphos** are outlined in Scheme 2. Addition of **pzphos** in dichloromethane to $Pd(COD)Cl_2$ in a 1 : 1 molar ratio gave a yellow precipitate that could be crystallised by slow diffusion of pentane into a chloroform solution of the complex. This complex **1a** was analysed by NMR spectroscopy and X-ray crystallography and was found to be identical to the complex independently synthesised by Sun *et al.*[22] by the similar reaction of **pzphos** with $Pd(PhCN)_2Cl_2$. In this complex, a single **pzphos** ligand chelates to the palladium *via* the N and P donor groups with the remaining two coordination sites occupied by chloro ligands.

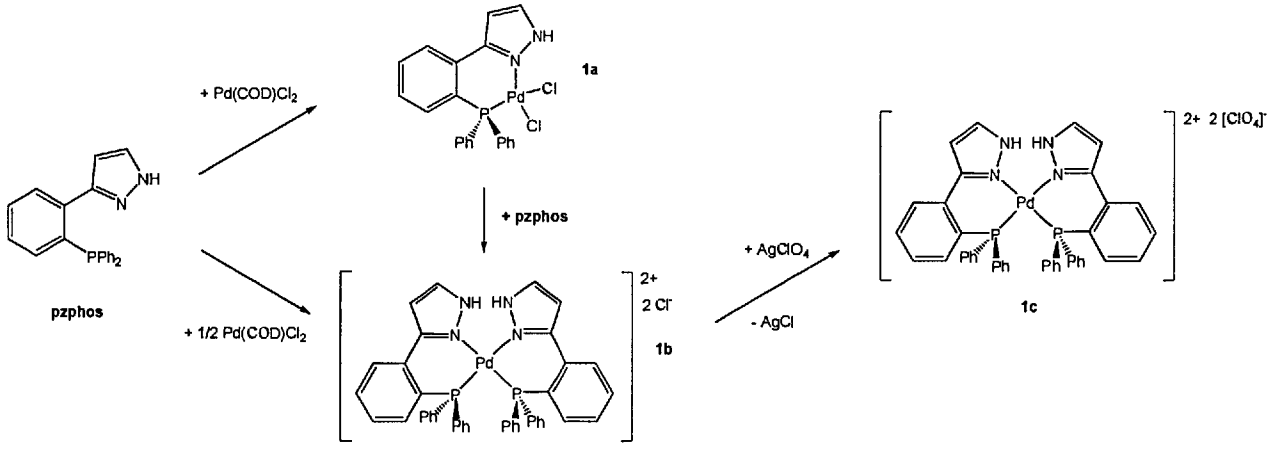
Upon increasing the ligand-to-metal ratio from 1 : 1 to 2 : 1, we found that addition of $Pd(COD)Cl_2$ to **pzphos** gave a different product in solution. This was evidenced by the ^{31}P NMR spectrum of the reaction solution (taken after 1 h of stirring) which contained a major peak at +31.8 ppm, corresponding to the new species, and an additional smaller peak at +25.7 ppm corresponding to traces of the 1 : 1 complex **1a**. Complex **1b** was isolated as a yellow solid by precipitation of a dichloromethane solution with hexane.

It was also possible to form **1b** by a stepwise process by first forming and isolating **1a** and then reacting this with a further equivalent of the **pzphos** ligand (shown in Scheme 2). The formation of the bis-chelate species **1b** is noteworthy as it has been previously reported that it was only possible to isolate the mono-chelate species **1a**, even when using a large excess of **pzphos** in the reaction with $Pd(PhCN)_2Cl_2$.[22]

The ^{31}P{H} NMR spectrum of **1b** showed one singlet at +31.6 ppm (*c.f.* **pzphos** ligand; $\delta = -11.4$ ppm) indicating the coordination of the **pzphos** ligands to the palladium centre in chemically equivalent environments. The N–H hydrogen of the pyrazole ring was found to be significantly shifted downfield in the ^{1}H NMR spectrum to 14.86 ppm compared to the free **pzphos** ligand ($\delta = 10.57$ ppm), suggesting coordination of the adjacent nitrogen atom of the pyrazole ring to the metal centre (Table 2). The bis-ligated nature of **1b** was confirmed by ESI mass spectrometry which showed a molecular ion peak at 761 *m/z* corresponding to $[Pd(pzphos)_2]^+$ and suitable crystals for X-ray diffraction were obtained by slow diffusion of pentane into a chloroform solution of **1b**.

The solid state structure of **1b** shows the palladium to have a distorted square planar geometry with the two **pzphos** ligands chelating in a *cis* fashion resulting in a dicationic species in which two chloride anions balance the charge (Fig. 2, Table 3). The N–H hydrogen atoms are linked to the chloride anions by N–H···Cl hydrogen bonds (see ESI).† Within each ligand the linked C_6 and C_3N_2 rings are distinctly twisted with respect to each other, the torsion angles for the C–C bond between them being *ca.* 20 and 26° for the N(4) and N(2) ligands, respectively. The two {Pd,P,N} coordination planes are twisted with respect to each other by *ca.* 15°, a distortion that may in part be due to a π–π stacking interaction between pendant phenyl rings on adjacent ligands (dashed line in Fig. 2). These interactions are supported by the ambient temperature ^{1}H NMR spectrum which shows some significantly broadened peaks in the aromatic region. Following this observation, variable temperature spectra were recorded upon cooling the solution to 223 K (aromatic region shown in Fig. 3).

At 223 K, the spectrum consists of sharp peaks and as the temperature is increased, some of these peaks coalesce forming broad signals. It is apparent that not all of these aromatic



Scheme 2 Reactions of **pzphos** with palladium(II).

Table 2 IR, ^{1}H and ^{31}P{H} NMR data for the complexes **1a–2c**

Complex	^{31}P{^{1}H} NMR[a] δ/ppm	^{1}H NMR[a] δ/ppm							IR[b] ν/cm^{-1}
	P	NH	5-pz	4-pz	3-Ph	4-Ph	5-Ph	6-Ph	Ph-H	NH
1a [Pd(pzphos)Cl$_2$]	+25.6	13.14 (s)	7.65 (dd)	6.86 (dd)	7.90 (ddd)	7.70 (dd)	7.42 (m)	7.05 (ddd)	7.4–7.7 (m)	3230
1b [Pd(pzphos)$_2$]Cl$_2$	+31.6	14.86 (s)	7.72 (d)	6.50 (d)	7.97 (m)	7.63 (dd)	7.28 (m)	6.82 (dd)	—[c]	~3290[d]
1c[e] [Pd(pzphos)$_2$][ClO$_4$]$_2$	+34.1	13.42 (s)	8.19 (dd)	6.99 (dd)	8.08 (ddd)	7.85 (dd)	7.59 (dd)	7.05 (ddd)	—[c]	3302[f]
2b [Pd{pzphos(O)}Cl$_2$]	+32.7	13.51 (s)	7.81 (dd)	6.19 (dd)	7.57 (dd)	7.61 (dd)	7.37 (dd)	7.22 (dd)	7.74 (m), 7.53 (m), 7.47 (m)	3196[g]
2c [Pd{pzphos(O)}$_2$][ClO$_4$]$_2$	+53.8	12.34 (s)	7.31 (d)	6.02 (dd)	8.27 (dd)	8.12 (dd)	overlap at ~7.4 (m)		7.6–7.9 (m)	3686[g]

[a] Recorded as $CDCl_3$ solution at 293 K unless indicated otherwise. [b] Recorded as KBr disc unless indicated otherwise. [c] Temperature dependent — see discussion. [d] Partially obscured by residual H_2O in disc. [e] Recorded as d^6-acetone solution. [f] Recorded as Nujol mull. [g] Recorded as CH_2Cl_2 solution.

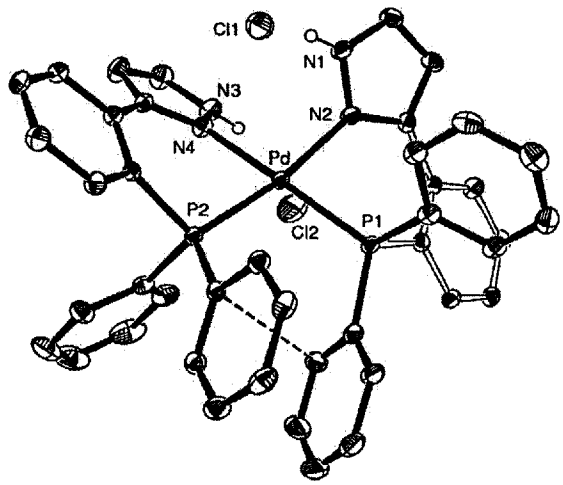


Fig. 2 Molecular structure of complex **1b** (30% probability ellipsoids). The π–π stacking interaction (dashed line) has centroid···centroid and mean interplanar separations of *ca.* 3.57 and 3.18 Å respectively, the two rings being inclined by *ca.* 7°.

Table 3 Selected bond lengths (Å) and angles (°) for **1b**

Pd–N(2)	2.072(4)	Pd–P(1)	2.2565(13)
Pd–N(4)	2.074(4)	Pd–P(2)	2.2541(13)
N(2)–N(1)	1.360(6)	N(4)–N(3)	1.344(6)
N(2)–Pd–P(1)	83.86(12)	N(4)–Pd–N(2)	92.77(16)
N(2)–Pd–P(2)	168.33(12)	P(1)–Pd–N(4)	169.39(12)
P(1)–Pd–P(2)	101.57(5)	N(4)–Pd–P(2)	83.63(12)

hydrogens are involved in fluxional behaviour as some resonances are temperature-independent. From the COSY ^{1}H NMR spectrum recorded at 223 K it has been possible to assign the peaks in these spectra; the non-fluxional hydrogens have been assigned as those attached to the pyrazolyl and phenyl rings which comprise the backbone of the ligand. The remaining hydrogens, which all display fluxional behaviour, are those which are present in the diphenylphosphine moiety of the ligand–metal complex. We ascribe this low temperature phenomenon to hindered rotation about the P–Ph bonds resulting in hydrogens occupying different spatial positions and hence unique chemical environments for periods of time comparable to the NMR timescale. These hydrogens are therefore observed as separate resonances while at higher temperatures, the energy barrier to rotation is overcome hence these peaks begin to coalescence.

Exchange of the chloride counter-anions in **1b** for perchlorate anions was achieved by addition of two equivalents of silver perchlorate, with the driving force of this reaction being the precipitation of silver chloride (Scheme 2). The ^{31}P NMR of the yellow solid product **1c** shows a single peak with chemical shift +34.1 ppm (*cf.* **1b**; $\delta = +31.6$ ppm) and the N–H in the ^{1}H NMR spectrum is found at 13.42 ppm (Table 2). The ^{1}H NMR shows broad peaks corresponding to the diphenylphosphine hydrogens. These broad peaks split into sharp resonances at low temperatures as seen previously for complex **1b** (see ESI).†

Layering of hexane above a dichloromethane solution of **1c** yielded single crystals suitable for X-ray analysis. The solid state structure of **1c** shows the palladium to have a distorted square planar geometry with the two **pzphos** ligands chelating in a *cis*

This journal is © The Royal Society of Chemistry 2007

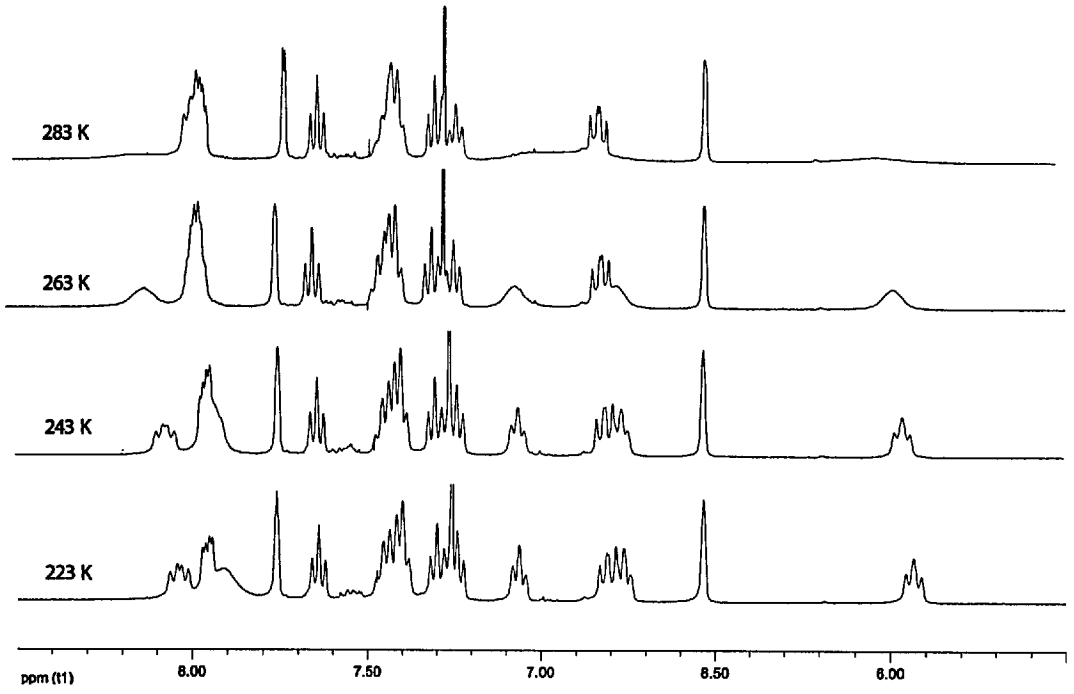


Fig. 3 Variable temperature (283 K to 223 K) ^{1}H NMR spectra of complex **1b**.

fashion (Fig. 4, Table 4). As seen for complex **1b**, a π–π stacking interaction between pendant phenyl rings on adjacent ligands is observed (dashed line in Fig. 4), and may be responsible for the twisting of the two {Pd,P,N} coordination planes with respect to each other (by *ca.* 14°). Within each ligand the linked C_6 and C_3N_2 rings are distinctly twisted with respect to each other, the torsion angles for the C–C bond between them being *ca.* 25 and 26° for the N(1) and N(31) ligands respectively. The N–H hydrogen atoms are linked to the perchlorate anions by N–H · · · O hydrogen bonds (see ESI).†

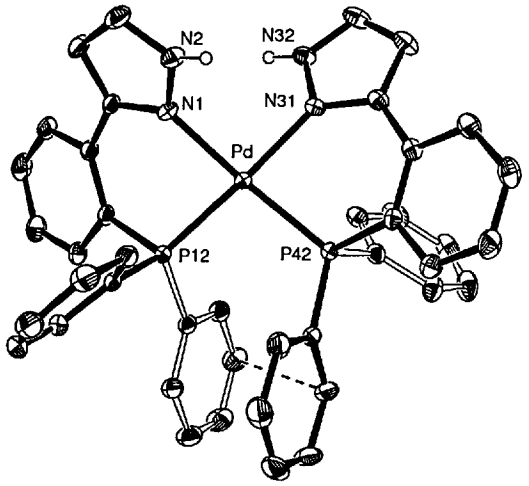


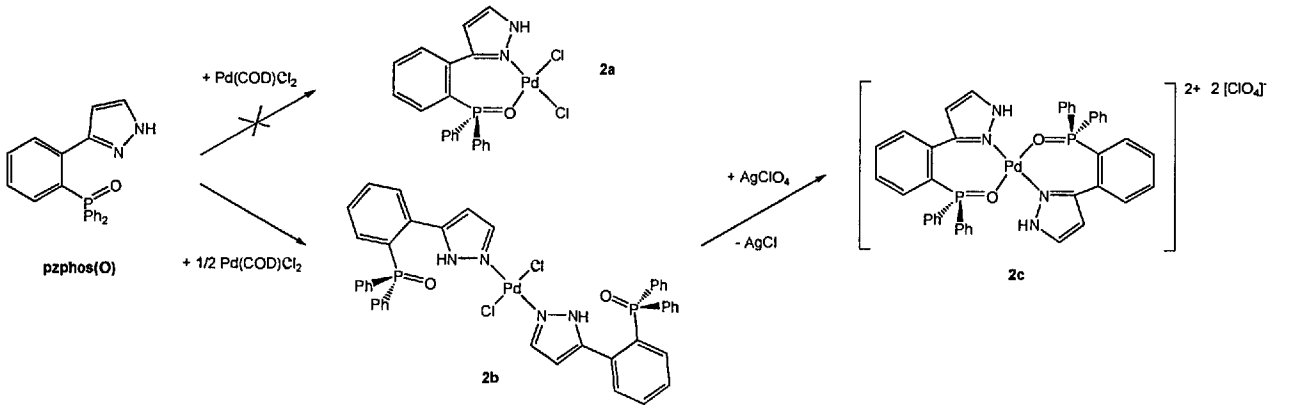
Fig. 4 Molecular structure of the cation in **1c** (30% probability ellipsoids). The π–π stacking interaction (dashed line) has centroid · · · centroid and mean interplanar separations of *ca.* 3.89 and 3.25 Å respectively, the two rings being inclined by *ca.* 2°.

Table 4 Selected bond lengths (Å) and angles (°) for **1c**

Pd–N(1)	2.0738(17)	Pd–P(12)	2.2614(6)
Pd–N(31)	2.0763(17)	Pd–P(42)	2.2545(6)
N(1)–N(2)	1.357(3)	N(31)–N(32)	1.352(2)
N(1)–Pd–P(12)	85.68(5)	N(1)–Pd–N(31)	91.73(7)
N(1)–Pd–P(42)	170.37(5)	P(12)–Pd–N(31)	169.37(5)
P(12)–Pd–P(42)	99.39(2)	N(31)–Pd–P(42)	84.71(5)

Reactions of *N,P(O)* ligand, pzphos(O). The *N,P(O)* ligand **pzphos(O)** displays different coordination behaviour since the 'soft' phosphine group is now replaced by a 'hard' phosphine oxide donor that has a lower affinity towards palladium(II). Formation of a chelate ring is now entropically disfavoured due to the increased size of the potential chelate ring, now seven-membered as opposed to the six-membered complexes of **pzphos** described above. The reactions performed between **pzphos(O)** and $Pd(COD)Cl_2$ are outlined in Scheme 3.

The reactivity of **pzphos(O)** was first examined by addition of a dichloromethane solution of $Pd(COD)Cl_2$ to two equivalents of **pzphos(O)**. The $^{31}P\{H\}$ NMR spectrum of the reaction solution was recorded after stirring at room temperature for 1 h, with the chemical shift of the predominant species occurring at +33.0 ppm (*cf.* free ligand; δ = 35.8 ppm). This indicated that the oxide group was not coordinated to the palladium as a significant downfield shift is expected to occur on coordination as a result of the inductive deshielding effect upon the phosphorus atom. The product **2b** was isolated by addition of hexane to the reaction solution and the $^{31}P\{H\}$ and ^{1}H NMR spectra were recorded of the resultant yellow solid (Table 2). The downfield position of the N–H in the ^{1}H NMR spectrum (13.51 ppm) suggests coordination of the pyrazolyl ring has occurred, in a similar fashion to the **pzphos** complexes described above. As such, it was hypothesised that a 2 : 1 ligand-to-metal complex had formed with the two ligands binding through their pyrazole nitrogens only and with the remaining



Scheme 3 Reactions of **pzphos(O)** with palladium(II).

coordination sites around the palladium centre being occupied by two chloro ligands. This stoichiometry was supported by FAB (+ve) mass spectral data showing a palladium isotope pattern at 869 *m/z* corresponding to $[Pd\{pzphos(O)\}_2Cl_2]^+$. To confirm this structure, crystals were grown by slow diffusion of pentane into a chloroform solution of the **2b** and were subsequently analysed by X-ray crystallography.

The solid state structure of **2b** shows the palladium to have a square planar geometry with the two **pzphos** ligands bound in a monodentate fashion *via* Pd–N bonds. In contrast to the **pzphos** complex **1b**, the two ligands are coordinated in a *trans* fashion with two chloro ligands occupying the remaining two sites around the palladium (Fig. 5, Table 5). Within each ligand the linked C_6 and C_3N_2 rings are distinctly twisted with respect to each other, the torsion angle for the C–C bond between them being *ca.* 39°. This distortion may be caused by the molecule adopting a conformation that facilitates intramolecular N–H···O hydrogen bonding between the N(1)–H donor and the O(1) acceptor.

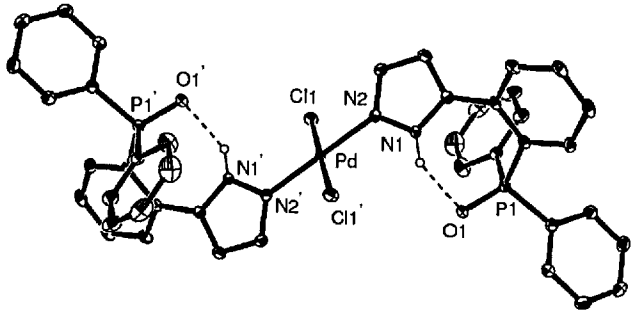


Fig. 5 Molecular structure of **2b** (30% probability ellipsoids). The intramolecular N–H···O hydrogen bonds (dashed lines) have N···O, H···O (Å), and N–H···O (°) of 2.69, 1.92 and 144 respectively.

The combination of the hard oxide donor on **pzphos(O)** and the increased size of the potential chelate ring (now seven-membered)

Table 5 Selected bond lengths (Å) and angles (°) for **2b**

Pd–N(2)	1.999(2)	Pd–Cl(1)	2.2995(7)
N(1)–N(2)	1.348(3)	P(1)–O(1)	1.496(2)
N(2)–Pd–Cl(1)	89.19(7)	N(2)–Pd–N(2')	180
N(2')–Pd–Cl(1)	90.81(7)	Cl(1')–Pd–Cl(1)	180

disfavours chelation, in contrast to the behaviour of the **pzphos** ligand. Since the ligands do not chelate, the *trans* form is observed as steric interactions between the two ligands are minimised. This structure further differs from the uncoordinated **pzphos(O)** ligand and the **pzphos** complexes **1a–1c** in that the N–H hydrogen has 'swapped' the nitrogen atom to which it is bonded, and consequently, coordination to palladium now occurs through the nitrogen in the 1'-position (Fig. 6).

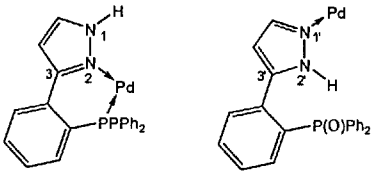


Fig. 6 Variable bonding modes of **pzphos** (left) and **pzphos(O)** (right).

This coordination mode in **2b** is presumed to result from the monodentate behaviour of the **pzphos(O)** ligand which permits the fluxional N–H hydrogen to reside on the nitrogen atom that produces the most energetically favourable configuration in the resultant complex, *i.e.* where steric interactions between the ligand moieties and the metal are minimised. This is achieved by coordination at the 1'-position, thus leaving the bulky triphenylphosphine oxide moiety on the 'other side' of the pyrazolyl ring, pointing away from the metal. This bonding mode has previously been observed for a palladium(II) complex of a 3-substituted pyrazole ligand.[38] Further stabilisation for this form is also achieved by the formation of intramolecular N–H···O hydrogen bonds.

The lack of formation of a seven-membered chelate has been observed previously with another *N,P(O)* ligand towards palladium(II).[36] Although formation of a seven-membered chelate has been observed in the palladium(II) complexes of *N,N*[39] and *N,P* ligands,[40] it is disfavoured in the case of oxygen donors due to the lower affinity of these donor groups towards palladium. In contrast, chelation of six-membered *N,P(O)* ligands around palladium has been observed previously,[31] although in one case it required an excess of palladium over ligand and heating at reflux for several hours.[35] In our attempts to synthesise the *mono* chelate structure **2a**, we found that even when using forcing conditions (extended reaction times, reflux, excess of palladium), the bis

This journal is © The Royal Society of Chemistry 2007

adduct **2b** would form preferentially with no traces of a chelated species being observed by ^{31}P NMR spectroscopy.

It was, however, anticipated that by adding two equivalents of silver perchlorate to a solution of **2b**, coordination of the oxide group could be encouraged by removal of the chloro ligands. This reaction was performed accordingly and after stirring the reaction solution at room temperature for 30 min, the $^{31}P\{H\}$ NMR spectrum revealed a mixture in which the predominant species occurred at 52.9 ppm, with smaller peaks present at 35.3 and 33.3 ppm. This species was subsequently isolated as a yellow powder by addition of hexane to the reaction mixture and recrystallisation from hot MeOH. The $^{31}P\{H\}$ NMR spectrum showed a singlet at 53.8 ppm enabling us to tentatively ascribe this complex as the bis-chelated species **2c** as its $^{31}P\{H\}$ chemical shift closely resembled that of a similarly coordinated *N,P(O)* species.[31] In order to confirm the structure of **2c**, X-ray analysis was performed on a single crystal grown by slow diffusion of pentane into a chloroform solution of the complex. Indeed, the solid state structure shows the palladium to have a square planar geometry with two **pzphos(O)** ligands chelating in a *trans* fashion (Fig. 7, Table 6). Each of the seven membered $C_3NP(O)Pd$ chelate rings has a distorted boat conformation. As a consequence of chelation, the linked C_6 and C_3N_2 rings within each ligand are distinctly twisted with respect to each other, the torsion angle for the C–C bond between them being *ca.* 50°.

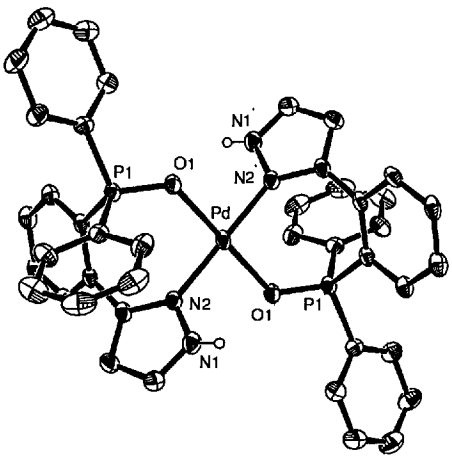


Fig. 7 Molecular structure of the cation in **2c** (30% probability ellipsoids).

This structure reveals that the N–H hydrogen of the **pzphos(O)** ligand has reverted back to the 1-position of the pyrazole ring (Fig. 7). This makes available the nitrogen in the 2-position for coordination to the metal and thus allows formation of the seven-membered chelate. Tautomerisation of this kind is required for chelation as when the ligand coordinates *via* the nitrogen in the 1′-position (as in **2b**), the rigidity of the ligand prevents the oxide group from approaching the palladium centre.

Table 6 Selected bond lengths (Å) and angles (°) for **2c**

Pd–N(2)	2.008(4)	Pd–O(1)	2.009(3)
N(1)–N(2)	1.339(7)	P(1)–O(1)	1.526(4)
N(2)–Pd–O(1)	92.89(16)	N(2′)–Pd–O(1)	87.11(16)
N(2)–Pd–N(2′)	180	O(1)–Pd–O(1′)	180

Conclusions

Relatively simple ligand tuning has been employed to demonstrate the variable coordination behaviour of the *N,P* ligand **pzphos** and the related *N,P(O)* ligand, **pzphos(O)** towards palladium(II). This tuning effect has demonstrated the potential hemilability of these species, while **pzphos** favoured chelation in all cases, **pzphos(O)** acted as a monodentate N-donor that could be forced into a bidentate chelating mode by abstraction of the chloro ligands. To our knowledge, this is the first structurally characterised example of an *N,P(O)* hybrid ligand chelating at a palladium(II) centre.[41] Investigations are currently underway in our laboratory into the catalytic properties of these complexes as well as the further functionalisation of the ligands *via* substitution at the pyrazolyl nitrogen. We have found the coordination chemistry of the *N,P(S)* ligand **pzphos(S)** to be less straightforward, and the results of these investigations will be presented in due course.

Experimental

All reagents, unless stated otherwise were purchased from commercial suppliers without further purification. Elemental analyses were performed by Stephen Boyer at the London Metropolitan University. ^1H, $^{13}C\{H\}$ and $^{31}P\{H\}$ NMR spectra were recorded on Bruker Av-400, DRX-400 or Av-500 spectrometers. Chemical shifts are reported in ppm using the residual proton impurities in the solvents. Pseudo-triplets which occur as a result of identical *J*-value coupling to two chemically inequivalent protons are assigned as dd and are recognised by the inclusion of only one *J*-value. Mass spectra were recorded on a Micromass Autospec Q spectrometer by Mr J. Barton and Mr G. Tucker of the Department of Chemistry, Imperial College, London. Infrared absorption spectra were collected either as KBr discs or Nujol mulls using a Perkin Elmer RX FT-IR spectrometer. Ligand precursor A was prepared as reported previously.[37]

Ligand syntheses

1-(2′-Diphenylphosphino)3-dimethylamino-2-propene-1-one B. Using a variation of a literature procedure,[42] 2′-(diphenylphosphino)acetophenone (12.35 g, 40.6 mmol) and *N,N*-dimethylformamide dimethylacetal (25 ml, excess) were heated at 120 °C for 12 h over which time the yellow solution turned deep brown. After cooling to room temperature, the excess *N,N*-dimethylformamide dimethyl acetal was removed *in vacuo* to leave a dark orange solid which was broken up and stirred in pentane (100 ml) and filtered to produce an orange solid which was dried *in vacuo* (13.48 g, 92%). Analysis was carried out on a sample recrystallised from CH_2Cl_2/hexane. ^1H NMR (+25 °C, $CDCl_3$, 400 MHz), δ = 7.64 [dd ($^3J_{HH}$ = 6.9 Hz, $^4J_{HH}$ = 3.8 Hz), 1H, 3-Ph], 7.38 [ddd ($^3J_{HH}$ = 7.7 Hz, $^3J_{HH}$ = 7.6 Hz, $^4J_{HH}$ = 1.2 Hz), 1H, 4-Ph], 7.27–7.35 [m, 12H, 5-Ph + *o,m,p*-Ph + $CHNMe_2$], 7.06 [dd ($^3J_{HH}$ = 7.3 Hz, $^4J_{HH}$ = 3.5 Hz), 1H, 6-Ph], 5.43 [d ($^3J_{HH}$ = 12.6 Hz), 1H, COCH], 2.96 [s, 3H, NCH_3], 2.71 [s, 3H, NCH_3]. $^{31}P\{H\}$ NMR (+25 °C, $CDCl_3$, 162.05 MHz), δ = −10.3. IR (KBr disc), ν/cm^{-1} 1637(CO). MS(EI), m/z = 359 [M]$^+$. Anal. (%); Calc. (found) for $C_{23}H_{22}NOP$: C, 76.9 (76.8); H, 6.17 (6.03); N, 3.90 (3.83).

[2-(3-Pyrazolyl)phenyl]diphenylphosphine pzphos. Hydrazine hydrate (10 ml, excess) was added dropwise to a solution of **B** (12.00 g, 33.4 mmol) in hot ethanol (150 ml) and stirred under reflux for 3 h. Removal of the solvent gave an orange solid to which was added water (50 ml) and the solid was collected by filtration. The aqueous washings were extracted into $CHCl_3$ (200 ml) and the organic fraction was separated and used to dissolve the solid. Drying ($MgSO_4$), filtration and concentration followed by recrystallisation from $CHCl_3$/hexane gave a colourless solid. Yield = 9.33 g (91%). ^{1}H NMR (+25 °C, $CDCl_3$, 500 MHz), δ = 10.57 [s, 1H, NH], 7.60 [dd ($^3J_{HH}$ = 7.1 Hz, $^4J_{HH}$ = 3.7 Hz), 1H, 3-Ph], 7.48 [d ($^3J_{HH}$ = 2.0 Hz), 1H, 5-pz], 7.42 [ddd ($^3J_{HH}$ = 7.7 Hz, $^3J_{HH}$ = 7.6 Hz, $^4J_{HH}$ = 1.3 Hz), 1H, 4-Ph], 7.33–7.37 [m, 6H, *m,p*-Ph], 7.26–7.31 [m, 4H, *o*-Ph], 7.03 [ddd ($^3J_{HP}$ = 7.8 Hz, $^3J_{HH}$ = 4.2 Hz, $^4J_{HH}$ = 1.1 Hz), 1H, 6-Ph], 6.34 [m, 1H, 4-pz]. ^{31}P{H} NMR (+25 °C, $CDCl_3$, 162.05 MHz), δ = −11.4. ^{13}C{H} NMR (+25 °C, $CDCl_3$, 500 MHz), δ = 146.9 [s, 3-pz], 140.0 [s, 5-pz], 137.1 [d, ($^1J_{CP}$ = 10.6 Hz), *i*-Ph], 136.1 [d ($^2J_{CP}$ = 17.3 Hz), 2-Ph], 134.3 [s, 6-Ph], 133.9 [d, ($^2J_{CP}$ = 19.7 Hz), *o*-Ph], 131.8 [s, 1-Ph], 130.0 [d ($^3J_{CP}$ = 5.5 Hz), 3-Ph], 128.9 [s, 5-Ph], 128.8 [s, 4-Ph], 128.6 [d ($^3J_{CP}$ = 7.6 Hz), *m*-Ph], 128.3 [s, *p*-Ph], 106.5 [s, 4-pz]. IR (KBr disc), ν/cm^{-1} 3187 cm^{-1}(NH). MS(EI), m/z = 328 [M]$^+$. Anal. (%): Calc. (found) for $C_{21}H_{17}N_2P$: C, 76.8 (77.0); H, 5.22 (5.00); N, 8.53 (8.35).

[2-(3-Pyrazolyl)phenyl]diphenylphosphine oxide pzphos(O). A solution of **pzphos** (0.30 g, 0.91 mmol) and H_2O_2 (27.5% in H_2O, 135 μL, 1.10 mmol) in CH_2Cl_2 (30 ml) was stirred for 1 h after which time H_2O (40 ml) was added and the organic layer separated, dried ($MgSO_4$) and concentrated to dryness to give a colourless solid. Yield = 0.20 g (63%). ^{1}H NMR (+25 °C, $CDCl_3$, 500 MHz), δ = 13.24 [s, 1H, NH], 7.78 [ddd ($^3J_{HH}$ = 7.8 Hz, $^4J_{HH}$ = 4.2 Hz, $^5J_{HH}$ = 1.0 Hz), 1H, 3-Ph], 7.61 [m, 5H, *o*-Ph + 4-Ph], 7.50 [m, 2H, *p*-Ph], 7.41 [m, 4H, *m*-Ph], 7.32 [d ($^3J_{HH}$ = 1.8 Hz), 1H, 5-pz], 7.30 [m, 1H, 5-Ph], 7.14 [ddd ($^3J_{HP}$ = 14.6 Hz, $^3J_{HH}$ = 7.8 Hz, $^4J_{HH}$ = 1.1 Hz), 1H, 6-Ph], 6.25 [s, 1H, 4-pz]; ^{31}P{H} NMR (+25 °C, $CDCl_3$, 162.05 MHz), δ = +35.8. ^{13}C{H} NMR (+25 °C, $CDCl_3$, 500 MHz), δ = 141.8 [s, 3-pz], 139.7 [s, 5-pz], 134.9 [d ($^2J_{CP}$ = 8.0 Hz), 2-Ph], 134.1 [d ($^2J_{CP}$ = 12.1 Hz), 6-Ph], 132.7 [s, 4-Ph], 132.2 [s, *p*-Ph], 131.7 [d ($^2J_{CP}$ = 9.8 Hz), *o*-Ph], 131.3 [d ($^3J_{CP}$ = 9.6 Hz), 3-Ph], 130.9 [s, *i*-Ph], 130.0 [s, 1-Ph], 128.6 [d ($^3J_{CP}$ = 12.4 Hz), *m*-Ph], 127.3 [d ($^3J_{CP}$ = 12.4 Hz), 5-Ph], 105.3 [s, 4-pz]. IR (Nujol), ν/cm^{-1} 3186 cm^{-1}(NH); MS(EI), m/z = 344 [M]$^+$. Anal. (%): Calc. (found) for $C_{21}H_{17}N_2OP$: C, 73.3 (73.1); H, 4.98 (5.01); N, 8.14 (8.02). Crystals suitable for X-ray studies were grown by slow diffusion of pentane in a chloroform solution of this complex.

[2-(3-Pyrazolyl)phenyl]diphenylphosphine sulfide pzphos(S). A solution of **pzphos** (0.30 g, 0.91 mmol) and S_8 (44 mg, 0.17 mmol) in CH_2Cl_2 (15 ml) was stirred for 1 h and then reduced in volume to ~5 ml and hexane added dropwise. The resultant off-white precipitate was collected by filtration, washed with hexane and dried *in vacuo*. Yield = 0.25 g (76%). ^{1}H NMR (+25 °C, $CDCl_3$, 500 MHz), δ = 12.54 [s, 1H, NH], 7.82 [dd ($^3J_{HH}$ = 13.6 Hz, $^4J_{HH}$ = 7.1 Hz), 4H, *o*-Ph], 7.57 [m, 2H, 3-Ph + 4-Ph], 7.44 [m, 2H, *p*-Ph], 7.37 [m, 4H, *m*-Ph], 7.37 [m, 1H, 5-Ph], 7.18 [dd ($^3J_{HP}$ = 14.9 Hz, $^3J_{HH}$ = 8.0 Hz), 1H, 6-Ph], 7.17 [d ($^3J_{HH}$ = 1.8 Hz), 1H, 5-pz], 6.08 [s, 1H, 4-pz]. ^{31}P{H} NMR (+25 °C, $CDCl_3$, 162.05 MHz), δ = +43.3. ^{13}C{H} NMR (+25 °C, $CDCl_3$, 500 MHz), δ = 139.7 [s, 3-pz], 139.3 [s, 5-pz], 133.4 [d ($^2J_{CP}$ = 11.2 Hz), 6-Ph], 133.2 [s, *i*-Ph], 132.6 [s, 1-Ph], 132.4 [d ($^3J_{CP}$ = 9.8 Hz), 3-Ph], 132.0 [d ($^2J_{CP}$ = 10.7 Hz), *o*-Ph], 131.9 [s, 4-Ph], 131.7 [s, *p*-Ph], 130.7 [s, 2-Ph], 128.4 [d ($^3J_{CP}$ = 12.7 Hz), *m*-Ph], 128.1 [d ($^3J_{CP}$ = 12.3 Hz), 5-Ph], 105.9 [s, 4-pz]. IR (KBr disc), ν/cm^{-1} 3220 cm^{-1}(NH). MS(EI), m/z = 360 [M]$^+$. Anal. (%): Calc. (found) for $C_{21}H_{17}N_2PS$: C, 70.0 (70.1); H, 4.75 (4.83); N, 7.77 (7.66).

Complex syntheses

Synthesis of palladium perchlorate complexes. Caution! Although we did not observe any explosive behaviour with the perchlorate compounds described below, all metal perchlorates must be treated as potentially explosive species and appropriate safety measures must be taken. See for example reference.[43]

[Pd(pzphos)Cl$_2$] 1a. **Pzphos** (0.33 g, 1.0 mmol) in CH_2Cl_2 (10 ml) was added dropwise to a stirred solution of Pd(COD)Cl_2 (0.29 g, 1.0 mmol) in CH_2Cl_2 (20 ml). The orange solution was stirred for 10 min causing a yellow solid to precipitate. This was collected by filtration, stirred with hexane (20 ml), filtered and dried *in vacuo* to give a bright yellow solid. Yield = 0.46 g (91%). ^{1}H NMR (+25 °C, $CDCl_3$, 500 MHz), δ = 13.14 [s, 1H, NH] 7.90 [ddd ($^3J_{HH}$ = 7.9 Hz, $^4J_{HH}$ = 4.4 Hz, $^5J_{HH}$ = 1.0 Hz), 1H, 3-Ph], 7.70 [dddd ($^3J_{HH}$ = 7.9 Hz, $^4J_{HH}$ = 1.5 Hz), 1H, 4-Ph], 7.65 [dd ($^3J_{HH}$ = 2.8 Hz, $^3J_{HH}$ = 1.8 Hz), 1H, 5-pz], 7.61 [m, 4H, *o*-Ph], 7.54 [m, 2H, *p*-Ph], 7.44 [m, 4H, *m*-Ph], 7.42 [m, 1H, 5-Ph], 7.05 [ddd ($^3J_{HP}$ = 10.8 Hz, $^3J_{HH}$ = 7.9 Hz, $^4J_{HH}$ = 1.2 Hz), 1H, 6-Ph], 6.86 [m, 1H, 4-pz]. ^{31}P{H} NMR (+25 °C, $CDCl_3$, 162.05 MHz): δ = +25.6. IR (KBr disc), ν/cm^{-1} 3230 cm^{-1}(NH). MS(EI), m/z = 471 [M–Cl]$^+$. Anal. (%): Calc. (found) for $C_{21}H_{17}Cl_2N_2PPd$: C, 49.9 (49.8); H, 3.39 (3.33); N, 5.54 (5.42). Yellow needles suitable for X-ray studies were grown by slow diffusion of pentane in a chloroform solution of the complex.

[Pd(pzphos)$_2$]Cl$_2$ 1b. Pd(COD)Cl_2 (65 mg, 0.23 mmol) in CH_2Cl_2 (15 ml) was added dropwise to a solution of **pzphos** (150 mg, 0.46 mmol) in CH_2Cl_2 (15 ml). After stirring overnight, the volume of the solvent was reduced to 10 ml and hexane (10 ml) was added causing a yellow solid to precipitate. This was collected by filtration and dried *in vacuo*. Yield = 150 mg (78%). ^{1}H NMR (−50 °C, $CDCl_3$, 400 MHz), δ = 14.54 [s, 1H, NH], 8.05 [dd ($^3J_{HH}$ = 12.8 Hz, $^4J_{HH}$ = 7.9 Hz), 1H, Ph], 7.96 [dd ($^3J_{HH}$ = 7.5 Hz, $^4J_{HH}$ = 3.4 Hz), 1H, 3-Ph], 7.96 [br s, 2H, Ph], 7.76 [s, 1H, 5-pz], 7.64 [dd, ($^3J_{HH}$ = 7.6 Hz), 1H, 4-Ph], 7.42 [m, 3H, Ph], 7.30 [dd ($^3J_{HH}$ = 7.7 Hz), 1H, 5-Ph], 7.22 [m, 1H, Ph], 7.06 [dd ($^3J_{HH}$ = 7.4 Hz), 1H, Ph], 6.79 [m, 2H, 6-Ph + Ph], 6.53 [s, 1H, 4-pz], 5.94 [dd ($^3J_{HH}$ = 9.0 Hz), 1H, Ph]. ^{31}P{H} NMR (+25 °C, $CDCl_3$, 162.05 MHz), δ = +31.6 (s). IR (KBr disc), ν/cm^{-1} 3290 cm^{-1}(NH). MS(ESI), m/z = 761 [Pd(pzphos)$_2$]$^+$. Anal. (%): Calc. (found) for $C_{42}H_{34}Cl_2N_4P_2Pd.2CH_2Cl_2$: C, 52.6 (52.6); H, 3.82 (3.62); N, 5.58 (5.37). Yellow crystals suitable for X-ray studies were grown by slow diffusion of pentane in a chloroform solution of this complex.

Alternative synthesis of 1b. A solution of **pzphos** (32 mg, 0.10 mmol) in CH_2Cl_2 (10 ml) was added to a solution of **1a** (50 mg, 0.10 mmol) in CH_2Cl_2 (10 ml) and stirred overnight. The solution was concentrated to half the volume and hexane (10 ml) added dropwise causing a yellow solid to precipitate. The solid was collected by filtration and dried *in vacuo* to give **1b** as evidenced by

This journal is © The Royal Society of Chemistry 2007

identical ^{1}H and ^{31}P{H} NMR data for both compounds. Yield = 55 mg (70%).

[Pd(pzphos)$_2$][ClO$_4$]$_2$ 1c. Pd(COD)Cl$_2$ (87 mg, 0.30 mmol) in CH_2Cl_2 (5 ml) was added dropwise to a solution of **pzphos** (200 mg, 0.61 mmol) in CH_2Cl_2 (20 ml). After stirring for 1 h, silver perchlorate (114 mg, 0.64 mmol) was added and the flask stirred overnight in the dark during which time AgCl precipitated. Filtration through a pad of Celite and concentration of the filtrate to dryness gave a yellow powder which was stirred with hexane (20 ml), filtered and recrystallised from hot methanol to give a yellow solid. Yield = 180 mg (61%). ^{1}H NMR (+25 °C, d^6-acetone, 400 MHz), δ = 13.42 [s, 1H, NH], 8.19 [dd ($^3J_{HH}$ = 2.8 Hz, $^4J_{HH}$ = 0.7 Hz), 1H, 5-pz], 8.08 [ddd ($^3J_{HH}$ = 7.8 Hz, $^4J_{HH}$ = 4.3 Hz, $^5J_{HH}$ = 1.2 Hz), 1H, 3-Ph], 7.90 (br m, 2H, Ph), 7.85 [dd ($^3J_{HH}$ = 7.8 Hz), 1H, 4-Ph], 7.40–7.70 [br m, 4H, Ph], 7.59 [dd ($^3J_{HH}$ = 8.0 Hz), 1H, 5-Ph], 7.08–7.25 [br m, 2H, Ph], 7.05 [ddd ($^3J_{HP}$ = 11.1 Hz, $^3J_{HH}$ = 7.9 Hz, $^4J_{HH}$ = 0.8 Hz), 1H, 6-Ph], 6.99 [dd ($^3J_{HH}$ = 7.8 Hz, $^3J_{HH}$ = 1.6 Hz), 1H, 4-pz]. ^{31}P{H} NMR (+25 °C, d^6-acetone, 162.09 MHz): δ = +34.1. IR (Nujol), ν/cm^{-1} 3302 cm^{-1}(NH). MS(FAB +ve), m/z = 761 [Pd(pzphos)$_2$]$^+$. Anal. (%): Calc. (found) for $C_{42}H_{34}Cl_2N_4O_8P_2Pd$: C, 52.4 (52.5); H, 3.56 (3.69); N, 5.82 (5.73). Single crystals for X-ray analysis were grown in an NMR tube by layering hexane above a CH_2Cl_2 solution of the product.

Attempted synthesis of [Pd{pzphos(O)}Cl$_2$] 2a. **Pzphos(O)** (30 mg, 0.09 mmol) in CH_2Cl_2 (10 ml) was added dropwise to a refluxing solution of Pd(COD)Cl$_2$ (30 mg, 0.10 mmol) in CH_2Cl_2 (20 ml). The refluxing solution was stirred for 16 h and ^{31}P{H} NMR of the reaction solution recorded (+25 °C, CH_2Cl_2/$CDCl_3$, 162.05 MHz): δ = +32.8, indicating formation of the bis adduct **2b**.

[Pd{pzphos(O)}$_2$Cl$_2$] 2b. Pd(COD)Cl$_2$ (21 mg, 0.07 mmol) in CH_2Cl_2 (10 ml) was added dropwise to a solution of **Pzphos(O)** (50 mg, 0.15 mmol) in CH_2Cl_2 (20 ml). After stirring for 2 h, half the solvent was evaporated under a stream of N_2 to give a yellow solution to which hexane was added dropwise (5 ml) causing a pale yellow precipitate to form. This was collected by filtration, washed with hexane (5 ml) and dried *in vacuo* to give a pale yellow powder. Yield = 52 mg (83%). ^{1}H NMR (+25 °C, $CDCl_3$, 400 MHz), δ = 13.51 [s, 1H, NH], 7.81 [dd ($^3J_{HH}$ = 2.1 Hz), 1H, 5-pz], 7.74 [m, 4H, *o*-Ph], 7.61 [dd ($^3J_{HH}$ = 7.5 Hz), 1H, 4-Ph], 7.57 [dd ($^3J_{HH}$ = 7.6 Hz), 1H, 3-Ph], 7.53 [m, 2H, *p*-Ph], 7.47 [m, 4H, *m*-Ph], 7.37 [dd ($^3J_{HH}$ = 7.5 Hz), 1H, 5-Ph], 7.22 [dd ($^3J_{HP}$ = 14.2 Hz, $^3J_{HH}$ = 7.5 Hz), 1H, 6-Ph], 6.19 [dd ($^3J_{HH}$ = 2.2 Hz), 1H, 4-pz]. ^{31}P{H} NMR (+25 °C, $CDCl_3$, 162.05 MHz), δ = +32.7 (s). IR (Nujol), ν/cm^{-1} 3196 cm^{-1}(NH). MS(FAB +ve), m/z = 869 [Pd{pzphos(O)}$_2$Cl$_2$]$^+$. Anal. (%): Calc. (found) for $C_{42}H_{34}Cl_2N_4O_2P_2Pd$: C, 58.3 (58.2); H, 3.96 (4.00); N, 6.47 (6.39). Yellow crystals suitable for X-ray studies were grown by slow diffusion of pentane in a chloroform solution of this complex.

[Pd{pzphos(O)}$_2$][ClO$_4$]$_2$ 2c. $AgClO_4$ (25 mg, excess) was added to a suspension of **2b** (34 mg, 0.04 mmol) in CH_2Cl_2 (5 ml). After stirring overnight, half the solvent was evaporated under a stream of N_2 to give a yellow solution to which hexane was added dropwise (5 ml) causing a yellow precipitate to form. This was collected by filtration, washed with hexane (5 ml) and dried *in vacuo* to give **2c** as yellow powder. Yield = 24 mg (60%). ^{1}H NMR (+25 °C, $CDCl_3$, 400 MHz), δ = 12.35 [s, 1H, NH], 8.27 [dd ($^3J_{HH}$ = 7.4 Hz, $^4J_{HH}$ = 4.4 Hz), 1H, 3-Ph], 8.12 [dd ($^3J_{HH}$ = 7.7 Hz), 1H, 4-Ph], 7.60–7.85 [m, 10 H, *o,m,p*-Ph], 7.35–7.50 [m, 2 H, 5,6-Ph], 7.31 [d ($^3J_{HH}$ = 2.0 Hz), 1H, 5-pz], 6.02 [m, 1H, 4-pz]. ^{31}P{H} NMR (+25 °C, $CDCl_3$, 162.05 MHz), δ = +53.9 (s). IR (CH_2Cl_2 solution), ν/cm^{-1} 3686 cm^{-1}(NH). MS(FAB +ve), m/z = 900 [Pd{pzphos(O)}$_2$ClO$_4$]$^+$. Anal. (%): Calc. (found) for $C_{42}H_{34}Cl_2N_4O_{10}P_2Pd$: C, 50.8 (50.7); H, 3.45 (3.43); N, 5.64 (5.58). Yellow crystals suitable for X-ray studies were grown by slow diffusion of pentane in a chloroform solution of this complex.

CCDC reference numbers 640789–640793.

For crystallographic data in CIF or other electronic format see DOI: 10.1039/b704051b

Acknowledgements

We gratefully acknowledge financial support from GlaxoSmithKline and the Department of Chemistry, Imperial College, London.

References

1 P. Braunstein and F. Naud, *Angew. Chem., Int. Ed.*, 2001, **40**, 680.
2 A. D. Burrows, *Sci. Prog.*, 2002, **85**, 199.
3 C. S. Slone, D. A. Weinberger and C. A. Mirkin, *Prog. Inorg. Chem.*, 1999, **48**, 233.
4 F. Fache, E. Schulz, M. L. Tommasino and M. Lemaire, *Chem. Rev.*, 2000, **100**, 2159.
5 P. Braunstein, *J. Organomet. Chem.*, 2004, **689**, 3953.
6 U. Schubert, J. Pfeiffer, F. Stohr, D. Sturmar and S. Thompson, *J. Organomet. Chem.*, 2002, **646**, 53.
7 A. Bader and E. Lindner, *Coord. Chem. Rev.*, 1991, **108**, 27.
8 A. Ramirez, X. Sun and D. B. Collum, *J. Am. Chem. Soc.*, 2006, **128**, 10326.
9 G. Kohl, R. Rudolph, H. Pritzkow and M. Enders, *Organometallics*, 2005, **24**, 4774.
10 M. Sauthier, F. Leca, L. Toupet and R. Reau, *Organometallics*, 2002, **21**, 1591.
11 C. Abu-Gnim and I. Amer, *J. Organomet. Chem.*, 1996, **516**, 235.
12 S. E. Angell, C. W. Rogers, Y. Zhang, M. O. Wolf and W. E. Jones, Jr, *Coord. Chem. Rev.*, 2006, **250**, 1829.
13 A. M. Allgeier and C. A. Mirkin, *Angew. Chem., Int. Ed.*, 1998, **37**, 894.
14 D. A. Weinberger, T. B. Higgins, C. A. Mirkin, L. M. Liable-Sands and A. L. Rheingold, *Angew. Chem., Int. Ed.*, 1999, **38**, 2565.
15 H. Werner, M. Schulz and B. Windmuller, *Organometallics*, 1995, **14**, 3659.
16 G. P. C. M. Dekker, A. Buijs, C. J. Elsevier, K. Vrieze, P. W. N. M. van Leeuwen, W. J. J. Smeets, A. J. Spek, Y. F. Wang and C. H. Stam, *Organometallics*, 1992, **11**, 1937.
17 P. L. Arnold, A. J. Blake and C. Wilson, *Chem.–Eur. J.*, 2005, **11**, 6095.
18 M. Bressan, F. Morandini and P. Rigo, *J. Organomet. Chem.*, 1983, **247**, c8–c10.
19 S. Park, D. Hedden and D. M. Roundhill, *Organometallics*, 1986, **5**, 2151.
20 E. Lindner, B. Keppleler, H. A. Mayer, K. Gierling, R. Fawzi and M. Steimann, *J. Organomet. Chem.*, 1996, **526**, 175.
21 D. Sellmann, A. Fetz, M. Moll and F. Knoch, *J. Organomet. Chem.*, 1988, **355**, 495.
22 Y. Sun, A. Hienzsch, J. Grasser, E. Herdtweck and W. R. Thiel, *J. Organomet. Chem.*, 2006, **691**, 291.
23 Y. Sun and W. R. Thiel, *Inorg. Chim. Acta*, 2006, **359**, 4807.
24 A. Mukherjee, U. Subramanyam, V. G. Puranik, T. P. Mohandas and A. Sarkar, *Eur. J. Inorg. Chem.*, 2005, 1254.
25 A. Otero, F. Carrillo-Hermosilla, P. Terreros, T. Exposito, S. Rojas, J. Fernandez-Baeza, A. Antinolo and I. Lopez-Solera, *Eur. J. Inorg. Chem.*, 2003, 3233.
26 D. B. Douglas, Y. Gong, L. Zakharov, J. A. Golen and A. L. Rheingold, *J. Am. Chem. Soc.*, 2006, **128**, 438.
27 K. S. Coleman, M. L. H. Green, S. I. Pascu, N. H. Rees, A. R. Cowley and L. H. Rees, *J. Chem. Soc., Dalton Trans.*, 2001, 3384.
28 P. Espinet and K. Soulantica, *Coord. Chem. Rev.*, 1999, **193**, 499and references therein.

29 P. Guillame and M. Postel, *Inorg. Chim. Acta*, 1995, **233**, 109.
30 F. E. Wood, M. M. Olmstead, J. P. Farr and A. L. Balch, *Inorg. Chim. Acta*, 1985, **97**, 77.
31 G. Minghetti, S. Stoccoro, M. A. Cinellu, A. Zucca, M. Manassero and M. Sansoni, *J. Chem. Soc., Dalton Trans.*, 1998, 4119.
32 G. Minghetti, A. Doppiu, S. Stoccoro, A. Zucca, M. A. Cinellu, M. Manassero and M. Sansoni, *Eur. J. Inorg. Chem.*, 2002, 431.
33 L. Prodi, M. Montalti, N. Zaccheroni, G. Pickart, L. Charbonniere and R. Ziessel, *New J. Chem.*, 2003, **27**, 134.
34 L. Tusek-Bozic, A. Furlani, V. Scarcia, E. De Clercq and J. Balzarini, *J. Inorg. Biochem.*, 1998, **72**, 201.
35 L. Tusek-Bozic, I. Matijasic, G. Bocelli, G. Calestani, A. Furlani, V. Scarcia and A. Papaioannou, *J. Chem. Soc., Dalton Trans.*, 1991, 195.
36 L. Tusek-Bozic, P. Sgarabotto, A. Furlani, V. Scarcia and A. Papaioannou, *Inorg. Chim. Acta*, 1991, **185**, 229.
37 S. J. Coote, G. J. Dawson, C. G. Frost and J. M. J. Williams, *Synlett*, 1993, 509.
38 M. C. Torralba, M. Cano, J. A. Campo, J. V. Heras, E. Pinilla and M. R. Torres, *Inorg. Chem. Commun.*, 2002, **5**, 887.
39 C. Navarro-Ranniger, J. M. Perez, F. Zamora, V. M. Gonzalez, J. R. Masaguer and C. Alonso, *J. Inorg. Biochem.*, 1993, **52**, 37.
40 S. Stoccoro, G. Chelucci, A. Zucca, M. A. Cinellu, G. Minghetti and M. Manassero, *J. Chem. Soc., Dalton Trans.*, 1996, 1295.
41 *Search on CSD version 5.27 (November 2004) + 3 updates.*
42 A.-K. Pleier, H. Glas, M. Grosche, P. Sirsch and W. R. Thiel, *Synthesis*, 2001, **1**, 55.
43 W. C. Wolsey, *J. Chem. Educ.*, 1973, **50**, A335.

 This journal is © The Royal Society of Chemistry 2007

A novel tetrakis(pyrazolyl)borate ligand bearing triphenylphosphine oxide substituents†‡

Steven Kealey,[a] Nicholas J. Long,*[a] Andrew J. P. White[a] and Antony D. Gee[a,b]

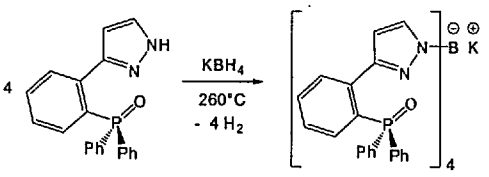
Received 20th July 2007, Accepted 14th September 2007
First published as an Advance Article on the web 20th September 2007
DOI: 10.1039/b711121e

A new tetrakis(pyrazolyl)borate ligand bearing triphenylphosphine oxide moieties appended to the 3-position of the pyrazolyl rings is reported and shown to display varied coordination chemistry from tridentate N_2O coordination with thallium to hexadentate N_3O_3 coordination with europium.

Over the last 10 years a number of poly(pyrazolyl)borate ligands bearing coordinating groups attached to the 3-pyrazolyl position of the ligand core have emerged. In these species, each 'arm' of the ligand is capable of bidentate coordination to a metal *via* the pyrazolyl nitrogen and the appended donor site resulting in the formation of several podand ligands, which in the case of the tris(pyrazolyl)borates (Tp) and the tetrakis(pyrazolyl)borates (T_kp)[1] are capable of up to hexadentate coordination. Examples of such species include poly(pyrazolyl)borates bearing pyridyl,[2] bipyridyl,[3] anisyl,[4] thioanisyl,[5] pyrazinyl,[6] carboxamide,[7] and ether[8] appendages. Examples of functionalised poly(pyrazolyl)-borates that do not exhibit coordination at the appended donor sites, include the furyl,[9] thienyl,[10] anisyl,[11] and carboxyl[12] derivatives. It is interesting to note that to date, there are no examples of poly(pyrazolyl)borates featuring phosphorus-containing substituents.

Recently, our group presented the synthesis and coordination chemistry of a novel pyrazolyl ligand bearing triphenylphosphine oxide units attached in the 3-position of a pyrazolyl ring.[13] Our interest in this compound, 3-(2-diphenylphosphinylphenyl)pyrazole, $pz^{phos(O)}$ is centred on its hemilabile behaviour coupled with its ease of derivatisation by substitution at the pyrazole N–H moiety, thus leading to tunable electronic and steric properties. In this communication, we present the synthesis and preliminary coordination chemistry of a novel tetrakis(pyrazolyl)borate ligand, $T_kp^{phos(O)}$,[14] derived from this pyrazole precursor.

$K[T_kp^{phos(O)}]$ was synthesised by reaction of one equivalent of potassium borohydride with five equivalents of $pz^{phos(O)}$ (excess of one eq.) according to the equation in Scheme 1. The small quantity of reagents employed in this reaction (mmols), meant that it was difficult to reliably measure the volume of H_2 gas evolved and as such we were unable to follow the progress of this reaction in the usual manner. The reaction was performed under typical conditions, heating at a high temperature (260 °C), for 2 h and under an inert atmosphere to avoid any possible degradation of the reagents. Following this, the ligand was purified by recrystallisation from hot THF and isolated as a white, air-stable solid. Evidence for the formation of a new species was given by ^{31}P NMR spectroscopy, showing a sharp singlet at 30.9 ppm (*cf.* starting material at 35.8 ppm). Crucially, proton-coupled ^{11}B NMR spectroscopy showed a sharp singlet at 0.70 ppm, indicating that no B–H bonds remain and thus the tetrakis-substituted species had formed. This was supported by negative ion ESI mass spectrometry, in which the $[T_kp^{phos(O)}]^-$ anion was observed at 1383 *m/z* as expected. Indeed, the facile formation of this T_kp species is expected here as there is no substituent at the 5-pyrazolyl position to provide the steric block that prevents addition of the fourth and final pyrazolyl unit in 3,5-disubstituted species.[15]



Scheme 1 Synthesis of $K[T_kp^{phos(O)}]$.

This species was converted to the thallium salt, $Tl[T_kp^{phos(O)}]$, by the equimolar reaction with thallous nitrate, and the solid-state structure§ was determined by X-ray analysis (Fig. 1). In contrast to most other Tl[Tp] and Tl[T_kp] derivatives where three of the pyrazolyl arms bind to the metal, here in $Tl[T_kp^{phos(O)}]$ only two of the arms coordinate. This mode of coordination has only previously been seen in a handful of related thallium structures.[2,16–19] The third coordination site at the thallium in $Tl[T_kp^{phos(O)}]$ is occupied by the phosphine oxide donor attached to one of the already bound pyrazolyl arms, making this arm bidentate. Only one of the literature examples cited above has an extra donor on the pyrazolyl arms (3-pyridyl groups), and in this case the extra donor is used to bind to a different metal atom, generating a polymer.[2] Thus, the $T_kp^{phos(O)}$ bonding mode seen here is the first example of its type. The metal has a hemidirected coordination geometry,[20] the three donors occupying the facial sites of a pseudo-octahedron. The *ca.* 0.05 Å disparity between the Tl–N bond lengths (see Table S1, ESI‡) is not related to the bidentate coordination of one of the $T_kp^{phos(O)}$ pyrazolyl arms as this pattern of bonding is also seen in each of the related literature examples cited above.[16–19]

We attribute this η^3-N_2O coordination behaviour to steric interactions between the fourth pyrazolyl unit and the 5-H substituents of the other pyrazolyl rings (Scheme 2). These interactions can

[a]*Department of Chemistry, Imperial College London, South Kensington, London, UK SW7 2AZ. E-mail: n.long@imperial.ac.uk; Tel: +44 (0)20 7594 5781*
[b]*GSK Clinical Imaging Centre, Imperial College London, Hammersmith Hospital, Du Cane Road, London, UK W12 0NN*

† CCDC reference numbers 653717 and 653718. For crystallographic data in CIF or other electronic format see DOI: 10.1039/b711121e

‡ Electronic supplementary information (ESI) available: Experimental details and characterisation data for represented compounds. See DOI: 10.1039/b711121e

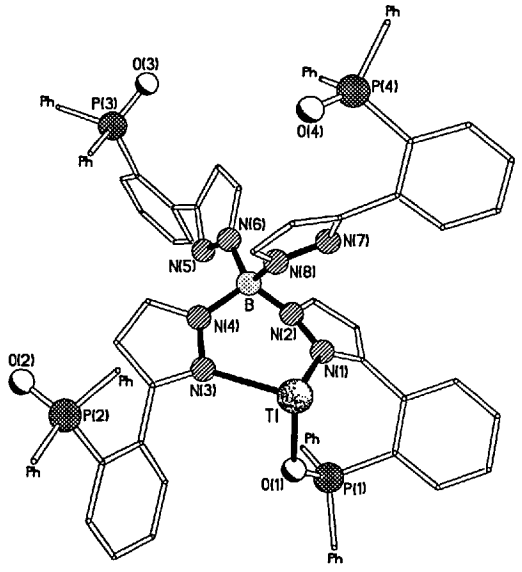
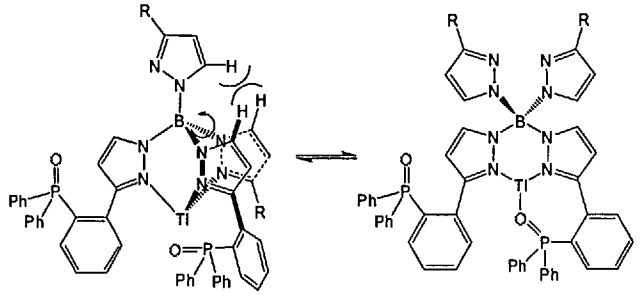


Fig. 1 The molecular structure of Tl[$T_kp^{phos(O)}$]. Selected hond lengths (Å); Tl–O(1) 2.541(2), Tl–N(1) 2.536(3), Tl–N(3) 2.587(3).



Scheme 2 Steric clash (left) resulting in an unusual thallium bonding mode (right). R = 2-($POPh_2$)Ph.

be minimised by rotation of one of the B–N bonds which, in turn, impedes coordination of that pyrazolyl unit. In this case, the thallium may still achieve coordinative saturation by bonding to one of the phosphine oxide moieties which has been brought into close proximity to the metal as a consequence of coordination of the remaining pyrazolyl units.

In an attempt to achieve full η^6-N_3O_3 chelation (excluding the fourth pyrazolyl arm which cannot coordinate due to structural rigidity) we decided to examine the coordination chemistry of this ligand towards lanthanide ions due to their comparable size to the ligand cavity. Reaction of K[$T_kp^{phos(O)}$] with one equivalent of $Eu(NO_3)_3{\cdot}5H_2O$ in the minimum amount of methanol yielded a clear solution, which to our surprise did not result in any precipitation of product after continued stirring, perhaps as a result of the non-coordinating ligand arm imparting increased solubility. ^{31}P NMR spectroscopy of the reaction solution showed a major species at 34.2 ppm and a minor species at 31.6 ppm (*cf.* free ligand at 30.9 ppm); the former was tentatively ascribed as the resonance of the three coordinated bidentate N,P=O arms and the latter from the fourth uncoordinated arm, pointing away from the metal. Complexation was supported by ESI mass spectrometry (m/z = 1581) which suggested the formation of an Eu : ligand : NO_3 complex in a 1 : 1 : 1 ratio ([Eu{$T_kp^{phos(O)}$}NO_2]$^+$ = 1581). The product was isolated as a white powder by extraction into CH_2Cl_2, filtration through Celite and concentration to dryness.

The X-ray structure§ of this species (Fig. 2) supports these predictions and we find that the europium is eight-coordinate with a hexadentate N_3O_3 podand and one bidentate nitrate group. This results in a cationic species, [Eu{$T_kp^{phos(O)}$}NO_3]$^+$, with the charge balanced by a non-coordinating nitrate anion. This is in contrast to the europium complex of the hexadentate N_6-donor, Tp^{py},[21] which is able to accommodate the hexadentate ligand and both nitrates to form a neutrally charged 10-coordinate species. The reason for the difference lies in the size of the chelate rings which are 5-membered in [Eu{Tp^{py}}$(NO_3)_2$] (with *N,N′* bite angles of *ca.* 62.2°), and 7-membered here in [Eu{$T_kp^{phos(O)}$}NO_3]$^+$ (with *N,O* bite angles of *ca.* 72.9°), and thus the space remaining for nitrate coordination is reduced in [Eu{$T_kp^{phos(O)}$}NO_3]$^+$ *cf.* [Eu{Tp^{py}}$(NO_3)_2$].

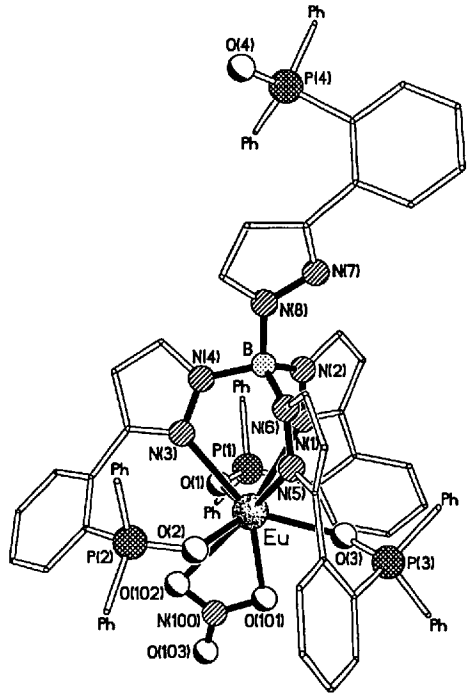


Fig. 2 The molecular structure of [Eu{$T_kp^{phos(O)}$}NO_3][NO_3]. Selected bond lengths (Å); Eu–O(1) 2.303(2), Eu–O(2) 2.299(2), Eu–O(3) 2.2710(19), Eu–N(1) 2.608(2), Eu–N(3) 2.529(2), Eu–N(5) 2.546(2), Eu–O(101) 2.442(2), Eu–O(102) 2.664(3).

In summary, synthesis of a new poly(pyrazolyl)borate ligand containing phosphine oxide appendages has been achieved to form a mixed N,O donor ligand. In coordination to thallium an unexpected η^3-N_2O species was isolated, while complete η^6 chelation could be achieved by coordination to europium. In the latter case, unfavourable steric interactions between the fourth pyrazolyl arm and the 5-H substituents of the ligated arms are compensated for by the increased stability gained from chelating to a metal which is well matched in terms of size and its ability to accommodate high coordination numbers. This phosphinyl-substituted ligand provides a useful NMR handle which facilitates the monitoring of the complexation reactions. We hope to extend this work to the synthesis of phosphino-substituted poly(pyrazolyl)borates for their potential application in homogenous catalysis.

This journal is © The Royal Society of Chemistry 2007

Acknowledgements

We gratefully acknowledge financial support from GlaxoSmithKline and the Department of Chemistry, Imperial College, London.

Notes and references

§ *Crystal data for* $Tl[T_kp^{phos(O)}]$: $[C_{84}H_{64}BN_8O_4P_4Tl]\cdot 3.5CHCl_3\cdot 0.5C_5H_{12}$, $M = 2042.35$, triclinic, $P\bar{1}$ (no. 2), $a = 14.6110(3)$, $b = 19.0394(3)$, $c = 19.8132(4)$ Å, $\alpha = 62.012(2)$, $\beta = 73.056(2)$, $\gamma = 85.878(2)°$, $V = 4642.07(15)$ Å^3, $Z = 2$, $D_c = 1.461$ g cm^{-3}, μ(Mo-Kα) = 2.164 mm^{-1}, $T = 173$ K, colourless blocks, Oxford Diffraction Xcalibur 3 diffractometer; 21 105 independent measured reflections, F^2 refinement, $R_1 = 0.043$, $wR_2 = 0.085$, 14 291 independent observed absorption-corrected reflections [$|F_o| > 4\sigma(|F_o|)$, $2\theta_{max} = 58°$], 1165 parameters. *For* $[EuT_kp^{phos(O)}\{NO_3\}][NO_3]$: $[C_{84}H_{64}BN_9O_7P_4Eu](NO_3)\cdot 4MeOH$, $M = 1788.27$, monoclinic, $P2_1/c$ (no. 14), $a = 25.0529(2)$, $b = 13.1352(1)$, $c = 26.4601(2)$ Å, $\beta = 106.560(1)°$, $V = 8346.19(11)$ Å^3, $Z = 4$, $D_c = 1.423$ g cm^{-3}, μ(Cu-Kα) = 6.686 mm^{-1}, $T = 173$ K, colourless blocks, Oxford Diffraction Xcalibur PX Ultra diffractometer; 16 144 independent measured reflections, F^2 refinement, $R_1 = 0.034$, $wR_2 = 0.092$, 14231 independent observed absorption-corrected reflections [$|F_o| > 4\sigma(|F_o|)$, $2\theta_{max} = 143°$], 1093 parameters.

1 We use the usual notation of Tp to denote a tris(pyrazolyl)borate and T_kp to denote a tetrakis(pyrazolyl)borate.
2 H. Adams, S. R. Batten, G. M. Davies, M. B. Duriska, J. C. Jeffery, P. Jensen, J. Lu, G. R. Motson, S. J. Coles, M. B. Hursthouse and M. D. Ward, *Dalton Trans.*, 2005, 1910.
3 J. S. Fleming, E. Psillakis, S. M. Couchman, J. C. Jeffery, J. A. McCleverty and M. D. Ward, *J. Chem. Soc., Dalton Trans.*, 1998, 537.
4 A. L. Rheingold, B. S. Haggerty, L. M. Liable-Sands and S. Trofimenko, *Inorg. Chem.*, 1999, **38**, 6306.
5 E. R. Humphrey, K. L. V. Mann, Z. R. Reeves, A. Behrendt, J. C. Jeffery, J. A. McCleverty and M. D. Ward, *New J. Chem.*, 1999, **23**, 417.
6 K. L. V. Mann, J. C. Jeffery, J. A. McCleverty and M. D. Ward, *Polyhedron*, 1999, **18**, 721.
7 A. L. Rheingold, C. D. Incarvito and S. Trofimenko, *J. Chem. Soc., Dalton Trans.*, 2000, 1233.
8 M. H. Chisholm, J. C. Gallucci and G. Yaman, *Chem. Commun.*, 2006, 1872.
9 J. A. Maldonado Calvo and H. Vahrenkamp, *Inorg. Chim. Acta*, 2006, **359**, 4079.
10 J. Kisala, A. Bialonska, Z. Ciunik, S. Kurek and S. Wolowiec, *Polyhedron*, 2006, **25**, 3222.
11 P. L. Jones, K. L. V. Mann, J. C. Jeffery, J. A. McCleverty and M. D. Ward, *Polyhedron*, 1997, **16**, 2435.
12 G. Bandoli, A. Dolmella, G. G. Lobbia, G. Papini, M. Pellei and C. Santini, *Inorg. Chim. Acta*, 2006, **359**, 4036.
13 S. Kealey, N. J. Long, P. W. Miller, A. J. P. White, P. B. Hitchcock and A. Gee, *Dalton Trans.*, 2007, 2823.
14 The ligand tetrakis{3-[2-(diphenylphosphinyl)-phenyl]pyrazolyl}-borate is referred to as $T_kp^{phos(O)}$ throughout this paper. Its full name, using the standard nomenclature, is $(2\text{-}\{POPh_2\}Ph)Tp^{2\text{-}\{POPh_2\}Ph}$.
15 S. Trofimenko, *Scorpionates: The Coordination Chemistry of Polypyrazolylborate Ligands*, Imperial College Press, London, 1999.
16 S. Guo, J. W. Bats, M. Bolte and M. Wagner, *J. Chem. Soc., Dalton Trans.*, 2001, 3572.
17 C. Janiak, L. Braun and F. Girgsdies, *J. Chem. Soc., Dalton Trans.*, 1999, 3133.
18 J. L. Kisko, T. Hascall, C. Kimblin and G. Parkin, *J. Chem. Soc., Dalton Trans.*, 1999, 1929.
19 F. Jakle, K. Polborn and M. Wagner, *Chem. Ber.*, 1996, **129**, 603.
20 L. Shimoni-Livny, J. P. Glusker and C. W. Bock, *Inorg. Chem.*, 1998, **37**, 1853.
21 P. L. Jones, A. J. Amoroso, J. C. Jeffery, J. A. McCleverty, E. Psillakis, L. H. Rees and M. D. Ward, *Inorg. Chem.*, 1997, **36**, 10.

This journal is © The Royal Society of Chemistry 2007

ScorpoPhos: a novel phosphine-nitrogen ligand containing a tris(pyrazolyl)borate ligand core†

Steven Kealey,[a] Nicholas J. Long,*[a] Philip W. Miller,[a] Andrew J. P. White[a] and Antony D. Gee[a,b]

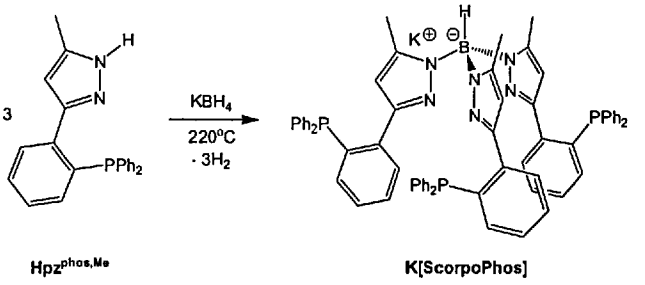
Received 17th March 2008, Accepted 26th March 2008
First published as an Advance Article on the web 10th April 2008
DOI: 10.1039/b804608p

A new tris(pyrazolyl)borate ligand bearing phosphine donor groups appended to the 3-position of the pyrazolyl rings is reported, and the hemilabile behaviour of this tris-N,P ligand in coordination with K^+, Tl^+ and Cu^+ ions is investigated.

To date a great deal of attention has been paid towards the development of new phosphine-containing hybrid ligands due to their widespread use in catalysis.[1] Similarly, since their conception in the late 1960s, a large amount of research has been focused on the many poly(pyrazolyl)borate 'scorpionate' ligands[2,3] and their second generation analogues containing extra coordinating groups bound to the pyrazolyl rings of the ligand core. It is therefore somewhat surprising to find that these two fields have not overlapped and that out of all of the functionalised scorpionate ligands produced to date, the most common appendages contain nitrogen,[4–6] sulfur[7,8] and oxygen[9–15] donors, and that no phosphine donor scorpionates have been reported. As such, we proposed to synthesise a tris(pyrazolyl)borate (Tp) ligand bearing phosphine donor appendages for its potentially favourable hemilabile properties. In such a species, the tripodal array of pyrazolyl donors would have an anchor effect of binding a metal ion firmly in place. Meanwhile, coordination of the appended phosphine donor moiety could stabilise the complex, but upon temporary dissociation a vacant site would be created to allow binding of a reactive substrate. The dissociation of a labile group occurs in a range of catalytic processes and the Tp-stabilised complex, $RuTp(PPh_3)_2H$,[16–18] is one such example, whereby the phosphine ligand dissociates initially to make way for substrate binding. A tris(pyrazolyl)borate ligand with phosphine appendages is therefore particularly desirable as it may find similar applications in catalysis, and possess its own unique steric and electronic attributes.

The absence of these species in the literature probably stems from the limited availability of phosphorus-containing pyrazoles to transform into new phosphorus-containing Tp ligands (*via* their reaction with metal borohydrides). Recently, however, we published a synthetic route to a pyrazole, Hpz^{phos}, consisting of a triphenylphosphine moiety appended to the 3-position of the pyrazolyl ring.[19] The corresponding phosphine oxide, $Hpz^{phos(O)}$, was easily obtained and was reacted with KBH_4 to form the tetrakis(pyrazolyl)borate ligand, $T_kp^{phos(O)}$. This N_4,O_4 ligand was shown to display varied coordination behaviour depending on the requirements of the metal involved.[15] With this reactivity in mind, we proposed further ligand modifications to form a new phosphine-appended pyrazole for the synthesis of a novel phosphine-appended Tp ligand. In this paper we present the ligand's synthesis and some preliminary complexation reactions which demonstrate its versatile coordination behaviour.

Since a tris(pyrazolyl)borate was desired rather than the tetra-substituted species (which often forms as a result of over-reaction of the pyrazole starting material), we placed a methyl group in the 5-position of the pyrazole unit to provide a steric block thus preventing addition of the fourth pyrazolyl arm during the ligand formation reaction. The desired pyrazole ($Hpz^{phos,Me}$ in Scheme 1) was formed in two steps in high yield from 2-(diphenylphosphino)acetophenone (see ESI†). Subsequent reaction of this pyrazole with KBH_4 at high temperature gave the crude product potassium tris(3-[2-(diphenylphosphino)phenyl]-5-methylpyrazolyl)borate, K[ScorpoPhos], which was recrystallised from CH_2Cl_2–hexane to give an analytically pure sample in reasonable yield (64%).‡ Evidence of the formation of the desired species was provided by negative ion ESI mass spectrometry in which the $[ScorpoPhos]^-$ ion was observed at 1035 *m/z* and further characterised by ^1H, $^{31}P\{^1H\}$ (−11.7 ppm), $^{11}B\{^1H\}$ (−5.11 ppm) NMR and IR spectroscopy (ν_{BH} = 2363 cm^{-1}). As shown in Scheme 1, the $[ScorpoPhos]^-$ ligand comprises three potentially bidentate 'arms', each containing N- and P-donor moieties. The $^{31}P\{^1H\}$ NMR spectrum suggests that the phosphine units are not involved in coordination to the potassium ion in solution as the chemical shift is identical to that of the metal-free pyrazole starting material ($\delta = -11.7$ ppm).



$Hpz^{phos,Me}$ K[ScorpoPhos]

Scheme 1 Synthesis of K[ScorpoPhos].

The potassium salt was converted to the corresponding thallium complex, Tl[ScorpoPhos], *via* an equimolar reaction with thallous nitrate. This reaction proceeded cleanly and in good yield (91%) and crystals suitable for X-ray analysis were obtained by slow

[a]*Department of Chemistry, Imperial College London, South Kensington, London, UK SW7 2AZ. E-mail: n.long@imperial.ac.uk; Tel: +44 (0)20 7594 5781*
[b]*GSK Clinical Imaging Centre, Imperial College London, Hammersmith Hospital, Du Cane Road, London, UK W12 0NN*

† Electronic supplementary information (ESI) available: Experimental details and characterisation data for represented compounds. CCDC reference numbers 674937 and 674938. For ESI and crystallographic data in CIF or other electronic format see DOI: 10.1039/b804608p

This journal is © The Royal Society of Chemistry 2008

evaporation of an acetone solution. The solid-state structure§ of Tl[ScorpoPhos] revealed the presence of five crystallographically independent complexes, one of which (Tl[ScorpoPhos]-*A*) is shown in Fig. 1 (see ESI† for details of the others). In each case the metal centre is encapsulated in an approximately C_3 symmetric manner by all six available donor atoms with Tl–N and Tl–P distances of *ca.* 2.64 and 3.29 Å respectively. In each complex the metal lies in the plane of the three phosphorus atoms, the mean deviation across the five complexes being *ca.* 0.12 Å. Despite the length of the Tl–P interaction, this contact is also present in solution at room temperature as evidenced by $^{31}P\{^1H\}$ NMR spectroscopy. Coupling between the three equivalent ^{31}P nuclei and the thallium centre (consisting of $^{203}Tl/^{205}Tl$, both of which are spin $\frac{1}{2}$ with near-identical gyromagnetic ratios) produces a sharp doublet at −3.1 ppm (J = 1253 Hz), suggesting that the thallium remains encapsulated by the podand ligand.

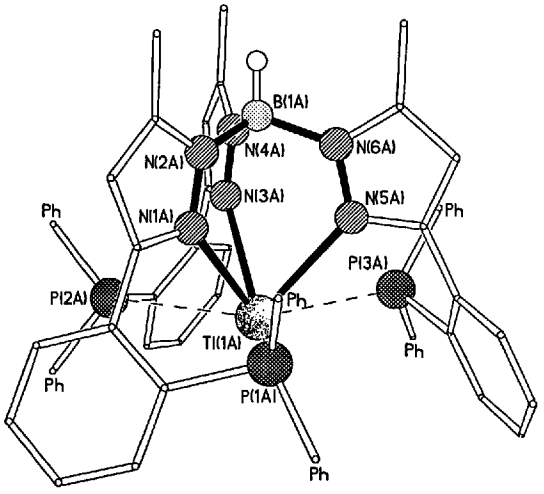


Fig. 1 The molecular structure of Tl[ScorpoPhos]-*A*, one of the five crystallographically independent complexes present in the crystals of Tl[ScorpoPhos]. Selected bond lengths for Tl[ScorpoPhos]-*A* (Å): Tl(1A)–N(1A) 2.642(3), Tl(1A)–N(3A) 2.678(3), Tl(1A)–N(5A) 2.637(3), Tl(1A)–P(1A) 3.2273(9), Tl(1A)–P(2A) 3.2122(9), Tl(1A)–P(3A) 3.2488(9).

To explore the potential of the phosphine moieties to coordinate with metal centres in a formal coordination bond, the reaction of K[ScorpoPhos] towards copper(I) ions was investigated. Mononuclear copper(I) complexes of Tp ligands are well known, with the copper achieving coordinative saturation by binding to the tripodal array of pyrazolyl donors and a second monodentate ligand to form a tetrahedral complex. In the case of ScorpoPhos, it was hoped that a single ligand unit would be able to stabilise the copper centre *via* coordination of the three pyrazolyl units plus coordination of one of the appended phosphine groups. Accordingly, the reaction between K[ScorpoPhos] and CuCl was performed in THF at room temperature to produce a yellow solution. $^{31}P\{^1H\}$ NMR spectroscopy of the reaction solution showed a sharp singlet at −9.0 ppm (*cf.* K[ScorpoPhos] at −11.7 ppm), indicating formation of a new species. Subsequent filtration and removal of the solvent gave a pale yellow powder which was attributed as the Cu[ScorpoPhos] complex based on ESI(+ve) mass spectrometry (m/z = 1099, corresponding to Cu[ScorpoPhos]$^+$). The downfield shift of the single peak in the $^{31}P\{^1H\}$ NMR (compared to the starting material) prompted further studies to probe the solution behaviour of this complex. Variable temperature $^{31}P\{^1H\}$ NMR studies were performed by cooling of a CD_2Cl_2 solution of the complex to 183 K (Fig. 2). At approximately 213 K (−60 °C) decoalescence of the single peak becomes apparent, and when the temperature is lowered to its minimum of 183 K (−90 °C) two separate peaks are observed at −14.6 ppm and +0.0 ppm with relative integrals of approximately 2 to 1, respectively. The chemical shift and the integral of these peaks suggest that the downfield resonance is that of a single copper-bound phosphine moiety, while the upfield resonance is attributed to the two remaining phosphine moieties which remain unbound in solution.

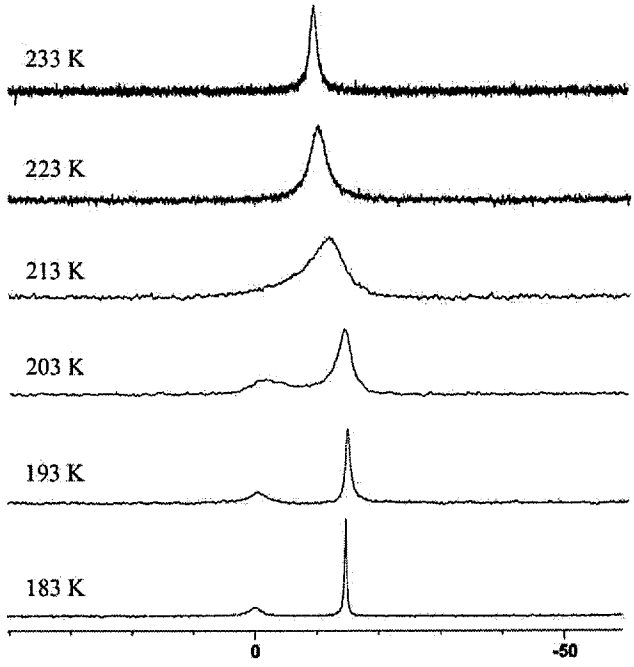


Fig. 2 VT $^{31}P\{H\}$ NMR spectra of Cu[ScorpoPhos].

X-Ray analysis of this complex§ supports the low temperature solution behaviour. As shown in Fig. 3, the ligand coordinates in a κ^4-N_3,P fashion *via* three pyrazolyl donors and one phosphino

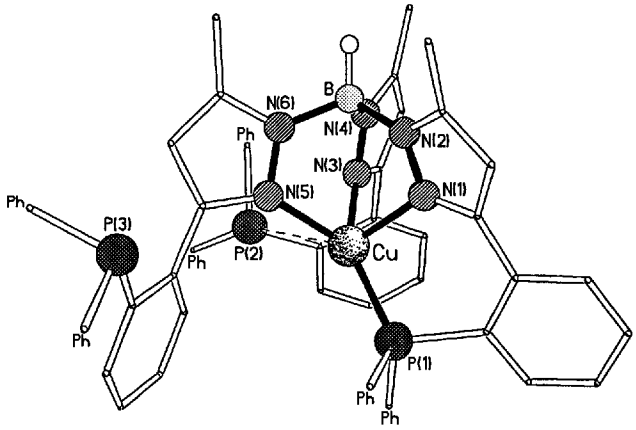


Fig. 3 The molecular structure of Cu[ScorpoPhos]. Selected bond lengths (Å): Cu–N(1) 2.0987(16), Cu–N(3) 2.0872(16), Cu–N(5) 2.0733(16), Cu–P(1) 2.1745(6), Cu···P(2) 3.7767(7), Cu···P(3) 5.7297(7).

This journal is © The Royal Society of Chemistry 2008

group with a Cu–P(1) separation of 2.1745(6) Å (*cf. ca.* 3.29 Å in Tl[ScorpoPhos]) to form a distorted tetrahedron around the copper. Excluding the PPh_2 units, the rest of the complex retains approximate C_3 symmetry, and the metal is, as expected, much closer to the boron centre (Cu···B 3.025(2) Å *cf. ca.* 3.79 Å for the Tl···B separations in Tl[ScorpoPhos]). Chelation of one bidentate arm to the copper forms a favourable six-membered [$CuNC_3P$] ring, with the coordinated phosphorus being observed as the downfield resonance in the low temperature $^{31}P\{^1H\}$ NMR spectrum. At room temperature, however, the phosphine moieties are so rapidly associating and dissociating that an average signal is observed in the $^{31}P\{^1H\}$ NMR spectrum.

In summary, a new tris(pyrazolyl)borate ligand containing phosphine appendages has been synthesised, and solution and solid-state studies have revealed that the appended phosphine moieties are able to stabilise a metal centre depending on the coordination requirements of the metal employed. With copper, a fluxional process of phosphorus coordination/dissociation at the 4th coordination site of the metal has been identified which should provide an opportunity for future substrate binding. Utilising this behaviour, we intend to investigate the use of this ligand for transition-metal catalysed reactions.

Acknowledgements

We gratefully acknowledge financial support from GlaxoSmithKline and the Department of Chemistry, Imperial College, London.

Notes and references

‡ *General procedure:* Under an atmosphere of nitrogen, a mixture of $Hpz^{Phos,Me}$ (4.000 g, 11.7 mmol) and potassium borohydride (0.158 g, 2.92 mmol) was heated gradually to 220 °C causing H_2 to evolve. After 5 h of stirring at this temperature, heating was stopped and the mixture allowed to cool, producing a yellow solid. Dissolution in CH_2Cl_2 and subsequent removal of the solvent by rotary evaporation gave an off-white powder. Recrystallisation from CH_2Cl_2–hexane gave a white powder which was analytically pure. Yield = 2.00 g (64%). Anal. calc. (found) (%) for $C_{66}H_{55}BKN_6P_3$: C 73.7 (73.8); H 5.16 (5.22); N 7.82 (7.90). MS-ESI(−ve): m/z = 1035 [ScorpoPhos]$^-$. $^{31}P\{^1H\}$ NMR (+25°C, $CDCl_3$, 162 MHz): $\delta = -11.7$.

§ *Crystal data for* Tl[ScorpoPhos]: $C_{66}H_{55}BN_6P_3Tl$, M = 1240.25, trigonal, $P3$ (no. 143), $a = b = 38.2173(2)$ Å, $c = 10.39625(8)$ Å, $V = 13150.1(3)$ Å^3, $Z = 9$ (there are five independent complexes, two of which have C_1 symmetry whilst the other three have C_3 symmetry, making a total of three complexes in the asymmetric unit), $D_c = 1.410$ g cm^{-3}, μ(Mo-Kα) = 2.891 mm^{-1}, T = 173 K, colourless tablets, Oxford Diffraction Xcalibur 3 diffractometer; 53602 independent measured reflections, F^2 refinement, $R_1 = 0.037$, $wR_2 = 0.063$, 42785 independent observed absorption-corrected reflections [$|F_o| > 4\sigma(|F_o|)$, $2\theta_{max} = 63°$], 2095 parameters. The structure of Tl[ScorpoPhos] was shown to be a partial racemic twin by a combination of R-factor tests ($R_1^+ = 0.0397$, $R_1^- = 0.0731$) and by use of the Flack parameter [$x^+ = +0.16(1)$, $x^- = +0.84(1)$]. *Crystal data for* Cu[ScorpoPhos]: $C_{66}H_{55}BCuN_6P_3 \cdot Me_2CO$, M = 1157.50, triclinic, $P\bar{1}$ (no. 2), $a = 14.4370(7)$ Å, $b = 14.6381(4)$ Å, $c = 17.2046(7)$ Å, $\alpha = 80.770(3)°$, $\beta = 68.299(4)°$, $\gamma = 61.978(4)°$, $V = 2981.75(19)$ Å^3, $Z = 2$, $D_c = 1.289$ g cm^{-3}, μ(Cu-Kα) = 1.659 mm^{-1}, T = 173 K, colourless blocks, Oxford Diffraction Xcalibur PX Ultra diffractometer; 11176 independent measured reflections, F^2 refinement, $R_1 = 0.034$, $wR_2 = 0.077$, 7403 independent observed absorption-corrected reflections [$|F_o| > 4\sigma(|F_o|)$, $2\theta_{max} = 143°$], 739 parameters. CCDC reference numbers 674937 and 674938.

1 P. Braunstein and F. Naud, *Angew. Chem., Int. Ed.*, 2001, **40**, 680.
2 S. Trofimenko, *Scorpionates: The Coordination Chemistry of Polypyrazolylborate Ligands*, Imperial College Press, London, 1999.
3 J. A. McCleverty and T. J. Meyer, *Comprehensive Coordination Chemistry II – From Biotechnology to Nanotechnology*, Elsevier, Oxford-Amsterdam, 2003.
4 H. Adams, S. R. Batten, G. M. Davies, M. B. Duriska, J. C. Jeffery, P. Jensen, J. Lu, G. R. Motson, S. J. Coles, M. B. Hursthouse and M. D. Ward, *Dalton Trans.*, 2005, 1910.
5 J. S. Fleming, E. Psillakis, S. M. Couchman, J. C. Jeffery, J. A. McCleverty and M. D. Ward, *J. Chem. Soc., Dalton Trans.*, 1998, 537.
6 K. L. V. Mann, J. C. Jeffery, J. A. McCleverty and M. D. Ward, *Polyhedron*, 1999, **18**, 721.
7 E. R. Humphrey, K. L. V. Mann, Z. R. Reeves, A. Behrendt, J. C. Jeffery, J. A. McCleverty and M. D. Ward, *New J. Chem.*, 1999, **23**, 417.
8 J. Kisala, A. Bialonska, Z. Ciunik, S. Kurek and S. Wolowiec, *Polyhedron*, 2006, **25**, 3222.
9 A. L. Rheingold, B. S. Haggerty, L. M. Liable-Sands and S. Trofimenko, *Inorg. Chem.*, 1999, **38**, 6306.
10 A. L. Rheingold, C. D. Incarvito and S. Trofimenko, *J. Chem. Soc., Dalton Trans.*, 2000, 1233.
11 M. H. Chisholm, J. C. Gallucci and G. Yaman, *Chem. Commun.*, 2006, 1872.
12 J. A. Maldonado Calvo and H. Vahrenkamp, *Inorg. Chim. Acta*, 2006, **359**, 4079.
13 P. L. Jones, K. L. V. Mann, J. C. Jeffery, J. A. McCleverty and M. D. Ward, *Polyhedron*, 1997, **16**, 2435.
14 G. Bandoli, A. Dolmella, G. G. Lobbia, G. Papini, M. Pellei and C. Santini, *Inorg. Chim. Acta*, 2006, **359**, 4036.
15 S. Kealey, N. J. Long, A. J. P. White and A. D. Gee, *Dalton Trans.*, 2007, 4763.
16 M. Jimenez-Tenorio, M. C. Puerta, P. Valerga, F. J. Moreno-Dorado, F. M. Guerra and G. M. Massanet, *Chem. Commun.*, 2001, 2324.
17 Y. Fukumoto, T. Dohi, H. Masaoka, N. Chatani and S. Murai, *Organometallics*, 2002, **21**, 3845.
18 C. Slugovc, K. Mereiter, E. Zobetz, R. Schmid and K. Kirchner, *Organometallics*, 1996, **15**.
19 S. Kealey, N. J. Long, P. W. Miller, A. J. P. White, P. B. Hitchcock and A. Gee, *Dalton Trans.*, 2007, 2823.